Carbon Nanotube/Polymer

Hybrid Material Design

via Modular Ligation Techniques

Zur Erlangung des akademischen Grades eines

DOKTORS DER NATURWISSENSCHAFTEN

(Dr. rer. nat.)

Fakultät für Chemie und Biowissenschaften

Karlsruher Institut für Technologie (KIT) – Universitätsbereich

genehmigte

DISSERTATION

von

Nicolas Pierre Stéphane Zydziak

aus

Thiais, Frankreich

Die vorliegende Arbeit wurde von Januar 2010 bis März 2013 unter Anleitung von Prof. Dr. Christopher Barner-Kowollik am Karlsruher Institut für Technologie (KIT) – Universitätsbereich angefertigt.

« Un voyage de mille li a commencé par un pas. » Tao Te King

Abstract

The Diels-Alder (DA) reaction is employed to functionalize Single-Walled Carbon Nanotubes (SWCNTs) by means of a library of end functional polymers. Given the dienophilic character of the SWCNTs, the functionalization with a specific polymer chain terminus was conducted for the first time in a one pot [4+2] cycloaddition reaction, under ambient conditions, without any catalyst and pre-treatment of the SWCNTs. These mild conditions are enabled by the high reactivity of the cyclopentadienyl (Cp) moiety, reacting as diene, localized at the terminus of the polymer chains. The polymerizations of the different monomers – (methyl)methacrylate, N-isopropylacrylamide, 3-hexylthiophene – occurred under living conditions leading to well-defined polymer chains and chain termini. The polymer chain-end transformation was in-depth characterized prior to the functionalization of the SWCNTs, after which analytic methods unambiguously evidenced the covalently bonded nature of the polymer chains and enabled to accurately determine their grafting density at the surface of the SWCNTs. A first *'proof-of-principle'* with Cp functional poly(methyl)methacrylate (M_n = 2900 g·mol^{-1}, $Đ$ = 1.2), synthesized via ATRP (Atom Transfer Radical Polymerization), illustrates the success of the SWCNT functionalization with Cp end-capped polymer chains. In that case, the grafting density reached 0.0293 chain·nm^{-2}. Subsequently, Cp end-capped poly(N-isopropylacrylamide) (M_n = 5400 g·mol^{-1}, $Đ$ = 1.1) was synthesized via RAFT (Reversible Addition Fragmentation chain Transfer) polymerization and a sequential chain-end transformation to Cp. The grafting density of the resulting PNIPAM functionalized SWCNTs was evaluated to be close to 0.0288 chain·nm^{-2}; the functionalized SWCNTs showed thermo-responsive properties. Thirdly, the Cp driven functionalization of SWCNTs was additionally carried out with a conjugated polymer, i.e. poly(3-hexylthiophene) (M_n = 6500 g·mol^{-1}, $Đ$ = 1.2) generated via GRIgnard Metathesis (GRIM). The grafting density of polymer chains at the surface of the SWCNTs was estimated to be close to 0.0510 chain·nm^{-2}. Finally, in an approach to increase the polymer grafting density on the SWCNTs surface, a pre-functionalization of the SWCNTs with a newly synthesized pyridine based dithioester, employed as diene for a hetero Diels-Alder (HDA) reaction, enabled to increase the grafting density of polymer strands on the SWCNTs to 0.0774 chain·nm^{-2} with Cp end-capped poly(methyl)methacrylate (M_n = 2700 g·mol^{-1}, $Đ$ = 1.2). Thus, the present thesis introduces novel, mild, efficient avenues for the functionalization of SWCNTs with highly defined polymer strands of variable chemical constitution, leading to high grafting densities, while leaving the SWCNTs primary structure largely intact.

Table of Contents

---

* The results reported in Chapter 6 have been produced in collaboration with Dr. Basit Yameen (KIT).

Chapter 1 – Introduction

1.1. Motivation

Whereas the effects of nanoparticles were applied by humanity thousand years ago,[1] the contemporary interest for the phenomena induced by nano-objects led to the recent emergence of nanotechnology, exploring the properties of systems organized at the nanometric scale. While the Nobel Prizes for Chemistry in 1996 were awarded to Curl Jr., Sir Kroto and Smalley for their discovery of fullerenes, and in Physics to Geim and Novoselov in 2010 for their groundbreaking experiments on graphene, one is often astonished by the proximity of such carbon nanostructures in everyday life – fullerenes are e.g. present in candle soot.[2] While recent interest focused on the properties of graphene – an interest reinforced by the accumulated knowledge over decades on fullerenes, carbon nanotubes and other carbon nanostructures – significant efforts are made to chemically modify these structures for specific applications. With the aim to promote the transfer of carbon nanostructures, especially Single-Walled Carbon Nanotubes (SWCNTs) to concrete applications, the investigations in the present thesis are guided by the desire to employ a modification reaction that leaves the primary structure of the SWCNTs as much as possible intact.

Many reviews and articles describe the properties of the carbon nanotubes (CNTs) and their applications. Alongside their particular nanometric size and cylindrical shape, one can compile the following characteristics which make SWCNTs, such as graphene, unique materials. SWCNTs have a high current capacity (10^9 A·cm^{-2}), a high thermal conductivity (3500 W·m^{-1}·K^{-1}), an axial Young's modulus in the range of 1–1.8 TPa, and a fracture stress

of 50 GPa, which is to 50 times larger than for steel wires.[3] Therefore, multiple applications based on these nanomaterials were developed in many research areas, such as CNT fibers,[4,5] supercapacitors,[6] electrodes[7] and batteries,[8] electrochemical sensors,[9,10] and in the medical domain with drug delivery[11,12] and bioelectronic devices.[13] Introduced in polymer matrices,[14,15] CNTs enable to enhance the properties of the nanocomposite materials: mechanically,[16,17] electrically,[18] or both simultaneously.[19]

However, without any treatment of the CNTs, a composite material displays poorer properties than one could expect, firstly because of the presence of Van der Waals forces[20] which lead the CNTs to form bundles[21] and not to disperse homogeneously into the material; secondly, because of incompatible interfacial energies between the CNTs and the polymer matrix, especially when an enhancement of the mechanical properties is targeted.[22,23] Physico-chemical processes are often employed in order to solve these issues. Among the most popular, sonication can be used to disrupt the bundles,[24] surfactants or wrapping molecules around the CNTs surfaces can decrease the differences between the interfacial energy of the CNTs and the polymer matrix or the solvent.[25] Other engineering procedures such as melt-mixing or *in situ* polymerization[26,27] are employed to better the properties of the generated composite materials. A chemical pre-functionalization, for example oxidation, can enhance the solubility[28] of CNTs in polar solvents and enable a further functionalization to anchor small molecules or polymers at the surface of the SWCNTs.[29,30]

In other words, efficient and facile strategies are required for a covalent modification of CNTs with suitable polymer strands and for good embedding of the CNTs into the polymer matrices. Ideally, one would envisage a functionalization process that requires no prior treatment of the employed CNTs, as well as leaving the CNTs' structure as much as possible intact. In the past, several strategies for the covalent functionalization of CNTs have been suggested. These strategies are described in several reviews[31] and include, among others: oxidation,[32,33] fluorination,[34] free radical addition,[35] addition of carbenes and nitrenes,[36] 1,3 dipolar cycloaddition,[37] Bingel reaction,[38] nucleophilic addition[39] and alkylation.[40] All these strategies require relatively demanding reaction conditions as the chemicals involved can be highly sensitive to atmospheric exposure (moisture, air) and several synthetic steps are required in order to functionalize the CNTs. Moreover, typical acid based pre-treatments are often highly detrimental to the properties of the CNTs that one wishes to impart within their embedding into polymer matrices.[41] Although a wide range of all these covalent strategies have been explored to control the chemical nature of the CNT surface of, there still exists a genuine challenge to develop facile and direct surface functionalization of pristine CNTs.

Therefore, the investigations performed herein were conducted to explore the potential of a simple reaction, for the grafting of well defined polymer chains onto carbon nanotubes: the Diels-Alder (DA) reaction. Specific interest is focused on polymer chains of different chemical composition able to react with the surface of SWCNTs in a one pot reaction, conducted under mild conditions, without any catalyst and pre-treatment of the SWCNTs.

1.2. Overview

In order to investigate a wide spectrum of possible applications of polymer functionalized SWCNTs, three polymers were chosen: poly(methyl)methacrylate (PMMA) useful for the compatibilization of SWCNTs into thermoplastic matrices, the thermo-responsive poly(N-isopropylacrylamide) (PNIPAM) and the conjugated poly(3-hexylthiophene) for energy harvesting purposes. These polymers were prepared via polymerization techniques able to guarantee an exceptionally high chain-end fidelity of the polymer chains. For each kind of polymer, a specific chain terminus was attached to the polymer chain for its high reactivity in [4+2] cycloadditions, namely the cyclopentadienyl (Cp) moiety.

Installed either directly or indirectly via Atom Transfer Radical Polymerization (ATRP), Reversible Addition Fragmentation chain Transfer (RAFT) and GRIgnard Metathesis (GRIM) polymerization, respectively, the bromine chain end-group of the polymer chains was transformed in each case into a Cp moiety, imparting a diene character to the polymer chains. The polymer chain terminus transformation was characterized via a combination of ^{1}H Nuclear Magnetic Resonance (NMR) spectroscopy and soft ionization mass spectrometry.

The reactions between the SWCNTs and the Cp end-capped polymers were performed in a solvent at ambient temperature or at elevated temperature (80 °C). The success of the reaction was investigated via complementary analytic methods in bulk, e.g. Thermogravimetric Analysis (TGA) and Elemental Analysis (EA), and at the surface with X-Ray Photoelectron Spectroscopy (XPS), while systematic control experiments with non-functional polymer chains were conducted. Supplementary analytic methods such as High Resolution Transmission Electron Microscopy (HRTEM) for imaging the SWCNTs, Fourier Transform Infrared (FTIR) spectroscopy, Dynamic Light Scattering (DLS) and ultraviolet (UV) spectroscopy were additionally employed.

Regardless of the degree of functionalization of the SWCNTs with the different Cp end-capped polymer chains in the above cited conditions, the analytic results were further evaluated to arrive at grafting densities, i.e. the concentration of polymer chains at the surface

of the SWCNTs. In addition, an alternative route to polymer SWCNT functionalization was explored via pre-functionalization of the SWCNTs with a dithioester moiety, sustainable for a hetero Diels-Alder (HDA) reaction with Cp end-capped polymer chains.

Consequently, the current thesis is structured (see **Scheme 1.1**) according to the nature of the polymer chains employed to functionalize the SWCNTs as follows: PMMA in the first part, PNIPAM in the second part and P3HT in the third part. The exploration of a pre-functionalization approach and the subsequent HDA reaction is reported towards the end of the thesis.
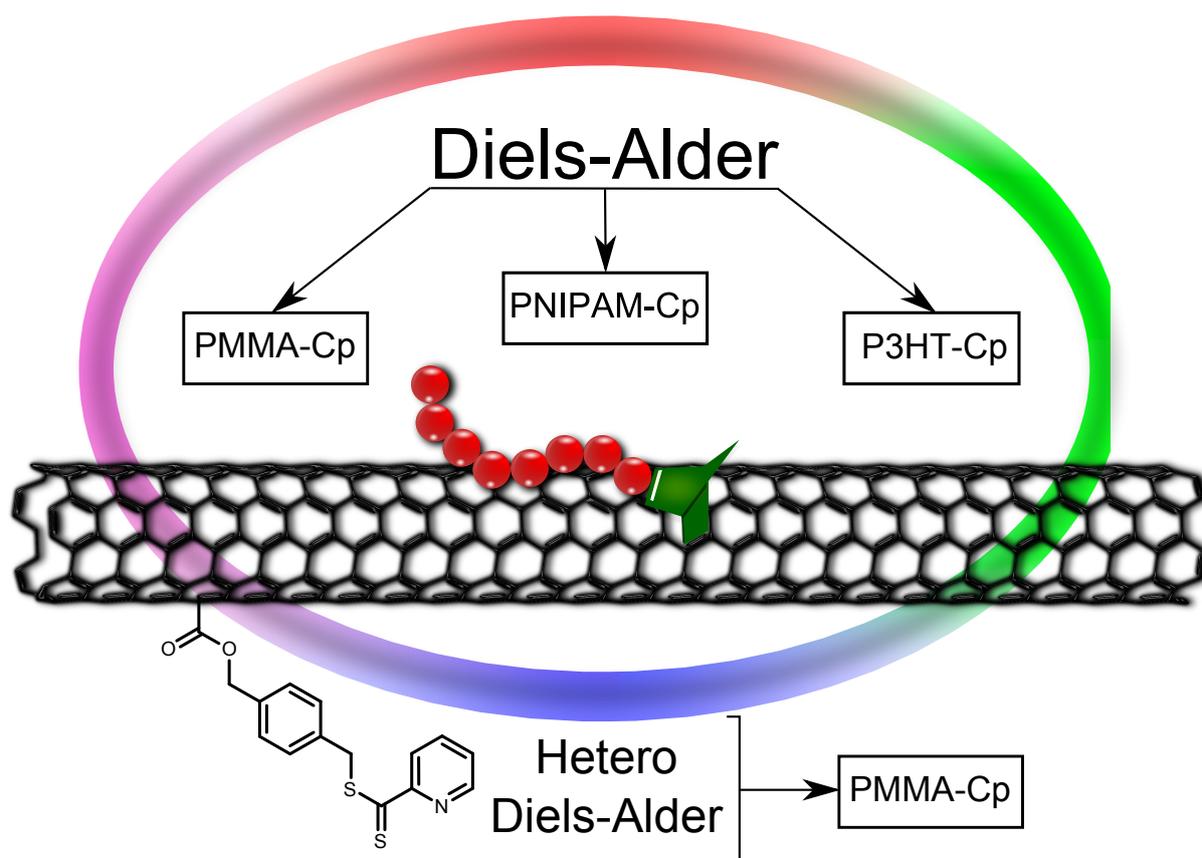
Scheme 1.1. Thesis overview depicting the four studied SWCNT/polymer hybrid materials generated via Diels-Alder and hetero Diels-Alder ligation.

1.3. Objectives

Following these intentions, the proposed investigations in the present thesis tend to satisfy the following objectives:

- Perform the synthesis of highly defined Cp end-capped PMMA, PNIPAM and P3HT and characterize the chain end-group fidelity for each polymer in-depth
- Assess the success of the DA reaction between SWCNTs and the functional polymer chains
- Quantify the grafting density of the polymer chains localized at the SWCNTs surface in order to describe the morphology of the obtained polymer/SWCNT hybrid materials
- Compare the grafting density between the direct DA reaction and the HDA strategy involving a SWCNT pre-treatment
- Verify the properties of the functionalized SWCNTs, especially in the case of their functionalization with thermo-responsive polymer chains.

Chapter 2 – Theory and Background
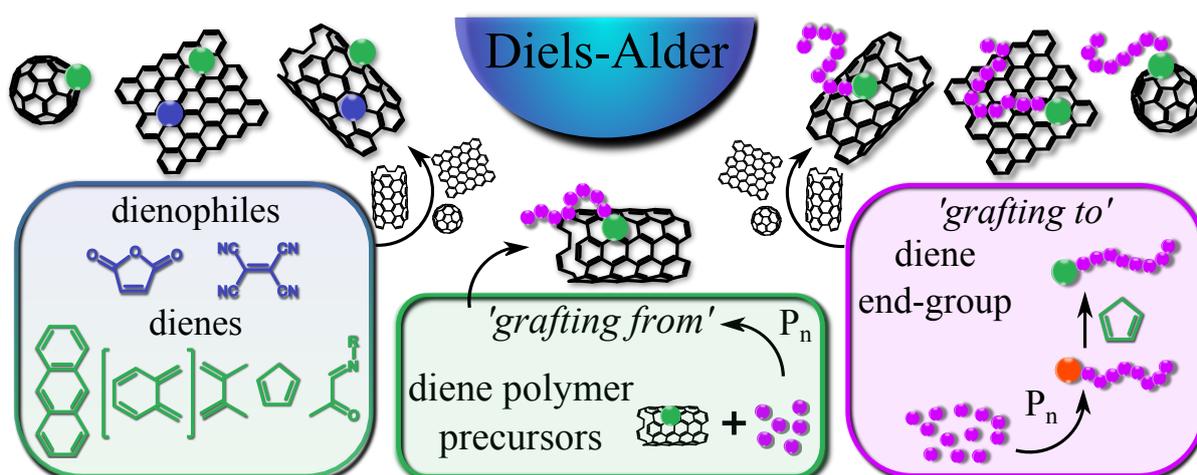
In the present chapter, some synthetic and structural characteristics of carbon nanostructures with a focus on SWCNTs, as well as the principle of the DA reaction are introduced. Considering these two topics, the role of the DA reaction, which is a fundamental reaction for the synthesis of carbon materials, is highlighted, and a state-of-the-art on previous and present works reporting the functionalization of carbon materials involving the DA reaction is given. Finally, the last part describes relevant polymerization techniques for the modular ligation of SWCNTs via a *'grafting to'* strategy applied in the present work.

2.1. Carbon materials

Carbon (Z = 6) is one primordial element, present in the nature, for the construction of organic molecules essential for life. From its ancestral use as energetic source (wood, coal), this element plays an essential role in new materials' discovery as evidenced from with the development of human technologies in the last centuries. Alongside the metallurgic importance of carbon for the fabrication of steel and cast iron, the diversity of the chemical bonding of this element underlines the fascination for carbon by the scientists. From the well-known carbon hybridization sp, sp^2 and sp^3, one can also distinguish unusual configurations such as the *platonic hydrocarbons* (C_8H_8 cubane[42], $C_{20}H_{20}$ dodecahedrane[43]) and carbon clusters, e.g. C_2, C_4, C_{10}.[44] As variation from the common allotropic forms such as diamond (sp^3 hybridization) and graphite (sp^2 hybridization), amorphous carbon allotropes raise the researchers' attention since 20 years, with the discovery of fullerenes, carbon nanotubes and graphene and their applications.

From their synthesis via graphite laser ablation,[45] arc vaporization[46] or flash vacuum pyrolysis of corannulene,[47,48] different forms of fullerenes can be synthesized. Within the wide fullerene family,[49] C_{60} represents one of the most studied fullerenes and appears in several recent applications (see section 2.4). The icosahedral sphere is constituted of 12 pentagonal and 20 hexagonal faces. Each carbon is bonded to three carbon atoms in a sp^2 configuration, although the curvature of the fullerenes leads to a mixture with the sp^3 configuration.[50] Graphene can be described as a single graphitic plane and is constituted of sp^2 carbon atoms. The synthesis of these 2D carbon nanostructures results from the exfoliation of graphite, from the CVD process or from the graphitization of SiC crystals.[51] Carbon nanotubes (CNTs) represent the cylindrical forms of a rolled graphene sheet. Constituted from a single graphene sheet (SWCNTs) or from concentric cylinders (Multi-Walled Carbon Nanotubes, MWCNTs), CNTs are commonly synthesized in the gas phase via chemical vapor deposition (CVD), laser ablation or arc discharge.[52] The synthesis of the CNTs leads to a sample containing nanotubes with a diameter varying in the range from

0.7 nm (diameter of the end-cap, a hemi-fullerene derived from C_{60}) to 1.6 nm[53] for SWCNTs, and 5–30 nm for MWCNTs, and with different length (from hundreds of nanometers to some micrometers).[54] Despite the difficulty to accurately control the gas phase process, many efforts are made to synthesize SWCNTs with a very well-defined diameter (refer to section 2.3 for further details). Yet, a well-defined diameter does not ensure the purity of the sample from a chiral and electronic point of view. Theoretically, a 1 nm (with an approximation of ±0.04 nm in the diameter) SWCNT can be described as the result of the rolling of the graphene sheet in 8 different fashions. These fashions are mathematically defined via a chiral vector C_h with two coordinates (n, m). The chiral vector C_h is the result of the linear combination of the two unit vectors a_1 and a_2 from the hexagonal graphene lattice (see **Figure 2.1**)[55] These coordinates determine the structure of the SWCNTs: the (n, n) vectors form armchair SWCNTs, the $(n, 0)$ vectors constitute the so-called zig-zag SWCNTs, and any other (n, m) combination describes chiral SWCNTs. The indices n and m also give access to the electronic properties of the SWCNTs: if $n – m = 3r$ (r integer), the SWCNT is metallic, otherwise the SWCNT is a semi-conductor.[56]
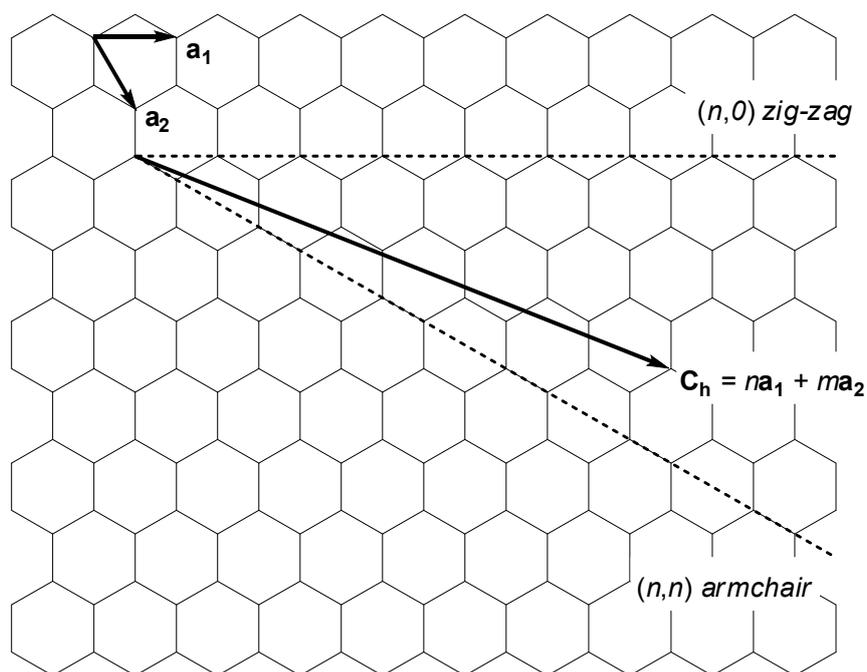
Figure 2.1. Representation of the graphene sheet and the chiral vector C_h of the SWCNTs. a_1 and a_2 are unit vectors (norm $a_{C-C}·\sqrt{3} = 2.46$ Å). The configuration (n, m) represents the armchair SWCNTs, $(n, 0)$ the zig-zag SWCNTs, and any other (n, m) pairs chiral SWCNTs.

2.2. Diels-Alder reactions

DA processes are conjugation reactions between a molecule containing a conjugated π-system of two double bonds (diene) and an alkene (dienophile). The reaction involves 4

electrons from the diene and 2 electrons from the dienophile – the DA reaction is also called [4+2] cycloaddition – and is thermodynamically favored due to the formation of two σ-bonds. The DA cycloaddition is a unique thermal controlled reaction, which can operate in a reverse fashion via a retro-DA process (rDA), thermally[57,58] or photochemically.[59,60] The simplicity of the DA reaction does not reflect its diversity, since many aspects influence the mechanism of this reaction such as stereochemistry, regiospecificity and kinetics (solvent effects, temperature and pressure effects).[61] Such as the Cu(I)-catalyzed azide-alkyne cycloaddition,[62,63] as well as the Michael-type thiol-ene and thiol-yne reactions,[64] the DA reaction, under certain conditions, belongs to the *'click'* reaction category. Its potential *'click'* character[65,66] is also prevalent in its hetero variant (HDA reaction, in which hetero atoms such as nitrogen, oxygen and sulfur are involved).[67] The *'click'* concept was introduced by Sharpless[68] in 2001 describing innovative orthogonal reactions which are quantitative, highly selective, proceed under mild conditions and have a high atom economy.[69] A wide range of research groups extended this concept, which was originally defined for small molecules,[70,71] to polymer chemistry,[72,73] for which, concretely, the design of macromolecular architectures with a specific functionality placed at a well-defined position is of crucial importance.[74,75] Driven by the simplicity of these modular orthogonal conjugations, numerous innovations have been specifically developed for the functionalization of surfaces. Indeed, under the so-called *'click'* conditions, a polymer strand equipped with a specific functionality can react orthogonally with a specific counter functionality, which is attached to another polymer chain, a surface[76] or a biomolecule.[77] The implementation of such polymer functionalization onto nanomaterials enables to ease the handling of such nanometric materials and imparts them with additional properties.[78]

The work performed in the present thesis is driven by these attracting aspects of the DA reaction. Firstly, the main advantage of the thermodynamically driven equilibrium concerns the absence of catalyst (e.g. copper) or radicals such as in the azide-alkyne cycloaddition or radical variant of the thiol-ene reaction. Moreover, this equilibrium involves a thermally driven retro DA reaction (rDA), which is mainly employed for the generation of self-healing materials,[79,80] with a theoretically infinitive numbers of reactants / products cycles. A further thermodynamic aspect is the ability to displace this equilibrium with more suitable systems[81] to the product side at mild conditions (e.g. at ambient pressure and temperature),[82,83] whilst the simplest example for a [4+2] cycloaddition between ethylene and butadiene molecules involves high pressure and high temperature.[84] Finally, the recent design of diene-dienophile pairs with high affinity enabled to the generation of complex surface designs. The design of

specific RAFT agents, sulfonyl, pyridinyl or phosphoryl based, reacting as electron deficient dienophiles with highly reactive dienes, such as cyclopentadienyl or sorbic acid moieties[85,86] imparts *'click'* character to the HDA chemistry. These recent developments of HDA reaction, for which the dienophiles are free or located at the terminus of a polymer chain, and the dienes are located at the terminus of the polymer chain or at a surface, make this reaction a strategy of choice for readily decorating complex surfaces with polymers or proteins on gold nanoparticles,[87] cellulose[88] or microspheres.[89]

Among all these above cited aspects, which highlight the high potential of the DA reaction, the DA reaction and its derivatives (HDA, rDA) may embody a breakthrough in the functionalization of SWCNTs, especially by their capability to simply decorate SWCNTs with polymer strands. The interest in the DA reaction and SWCNTs requires to review to what extent this reaction has been employed in the context of SWCNTs and other carbon materials (MWCNTs, fullerenes and graphene). In the following, the most recent investigations for understanding the synthetic approaches towards these carbon materials involving the DA reaction are explored in a first part (section 2.3.). In a second part, the necessity of functionalizing these carbon materials with polymer strands by citing concrete applications to functionalized carbon materials and the resulting properties (section 2.4.) is highlighted. Finally, the developed chemical systems reacting with the carbon materials via the DA reaction, being a small molecule or a polymer strand (section 2.5.) is described. For this particular point, two functionalization strategies are distinguished, e.g. *'grafting from'* and *'grafting to'*. Finally the question whether the DA process can be a suitable reaction for the functionalization of the SWCNTs, and to what extend its *'click'* character could be employed in the realization of a simple SWCNT functionalization approaches is explored.

2.3. Use of Diels-Alder reactions for the synthesis carbon materials

In the past 20 years substantial efforts were made to produce carbon materials in controlled processes at large scales in order to achieve very well-defined nanostructures with a high degree of purity and at reasonable costs, especially for CNTs and graphene.[90,91] For CNTs, many post-synthetic strategies were developed to purify (e.g. via acidic treatment,[92,93] or annealing[94]) and selectively isolate the CNTs (via chromatography[95] or via employing surfactants[96]) obtained from gas phase processes.[97] Purity, e.g. the quality of the synthesized CNTs, is primordial to design materials or systems with tailored properties.[98] From a synthetic process perspective, many efforts are being undertaken not only to reduce the amount of catalyst and amorphous carbon associated with the generation of CNTs, but also to control the dispersity of the CNTs population in terms of diameter,[99,100] helicity (chirality),[101]

length[102] or absence of defects.[103] Inspired by the advantages (e.g. purity) of the synthetic alternates provided by flash vacuum pyrolysis of corannulene,[47,48] over the graphite laser ablation[45] or arc vaporization[46] for the synthesis of fullerenes, organic strategies employing synthetic templates were recently developed to control the quality and to selectively synthesize CNTs with a unique diameter and chirality, directly in the gas phase. Recently, a so called *'polymer approach'* (refer to **Figure 2.2**) based on the successive DA reactions for the synthesis of CNTs has been introduced.[104,105]
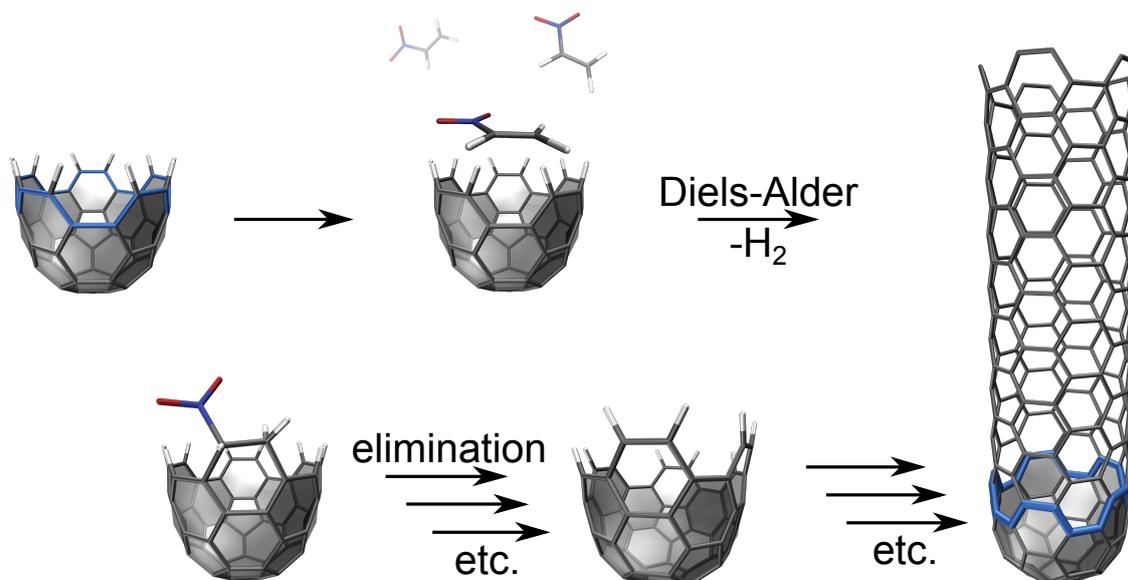
Figure 2.2. *'Polymer approach'* for the synthesis of SWCNTs via successive DA reactions of nitroethylene on a CNT end cap and subsequent elimination reactions. Reproduced with permission from Ref.104 (Schrettl *et al*). Copyright 2012, Wiley-VCH.

A deeper investigation into the underpinning mechanism will allow the application of DA reactions for the controlled synthesis of a variety of carbon nano-architectures. Scott *et al*.[106,107] have reported a DA reaction of 7,14-dimesitylbisanthene (perylene), with diethyl acetylene derivatives, evidencing the possibility of an elongation of planar polyaromatic hydrocarbons. The same research group has employed semi-empirical quantum calculations (AM1 and B3LYP/6–31G*) predicting the growth of cylindrical polyaromatic hydrocarbons through successive DA reactions between end-capped or belt polyarenes and acetylene followed by dehydrogenation (re-aromatization).[108] However, Li *et al*.[109,110] have proposed a self-assembly mechanism for low-temperature SWCNT growth from the [6]cycloparaphenylene precursor through ethynyl radical addition. These authors have employed non-equilibrium quantum chemical molecular dynamics (QM/MD) simulations and density functional theory (DFT) calculations which predicted that the self-assembly mechanism is energetically more favorable as compared to the DA based growth mechanism.

These reports suggest that the exact nature of the CNTs growth is still a subject of scientific debate. A similar evolution for the synthesis of graphene from gas phase procedures to organic synthesis as for the synthesis of CNTs is also observed. Graphene sheets are conventionally synthesized from graphite exfoliation (mechanically or chemically),[111,112] or obtained from the unzipping of CNTs.[113] Currently, new procedures are being developed with large polyaromatic hydrocarbons condensed into graphene nanoribbons via successive DA reactions between cyclopentadienone and phenyl-substituted alkyne (dendritic polyphenylene, DDP), and subsequent dehydrogenation.[114,115] Other examples for synthesizing large polyaromatic hydrocarbons employing DA reactions include the reaction of cyclopentadienone with aryne precursors[116] and the domino cycloaddition of arynes.[117] These recent investigations evidence that the DA reaction will play a fundamental role for the development of a more targeted synthesis of carbon nanostructures.

2.4. Applications of carbon materials: Necessity of functionalization

In addition to the development of less expensive and more selective synthetic procedures for the synthesis of carbon nanomaterials, scientists are also exploring their application potential in a variety of fields ranging from electronics and communications, to optics, chemistry, energy and biology. In the following, selected examples from various application domains are described in which carbon nanomaterials are being used either alone or are incorporated into polymer based composites. In addition, efforts of employing their surface functionalization as a means for achieving superior mechanical, thermal, electrical, or optoelectronic properties are highlighted.

2.4.1. Mechanical, thermal and electrical reinforcement of polymer matrices

The high electrical and thermal conductivities and the superior mechanical properties of CNTs have stimulated significant efforts to prepare polymer/CNTs nanocomposites aiming at synergistically combining the merits of the each individual component. For mechanical reinforcements, polymer/CNTs nanocomposites are widely studied and display enhanced mechanical properties of polymer matrices as reported by Logakis *et al.*[118] for poly(methyl) methacrylate (PMMA) and MWCNTs.[119] Additional properties such as conductivity[120,121] and thermoelectric properties[122] of CNTs nanocomposites are of interest for their application as sensors.[123] The absence of chirality in a graphene sheet, contrary to CNTs, extends the properties of carbon based systems to wider research domains, e.g. graphene displays a super capacitance[124] induced by reversible oxidation – reduction cycles, and a high heat transfer.[125] To date, the embedding of graphene in polymer matrices is exploited for

similar applications[126] as for CNTs based composites. Depending on the degree of oxidation of graphene, Zhang *et al.* have incorporated variable amounts of graphene into PMMA (refer to **Figure 2.3**) showing that a lower content of graphene is required when the degree of oxidation is higher.[126]
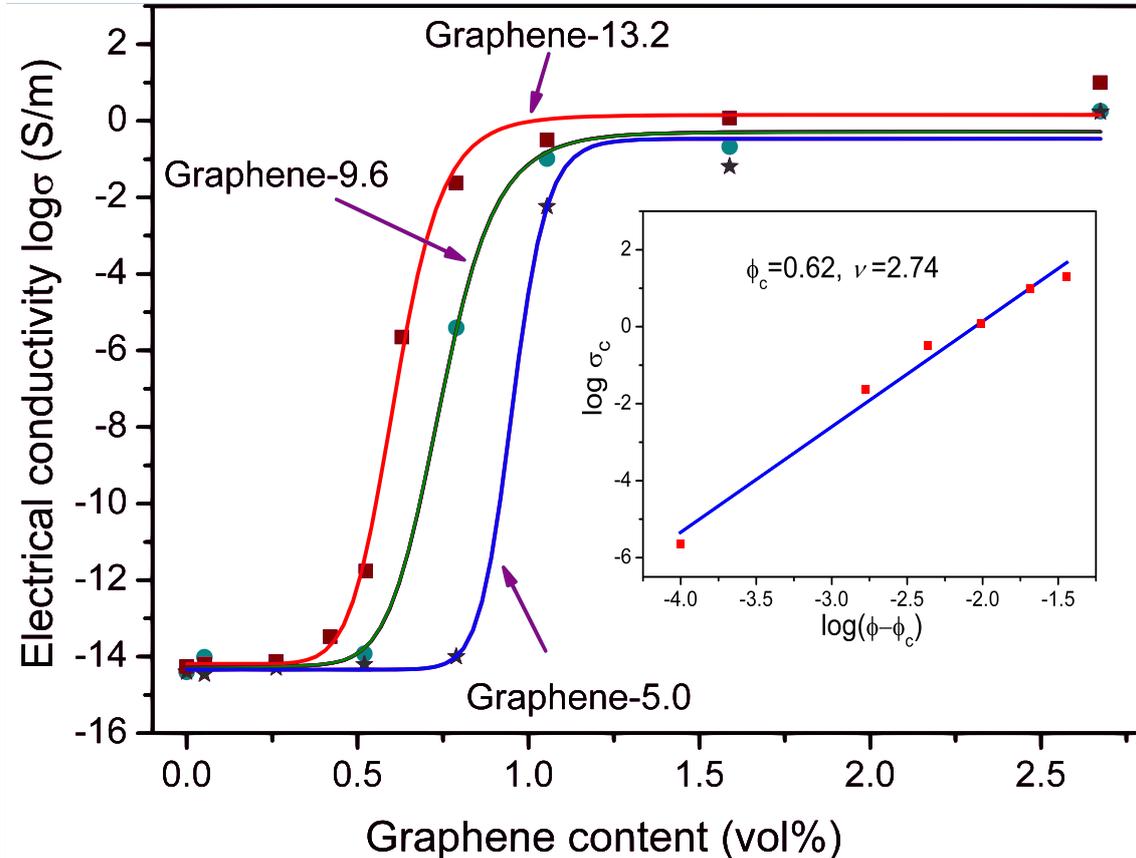
Figure 2.3. Electrical conductivity of graphene/PMMA composites as a function of graphene content characterized by different C/O ratios (5.0, 9.6 and 13.2 via XPS). Reproduced with permission from Ref. 126 (Zhang *et al.*). Copyright 2012, Elsevier.

Concerning the mechanical reinforcement and the enhanced electrical properties gained by the incorporation of carbon materials into polymer matrices, the discussion of carbon materials functionalization can be divided into covalent or non-covalent functionalization. Further dimensions in this context are the nature of the functionalizing molecule, i.e. a polymer or a small molecule, and the degree of functionalization. As suggested by Bose and Rahmat,[127,128] the degree of carbon nanomaterial functionalization must be carefully controlled since an unnecessarily high degree of functionalization can lead to the loss of the intrinsic properties. Nevertheless, for the mechanical reinforcement of polymer matrices, the functionalization of CNTs with small molecules and with polymer chains increases the interactions between the CNTs and the polymer matrix. For example, Selvin *et al.*[129] have investigated the influence of phenol functionalization of MWCNTs on the mechanical

properties of an isotactic poly(propylene) matrix. These authors have reported superior mechanical properties, namely Young's modulus, maximum stress and elongation at break, of the polymer matrix by the incorporation of functionalized MWCNTs as compared to the non-functionalized MWCNTS (**Figure 2.4**).
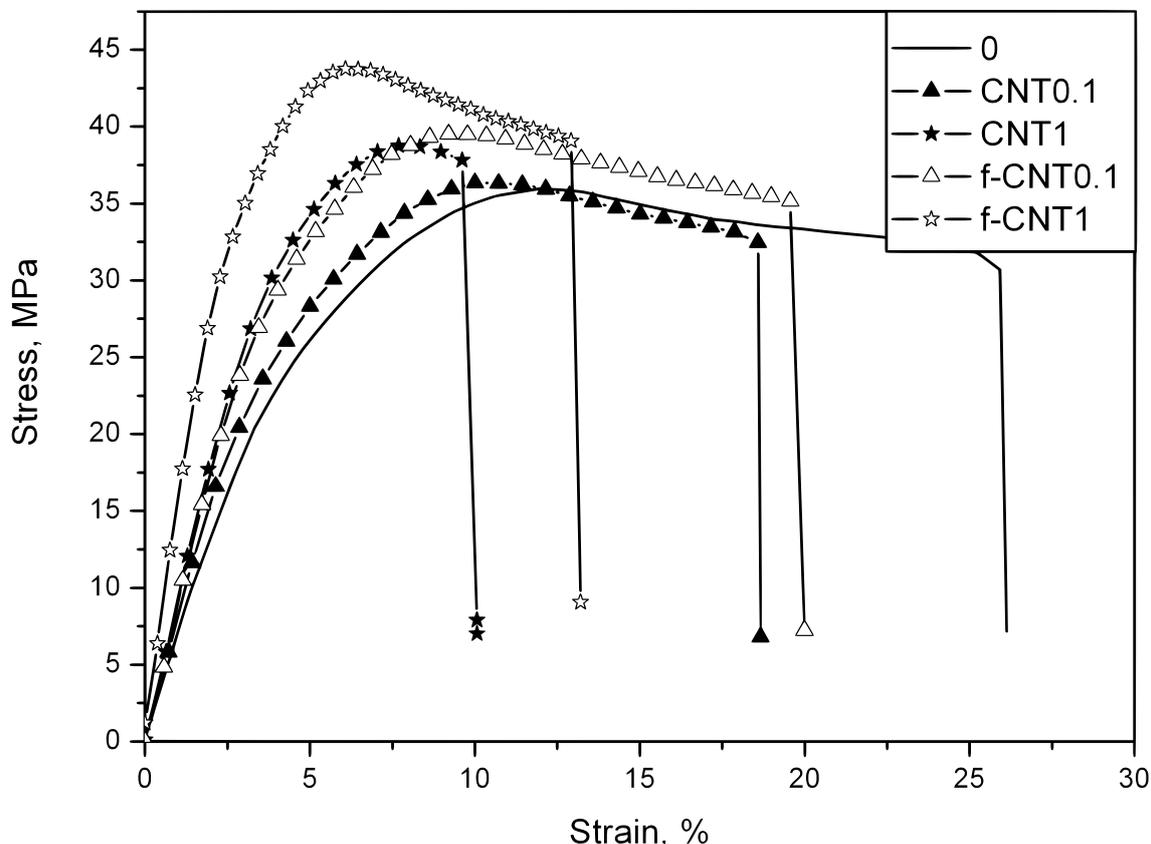
Figure 2.4. Stress-strain plots of isotactic poly(propylene) composites of 0.1 to 1.0 *wt.-%* of untreated and phenol functionalized MWCNTs. Reproduced with permission from Ref. 129 (Selvin *et al.*). Copyright 2012, Wiley-VCH.

2.4.2. Photovoltaics and photo-devices

The surface functionalization of carbon nanomaterials, with small molecule or polymer for the improvement of the opto-electronics properties, is an active area of research.[130,131] Functionalization generally increases the solubility of carbon nanostructures in solvents leading to a better processability. This is especially the case for fullerenes underlined by the popularity of (6,6)-phenyl-C_{61}-butyric acid methyl ester (PCBM) since 1995 in photovoltaics.[132] Due to their superior opto-electronic properties, the use of CNTs and graphene is expected to increase for the development of solar cells and photo-devices compared to the presently used C_{60}.[133,134] CNTs display useful properties when incorporated into solar cells, e.g. CNTs are electron acceptors,[135] trigger ultrafast charge separation,[136,137] and display high photocurrent mobility.[138] The optoelectronic properties achievable via

combination of fullerenes and CNTs may well lead to polymer-free all-carbon photovoltaic devices.[139] Based on the predictable carrier multiplication behavior of graphene,[140] complex photo-devices combining graphene with the other carbon nanostructures may even become relevant in the future.[141,142] C_{60} or CNTs/conjugated polymer derived hybrid photo-devices are of interest based on their convenient solution based processing.[143,144]

2.4.3. Biomedical – Disease diagnostics and treatment

The properties associated with carbon nanostructures, such as near infrared fluorescence, the ability to quench fluorescence, provision of photo-acoustic imaging, the ability to form field effect transistors, and well defined Raman scattering spectra, have attracted substantial interest within the biomedical related research community (**Figure 2.5**). Consequently, an enormous wealth of literature is available highlighting the potential of these materials for (bio)sensing and imaging applications (**Figure 2.5**).[145] There are especially no concerns regarding the use of carbon materials for *in vitro* applications, however the scientific opinion regarding the *in vivo* toxicity of these materials is rather divided.[146] Nevertheless, as a result of several investigations, there seems to be a consensus that appropriate surface functionalization can lead to the required non-toxicity and biocompatibility.[147] These findings, along with the results showing convenient internalization of carbon nanomaterials into the cells,[148] have even triggered the exploration of carbon nanomaterials potential for drug/gene delivery in addition to tissue engineering applications.[149]
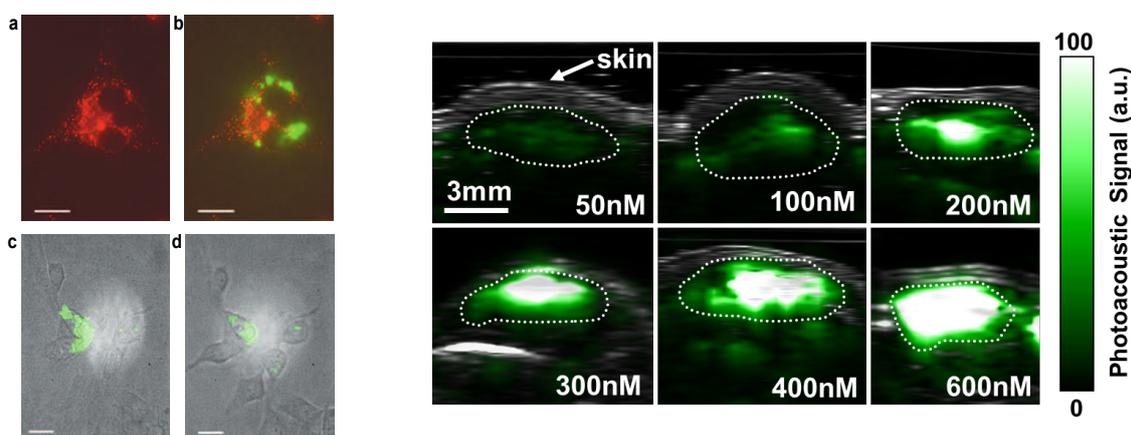
Figure 2.5. Left images (a-d): Real time multiplexed detection of genotoxins in live mammalian cells. (a) NIR fluorescence of lysosomal stain Lysotracker in 3T3 cells. (b) DNA-SWCNT photoluminescence (green) showing partial co-localization with Lysostracker emission. Photoluminescence of DNA-SWCNT (green) overlaying visible 3T3 cells (grey) in the presence of Fe2+ before (c) and after (d) introduction of H_2O_2. Adapted and reproduced with permission from Ref. 145 (Heller *et al.*). Copyright 2009, Nature. Right images: Photoacoustic detection of SWCNTs in living mice. The mice were injected subcutaneously with SWCNTs at concentrations of 50–600 nM. One vertical slice in the 3D photoacoustic image (green) was overlaid on the corresponding slice in the ultrasound image (grey). Reproduced with permission from Ref. 145 (Zerda *et al.*). Copyright 2008, Nature.

2.5. Diels-Alder functionalization of carbon materials: *'State-of-the-art'*

In addition to the scientific efforts focused on the controlled synthesis of carbon nanostructures, the development of convenient surface functionalization strategies is of paramount importance from the application perspective. In this context the tendency of carbon nanostructures to undergo DA reactions is attracting increasing attention. Compared to other functionalization strategies, the DA reaction based surface modifications are simple, capable of working under ambient conditions, applicable to all the graphitic carbon allotropes and require no surface pre-treatment or catalyst.[150] In the following sections, the theoretical studies predicting and simulating the tendency of carbon nanostructures (fullerenes, CNTs, and graphene) to undergo DA reactions are summarized. The examples of DA reactions of carbon nanostructures with the small molecules are also included (refer to **Scheme 2.1** and **Table 2.1** for the reactions with the compounds **1** to **29**, and **Scheme 2.2** and **Table 2.2** for the reactions with the compounds **30** to **43b**) followed by an up-to-date overview of the recent literature related to the DA reactions assisted functionalization of carbon nanostructures with polymer chains.

2.5.1. Small molecules

From a chemical point of view, carbon nanostructures display a rather unique reactive behavior and understanding their reactivity is a requirement for employing them efficiently. In the case of fullerenes, the C-C bond at the 6,6-ring junction between two annulated six-membered ring is more reactive (electron donor and electron acceptor character) than the C-C bond at the 5,6-ring junction common to a five-membered and a six-membered ring. This renders fullerene reacting more like a dienophile, and being a less reactive diene molecule than cyclopentadiene (Cp) and anthracene.[151,152] The reaction of all the reactive bonds of the fullerene will lead to a hexa-substituted fullerene derivative. DA reaction can occur between C_{60} and different dienes. The reactions with dienes such as acenes[153] have been widely studied (compounds **1-6** in **Scheme 2.1**). In particular, the effect of acene length (anthracene,[154,155] pentacene[156]), the functionality[157] and the number of adducts has been investigated.[155,156,158] Intermediate dienes such as *o*-quinodimethanes (**Int1**), produced *in situ* from the ring opening of benzocyclobutenes (compounds **8-12b**),[159,160] by the decarboxylation of norbornadiene-7-one (**13**),[161,162] through the elimination of bis(bromomethyl)-anthraquinone (**14**),[163] or via the thermolysis of sulfolenes[164] and sultines[165] (respectively compounds **15a-b** and **16a-b**) which are thermally (temperature superior to 100 °C) generated leading to unstable dienes, and for which the driving force of the reaction is the gain of aromaticity once reacted with C_{60}. Hetero Diels-Alder (HDA) reactions based on similar systems were also conducted by ring opening

of benzothiet (**17**) to generate *in situ o*-thioquinone methide (a hetero diene).[166] Using the same strategy, *in situ* generated butadienes (**Int2**, **Int3**) obtained from the decomposition of cyclic sulfur based compounds react efficiently with fullerenes: 1,2-diaza-1,3-butadienes (**Int2**) from the thermolysis of thiadiazoldioxides (**18a-e**),[167] 1,3-butadienedicarboxylates (**19a-c**),[168] (2-phenylsulfonyl)-1,3-butadiene and 2-nitro-1,3-butadiene[169] from the decomposition of the corresponding sulfolene (**20a-b**). Contrary to these examples, stable dienes derived from 1,3-butadiene require a lower reaction temperature and do not generate side-products. The reaction between C_{60} and stable dienes similar to 1,3-butadiene was described by Kräutler *et al.* with 2,3-dimethylbutadiene (**24**) and myrcene (**25**),[170] 2,3-dipropylbutadiene (**26**) and cyclohexa-1,3-diene (**27**) compounds.[171] Introducing electron donating or withdrawing groups into the 1,3-butadiene backbone (compounds **21a-23**), the DA reaction enabled decorating the surface of C_{60} with electron withdrawing or donating functionalities.[169] HDA reactions of linear 1,3-butadiene based structures were also performed with thioacrylamide (compound **28**).[172] Five-membered ring compounds such as Cp and furan are more reactive towards fullerenes as dienes in the DA reaction than butadiene,[173] or pyrrole and indole (compound **33** in **Scheme 2.2**).[174] For less reactive dienes, the reaction must be heated to high temperatures (180 °C).[175] In case of Cp (**30**),[155] furan (**32**) and furan derivatives (1,3-diphenylisobenzofuran **31**),[163] the reaction occurs at ambient temperature, with a higher reactivity predicted[176] and observed[177] for Cp. Under microwave heating, the chiral α-oxo imines (**36**) and α-diimines (**37**) were employed in a more recent application[178] evidencing the ability of conducting HDA reactions on fullerenes. A recent example was published by Ray *et al.* regarding the anthracene assisted immobilization of fullerenes as a monolayer on silicon oxide substrates (refer to Scheme 3, structure **7**) to design organic field effect transistors (OFET) and sensors.[179] In a more recent publication, the DA reaction of fullerenes with *o*-quinodimethane (generated from dimethoxybenzocyclobutenyl acetate, **11**) led to functionalized C_{60} and C_{70} with increased solubility and development of new systems for photovoltaics with low band gap. This system is reported to exhibit a higher photovoltaic performance when compared to the [6,6]-phenyl-C_{61}-butyric acid methyl ester (PCBM) based system.[180]

Dienes

Acenes

1

2

3a R = -(CH₂OH)
3b R = -(CH₂OCH₃)

4

5

6

7

o-Quinodimethanes

Int1

8

9

10a R₁ = R₂ = -SMe
10b R₁ = R₂ = -SO₂Me
10c R₁ = -SO₂Me, R₂ = -NH₂
10d R₁ = R₂ = -OMe

11

12a R = (-CH₂CH₂O-)₁₋₂H
12b R = (-C(CH₂)-C₆H₅)

13

14

R = -NH-AA-Me
15a Gly, **15b** Leu, **15c** Met
15d Asp, **15e** Ser, **15f** Lys
15g disulfolene

16a R = -H
16b R = -OC₆H₁₃

17

Butadienes

Int2

18a R₁ = R₂ = Ph
18b R₁ = 4-ClPh, R₂ = Ph
18c R₁ = 4-CH₃OPh, R₂ = Ph
18d R₁ = CH₃, R₂ = Ph
18e R₁ = Ph, R₂ = 4-ClPhCH₂

Int3

19a R = Me, **19b** R = Et
19c R = *i*Pr, **19d** R = *t*Bu

20a R= -SO₂Ph
20b R = -NO₂

21a R₁ = R₂ = R₃ = H
21b R₁ = -OMe, R₂ = R₃ = H
21c R₁ = R₂ =Me, R₃ = H
21d R₁ =Ph, R₂ = R₃ = H
21e R₁ = H, R₂-R₃ = -CH₂-CH₂-

22a R = -COOEt
22b R = -(CO)Me
22c R = -CN

24

23

25

26

27

29

28a R₁ = R₂ = Me
28b R₁ = Me, R₂ = Ph
28c R₁ = Ph, R₂ = Me
28d R₁ = R₂ =Ph

Scheme 2.1. Dienes (acenes, *o*-quinodimethanes, butadienes) reacting via DA reaction with carbon materials. The *o*-quinodimethane model intermediate (**Int1**) is generated by **8-17**, and the butadiene model intermediates **Int2** and **Int3** from **18a-e** and **19a-20b** respectively. The yields and reaction parameters with specific carbon materials are collated in **Table 2.1**.

Table 2.1. Summary of reaction conditions and yields of DA reactions of carbon materials with dienes (acenes, *o*-quinodimethanes, butadienes).

Dienes		Carbon material[a]	Conditions			Yield[d]	Ref.
			Solvent[b]	T /°C (P /W)[c]	Time		
Acenes[e]	1	C$_{60}$	Toluene	70	72 h	13%	154a
	1		Naphthalene	200	48 h	39%	154b
	1		Toluene	(800)	15 min	35%	154c
	1		C$_6$H$_6$	80	12 h	25% (24%)	155
	1		-[h]	-	1 h	55% (19%)	156a
	2		-[h]	-	1 h	19% (15%)	156a
	3a-b, 4		-[h]	-	30, 45, 40 min	3a: 70%, 3b: 70%, 4: 34%	156b
	5		-[i]	-	9 h	30% (19%)	157
	6		Toluene	a.t.	48 h	43%	179a
	7		Toluene	45	3.5 days	-	179b
	1	F-SWCNT	ODCB	90	3 h	-	186
	5	Graphene	*p*-xylene	130	12 h	-	186
o-Quinodimethanes[f]	8	C$_{60}$	*m*-xylene	140	20 h	4.4% (81%)	159
	9		*m*-xylene	140	20 h	15.6% (5.3%)	159
	10a-d		ODCB	180	48 h	a 43%, b 19%, c 41%, d 47%	160
	11		C$_6$H$_3$Cl$_3$	214	several h	-	180
	12a-b	MWCNTs	C$_{14}$H$_{30}$	235	90, 100 min	-	189
	13	C$_{60}$	Toluene	120	5 h	60%	161
	14		Toluene[j]	120	8 h	83%	163
	15a-g		C$_6$H$_3$Cl$_3$	214	3 h	a 56%, b 47%, c 52%, d 41%, e 40%, f 40%, g 42%	164
	16a-b		C$_6$H$_6$	80 (800)	18 h 20 min	a 30% (17%), b 45% (10%), a 39% (5%)	165
	16a	SWCNTs	ODCB	(150)	45 min	-	187
	17	C$_{60}$	ODCB[k]	180	5 min	21% (33%)	166
Butadienes[g]	18a-e	C$_{60}$	Toluene[k]	120	60, 45, 40, 180, 480 min	a 47%, b 48%, c 48%, d 36%, e 27%	167
	19a-d		ODCB	180	30 min	a 44%, b 43%, c 32%, d 47%	168
	20a-b		ODCB	135, 180	30 min, 8 h	a 79 %, b 27 %	169
	21a-e		Toluene	110 50,80	8 h, 0.5 h, 24 h 5 h, 3 h	a 48%, b 35%, c 30%, d 29%, e 47%	169
	22a-c		ODCB	150	3 h, 30 min, 3 h	a 68%, b 50%, c 49%	169
	23		ODCB	180	8 h	27%	169
	24		C$_6$H$_6$	a.t.	12 h	23%	170
	25		C$_6$H$_6$	a.t.	12 h	43%	170
	26		C$_6$H$_6$	80	14 h	51.4%	171
	27		Toluene	90	2 h	30.3%	171
	28a-d		Toluene[k]	65	30 min	a 57%, b 69%, c 43%, d 43%	172
	24	F-SWCNTs	ODCB	90	3 h	-	186
	21a	F-SWCNTs	THF	75	16 h	-	186
	29	SWCNTs	1,4-dioxane/THF[l]	50	60 h	-	190
	29	Graphene	*p*-xylene	50	16 h	-	197

[a]F-SWNCT: fluorinated SWCNTs, CNTs: SWCNTs and MWCNTs; [b]ODCB: *o*-dichlorobenzene, C$_6$H$_3$Cl$_3$: 1,2,4-trichlorobenzene; [c]microwave power in brackets; [d]of C$_{60}$ monoadduct, bisadduct in brackets, [e]anthracene and derivatives (**1**, **3a-7**) and pentacene (**2**), [f]*in situ* generated *o*-quinodimethanes (**Int1**) by benzocyclobutenes (**8-12b**), norbornadiene-7-one (**13**), bis(bromo)anthraquinone (**14**), sulfolenes (**15a-g**), sultines (**16a-b**), benzothiet (**17**) via *o*-thioquinone methide; [g]*in situ* generated by thiadiazoldioxides (**18a-e**) via the 1,2-diazo-1,3-butadiene intermediates (**Int2**), by sulfolenes (**19a-20b**) via the 1,3-butadiene intermediates (**Int3**), and substituted 1,3-butadienes (**21a-29**); [h]in solid state and high speed vibration milling; [i]UV (pressure mercury lamp); [j]addition of KI and 18C6; [k]hetero Diels-Alder; [l]pressure 1.3 GPa.

Dienes

Five-membered rings

Imines

30
31
32
33
34
35
36
37

Dienophiles

Arynes

Five-membered rings

Alkenes

38
39
40
41
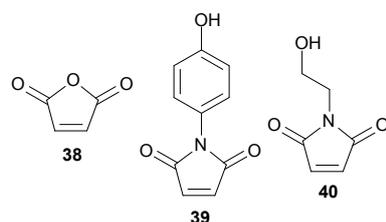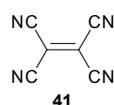
Int4
42
43a R = H
43b R = OC6H13
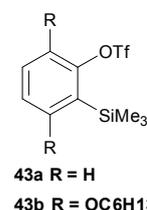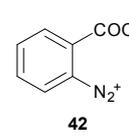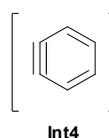
Scheme 2.2. Dienes (five-membered rings, imines), arynes and dienophiles (five-membered rings, alkenes) reacting via DA reaction with carbon materials. The reactivity of arynes (intermediate *in situ* generated **Int4** from **42** and **43a-b**) as dienes ([2+2] cycloaddition) or dienophiles ([4+2] cycloaddition) is still an open question. The yields and reaction parameters with specific carbon materials are collated in **Table 2.2**.

For SWCNTs – at first glance – the lack of 'superaromaticity' of the almost infinite number of benzene rings is surprising.[181] The reactive behavior of the CNTs is often compared to the reactivity of fullerenes to highlight the principle of directional-curvature theory: the curvature (or pyramidalization angle of the carbon atoms) is more pronounced in the case of fullerenes and leads to higher reactivity than SWCNTs;[182] the higher the diameter of the SWCNTs, the less reactive are the SWCNTs.[183] Independent from their chirality, SWCNTs react as dienophiles.[184] The DA reaction of CNTs with *o*-quinodimethanes (dienes) has been predicted via *ab initio* quantum mechanical calculation (ONIOM(B3LYP/6-31G*:AM1).[185] Based on this prediction, further DA reactions involving SWCNTs and dienes were conducted, with similar compounds as for the case of fullerenes. The reactivity of SWCNTs towards acenes was assessed by Zhang *et al.* after the fluorination of the SWCNTs. Introducing electron withdrawing fluorine atoms (activating the sidewalls), the dienophilic character of the SWCNTs increased and the DA reaction was possible with anthracene (**1**), 2,3-dimethylbutadiene (**24**) and 2-trimethylsiloxy-1,3-butadiene (**21a**).[186] As for fullerenes, *o*-quinodimethanes (**Int1**) are also found to react with CNTs. The degradation of sultine (4,5-

benzo-1,2-oxathiin-2-oxide, **16a**) under microwave[187] or the thermal degradation of benzocyclobutenes (**12a-b**)[188] at 235 °C thermal degradation of benzocyclobutenes (**12a-b**)[189] at 235 °C under an inert atmosphere was performed to generate reactive intermediates, *o*-quinodimethanes, which react as dienes at the surface of SWCNTs and MWCNTs.

Table 2.2. Summary of reaction conditions and yields of DA reactions of carbon materials with dienes (five-membered rings, imines), arynes, and dienophiles (five-membered rings, alkenes).

Dienes		Carbon material	Conditions			Yield[c]	Ref.
			Solvent[a]	T /°C (P /W)[b]	Time		
Five-membered rings[d]	30	C_{60}	Toluene	a.t.	12 h	68% (28%)	155
	31		C_6H_6	a.t.	16 h	-	163
	30, 32		Toluene	a.t.	24 h	-	177
	33		ODCB	180	12 h	35%	175
	34	MWCNTs	DMSO	50	96 h	-	192
	34	CNTs	-	75	24 h	-	193
	35	MWCNTs	Anisole	80	48 h	-	193
Imines[e]	36	C_{60}	C_6H_6	80 (600)	72 h 20 min	44-47% 78-83%	178
	37		C_6H_6	80 (600)	72 h 20 min	39-41% 59-63%	178
Dienophiles							
Five-membered rings[f]	38	MWCNTs	-	130	40 h	-	191
			1,4-dioxane/THF	110	48 h	-	
	39		DMSO	50	96 h	-	192
	38		Benzyl ether	75	48 h	-	193
	40		Toluene	75	24 h	-	193
	40	SWCNTs	THF	75	24 h	-	193
	38	Graphene	-	120	3 h	-	197
Alkenes[g]	41	Graphene	1,4-dioxane/H_2CCl_2	a.t.	3 h	-	197
Arynes[h]							
	42	SWCNTs	ODCB/THF	80	4 h	-	196
	43a-b	SWCNTs	ODCB/CH_3CN[i]	70	16 h	-	196
	43a	Graphene	CH_3CN[j]	45	24 h	-	198

[a]ODCB: *o*-dichlorobenzene, $C_6H_3Cl_3$: 1,2,4-trichlorobenzene; [b]microwave power in brackets; [c]of C_{60} monoadduct, bisadduct in brackets; [d]cyclopentadiene (**30**); furan derivatives (**31-35**); [e]α-oxo imines (**36**), α-diimines (**37**); [f]maleic anhydride (**38**); maleimide derivatives (**39**, **40**); [g]tetracyanoethylene; [h]*in situ* generated arynes (**Int4**) from benzenediazonium-2-carboxylate (**42**) and 2-(trimethylsilyl)triflate (**43a-b**); [i]CsF, 16C8; [j]CsF.

Similar to fullerenes, the reactivity of CNTs with butadiene based compounds has been assessed, however, it requires high pressure (1.3 GPa) and a $Cr(CO)_6$ catalyst to boost the reactivity of SWCNTs towards the DA reaction based cycloaddition with electro-rich diene, i.e. 2,3-dimethoxy-1,3-butadiene (**29**).[190] In this example, the use of an electron acceptor, e.g. a dienophile, was not successful. Nevertheless, the reactivity of carbon nanotubes as dienes has been explored. Without any pre-functionalization, maleic anhydride (**38**) was employed as dienophile in the molten state or in solution to functionalize MWCNTs, which reacted as

dienes.[191] The maleimide based derivative (**39**) was also employed as dienophile in a reaction with MWCNTs to increase the solubility.[192] Under milder conditions, Abetz *et al.* reported furan based dienes (**34**, **35**), and dienophiles such as maleic anhydride (**38**) and ethanolmaleimide (**40**) to functionalize CNTs in all cases at 75 °C.[193] The last example highlights a still open issue regarding the reactivity of CNTs with *in situ* generated arynes (**Int4**). Whereas arynes are known to react in a [2+2] cycloaddition with C_{60},[194] they can also undergo a [4+2] DA cycloaddition when reacted with dienes.[195] Functionalizing SWCNTs with arynes is possible; however it is presently not clear whether a [2+2] cycloaddition occurs at the surface of the SWCNTs leading to a cyclobutene moiety, or a [4+2] cycloaddition leading to a norbornadiene moiety. The diameter of the SWCNTs (more or less pronounced curvature) has been proposed to influence the type of cycloaddition occurring with different compounds (**42**, **43a-b**).[196]

The reactivity of graphene towards DA reactions is not completely understood. Contrary to fullerenes and CNTs, the dienophilic character of graphene is still debated. The reactivity of graphene may be only controlled by the reactivity of the bay regions. Sarkar *et al.* have characterized the ambivalent character, being a diene or a dienophile, of graphene via infrared and Raman spectroscopy. Given that the valence band is located at the Fermi level, graphene reacted as diene with tetracyanoethylene (**41**) at ambient temperature and maleic anhydride (**38**) at 120 °C, and as dienophile with 2,3-dimethoxybutadiene (**29**) at 50 °C and 9-methylanthracene (**5**) at 130 °C.[197] These examples emphasize the ambivalent reactivity of graphene, which is of interest for the future understanding of the reactivity of these materials. As for the DA reaction between SWCNTs and arynes, Zhong *et al.* have reported the functionalization of graphene with arynes which were generated *in situ* from 2-(trimethylsilyl)aryl triflate (**43a**) and caesium fluoride.[198] Despite Raman and infrared characterization evidencing the success of the surface functionalization, the nature of the cycloaddition, [2+2] or [4+2], involved is still unknown. This last example illustrates the fundamental role of the DA reactions in the synthesis and functionalization of graphene. On the one hand arynes can be employed to functionalize graphene via DA cycloadditions, while on the other hand they are involved in the synthesis of graphene precursors via the same cycloaddition reaction (refer to the earlier section of this review addressing the synthesis of carbon materials via DA reactions).

2.5.2. Polymers (*'grafting from'* and *'grafting to'* approaches)

In the realm of attaching polymers to carbon materials, the well-known *'grafting from'* and *'grafting to'* approaches can also be implemented via DA reactions for carbon materials

surface functionalization. The *'grafting from'* strategy implies the reaction of carbon materials with a diene bearing a functional group which is capable of directly undergoing a surface initiated polymerization or requires further modifications for transformation into an appropriate functionality suitable to initiate a polymerization. The *'grafting from'* strategy does not allow perfect control over polymer chains which are grafted at the surface while in the case of the *'grafting to'* approach pre-synthesized and well-defined polymer chains can be employed for surface functionalization. In most cases where the *'grafting to'* approach is applied, the synthesis of well-defined polymer is followed by an end-group transformation. In the context of DA cycloaddition assisted functionalization of polymers onto the surface of carbon materials, a diene or dienophile end-group is installed at the terminus of the polymer.

The *'grafting from'* approach involving a pre-functionalization of the carbon materials via a DA reaction is mainly employed for CNTs. In a recent review by Sakellariou *et al.* addressing the *surface initiated polymerization* of CNTs,[199] three main classes of dienes undergoing DA cycloaddition are highlighted. An acene, more precisely 1-aminoanthracene, was heated with SWCNTs at 120 °C and subsequently reacted with 2-bromomethylpropionyl bromide leading to the SWCNTs functionalized with the atom transfer radical polymerization (ATRP) initiator.[200] A subsequent surface initiated polymerization of styrene led to the separation of metallic (m) and semi-conductive (s) SWCNTs, since 1-aminoanthracene appeared to selectively functionalize s-SWCNTs. In another report from Sakellariou *et al.*,[201] the surface of MWCNTs was functionalized with 4-hydroxyethyl benzocyclobutene and 1-benzocyclobutene-1'-phenylethylene via DA cycloadditions at 235 °C. The functionalization involved the *in situ* generation of *o*-quinodimethanes via the thermal degradation of functional cyclobutenes and subsequent DA reaction with MWCNTs. These authors have grafted a library of functional benzocyclobutenes at the surface of MWCNTs via DA [4+2] cycloadditions. The hydroxy group of 4-hydroxyethyl benzocyclobutene was employed to initiate the ROP (ring opening polymerization) of ethylene oxide from the surface of MWCNTs. 1-Benzocylcobutene-1'-phenylethylene functionalized MWCNTs were employed to initiate the anionic polymerization of styrene with *sec*-BuLi. In both cases, the *'grafting from'* polymerization was carried out after the degradation of benzocyclobutenes at high temperature to react with the surface of the MWCNTs. In a similar fashion, MWCNTs were simultaneously functionalized with ROP and ATRP initiators. These so called binary functionalized CNTs were simultaneous functionalized with polymers (poly(ε-caprolactone) and polystyrene) via ROP and ATRP, leading to polymer grafted MWCNTs capable of forming Janus type structures.[202] Employing the same strategy and further modification of the

4-hydroxybenzocyclobutene with trichlorocyclopentadienyl-titanium, the living coordination polymerization of L-lactide, ε-caprolactone and *n*-hexyl isocyanate was performed at the surface of MWCNTs.[203] Due to the limited information about the molecular weight and the polydispersity of the polymer functionalized at the surface of carbon materials via the *'grafting from'* approach, the estimation of reliable grating densities is difficult and is seldom reported (refer to **Table 2.1** and **Table 2.2**). Milder conditions (75 °C) employing furan derivatives have been published by Abetz *et al.*[193] These authors have reported a *'grafting from'* approach based functionalization of MWCNTs with ATRP initiator via DA reaction employing an ATRP initiator functionalized furan molecule. Subsequently, the polymerization of styrene was initiated from the surface of the MWCNTs.[193] The examples of *'grafting from'* and *'grafting to'* based approaches for functionalization of polymers at the surface of carbon nanostructures are summarized in **Scheme 2.3** and in **Table 2.3**.

In the context of employing the DA reaction as *'grafting to'* approach for carbon materials surface functionalization, the synthesis of diene end-capped polymers is the main research focus. In addition, polymers with pendant diene groups are also being explored. Contrary to elevated temperatures (200 °C) necessary for conducting benzocyclobutene degradation, the choice of highly reactive dienes enables the functionalization of fullerenes, CNTs and graphene, at ambient to moderately high temperatures (80 °C). A *'grafting to'* approach employing furan derivatized polymers has been reported where the copolymerization of styrene (St), furfuryl methacrylate (FMA) and boron-dipyrromethene methacrylate (BODIPY-MA) lead to a polymer with pendant furan groups.[204] The functionalization of MWCNTs with P(St-*co*-FMA-*co*-BODIPY-MA) polymer was carried out via DA reactions with the pendant furan groups at 100 °C for 48 h. The grafted MWCNTs were soluble in THF and high resolution transmission electron microscopy (HRTEM) revealed a 3 nm thick layer of polymer surrounding the MWCNTs (refer to **Scheme 2.3** and **Table 2.3**).

'Grafting from' functionalizatiom

ATRP initiators

Precursor for anionic polymerization

Coordination polymerization

ROP initiator

Anthracene and furan derivatives
75 or 120 °C

Benzocyclobutene derivatives
T > 200 °C
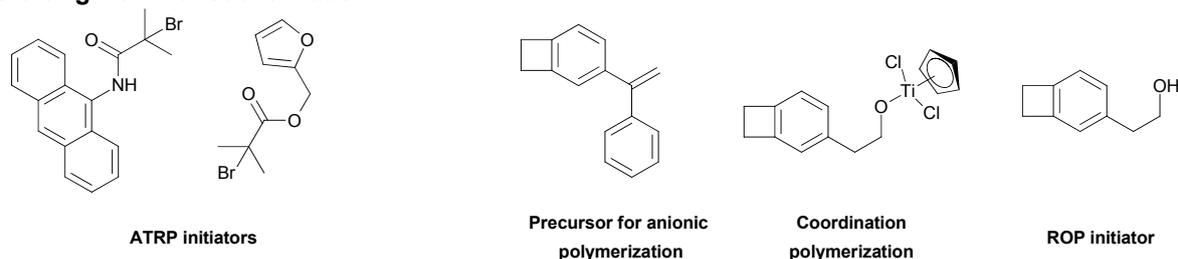
'Grafting to' functionalization

Cyclopentadienyl (Cp) end-capped polymers

Furfuryl based polymer
100 °C

ambient temperature or 80 °C

PMMA-Cp from ATRP

PNIPAM-Cp from RAFT

poly(Sty)-co-(FMA)-co-(BODIPYMA) from ATRP

Cyclopentadienyl (Cp) end-capped polymer

ambient temperature or 80 °C

ambient temperature

PEG-Cp
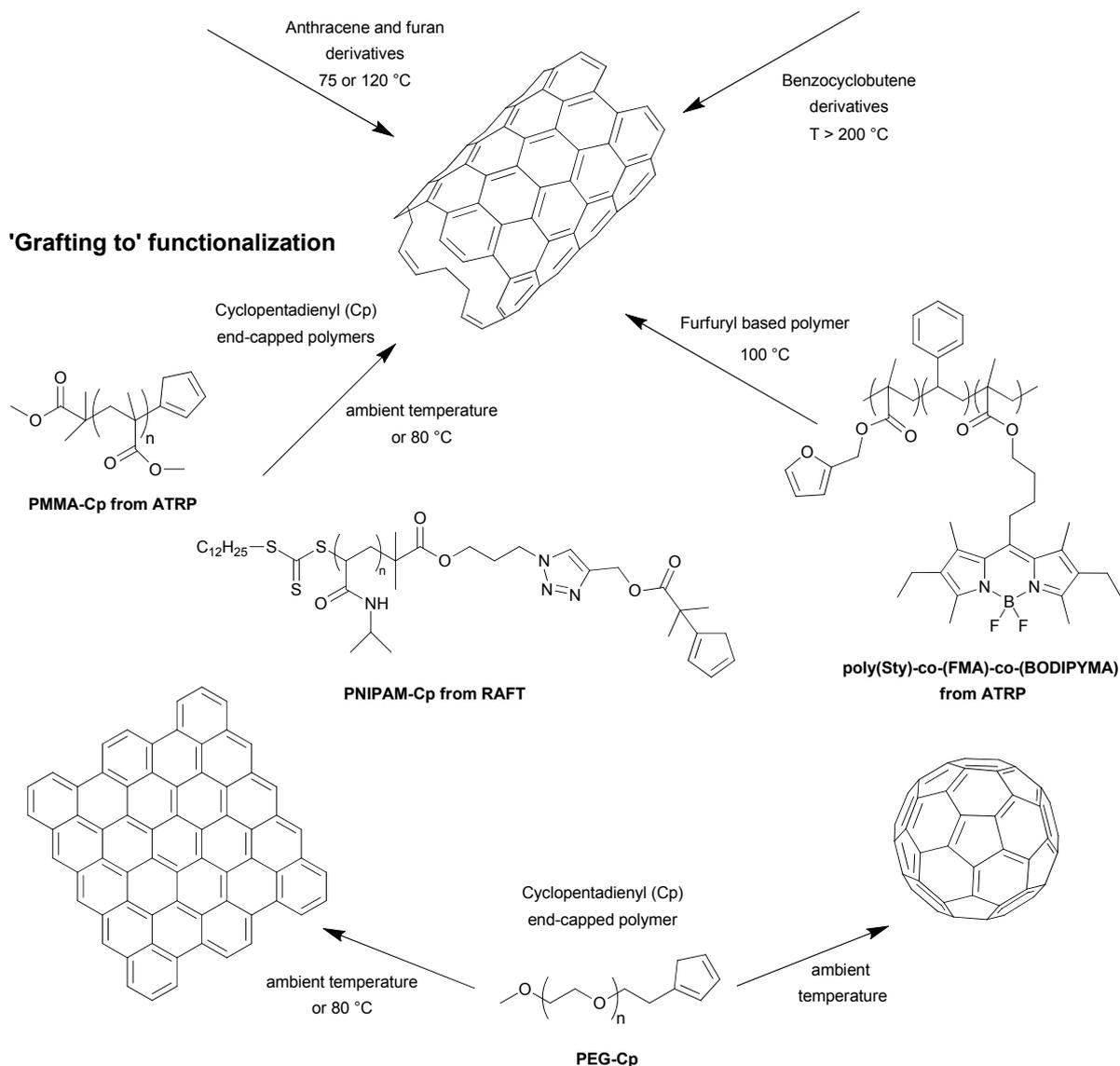
Scheme 2.3. Polymer functionalization of fullerenes, CNTs and graphene via DA reaction performed via *'grafting from'* and *'grafting to'* approaches. Five-membered ring functionalities react under mild conditions (ambient temperature to 80 °C).

Table 2.3. Reaction conditions and grafting densities for the surface functionalization of CNTs with polymers via *'grafting to'* and *'grafting from'* approaches.

'Grafting from'		Carbon material	Conditions			Grafting density[c]	Ref.
Anchoring moiety	Polymer[a]		Solvent	T /°C[b]	Time		
Anthracene	PS (ATRP)	SWCNTs	Diethylene glycol	120-200	24 h	-	200
4-Hydroxy-benzocyclobutene	PEO (ROP)	MWCNTs	Tetradecane	235	60-90 min	-	201
1-Benzocylcobutene-1'-phenylethylene	PS (anionic)	MWCNTs	Tetradecane	235	60-100 min	-	201
4-Hydroxy-benzocyclobutene	PS, PMMA, PLLA[d], PCL[e], (ATRP, ROP)	MWCNTs	Tetradecane	220	50 min	-	202
1-Benzocyclobutene-(ethoxy)dichlorocyclo-pentadienyltitanium	PLLA, PCL, HIC[f] (coordination)	MWCNTs	Tetradecane	235	60 min	-	203
Furfuryl-2-bromo-isobutyrate	PS (ATRP)	MWCNTs	Anisole	80	48 h	0.2[g]	203
'Grafting to'							
End-functionality	Polymer						
Furan	P(St-co-FMA-co-BODIPY-MA)[h] (ATRP)	MWCNTs	Toluene	80	48 h	-	204

[a]type of polymerization in brackets; [b]a.t. is ambient temperature; [c]in mmol·g^{-1}; [d]poly(L-lactide); [e]poly(ε-caprolactone); [f]poly(*n*-hexyl isocyanate); [g]measured for furfuryl-2-bromo-isobutyrate ATRP initiator by TGA; [h]copolymer of styrene, furfuryl methacrylate (FMA) and BODIPY-MA.

To date, polymers end-capped with Cp groups have been demonstrated to be most efficient towards DA reaction, as suggested by their 'ultrafast' (within 1 minute) conjugation to form block polymers with suitable ene-carrying chain termini.[205] Nebhani *et al.* have compared the reactivity of anthracenyl and Cp groups end-capped poly(ethylene)glycol (PEG) towards pristine C$_{60}$. The reaction between Cp end-capped PEG and C$_{60}$ was complete within 5 minutes at ambient temperature, whereas the reaction of C$_{60}$ with the anthracenyl terminated PEG required higher temperature and longer reaction times.[206] The high reactivity of the Cp end-capped polymer demonstrated for dienophilic end-capped polymers and for the fullerenes has been extended to SWCNTs and graphene. PEG-Cp has been successfully functionalized onto the graphene sheets which then displayed water solubility.[207]

From **Table 2.3**, only one example is reported for the functionalization of CNTs with polymer strands via DA reaction[204] in a *'grafting to'* approach. However, this work was performed on a triblock copolymer, the diene moieties were incorporated by polymerizing furfuryl based monomers (possible creation of a network), and MWCNTs were studied, reducing the ability to determine accurately the grafting density – accurate grafting density calculations being impossible due to the very broad diameter distribution of the MWCNTs. Thus it is proposed to deepen these previous investigations by extending the DA strategy to simpler macroarchitectures and SWCNTs – relatively easier to characterize than MWCNTs. Such as for the ligation of fullerenes and graphene with PEG terminated by a Cp moiety,[206,207]

and convinced by the possibility of functionalizing SWCNTs with polymer strands using the DA reaction under mild conditions in a *'grafting to'* approach, the present thesis aims at synthesizing different polymers (PMMA, PNIPAM and P3HT) with Cp terminus (more reactive than furan moiety at ambient conditions) and to investigate their reactivity with SWCNTs. The three following polymerization techniques were employed for the generation of well-defined linear polymer strands: ATRP for PMMA, RAFT polymerization for PNIPAM, and GRIM polymerization for P3HT, in order to, on the one hand be able to assess the chain terminus transformation into Cp, on the other hand to facilitate the in-depth characterization of the hybrid material and perform quantification, i.e. evaluation of the grafting density on the hybrid material.

2.6. Polymerization techniques

The employed polymerization techniques differ fundamentally in their basic mechanisms. While ATRP is based on a persistent radical effect, RAFT polymerization is governed by a degenerative chain transfer process. GRIM is not a radical polymerization method, since the polymerization is based on the reactivity of Grignard reagent and is formally a polycondensation (release of magnesium halide). However, a chain growth mechanism has been evidenced[208] and the term *quasi-living* for GRIM polymerization is more appropriate. As emphasized by the relatively brief introduction of their polymerization mechanisms in the following section, these techniques enable to synthesize polymer strands with well-defined termini based on the monomers relevant for the present thesis. In the following, the key points governing CLRP and GRIM polymerization are highlighted.[209]

ATRP and RAFT polymerization belong to the controlled/living radical polymerization processes (CLRP), a sub-classification of living polymerizations such as anionic polymerization, coordination polymerization or Ring Opening Metathesis Polymerization (ROMP). The living character of the CLRP polymerizations differentiates them from free radical polymerizations, in which the polymerization process is often not controlled. The uncontrolled nature of the polymerization is mainly characterized by a high tendency of the generated radicals to terminate rapidly. Kinetically, while the propagation rate coefficient (k_p) is close to 162 $L \cdot mol^{-1} \cdot s^{-1}$ for styrene at 40 °C,[210] the initiation rate coefficient (k_i) can be as high as 10^4 $L \cdot mol^{-1} \cdot s^{-1}$, and the diffusion controlled termination rate coefficient (k_t) is in the range of 10^8 $L \cdot mol^{-1} \cdot s^{-1}$. The mechanisms prevalent under CLRP conditions enable a reduction in inevitably terminated material. As indicated by its name, living polymerization is based on the principle that enables to restart a polymer chain via chain propagation. In principle, the control of the termination process in living radical polymerization is such that the generated

radicals after initiation react with the monomers with limited termination (combination/disproportionation), leading to polymers chains with ideally similar length. The chain growth continues until the monomer is completely consumed. The resulting chains are still active or reactivable. CLRP departs from this ideal case (anionic polymerization), since some irreversible termination takes place. Contrary to CLRP, in free radical polymerization, radicals undergo combination and disproportionation, and the polymer chains cannot be reactivated.

One can distinguish two main CLRPs, ones based on a persistent radical effect and others based on degenerative chain transfer processes. Via a persistent radical effect, the concentration of radicals is reduced by activation/deactivation cycles as in ATRP, or combination/dissociation cycles as in Nitroxide Mediated Polymerization (NMP). In the case of degenerative processes, e.g. RAFT, the concentration of radicals present in the reactive mixture is close to unaltered from the conventional process, and the generated radicals undergo equilibria which enables to prolongate the life time of each radical. In CLRP processes, the control of the polymerization is governed by fast exchange equilibria between the propagating radicals and the dormant species. The radical is thought to propagate during a short period of time (~1 ms) before returning into a dormant state for a few seconds. Undergoing a large number of equilibrium exchanges, the radical typically propagates for an overall period of time of 1 s (comparable to the life time as in free radical polymerization), and spends a longer time in the dormant state, extending its effective life time to hours.

Yet, reality is far from ideal, and termination still occurs in these polymerizations techniques; this phenomenon typically leads to 5 to 10% dead material. Nevertheless, as in the case of true (anionic) living polymerization, CLRPs are characterized by a linear evolution of the chain length (e.g. number average molecular weight M_n) with conversion, a linear evolution of $\ln([M]_0/[M])$ ([M] being the concentration of the monomer) with time, and a decrease of the polydispersity with conversion. The first criterion translates the living principle, i.e. the number of reactivable chains remains constant during the polymerization. Deviation from the ideal can be induced by slow initiation or chain coupling (upward deviation) or by transfer reactions (downward deviation). The second criterion reflects the first order kinetics, i.e. the concentration of propagating species remains constant. This criterion is also observed for any radical polymerization under steady-state conditions (no accumulation of radicals).[211] When living/controlled conditions are in operation, the polydispersity is thus relatively small and the chain termini are largely preserved.

2.6.1. Atom Transfer Radical Polymerization (ATRP)

The mechanism of ATRP is based on the reversible deactivation of the propagating radicals reducing their effective concentration. The activation/deactivation equilibrium consists in the transfer of an atom (halogen) via a metallic redox system. An ATRP system is composed of a monomer (M), a halogenated initiator, a transition metal catalyst (M_t) and a ligand (L), and typically a solvent. The living character of ATRP is based on the ability of the metal-ligand complex to accept, through a redox equilibrium, a halogen atom (X) abstracted from the dormant species (initiator, polymer chain P_n-X) with a concomitant one electron oxidation. The polymer chain radicals ($P_n\bullet$) propagate in the time period after their activation and before their deactivation. The ATRP system should fulfill the following criteria: the transition metal has two possible oxidation states (M_t^n and M_t^{n+1}) and has an affinity for halogen, the complex (M_t^n-L) should be able to be sufficiently flexible enough to adapt to the reversible expansion of the metal sphere coordination induced by the increase of the oxidation state and the presence of the halogen, the ligand should strong, and finally the equilibrium constant ($K_{eq} = k_{act}/k_{deact}$) high. The equilibrium is depicted in **Scheme 2.4**.

$$R\text{-}X \quad + \quad M_t^n\text{-}Y / Ligand \quad \underset{k_{deact}}{\overset{k_{act}}{\rightleftharpoons}} \quad R^\bullet \quad + \quad X\text{-}M_t^{n+1}\text{-}Y / Ligand$$

$$k_p \quad monomer \qquad k_t \quad termination$$
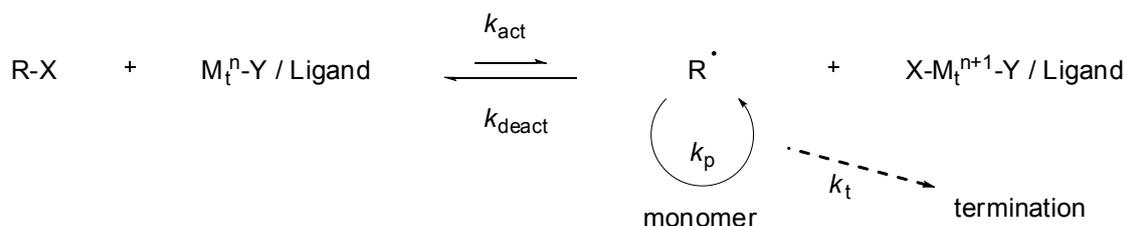
Scheme 2.4. Principle of Atom Transfer Radical Polymerization (ATRP).

The choice of the ATRP system depends on the selected monomer, which co-determines the polymerization rate: the equilibrium constant is thus adapted to the monomer. If the equilibrium constant is too low, the polymerization may be very slow (or maybe does not occur). In the case of a too high constant, the concentration of the radicals is high, leading to more termination. Thus ATRP was developed in many variants and adapted to a wide spectrum of monomers. Firstly, the above basic system may vary with the nature of the initiator: its structure should be ideally identical to the structure of the monomer, and a homolytic cleavage of the alkyl-halogen bond possible. Secondly, many articles report ATRP conditions with diverse transition metals: Mo, Cr (group VI), Re (group VII), Ru, Fe (group VIII), Rh (group IX), Ni, Pd (group X), Cu (group XI). The choice of the ligand (PMDETA, bipyridine, Me_6TREN being mostly used) varies also according to its chemical composition (nitrogen or phosphorus based) and its chelating properties (bidentate, tridentate).[212]

Furthermore, the redox equilibrium can be externally influenced by the addition of

radical or other metallic species, with different oxidation state than the initially chosen transition metal. The control of the polymerization can be thus increased by the addition of a deactivator which displaces the equilibrium in the direction of the reagents (deactivation).[213] Under SET (Single Electron Transfer) conditions, the Cu^I species are *in situ* generated in the reaction mixture through a redox equilibrium between Cu^0 and Cu^{II} species for the ready synthesis of high molecular weight polymer chains.[214] The addition of a radical source (e.g. AIBN) provides ICAR (Initiator for Continuous Activator Regeneration) conditions in order to continuously regenerate the activator Cu^I species consumed via termination. The ICAR technique enables to increase the molecular weight keeping the CLRP character with low amounts of copper.[215] Generally, high molecular weights with high end-group fidelity under classical ATRP conditions are difficult to achieve. Indeed, to generate high molecular weight, the conversion should be very high while termination is still present (~10% of the polymerized chains). Therefore, further conditions were investigated to achieve high molecular weights (around 10^5 g·mol^{-1}) with better chain-end fidelity. This is the case for AGET (Activator Generated by Electron Transfer) and ARGET (Activator Regenerated by Electron Transfer) conditions where the Cu^I species are slowly generated[216] or regenenated[217] by the reduction of Cu^{II} species via the presence of a reduction agent.

Indeed, the presence of any transition metal in the final product, even at low concentration, may also be an issue for biological applications (toxicity, denaturation of biomolecules) and may lead to – at an industrial scale – high costs (purification, metal recovery). Finally, the combination of ATRP with RAFT polymerization led to an interesting polymerization concept, enabling a dual control over the polymerization. On the one hand, the radical concentration is dictated by the deactivation/activation process from ATRP, on the other hand the growth of the polymer chains is controlled by the RAFT equilibria. This innovative combination of both CLRP methods may be of interest for the design of new macromolecular architectures and the reduction of the metal consumption as required in conventional ATRP procedures.[218]

2.6.2. Reversible Addition Fragmentation chain Transfer (RAFT) polymerization

Similarly to ATRP, RAFT polymerization consists in maintaining the radical species active over a longer period of time than in conventional free radical polymerization. Contrary to ATRP, for which the persistent radical effect is the key principle, RAFT polymerization relies on a degenerative chain transfer process. RAFT polymerization starts as soon as an external source of radical (initiator) decomposes, whereas the 'initiator' in ATRP is the halogen terminated polymer chain.[219] RAFT polymerization requires a monomer (M), an

initiator (I), a RAFT agent and sometimes a solvent. The initiator decomposes thermally and the generated radicals are subsequently involved in a dual equilibrium.

The generated radicals (I•) from the initiator fragments initially start the polymerization. The propagating chains (P_n•) react with the RAFT agent (addition) to form an intermediate radical. The formed radical fragments – at best fast – to release the primary radical (P_n•), which continues to propagate, or to release (fragmentation) the leaving R-group radical to initiate (reinitiation) the polymerization. The extremely low concentration (generally ratio 1:100, 1:1000) of the I• radicals compared to the RAFT agent concentration, e.g. the intermediate radicals, leads to a limited influence of the I• radicals over the polymerization, reflected in their low presence as polymer chain end-groups in the final synthesized sample. The first sequence is the pre-equilibrium. In the case of the R-group (or R• radical) being replaced by another polymer chain (P_m), the equilibrium is called main equilibrium as depicted in the **Scheme 2.5**.
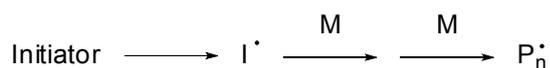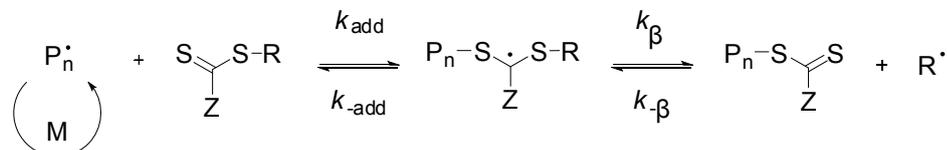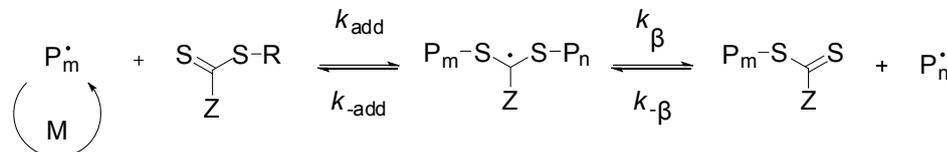
Scheme 2.5. Principle of Reversible Addition Fragmentation chain Transfer (RAFT) polymerization.

In order to be efficient, the RAFT agent is designed to ease the addition of the propagating radical to the initial RAFT agent, and also the fragmentation of the generated

intermediate radical, according to the monomer to be polymerized. Therefore, the RAFT agent is constituted of an R- and a Z-group. The R-group is chosen according to its ability to fragment readily and to react with the monomer. The Z-group is the stabilizing group which imparts stability to the intermediate radical, guiding the addition rate of the propagating radicals to the RAFT agent. Therefore, a wide library of molecules acting as RAFT agents has been established. The design of the RAFT agent for a specific monomer requires the fine tuning of the R- and Z-group. Indeed, the Z-group must stabilize the intermediate radical not more than necessary. The criteria for a good RAFT agent must be fulfilled as follows. The C=S bond reacts rapidly favoring the addition (k_{add} high), the R-S bond fragments readily (k_β high), the partition of the intermediate radical is directed to the product formation ($k_\beta > k_{-add}$), the R• radical reinitiates.

For the first criterion, the reactivity of C=S is high when electrophilically activated (for a favored addition of the radical), and the radical intermediate is stabilized. When Z is a phenyl group, the formed radical intermediate is well-stabilized, yet its fragmentation slow. Consequently, a phenyl Z-group, and generally speaking a stabilizing Z-group for the radical intermediate, should be ideally associated with an R-group easily undergoing homolytic scission. However, the choice of the R-group should be such that reinitiation is possible with the monomer. To guarantee the reinitiation efficiency of the R• radical, the R-group should be of the same structure as the monomer. To mimic the structure of highly substituted monomers (such as methacrylates), the R-group should also display the same substitution pattern, compensated with an electron withdrawing cyano group or s phenyl group (enabling the reinitiation of the already propagated polymer chain P_n). As an example for Z-group choice, styrene forms a stable propagating radical requiring a Z-group that sufficiently stabilizes the intermediate radical. However, the Z-group should not be too stabilizing, as a reduction in polymerization rate may result from slow fragmentation.[220,221] For acrylates and acrylamides, the high reactivity of the propagating radical allows the use of less stabilizing Z-groups. For high reactive monomer radicals (vinyl acetate), the addition to the RAFT agent is highly favored and a RAFT agent with less stabilizing Z-group must be employed. The fragmentation of the radical intermediate is then favored by electron donating groups as present in thiocarbamates or xanthates.

Similarly to ATRP, some deviation from ideal CLRP can be observed. Inhibition of the RAFT polymerization can be observed since RAFT agents act as radical scavengers. Retardation by slow polymerization occurs when the fragmentation is too slow or the reinitiation is poor. Hybrid behavior by an initial increase of molecular weight is due to slow

addition of the propagating radicals at the beginning of the polymerization ($DP_n^{inst} \gg 1$).[222]

RAFT polymerization is an attractive method not only based on its synthetic simplicity (simple mixture of the monomer, the initiator and the RAFT agent), but also for the wide spectrum of polymer structures that can be derived from the employed RAFT agent. Firstly, the polymer chain-end functionality can be guided by the structure of the RAFT agent (for example by RAFT agents carrying an azide group, see Chapter 5). Via derivatization of the dithioester (and trithioester),[223,224] it is possible to equip the polymer chain with a thiol (by aminolysis[225] or hydrolysis[226]), a vinyl (by thermolysis),[227] a hydrogen atom (by reduction),[228] a peroxide (by oxidation),[229] or a hydroxy group (successive oxidation and reduction).[230,231] As for ATRP, the living character of the RAFT polymerization enables to generate block copolymers, simply by adding the second monomer to the macro-RAFT agent (previous polymer chain) in the presence of an initiator.[232] Surface functionalization in a *'grafting from'* approach can be performed when the RAFT agent is immobilized at a surface via an R[233] or Z[234] strategy and the polymer grows from the surface, or in a *'grafting to'* approach when a pre-synthesized polymer is attached to the surface. In the present thesis, such an approach was followed via a HDA reaction by activation of the C=S bond with electron withdrawing groups (presented in section 2.2. and developed in Chapter 7).

2.6.3. GRIgnard Metathesis (GRIM) polymerization

GRIM polymerization is a chain growth polymerization such as ATRP and RAFT polymerization. As already noted, GRIM polymerization process is not a radical polymerization but relies on the metathesis of a Grignard reagent. Many studies have explored the mechanisms of this polymerization.[235]

GRIM polymerization is also called Kumada Catalyzed Transfer Polymerization (KTCP). The Kumada catalyst is based on nickel or palladium metal, complexed by a phosphine ligand.[236] The polymerization occurs via the C-C cross-coupling of an organohalide with an organomagnesium compound (Grignard reagent). The polymerization proceeds in three successive reactions:[208] oxidative addition, transmetalation and reductive elimination as proposed in the **Scheme 2.6**.
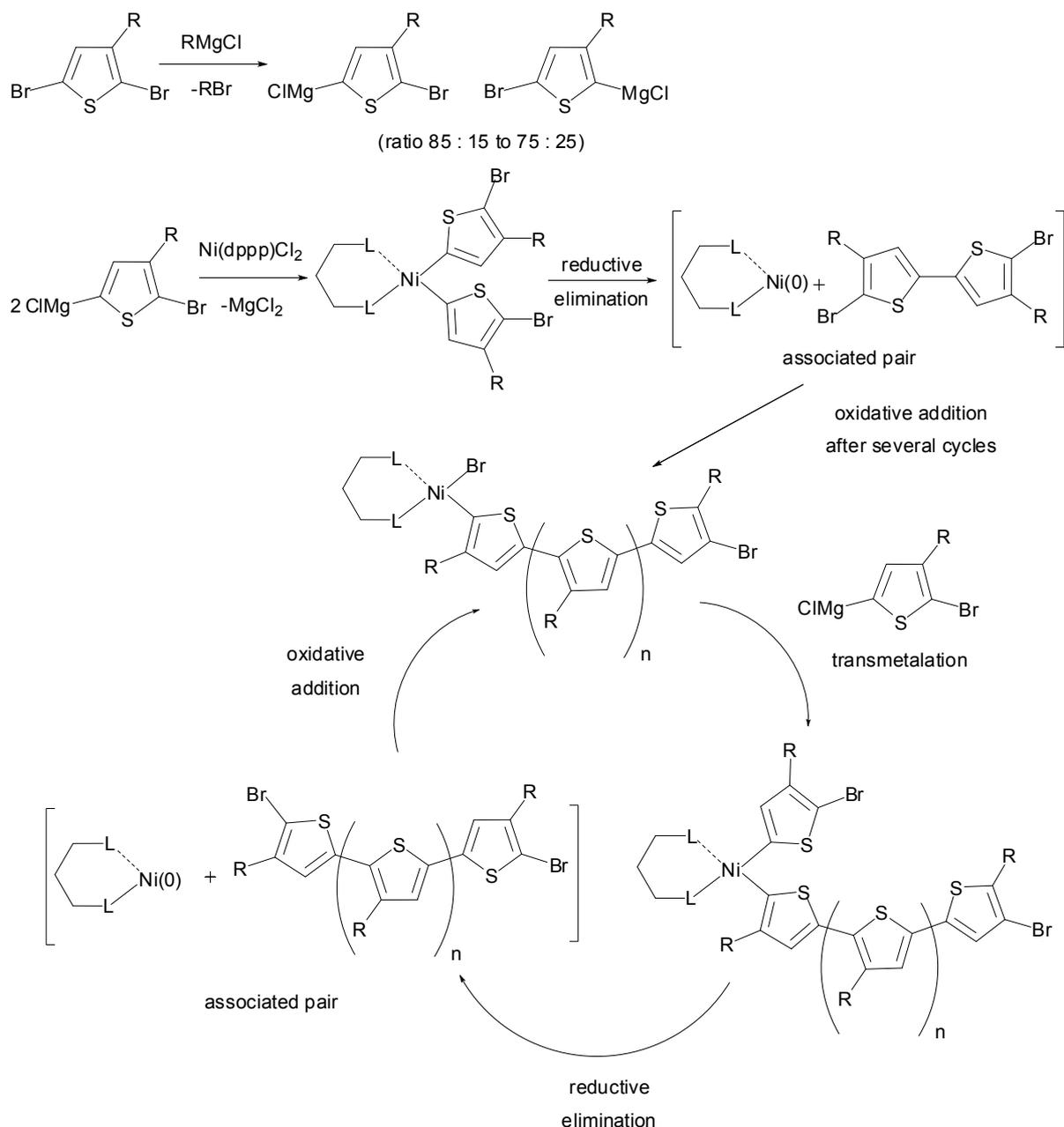
Scheme 2.6. Mechanism of GRIgnard Metathesis (GRIM) polymerization.

The nickel complex (in the example Ni(dppp)Cl$_2$) is oxidized via two additions of the Grignard reagent as *'initiation'* to form a Ni(II)-complex adduct. After the reductive elimination of the dimer, the hypothetic associated pair dimer/Ni(0)-complex is generated. The reduced Ni(0)-complex undergoes an oxidative addition reaction with the halogenated dimer. After transmetalation with the Grignard agent, a further Ni(II)-complex adduct is produced with an additional monomer unit in a head-to-tail configuration (case of alkylthiophene)[237] with release of magnesium halide (MgX$_2$). Subsequently, after the reductive elimination, the associated pair is regenerated with the growing polymer chain, e.g.

a trimer after the first cycle, and the associated reduced Ni(0)-complex. The polymerization cycle is complete, while the associated Ni(0)-complex undergoes the next oxidative addition with the halogen terminated polymer chain.

Depending on the initial synthesized Grignard (metal, halogen, monomer substitution), the polymerization differs in denomination (McCullough, Rieke, or GRIM) as reported in the literature.[238] GRIM polymerization is based on a Grignard reagent synthesized with 2,5-dibromo-3-alkylthiophene and magnesium, while the Rieke variant is based on the organozinc compound derivate from the 2,5-dibromo-3-alkylthiophene, and the McCollough variant with either organomagnesium or organozinc compounds derivates from 2-bromo-3-alkylthiophene. Other couplings without Grignard reagent, yet rather with a palladium based complex and 2-iodo-3-hexylthiophene, such as Suzuki coupling (with an organoborane) or Stille coupling (with an organostannane) can also polymerize alkylthiophene monomers. In each case, the regioregularity (head-to-tail) for alkyl monosubstituted thiophene lies above 96%. The main advantage of GRIM polymerization is its simplicity compared to the other techniques requiring cryogenic conditions or the use of highly reactive compounds. Termination occurs either by quenching the complex (hydrogen terminated polymer chains) or by the addition of another organomagnesium compound (vinyl, alkynyl, alkyl or aryl terminus).[239] In Chapter 6 of the present thesis, the vinyl version for the termination was preferred in order to form a mono-capped polymer. Via the addition of vinylmagnesium (alkynyl or allyl), the associated Ni(0)-complex is stabilized to form a π-complex and is hindered to react with the other bromine terminus of the polymer chain,[239] hence providing polymer chains with a single vinyl terminus.

The *quasi-living* character of such (GRIM) polymerization is illustrated in the study of Iovu *et al.*[208] concluding that the increase of the polymer chain length (molecular weight) is linear with conversion, the polydispersity is rather low and the degree of polymerization is determined by the concentration of the Kumada complex.

The GRIM polymerization technique focuses more and more interest on other monomers, different from thiophene based monomers for the generation of conjugated[240] and non-conjugated polymers.[241] The functionalization of the GRIM generated polymer chains is not only open to the chain end-group (hydrogen terminated or not), but also to the functional groups present within the monomer unit.[235] More complex macromolecular architectures can also be developed such as hyperbranched macrostructures by employing a two-arm or three-arm 'initiator',[242] copolymers by copolymerizing different monomers,[243,244] block copolymers by combining GRIM polymerization with controlled/living polymerization techniques such as

ATRP, RAFT, NMP and cationic polymerization[245] with targeted end-group, or by performing modular ligation reactions.[246]

2.7. Conclusions

The above described polymerization techniques (ATRP, RAFT and GRIM polymerizations) enable the generation of very well-defined polymer chains under CLRP and *quasi-living* (in the case of GRIM polymerization) polymerization conditions. The living character of these polymerizations represents a fundamental aspect of the applied strategy to functionalize SWCNTs in a *'grafting to'* approach and attain the objectives of the present thesis. Indeed, the structure of the polymer chains depends, in terms of topology (linear polymer) and chemical composition, on a well-controlled polymerization. On the one hand the chain length and the monodipersity, on the other hand the end-group fidelity, are readily controlled by these techniques. Once the structure of the polymer chains has been determined, the success of the chain-end transformation of the polymer chains terminus into Cp needs to be verified. Subsequently, the ligation of the Cp end-capped polymer chains with SWCNTs can be performed. Finally – based on the previous characterization of the polymer chains – the composition (grafting density) of the hybrid material can be accurately determined as described in the following chapters of the present thesis.

Chapter 3 – Methods, Instrumentation and Materials

In Chapter 3, the analytic methods employed in the current thesis are described, in a first part for the methods dedicated to the characterization of polymer chains and organic molecules; and in a second part for the analytic methods necessary for the characterization of the hybrid SWCNT/polymer materials. After a succinct description of each analytic principle, the *modus operandi* for each instrument is reported.

3.1. Size Exclusion Chromatography (SEC)

Size Exclusion Chromatography (SEC) was essentially employed in the present thesis to determine the molecular weight and the polydispersity of the different synthesized polymer chains. During SEC experiment, the polymer chains are separated according to their hydrodynamic volume. The analyte flows in an eluent through a column containing a stationary phase (porous silica or highly cross-linked organic gels),[247] and the change in refractive index of the eluent enables the recording of a weight distribution. The method requires a calibration with polymer standards[248] eluted at a specific retention time or via universal calibration,[249] e.g. a specific hydrodynamic volume corresponding to a well-defined molecular weight. SEC is a simple and rapid method to assess the molecular of the polymer chains (i.e. the polymer distribution).

The SEC measurements were performed on a Polymer Laboratories PL-GPC 50 Plus Integrated System, comprising an autosampler, a PLgel 5 μm bead-size guard column (50 ×

7.5 mm) followed by one PLgel 5 μm Mixed E column (300 × 7.5 mm), three PLgel 5 μm Mixed C columns (300 × 7.5 mm) and a differential refractive index detector using THF as the eluent at 35 °C with a flow rate of 1 mL·min^{-1}. The SEC system was calibrated using linear poly(methyl)methacrylate standards ranging from 700 to $2 \cdot 10^{6}$ g·mol^{-1}. From a 0.1 mg·mL^{-1} sample solution 100 μL were injected. The molecular weight distribution were corrected with the Mark-Houwink relation with $K = 12.8 \cdot 10^{-5}$ dL·g^{-1} and $\alpha = 0.69$ for PMMA (Chapter 4 and 7),[250] and for $K = 5.75 \cdot 10^{-5}$ dL·g^{-1}, $\alpha = 0.78$ for PNIPAM (Chapter 5).[251]

3.2. Nuclear Magnetic Resonance spectroscopy (NMR)

^{1}H and ^{13}C NMR spectroscopy were performed to characterize the structure and purity of organic intermediates. The characterization of the polymerization reaction mixtures via ^{1}H NMR spectroscopy enabled to determine the conversion of the polymerization reaction, while the ^{1}H NMR analyses of purified polymer samples allowed the determination of the chain length and the characterization of the chain end-group of the polymer chains after their transformation. More details of the materials characterized via NMR spectroscopy are to be found in the respective chapters.

The NMR measurements were conducted on a Bruker AM400 spectrometer at 400 MHz for hydrogen nuclei, and 100 MHz for carbon nuclei. Samples were dissolved in CDCl$_3$ using residual solvent peaks for shift correction.

3.3. Mass spectrometry of polymers

Contrary to SEC and NMR spectroscopy, mass spectrometry is a sensitive and accurate methodology to access the exact mass of individual polymer chains in a sample. Electrospray Ionization – Mass Spectrometry (ESI-MS) and Matrix Assisted Laser Desorption Ionization (MALDI) feature different ionization principles, yet remain two complementary mass spectrometric methods for the accurate characterization of polymer chains.

3.3.1. Electrospray Ionization – Mass Spectrometry (ESI-MS)

ESI-MS is based on an electrospray process, consisting of the nebulization of the solution containing the analyte, after its flow through a capillary needle at a high potential (3–5 kV).[252] Desolvatation takes place in the charged droplets by means of solvent evaporation (aided by an additional gas flow) and by successive *'coulombic explosions'*: the droplets shrink until the surface tension cannot sustain the repulsive *Coulomb* forces and they disintegrate. The charged polymer chains, then in the gas phase, reach the mass analyzer through a heated transfer capillary. In the present work, the mass analysis is performed by a linear quadrupole ion-trap. The quadrupole ion-trap consists of four electrodes subjected to

different voltage and high frequencies.[253] For a characteristic voltage, ions of a specific *m/z* value describe a stable trajectory within the quadrupole and the complete mass spectrum is subsequently obtained by varying the voltage. The particular design of the quadrupole ion-trap enables to isolate specific ions, allowing further fragmentation experiments (collision induced dissociation) to be conducted. ESI-MS is an efficient method for the characterization of polymer chains, as long as the molecular weight does not exceed 4000 Da. The presence of multiple charged species, however, enables to get access to higher molecular weight regimes. The preparation of the analyte occurs in a volatile solvent dotted with cations to enhance ionization and is very convenient. The resolution of the employed linear quadrupole ion trap is close to 0.3 Da.

The spectra were recorded on an LXQ mass spectrometer (Thermo Fisher Scientific, San Jose, CA, USA) equipped with an atmospheric pressure ionization source operating in the nebulizer assisted electrospray mode. The instrument was calibrated in the *m/z* range 195-1822 using a standard containing caffeine, Met-Arg-Phe-Ala acetate (MRFA) and a mixture of fluorinated phosphazenes (Ultramark 1621) (all from Aldrich). A constant spray voltage of 4.5 kV was used and nitrogen at a dimensionless sweep gas flow-rate of 2 (approx. 3 L·min^{-1}) and a dimensionless sheath gas flow-rate of 12 (approx. 1 L·min^{-1}) were applied. The capillary voltage, the tube lens offset voltage and the capillary temperature was set to 60 V, 110 V and 275 °C, respectively. The sample was directly injected with the addition of sodium trifluoroacetic acid at a concentration of 0.14 μg·L^{-1} from a 0.5 mg·mL^{-1} solution in THF:MeOH (3:2) for the PMMA samples (Chapter 4 and 7), and from a solution of methylene chloride:methanol (3:1) for the PNIPAM samples (Chapter 5).

3.3.2. Matrix Assisted Laser Desorption Ionization (MALDI)

The ionization in MALDI requires the analyte to be incorporated into an organic matrix sensitive to the wavelength of the laser.[254] A high amount of laser energy is absorbed by the matrix and subsequently transmitted to the analyte which is subsequently, transferred into the gas phase as ions. The mass analysis is often performed via a Time-of-Flight (ToF) analyzer. In a ToF analyzer, ions are accelerated under in an electric field, and the time needed to travel a certain distance gives access to their *m/z* value.[255] The main advantage of MALDI over ESI-MS is the ability to access high molecular weight regions (10^5 Da). However, several trials for determining the optimal choice of matrix interacting with the analyte are required. Moreover, fragmentation of the analyte can occur due to laser irradiation, while ESI-MS is an even softer ionization method. The achievable resolutions in the sub-4000 Da mass range, employing a ToF analyzer, are close to those observed with linear quadrupole ion traps.

For the P3HT sample (Chapter 6), MALDI-ToF mass spectrometry was performed on an Autoflex III Smartbeam MALDI (Bruker Daltonik, Bremen) operating at laser wavelength of 355 nm while using DCTB as the matrix. DCTB matrix (10 mg·mL^{-1}) and the polymer samples (2 mg·mL^{-1}) were separately dissolved in THF. 5 µL matrix solution was subsequently mixed with 2 µL sample solution. 1 µL of this mixture was pipetted onto the stainless steel target. After evaporation the target was inserted in the mass spectrometer and 2000 shots were accumulated from different regions of the sample spot.

3.4. Thermogravimetric Analysis (TGA)

Thermogravimetric analysis consists of continuously weighing a sample while it being heated. The sample is placed in a small inert crucible, attached to a microbalance, and is positioned into a furnace. The microbalance is equipped with a rotating pivot, used as a galvanometer, and is electronically controlled to keep the balance in the zero position, so that the sample remains at the same position in the furnace during its degradation. The variation of current (or voltage) is continuously recorded to deliver the mass variation of the sample with the temperature measured in the furnace by a thermocouple.[256]

Thermogravimetric measurements were carried out on a Q5000 thermogravimetric analyzer from TA-Instruments. Approximately 6 mg of sample was heated at 10 K·min^{-1} from ambient temperature to 100 °C for 30 min, and subsequently at the same heating rate from 100 to 700 °C for the polymers (and up to 1000 °C for the SWCNTs and their derivates) in a dynamic air atmosphere (*flow rate* = 25 mL·min^{-1}). The samples synthesized in Chapter 4 were heated at the same conditions, except for the isothermal step conducted at 210 °C in order to evaporate potentially adsorbed NMP from the sample.

3.5. Elemental Analysis (EA)

The elemental composition of an organic compound for the elements carbon, hydrogen, nitrogen and sulfur is determined from the composition of its combustion gases.[257] The sample is placed in a furnace at high temperature to be burnt via flash dynamic combustion under a continuous flow of an oxygen/helium mixture. The different gases resulting from the combustion are separated by gas chromatography and analyzed by thermoconductivity. The peak area associated with each gas in the chromatogram is subsequently compared to a calibration substance, and the quantity of each element reported to the mass of the sample to determine the weight percentage (*wt.-%*) of the corresponding element. To quantify the oxygen content, the sample is separately pyrolyzed in the presence of a nickel-coated carbon catalyst quantitatively converting the gases into carbon monoxide. After separation via gas

chromatography, the quantity of carbon monoxide detected is related to the calibration substance, and the quantity of oxygen detected is reported to the mass of the sample for the determination of the weight percentage of oxygen in the sample.

The elemental composition of the samples was analyzed using an automatic elemental analyzer Flash EA 1112 from Thermo Scientific, which was equipped with an MAS 200R auto sampler. The calibration standards methionine, and 2,5-bis-5-tert-butyl-2-benzoxazolylthiophene (BBOT), and vanadium pentoxide, tin capsules, and silver containers were purchased from IVA Analysentechnik e. K., Germany. Helium 5.0 for the GC-TCD analysis was purchased from Linde, Germany.

3.6. X-Ray Photoelectron Spectroscopy (XPS)

Contrary to TGA and EA, XPS is an almost destruction free method providing access to the chemical composition of a surface, via the electronic state of the detected elements. The method is based on the photoelectric effect induced by the exposure of matter to X-rays under high vacuum. For XPS, soft X-rays are involved (photon energy in the range 200–2000 eV).[258] The incident X-ray ejects an electron from a core shell (for example K shell for electron located in the 1s atomic orbital). The generated photoelectron quits the atom with a specific kinetic energy, and is subsequently detected by an electron energy analyzer, able to separate the electrons according to their kinetic energy and measure the corresponding electron flux. The emitted photoelectrons without energy loss (elastic interactions) constitute the characteristic peaks of the XPS spectrum associated with specific binding energies, while the photoelectrons undergoing inelastic scattering (secondary electrons) constitute the background of the spectrum. When the photoelectron is emitted, the ionized atom must relax, either by the emission of an X-ray photon (X-fluorescence) or by the reorganization of the electronic configuration from electrons located at higher energy levels. A higher energetic electron from superior shells will fill the vacancy left by the photoelectron emission, and release energy. When this energy is released as a photon, this photon can eject a second electron, called Auger electron. The spectroscopic method associated with this phenomenon is known as X-ray induced Auger Electron Spectroscopy (X-AES) and delivers complementary information.

The XPS measurements were performed using a K-Alpha XPS spectrometer (ThermoFisher Scientific, East Grinstead, UK). Data acquisition and processing using the Thermo Avantage software is described elsewhere.[259] All SWCNTs were deposited on Au substrates and analyzed using a microfocused, monochromated Al Kα X-ray source (30–400 μm spot size). The K-Alpha charge compensation system was employed during analysis,

using electrons of 8 eV energy and low-energy argon ions to prevent any localized charge build-up. The spectra were fitted with one or more Voigt profiles (BE uncertainty: ±0.2 eV). The analyzer transmission function, Scofield sensitivity factors,[260] and effective attenuation lengths (EALs) for photoelectrons[261] were applied for quantification. EALs were calculated using the standard TPP-2M formalism. All spectra were referenced to the Au $4f_{7/2}$ peak at 84.0 eV binding energy, the C 1s peak for hydrocarbons at 285.0 eV binding energy and the C 1s peak for the C-C sp^2 bond at 284.4 eV binding energy controlled by means of the well-known photoelectron peaks of metallic Cu, Ag, and Au, respectively.

3.7. High Resolution Transmission Electron Microscopy (HRTEM)

The observation of nanostructures requires the use of electron microscopy which resolution is higher (around 0.3 nm) than that of conventional light microscopy (around 200 nm). The higher resolution in electron microscopy is due to a shorter wavelength characteristic of the electrons (Broglie equation) compared to the wavelength of photons (limit of diffraction).[262] Similarly to conventional optics, the primary electrons are observed whether they are reflected (Reflexion Electron Microscope, REM) or transmitted (Transmission Electron Microscopy, TEM). Whereas REM and TEM images are based on the image of primary electrons reflected and passing through the sample respectively, Scanning Electron Microscopy (SEM) is based on imaging secondary electrons resulting from their interaction with the surface of the sample. During SEM, primary electrons are focused into a sub-nanometer electron probe that is scanned across the sample. The secondary electrons are detected in a raster (square surface) for each point of the sample, and the final image is generated by collecting the images of each scanned point. While TEM has a resolution generally around 0.2–0.5 nm (electron beam energy from 100 to 1000 keV), SEM is limited to 1–10 nm (electron beam energy from 1 to 30 keV).[263] Environmental Scanning Electron Microscopy (ESEM) is particularly useful for the observation of biological samples in a specific gas atmosphere. The TEM consists basically of an electron gun, a sample chamber, electron lenses and a vacuum system (10^{-7}–10^{-8} Pa for high voltage TEM).

The source of electrons is an electron gun constituted of a filament able to emit a beam of electrons with sufficient kinetic energy to pass through the sample. The electron sources can be differentiated by their physical principle, their operating parameters (voltage, temperature vacuum) and the brightness of their emission. After being accelerated in an electric field, the electrons are focused in a first strong magnetic lens and pass through a condenser aperture to control the convergence angle (maximum deviation angle from the optic axis). The focused electron beam (diameter of the focusing area of a few nanometers)

passes through the sample and is successively magnified by the objective composed of several condensing lenses and apertures. A final lens is employed as projector to generate the magnified image (10^6 times from the original) on CCD sensors protected with a fluorescent screen. As light microscope, TEM is limited by the quality of the lenses (astigmatism, spherical aberration), the quality of the electron source (geometry, brightness) and the quality of the objective (chromatic aberrations). The high resolution modus for TEM (High Resolution Transmission Electron Microscopy, HRTEM) can be used in order to increase the resolution to 0.8 Å. The diffracted electrons and the transmitted electrons interfere by their phase and generate an electron exit wave localized below the sample. This wave is subsequently treated by the system as an image and delivers an image with higher resolution than conventional TEM operative modus.[264]

HRTEM was performed in Chapter 4 with a Philips CM200FEG instrument, at 200 kV (large objective), the samples were prepared on copper grid with hollow polymer coverage. HRTEM was performed in Chapter 6 with a FEI Titan 80-300 instrument at 300 kV, equipped with a Cs (spherical aberration corrector) for high resolution condition (0.08 nm). The SWCNT based samples were dispersed in a 10 μg·mL^{-1} toluene dispersion via ultrasonic bath for 5 minutes. One drop of the dispersion was immediately applied onto a copper grid with holey polymer coverage.

3.8. Ultraviolet-Visible spectroscopy (UV-VIS)

Ultraviolet-visible spectroscopy (UV-VIS) was employed as a complementary analytic method to DLS for the characterization of thermo-responsive functionalized SWCNTs (see Chapter 5). The UV-VIS spectrophotometer was employed for turbidity measurements in transmission mode, i.e. the intensity of a light beam at a specific wavelength is measured after passing through the sample. Firstly, the spectrum of the solution and dispersion was recorded in the range of between 800–200 nm after tempering in a quartz cuvette at different temperatures. For generating such a spectrum, the wavelength region is scanned by splitting the light beam via a rotating grating. The subsequent diffracted light for a specific wavelength hits the detector at a pre-determined position and the spectrum can be recorded.[265] A transparent range of wavelength was determined where no absorption from the sample takes place. A specific wavelength was chosen in order to follow the evolution of the transmission of the sample, either water solution containing the thermo-responsive polymer or the dispersions of SWCNTs, as a function of the temperature in successive heating/cooling cycles.

The UV-spectroscopy experiments were conducted on a Varian Cary 300 Bio

spectrophotometer. In Chapter 5, the SWCNT based samples were added to deionized water at a concentration of 0.01 mg·mL^{-1} and left 24 h under refrigeration (6 °C). The solution was dispersed while being immersed in an ice-bath with a 450 W sonifier (W-450 G. Heinemann, 24 kHz) equipped with a sonotrode (20 mm diameter) and received a total energy of 4 kJ, and stored in the confinement of an ice-bath. After recording the all UV-Vis spectrum of the dispersion, the absorbance to perform turbidity experiments was fixed at 600 nm. PNIPAM solutions were prepared at 0.1 mg·mL^{-1}. All samples underwent a heating/cooling rate of 0.1 °C·min^{-1} with 10 min equilibration time for each temperature step, from 25 °C for the polymer solutions, and from 10 °C for the SWCNT based dispersions. The maximum temperature was 35 °C for all samples. In Chapter 6, the absorption spectra were recorded in chloroform from 200 nm to 800 nm with a resolution of 1 nm.

3.9. Dynamic Light Scattering (DLS)

Dynamic Light Scattering (DLS) measurements were employed for the size characterization of particles dispersed in water (refer to Chapter 5). The principle of DLS differs from the Static Light Scattering (SLS) principle. In the static mode, the scattered intensity at different angles and concentrations of the analyte is measured and is dependent on the form and structure factors. Model approximations for SLS measurements applied to polymers enables to access to the molecular weight, gyration radius and second virial coefficient.[266] The DLS measurement principle relies in the Brownian motion of the particles in solution (or dispersion). The intensity of the scattered light fluctuates according to time and is recorded. An autocorrelation function can be mathematically calculated over a period of time and for a specific angle (fixed at 90°), and this function gives direct access to the translation diffusion coefficient, and consequently to the hydrodynamic diameter of the studied particles.[267]

DLS was performed with a Nicomp 380 DLS spectrometer from Particle Sizing Systems (Santa Barbara, USA - laser diode: 90 mW, 632.8 nm), with an incident beam at 90°, in automatic mode. The measurements were evaluated with a standard Gaussian and an advanced evaluation method using an inverse Laplace algorithm for multimodal distribution. The hydrodynamic diameters were evaluated via the volume weighted average values. The thermal regulation is driven by a Peltier thermoelectric element (±0.2 °C). The same protocol was followed as for the UV-measurements to disperse the SWCNTs and the samples were kept immersed in an ice-bath after sonication prior to each measurement. For the SWCNT based dispersion, deionized water was filtered with a PFTE 0.2 μm filter and the flasks were washed with acetone and ethanol to eliminate any dust. The obtained SWCNTs dispersions

were not filtered after sonication, since some SWCNTs remain on the filter that would distort the result. In contrast, the polymeric solutions were filtered and fixed at 0.1 mg·mL^{-1} as for the UV-measurements. The temperature region from 10 to 40 °C was inspected with an increment of 5 °C. For a specific temperature, 5 cycles of 5 min were conducted and averaged. The system was allowed to stabilize at each temperature for 30 min between two temperature measurements. The complete measurement (10–40 °C) lasted approximately 7 h. To determine if the evolution of the hydrodynamic diameter of the dispersion was not related to instabilities, the dispersion was also tested for the same measurement time (7 h) at 10 °C. Those conditions were also employed to verify the stability of the dispersion after 24 h when placed in a cool place. These two measurements led to almost identical results and demonstrated the reliability of the DLS measurements for the SWCNT based dispersion.

3.10. Fourier Transform Infrared spectroscopy (FTIR)

Fourier Transform Infrared (FTIR) spectroscopy was employed as an analytic method for the characterization of organic compounds (see Chapter 5 and 7) and SWCNTs (refer to Chapter 7). Although many convenient and simple techniques exist for carrying out infrared spectroscopy experiments, the measurements were performed in transmittance mode with samples embedded in KBr pellets. This method was employed especially for the SWCNTs since other techniques were not feasible for these materials (Attenuated Transmitted Reflection ATR, confocal microscopy, reflexion, Diffuse Reflectance Infrared Fourier Transform spectroscopy DRIFT, Infrared Reflection Absorption Spectroscopy IRRAS). For uniformity reason, other organic compounds were characterized via the same experimental protocol. Depending on its functional group constitution and chemical bonds, the studied molecule, or system, absorbs infrared energy delivered from an infrared source. A typical FTIR spectrum of a sample is obtained via the comparison of the interferogramms obtained from the source infrared beam with the transmitted signal after irradiation of the sample. Concretely, before being detected and recorded, the interferogramm is generated as the infrared light beam passes through a Michelson interferometer. By comparing the difference between the incident signal and the transmitted signal after the Fourier transformation of the obtained interferogramm, the variation of the transmittance according to the wavenumber (equivalent to frequency) yields a typical FTIR spectrum.[268]

The infrared measurements were performed using a Bruker FT-IR microscope HYPERION 3000 coupled to a Bruker research spectrometer VERTEX 80.

3.11. Raman spectroscopy

Raman spectroscopy is complementary to FTIR spectroscopy. Generally speaking, the Raman and FTIR spectra display at first glance several similarities, although the physical principle and the information content are very different. Contrary to FTIR spectroscopy, Raman spectroscopy is not an absorption spectroscopy of infrared radiation, but the inelastic scattering of light from a molecule. Excited by a laser source, the molecule absorbs light at a virtual level (schematically located between the fundamental and the excited electronic levels of energy). The molecule relaxes as an electron returns to its initial energy level (Rayleigh scattering), at a higher energy level (Stockes scattering) or at a lower energy level (anti-Stokes scattering). The efficiency of the Raman scattering is relatively low (intensity of scattered energy 10^{-3}–10^{-4} of the incident energy) as most of the energy is recovered in the Rayleigh scattering or, if the laser excitation is not adapted (wavelength, power), by fluorescence.[269]

Typically, Raman spectroscopy is based on the variation of the polarizability of a molecule induced by light, while FTIR spectroscopy is based on the variation of dipole moment. An example for the complementarity of both methods is the possibility of performing Raman spectroscopy in water whereas this is difficult for FTIR spectroscopy (strong absorption of water). The Raman spectrometer is constituted of a laser source, a grating and a detector. Raman spectroscopy is the method of choice for the characterization of carbon materials, especially for SWCNTs since their diameter (radial breathing modes) and their quality (defect band peak) can be simply determined.[270] Surface Enhanced Raman Spectroscopy (SERS) and tip-enhanced Raman spectroscopy are two emerging methods for the characterization of CNTs. Via the participation of gold colloids or gold structured substrate, Raman scattering can be multiplied by a factor of 10^{10}–10^{11} via SERS,[271] increasing the quantity of information derived from the sample since CNTs also tend to absorb light. When coupled with tools such as AFM (Atom Force Microscopy), tip-enhanced Raman spectroscopy enables to perform local spectroscopy, directly at the surface of the CNTs, enhancing the chance to determine their electronic properties (metallic or semi-conducting) of the investigated region of the tube.[272] In Chapter 7, the Raman spectra of 0.1 mg·mL^{-1} water dispersions were recorded on a HoloLab (Kaiser Optical Systems) equipped with a 785 nm (1.58 eV) laser source. The final spectrum was obtained via 100 scans at a laser power of 400 mW. For the same samples, an additional Raman spectrometer (Bruker FT Raman RFS 100/S) with a Nd-YAG laser source of 1064 nm (1.17 eV) was employed at 1250 mW and the spectra were generated after cumulating 1000 scans.

3.12. Materials

3.12.1. Chemicals employed in Chapter 4

Methyl methacrylate (MMA, Acros) was passed through a column of basic alumina prior to use and stored at -20 °C. Copper (I) bromide ($Cu^{I}Br$, Fluka) was purified via sequential washing with sulphurous acid, acetic acid and ethanol, followed by drying under reduced pressure. Methyl 2-bromo-2-methylpropionate (MBMP, ≥99%, Aldrich), copper(II)bromide ($Cu^{II}Br$, ≥99%, Fluka), 2,2'-bipyridyl (bpy, ≥99%, Sigma-Aldrich), nickelocene ($NiCp_2$, 99%, Strem Chemicals), sodium iodide (NaI, ≥99%, Fluka), triphenylphosphine (PPh_3, ≥99%, Merck), and tetrahydrofuran (THF, anhydrous, ≥99.9%, Sigma-Aldrich) were used as received. Acetone (VWR) was purchased in the highest purity and used as received. N-methylpyrrolidone (NMP, ≥98%, Fluka) was distilled under vacuum before use. The SWCNTs were purchased from He Ji Ltd. (diameter: 1–2 nm, length: 10–50 μm). SWCNTs were used as received with a content of SWCNTs up to 90 *wt.-%* and less than 1.5 *wt.-%* ashes (characteristics from the supplier). Dispersions of SWCNTs were filtered using a PTFE-membrane (0.2 μm pore size, Sartorius).

3.12.2. Chemicals employed in Chapter 5

N-isopropylacrylamide (NIPAM, 98%, TCI) was recrystallized from *n*-hexane and stored at -20 °C. 2,2′-Azobis(2-methylpropionitril (AIBN, 98%, Acros) was recrystallized from ethanol before use. 1,4-Dioxane (≥99%, Acros) was freshly passed through a column of basic alumina before use. Copper (I) bromide ($Cu^{I}Br$, Fluka) was purified via sequential washing with sulphurous acid, acetic acid and ethanol, followed by drying under reduced pressure. *N,N,N',N'',N''*-pentamethyldiethylenetriamine (PMDETA, ≥ 99%, Acros), nickelocene ($NiCp_2$, 99%, ABCR), sodium iodide (NaI, ≥99%, Fluka), triphenylphosphine (PPh_3, ≥99%, Merck), *N*-maleimide (≥99%, Sigma Aldrich), tetrahydrofuran (THF, anhydrous, ≥99.9%, Sigma-Aldrich) and *N,N*-dimethylformamide (DMF, ≥99%, Sigma Aldrich) were used as received. *N*-methylpyrrolidone (NMP, 99%, Acros) was distilled under vacuum before use. All other solvents were purchased from VWR in the highest available purity and used as received. SWCNTs were purchased from Carbon Solutions Inc. (diameter: 1.4 nm) and used as received with a content of SWCNTs up to 90 *wt.-%* and less than 4–8 *wt.-%* ashes (supplier information). Dispersions of SWCNTs were filtered using a PTFE-membrane (0.2 μm pore size, Sartorius).

3.12.3. Chemicals employed in Chapter 6

2,5-Dibromo-3-hexylthiophene (>97.0%) was purchased from TCI, Deutschland

GmbH. Dry THF, [1,3-Bis(diphenylphosphino)propane]dichloronickel(II) Ni(dppp)Cl$_2$ (99%) was obtained from Acros Organics, Geel Belgium. Triethylamine (TEA, 99%), zinc chloride (ZnCl$_2$, ≥99%), *tert*-butylmagnesium chloride (2 M ether solution), and vinylmagnesium bromide (1 M THF solution) were obtained from Sigma-Aldrich, Schnelldorf, Germany. 9-Borabicyclo[3.3.1]nonane (9-BBN) monomer (97%, 0.5 M THF solution) and 2-bromopropionyl bromide (97%) were obtained from Alfa Aesar GmbH & Co KG, Karlsruhe, Germany. 35% aq. H$_2$O$_2$ solution was obtained from Carl Roth + Co. KG, Karlsruhe, Germany. Bis(cyclopentadienyl)nickel (NiCp$_2$, Nickelocene, 99%) was purchased from ABCR GmbH & Co KG, Germany. Sodium iodide (NaI) was obtained from Fisher Scientific UK Limited. Triphenylphosphine (PPh$_3$, ≥99%) was obtained from Merck Schuchardt OHG, Hohenbrunn Germany. PS (M_n = 3100 g·mol^{-1}, Đ = 1.1) with dithioester end-groups was synthesized according to a previously published RAFT procedure.[86] *N*-methylpyrrolidone (NMP, 99%, Acros) was distilled under vacuum before use. SWCNTs were purchased from Carbon Solutions Inc. (diameter: 1.4 nm) and used as received with a content of SWCNTs up to 90 *wt.-%* and less than 4–8 *wt.-%* ashes (supplier information). Dispersions of SWCNTs were filtered using a PTFE-membrane (0.2 μm pore size, Sartorius).

3.12.4. Chemicals employed in Chapter 7

Methyl methacrylate (MMA, Acros) was passed through a column of basic alumina prior to use and stored at -20 °C. Copper(I) bromide (Cu^{I}Br, Fluka) was purified via sequential washing with sulphurous acid, acetic acid and ethanol, followed by drying under reduced pressure. Picolylchloride hydrochloride (98%, Aldrich), phenylsulfinate sodium (technical grade, 85%, Aldrich), 1,8-diazabicycloundec-7-ene (DBU, ≥99%, Fluka), tetrapropylammoniumbromide (98%, Sigma-Aldrich), *p*-bromomethylbenzoic acid (97%, ABCR), diisobutylaluminum hydride in hexane (DIBAL-H, 1 mol·L^{-1}, Acros), elemental sulfur (powder, Sigma-Aldrich), potassium *tert*-butanolate (95%, Sigma-Aldrich), *N,N,N',N'',N''*-pentamethyldiethylenetriamine (PMDETA, ≥99%, Acros), nickelocene (NiCp$_2$, 99%, ABCR), sodium iodide (NaI, ≥99%, Fluka), triphenylphosphine (PPh$_3$, ≥99%, Merck), *N*-(3-Dimethylaminopropyl)-*N'*-ethylcarbodiimide hydrochloride (EDC, ≥99%. Sigma-Aldrich), 4-dimethylamino pyridine (DMAP, ≥99% Sigma-Aldrich), and trifluoroacteic acid (TFA, 99%, ABCR) were used as received. *N*-methylpyrrolidone (NMP, 99%, Acros) was distilled under vacuum before use. Anhydrous toluene (water content < 30ppm) was purchased from Sigma-Aldrich. For the esterification, dichloromethane was purchased in the highest purity from VWR and distilled over phorsphorus pentoxide (≥97%, Fluka) prior to use. All other solvents were purchased in the highest available purity from VWR and used as

received. SWCNTs (≥90%) were purchased from He Ji Ltd. (diameter: 1–2 nm, length: 10-50 µm) and used as received (≤ 5 *wt.-%* ashes). Dispersions of SWCNTs were filtered using a PTFE-membrane (0.2 µm pore size, Sartorius).

- 52 -

Chapter 4 – *'Proof of principle'*: SWCNTs functionalization with cyclopentadienyl end-capped poly(methyl)methacrylate

Diels-Alder cycloaddition
on carbon nanotubes
at ambient temperature
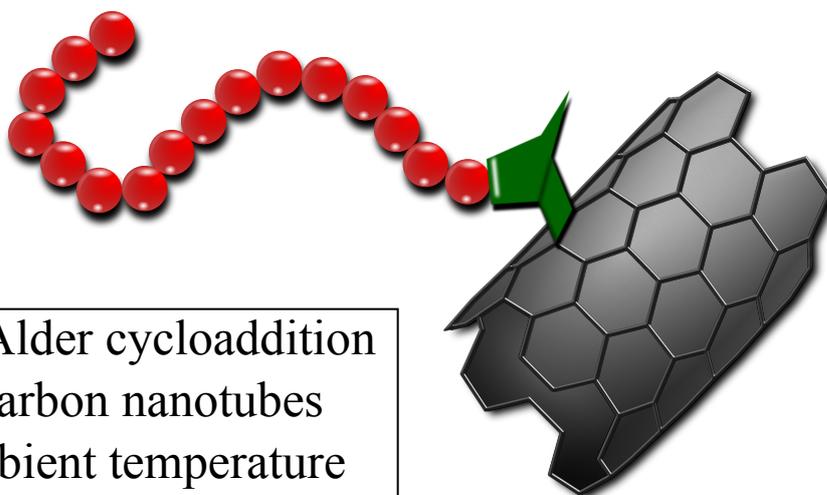
4.1. Introduction

While the characterization of Cp end-capped PMMA polymer chains is a relatively straight forward task (via SEC, NMR spectroscopy and ESI-MS), evidencing the success of the functionalization of CNTs with polymer strands is not as straight forward as in the case of functional fullerenes (characterization of the adduct possible via ESI-MS), as polymer-functionalized SWCNTs do not spontaneously dissolve in any solvent system and can thus not be analyzed via e.g. soft ionization mass spectrometric techniques.[273] The characterization approach taken in the current thesis combines quantitative (surface analysis) methods to prove the successful [4+2] cycloaddition of Cp-capped polymers onto the SWCNTs. TGA was conducted to observe changes in the thermal response profiles and to estimate the grafting density of polymer chains attached onto the SWCNTs. Complementary to TGA, EA and XPS enable the determination of the elemental composition (throughout the bulk and the surface) of the sample and enable the comparison of the grafting density estimated via these three methods. In addition, HRTEM was performed to visualize the modified surface of the SWCNTs after the [4+2] cycloaddition and to deduce the thickness of the grafted polymer layer. PMMA was initially chosen as it can be readily prepared with a pre-selected chain length and narrow polydispersity via ATRP, featuring a bromine chain terminus, which is readily switchable to a highly [4+2] active Cp entity in a quantitative fashion as recently demonstrated by Inglis *et al.*[274] Most importantly, PMMA contains oxygen atoms which can be readily distinguished from SWCNTs (constituted only of carbon atoms) by XPS and EA.

Chapter 4 is divided in two parts. In the first part (section 4.2), the synthesis and the characterization of PMMA-Cp is described and the quantitative presence of the Cp group at the terminus of the polymer chains is evidenced. In the second part (section 4.3), the hybrid material PMMA-Cp/SWCNTs, and a control sample, are characterized via the above cited and already discussed (refer to Chapter 3) techniques to quantitatively assess the success of the DA reaction of Cp-end functionalized PMMA with SWCNTs under ambient conditions without the use of any catalyst as depicted in **Scheme 4.1**.
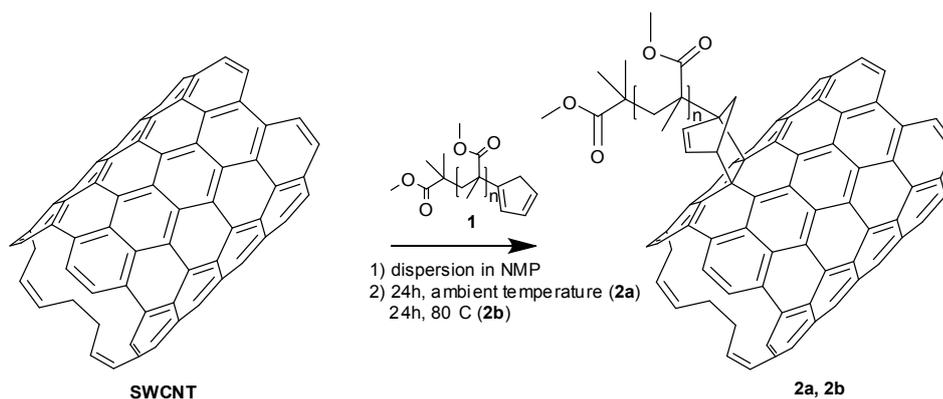
Scheme 4.1. Synthetic pathway for the direct [4+2] functionalization of SWCNTs with Cp-capped PMMA (PMMA-Cp, **1**) at ambient temperature (product **2a**) and at 80 °C (product **2b**).

4.2. Synthesis

4.2.1. Polymerization and Cp-transformation

The synthesis of Cp-capped PMMA-Cp was performed according to the procedure described by Inglis *et al.*[274] and requires the synthesis of the bromine terminated polymer PMMA-Br via ATRP. The list of the employed materials can be found in Chapter 3 (section 3.12.1).

The synthesis of the starting material PMMA-Br was proceeded as follows. To a dried Schlenk tube was added copper (I) bromide, copper (II) bromide and bpy which was then sealed with a rubber septum, evacuated and backfilled with nitrogen. To another Schlenk tube was added methyl methacrylate (MMA) and acetone were added (50:50) and equipped with a rubber septum. The monomer solution was then deoxygenated by three consecutive freeze-pump-thaw cycles and subsequently transferred to the first Schlenk tube via cannula. The tube was sealed under a nitrogen atmosphere and placed in a thermostatic oil bath held at 50 °C. After the polymerization mixture reached the desired temperature, methyl 2-bromo-2-methylpropanoate (MBMP) was added. The initial ratio of [MMA]:[MBMP]:[Cu^{I}Br]:[Cu^{II}Br]:[bpy] was 50:2:0.105:0.0125:0.25. The polymerization was stopped by cooling the mixture in an ice-bath and exposure to oxygen. The mixture was passed through a short column of neutral alumina to remove the copper catalyst. PMMA-Br was isolated by two-fold precipitation in cold hexane. The obtained polymer was characterized via SEC ($M_n = 2700$ g·mol^{-1}, $Đ = 1.18$).

The Cp transformation of PMMA-Br to obtain PMMA-Cp was conducted as follows. A solution of bromine terminated polymer PMMA-Br (0.18 mmol), triphenylphosphine (PPh$_3$, 0.36 mmol, 2 eq) and sodium iodide (NaI, 1.08 mmol, 6 eq) in anhydrous THF (2.0 mL) was prepared under a nitrogen atmosphere. Separately, a stock solution of nickelocene (NiCp$_2$) in

anhydrous THF (0.18 mol·L^{-1}) was prepared under a nitrogen atmosphere. The NiCp$_2$ solution (2.0 mL, 4 eq) was subsequently added to the polymer solution and allowed to stir overnight at ambient temperature. At the end of the reaction, the mixture was passed through a short column of basic alumina to remove the precipitated nickel (II) bromide and the polymer was recovered by precipitation. The resulting polymer was dissolved in chloroform and washed three times with distilled water. The obtained PMMA-Cp was isolated by successive precipitations in cold hexane. The obtained polymer was characterized via SEC (M_n = 2900 g·mol^{-1}, $Đ$ = 1.17).

The obtained bromine terminated polymer PMMA-Br and the Cp-capped polymer PMMA-Cp were characterized by SEC. The SEC traces in **Figure 4.1** depict the narrow distribution of the initial polymer chains PMMA-Br synthesized via ATRP. After the chain-end transformation, the molecular remains unchanged, which also guarantees the absence of any chain coupling that could potentially occur between two Cp moieties, leading to a doubling of the molecular weight.
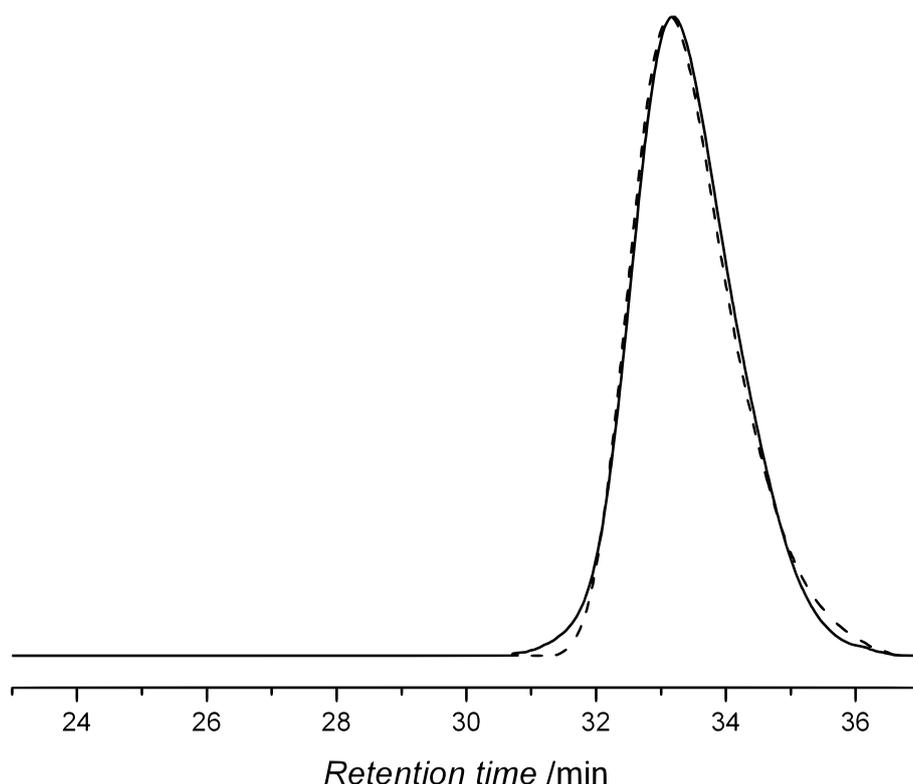
Figure 4.1. SEC traces of PMMA-Br (dot line) and PMMA-Cp (continuous line).

4.2.2. Chain-end fidelity

^{1}H Nuclear Magnetic Resonance spectroscopy (NMR)

The chain-end fidelity of the Cp end-capped polymer (PMMA-Cp) is demonstrated by

^{1}H NMR spectroscopy via the appearance of two signals allocated to the Cp group in the spectrum of PMMA-Cp (**Figure 4.2**). The protons *e* and *f* located at between 2.9 and 3.1 ppm and between 6.0 and 6.7 ppm, respectively evidence the successful transformation of the bromine end-group into a Cp end-group at the polymer chain terminus.
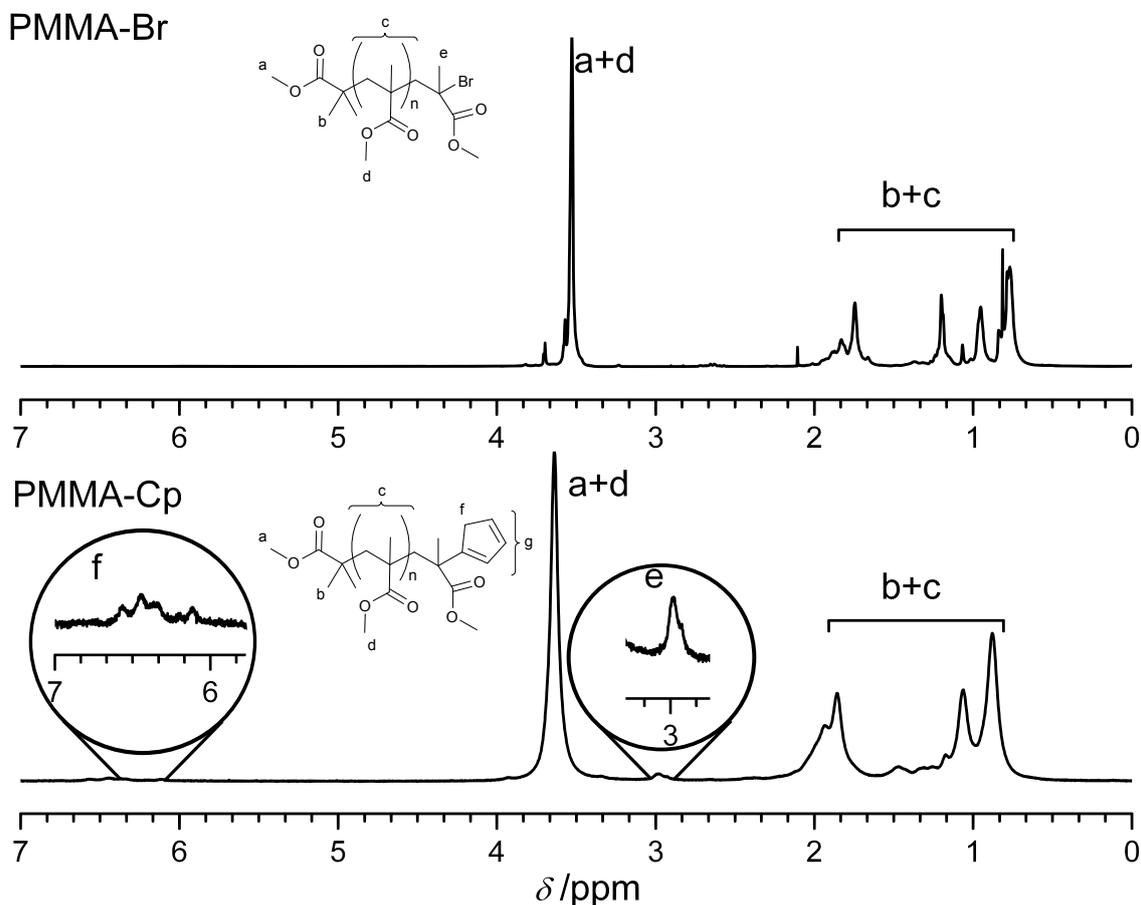
Figure 4.2. ^{1}H NMR spectra of the starting material PMMA-Br (top) and the final PMMA-Cp (bottom) after the end-group modification.

Mass Spectrometry (ESI-MS)

A detailed characterization of the initial and final polymer chains is performed via ESI-MS for the determination of the end-groups for each polymer chains. From the ATRP process, the main species present in the sample (and are of interest) are species **II** (see **Scheme 4.2**), being the bromine terminated polymer chains PMMA-Br, while further species (**III**, **IV**, **V**) are generated during the ATRP process.[274]

From the ESI-MS spectra in **Figure 4.3**, while bromine capped PMMA-Br is the main product (**II**), three minor species (**III**, **IV** and **V**) are identified. During the transformation to PMMA-Cp, only PMMA-Br reacts to generate the cyclopentadienyl capped polymer. Side products are not bromine terminated, hence they remain in the sample and can be still identified in the ESI-MS spectrum of PMMA-Cp at the same *m/z*. Via the transformation and

according to the ESI-MS spectra (see **Figure 4.3**), PMMA-Br is completely transformed to PMMA-Cp, leading to an effective mass change of 13.88 Da. Moreover, the isotopic pattern changed from the PMMA-Br (**II** species) peak featuring the characteristic bromine isotopic pattern (^{79}Br and ^{81}Br), to the PMMA-Cp (**I** species) peak with the characteristic carbon isotopic abundances (^{12}C and ^{13}C).
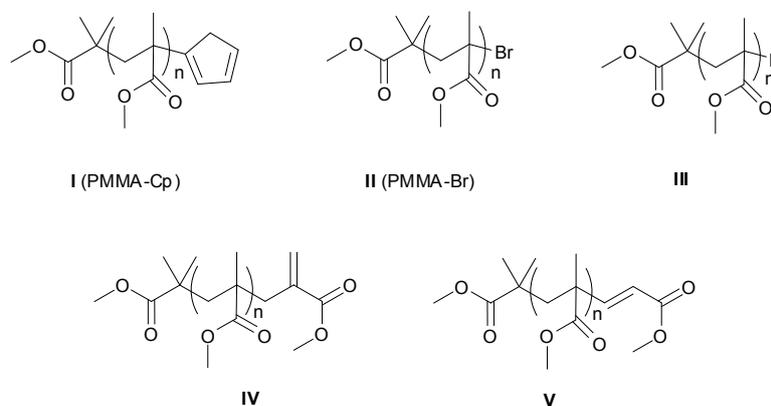
Scheme 4.2. Expected species during the ATRP process for the synthesis of **PMMA-Br** (**II**), and after elimination of Br (**III**), HBr (**IV**) and CH$_3$Br (**V**).
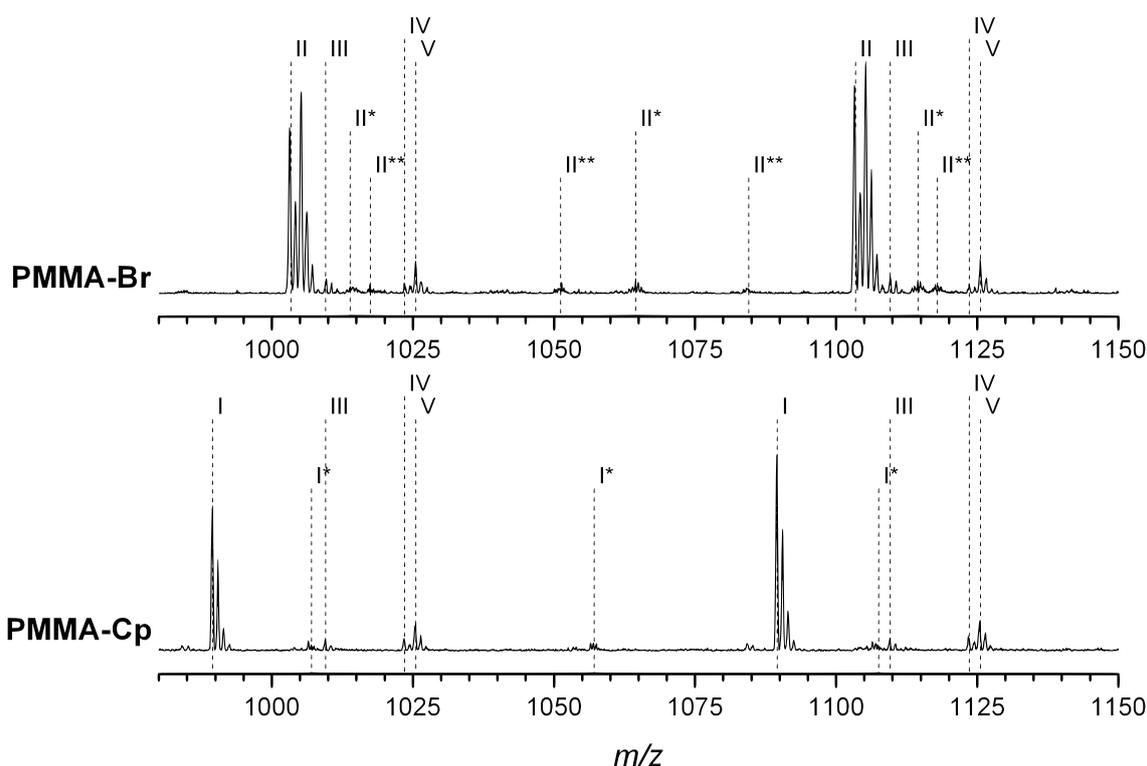
Figure 4.3. ESI-MS spectra of PMMA-Br (**II**) and PMMA-Cp (**I**) polymer obtained via direct source infusion. Signals marked with an asterisk represent double charged species (*) and triple charged species (**). Minor side products from ATRP process (**III**, **IV**, **V**) are also identified.

Peak identification was conducted according to the exact mass of the ATRP starting molecule (2-methyl 2-bromo-2-methylpropanoate, MBMP) and the number of monomer units

incorporated in the polymer chain (see **Table 4.1**). Only sodium adducts were observed and the analysis led to the identification of up to three times charged ions for PMMA-Br (**II** for single charged species, **II*** for double charged and **II**** for triple charged species).

Table 4.1. Identification of the charged species present in PMMA-Br sample. The main product is identified as the bromine terminated polymer chains (**II**) with the corresponding double (**II***) and triple (**II****) charged species, as well as minor side products (**III**, **IV**, **V**).

n^a	Species	Formula	m/z exp.	m/z th.	$\Delta m/z$
8	II	$[C_{45}H_{73}O_{18}BrNa]^+$	1003.12	1003.39	0.27
	III	$[C_{49}H_{78}O_{20}Na]^+$	1009.68	1009.50	0.18
	IV	$[C_{50}H_{80}O_{20}Na]^+$	1023.48	1023.51	0.03
	V	$[C_{50}H_{82}O_{20}Na]^+$	1025.48	1025.53	0.05
9	II	$[C_{50}H_{81}O_{20}BrNa]^+$	1103.24	1103.44	0.20
	III	$[C_{54}H_{86}O_{22}Na]^+$	1109.60	1109,55	0.05
	IV	$[C_{55}H_{88}O_{22}Na]^+$	1123.60	1123.57	0.03
	V	$[C_{55}H_{90}O_{22}Na]^+$	1125.56	1125.58	0.02
10	II	$[C_{55}H_{89}O_{22}BrNa]^+$	1203.28	1203.49	0.21
18	II*	$[C_{95}H_{153}O_{38}BrNa_2]^{2+}$	1013.92	1013.87	0.05
19	II*	$[C_{100}H_{161}O_{40}BrNa_2]^{2+}$	1064.44	1064.48	0.04
20	II*	$[C_{105}H_{169}O_{42}BrNa_2]^{2+}$	1114.44	1114.51	0.07
21	II*	$[C_{110}H_{177}O_{44}BrNa_2]^{2+}$	1164.44	1164.53	0.09
28	II**	$[C_{145}H_{233}O_{58}BrNa_3]^{3+}$	1017.36	1017.48	0.12
29	II**	$[C_{150}H_{241}O_{60}BrNa_3]^{3+}$	1051.36	1051.16	0.20
30	II**	$[C_{155}H_{249}O_{62}BrNa_3]^{3+}$	1084.08	1084.51	0.43
31	II**	$[C_{160}H_{257}O_{64}BrNa_3]^{3+}$	1117.48	1117.86	0.38
32	II**	$[C_{165}H_{265}O_{66}BrNa_3]^{3+}$	1151.12	1151.21	0.09
33	II**	$[C_{170}H_{273}O_{68}BrNa_3]^{3+}$	1184.48	1184.57	0.09

^{a}number of monomer units.

From the ESI-MS spectrum of PMMA-Cp, excellent agreement between the theoretically expected and experimentally observed species is found (see **Table 4.2**). As for the bromine capped polymer, sodium adducts are observed in the ESI-MS spectrum (species **I*** for the double charged ions). The side products **III**, **IV** and **V**, not terminated by a bromine group, remain inert towards the Cp transformation and are observed at unchanged m/z ratios.

Table 4.2. Identification of the charged species present in the PMMA-Cp sample. The main product is identified as the Cp terminated polymer chains (**I**) with the corresponding double (**I***) and triple (**I****) charged species (not observed in the ESI-MS spectrum), the non bromine terminated polymer chains (**III**, **IV**, **V**) remaining still present in the sample.

n^a	Species	Formula	m/z exp.	m/z th.	$\Delta m/z$
8	I	$[C_{50}H_{78}O_{18}Na]^+$	989.59	989.51	0.08
9	I	$[C_{55}H_{86}O_{20}Na]^+$	1089.60	1089.56	0.04
10	I	$[C_{60}H_{94}O_{22}Na]^+$	1189.64	1189.61	0.03
18	I*	$[C_{100}H_{158}O_{38}Na_2]^{2+}$	1007.08	1007.01	0.07
19	I*	$[C_{105}H1_{66}O_{40}Na_2]^{2+}$	1057.04	1057.12	0.08
20	I*	$[C_{110}H_{174}O_{42}Na_2]^{2+}$	1107.57	1107.57	0.00
21	I*	$[C_{115}H_{182}O_{44}Na_2]^{2+}$	1157.60	1157.59	0.01
28	I**	$[C_{150}H_{238}O_{58}Na_3]^{3+}$	1013.18	1013.12	0.06
29	I**	$[C_{155}H_{246}O_{60}Na_3]^{3+}$	1046.68	1046.54	0.14
30	I**	$[C_{160}H_{254}O_{62}Na_3]^{3+}$	1079.84	1079.89	0.05
31	I**	$[C_{165}H_{262}O_{64}Na_3]^{3+}$	1113.24	1113.23	0.01
32	I**	$[C_{170}H_{270}O_{66}Na_3]^{3+}$	1146.32	1146.58	0.26
33	I**	$[C_{175}H_{278}O_{68}Na_3]^{3+}$	1179.68	1179.94	0.26

^{a}number of monomer units.

By means of ^{1}H NMR spectroscopy and mass spectrometry (ESI-MS), the targeted Cp-capped polymer chains PMMA-Cp were characterized and based on the quantitative transformation of ATRP synthesized starting product PMMA-Br, bromine terminated, with a narrow distribution according to SEC measurements. Side products generated during the polymerization were identified, yet their concentration remains rather low ensuring a high purity of the polymer chains PMMA-Br, and thus consequently of the Cp terminated polymer chains PMMA-Cp, which are further reacted with the SWCNTs, as described in the following section 4.3.

4.3. Characterization of PMMA-Cp functionalized SWCNTs

In this section, the synthesis of two PMMA-Cp/SWCNT hybrid materials differing in their reaction conditions (ambient temperature for sample **2a** and 80 °C for sample **2b**) is reported. The characterization is referenced to a control sample (**3**) generated by the mixture of non reactive PMMA-Br polymer chains with SWCNTs under the same conditions as for the PMMA-Cp modified SWCNTs. In order to in-depth characterize the obtained hybrid material, e.g. to estimate accurately the grafting density of the polymer chains at the surface of the SWCNTs, the same analytic methods (TGA, EA and XPS) were employed to

characterize the Cp-capped polymer chains PMMA-Cp (noted for convenience **1** in the following) as the pristine **SWCNTs**.

4.3.1. Synthesis of the hybrid material PMMA-Cp/SWCNT

The lists of all materials employed can be found in Chapter 3 (section 3.12.1). In a 100 mL round bottom flask 25 mg of SWCNTs were dispersed in 50 mL of distilled NMP in an ultrasonic bath. After 30 min of dispersion, 250 mg PMMA-Cp (**1**) was added and the mixture was stirred overnight at ambient temperature (sample **2a**). The dispersion was subsequently filtered and washed with 100 mL THF and dried under vacuum. Sample **2b** was synthesized under the same conditions, except that the dispersion was heated at 80 °C after the ultrasonic treatment. The round bottom flask was capped with dried $CaCl_2$ to ensure no absorption of moisture. A control sample (**3**) was prepared under exactly the same reaction conditions (including the washing procedure) as sample **2a** by replacing the PMMA-Cp polymer by its polymeric precursor PMMA-Br.

4.3.2. Results and discussion

Thermogravimetric Analysis (TGA)

The thermogravimetric analysis of the studied samples in air atmosphere (see **Figure 4.4**) depicts noticeable differences between the non-modified **SWCNTs**, the control reference (sample **3**) on the one hand, and the PMMA-Cp modified SWCNTs **2a** and **2b** on the other hand. Whereas non-modified SWCNTs remain stable until degradation commences at 350 °C, the PMMA-Cp modified SWCNTs start to degrade at lower temperature in two steps.

The analysis of the first derivative curves of the TGA traces gives access to the degradations that the samples undergo with increasing temperature. **Figure 4.5** depicts the first derivative curves obtained for each sample.

The maximal temperature T_m for which the weight loss is maximal and the final temperature T_f of the observed degradation were obtained graphically from the first derivative of the thermogravimetric profile of the samples. This analysis indicates for **2a** and **2b** that the initial degradation sets in at 210 °C with a maximal temperature (T_m for which the weight loss is maximal) at 325 °C, while the subsequent degradation step has a similar maximal temperature T_m compared to non-modified SWCNTs (see **Table 4.3**).

Such a behavior is to be expected when a covalent attachment to the SWCNTs surface has indeed occurred: the tethered polymer strands on **2a** and **2b** should feature a similar degradation temperature as the pure polymer sample PMMA-Cp (**1**), indicating identical

maximal (T_m) and final (T_f) temperatures characteristic for the polymer degradation part.
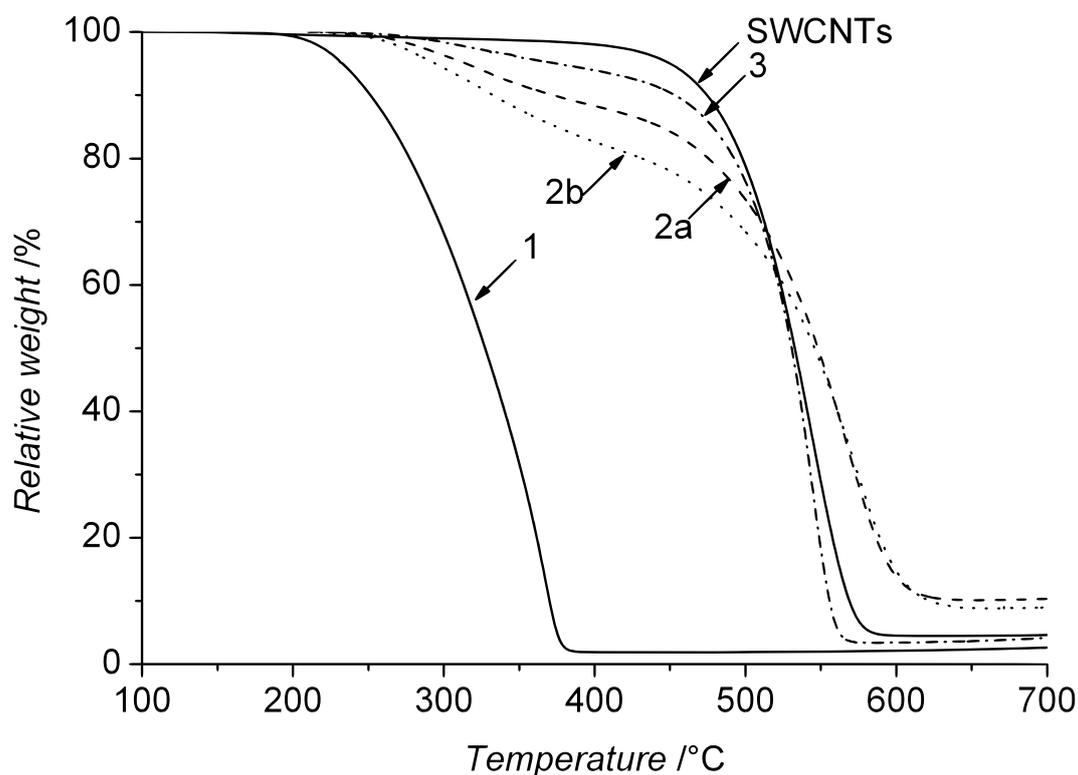
Figure 4.4. Thermogravimetric analysis in air atmosphere employing a heat flow of 10 °C·min^{-1} of non-modified **SWCNTs**, **1** PMMA-Cp, **2a** SWCNTs modified with PMMA-Cp at ambient temperature, **2b** SWCNTs modified with PMMA-Cp at 80 °C, **3** control sample (SWCNTs mixed with a non-DA reactive PMMA-Br at ambient temperature and subjected to the same washing procedure as **2a** and **2b**). Once the temperature reached 100 °C, the sample was equilibrated for 30 minutes at 100 °C for **SWCNTs** and **1**, as well as at 210 °C for **2a**, **2b** and **3** to evaporate residual solvent (NMP).

However, the overall degradation profile of **2a** and **2b** is indeed strongly altered when compared to the virgin SWCNTs (where *no* degradation is observed in the sub-350 °C region), providing evidence – underpinned by the below discussed control sample degradation profile – for a successful functionalization of SWCNTs via a [4+2] cycloaddition with PMMA-Cp. The final temperature degradation (T_f) represents the temperature at which the first degradation stops. Considering the weight loss at T_f, a further analysis of the obtained TGA curves allows the quantification of the amount of polymer chains grafted onto the surface of the SWCNTs. With observed weight percentages of 12.3% and 18.2% for **2a** and **2b** respectively, the amount of polymer on the surface of the SWCNTs after washing is relatively high. Further underpinning these results, the thermogravimetric profile of the
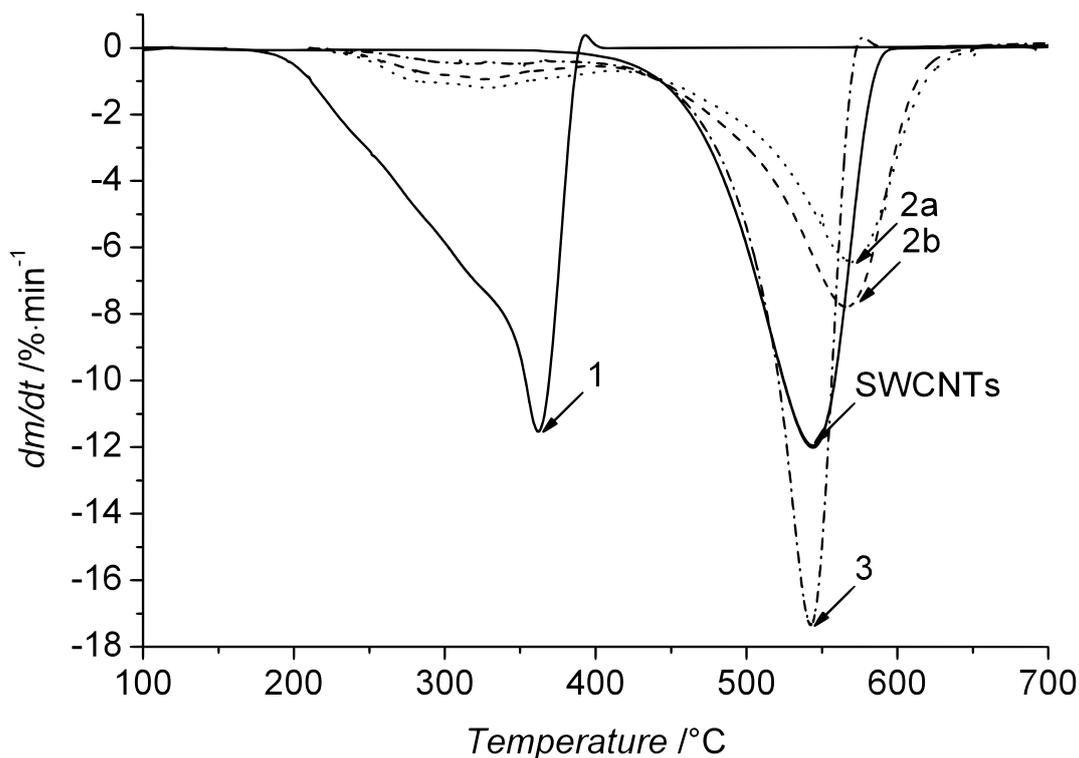
Figure 4.5. Derivatives of the thermogravimetric profiles in air atmosphere, with a heat flow of 10 °C·min⁻¹ for non-modified **SWCNTs**, **1** PMMA-Cp, **2a** SWCNTs modified with PMMA-Cp at ambient temperature, **2b** SWCNTs modified with PMMA-Cp at 80 °C, **3** SWCNTs mixed with PMMA-Br at ambient temperature. Once the temperature reached 100 °C, the sample was equilibrated for 30 minutes at 100 °C for **SWCNTs** and **1** as well as at 210 °C for **2a**, **2b** and **3** to evaporate residual solvent (NMP).

Table 4.3. Quantitative grafting results obtained via TGA[a] of non-modified **SWCNTs**, PMMA-Cp (**1**), SWCNTs modified with PMMA-Cp (**2a**)[b] and (**2b**)[c].

	T_i[e] /°C	T_f[f] /°C	T_m[g] /°C	wt.-% at T_f
SWCNTs[d]	350	600	545	4.5
1	140	400	290	1.9
2a	200	410	325	87.7
	410	650	565	10.1
2b	200	410	325	81.8
	410	650	570	8.8
3	200	410	325	93.5
	410	600	545	4.5

[a]TGA conditions: air atmosphere, heat flow of 10 °C·min⁻¹, after 30 minutes isothermal step at 100 °C for **SWCNTs** and **1**, and at 210 °C for **2a**, **2b** and **3**; [b]at ambient temperature; [c]at 80 °C; [d]non-modified SWCNTs; [e]initial temperature for degradation; [f]final temperature for degradation; [g]temperature of maximal weight loss (from first derivative); [h]number of carbon atoms covered by one polymer chain grafted on the surface of SWCNTs.

control sample **3** displays slight degradation, probably due to a small amount of PMMA-Br adsorbed at the surface of the SWCNTs. However, samples **2a** and **2b** display a much stronger degradation, unambiguously evidencing the covalent attachment of PMMA-Cp at the SWCNT's surface. The strongly altered thermal degradation profile observed in the profiles of the SWCNTs that have undergone a DA reaction with PMMA-Cp, compared to the control sample, provides direct proof for not an adsorption of the polymer chains onto the surface of the SWCNTs, but rather a covalent functionalization.

For a better understanding and comparison of the grafting density onto nanoparticles, these experimental values must be expressed in commonly used units for the grafting density. Moreover, a mathematical treatment must take into account the amount of impurities, the molecular weight of the polymer chains and the specific surface area of the graphene sheet. After the estimation of the amount of degraded polymer after the first reaction finishing at T_f ($x_{\text{polymer at } T_f}$ in *wt.-%*) and of the amount of residue at 700 °C ($x_{\text{residue at 700°C}}$ in *wt.-%*), the loading capacity (σ_1) in mol·g^{-1} was calculated based on the weight loss at T_f, the polymer chain molecular weight M_n and by assuming the rest of the samples is constituted purely of carbon. Based on the above procedure, the grafting density (σ_2) in chains·m^{-2} was calculated according to the polymer chain molecular weight M_n and the theoretical specific surface of the SWCNTs (1315 m^2·g^{-1}).[275] The third calculable parameter is the grafting density expressed as periodicity (σ_3) for which the number of polymer chains (also based on the molecular weight M_n) is reported relative to the area of one graphene hexagon ($A_{\text{hexagon}} = 5.25$ Å^2),[276] delivering the number of carbon atoms covered by one polymer chain (since one hexagon is constituted by two carbon atoms, according to the structure of graphene). The periodicity represents the surface occupied by the polymer chains for the specific application of CNTs grafting. Expressed by the number of carbon atoms covered by a single polymer chain, this value subsequently allows for a qualitative analysis with reference to the structure of the SWCNTs. In summary, the different grafting densities are given by the set **Equation 4.1**.

$$\sigma_1 = \frac{x_{\text{polymer at } T_f}}{M_n \cdot \left(100 - x_{\text{polymer at } T_f} - x_{\text{residue at 700°C}}\right)} \, (\text{mol·g}^{-1}) \qquad \text{(Eq. 1)}$$

$$\sigma_2 = \frac{\sigma_1 \cdot N_A}{1315} \, (\text{chain·m}^{-2}) \qquad \text{(Eq. 2)}$$

$$\sigma_3 = \frac{2}{A_{\text{hexagon}} \cdot \sigma_2} \, (\text{carbon atoms}) \qquad \text{(Eq. 3)}$$

Equation 4.1. Equations determining the grafting density from the thermogravimetric analysis. N_A represents Avogadro's number.

According to **Table 4.6**, where all quantitative grafting data from all three methods are compiled, a higher grafting ratio results for the sample reacted at 80 °C **2b** compared with that of the sample reacted at ambient temperature **2a**, with 0.040 and 0.025 chain·nm^{-2} respectively. A maximum theoretical grafting density can be calculated, assuming that every unsaturated carbon double bond reacts with a polymer chain, implying that the periodicity is reduced by one polymer chain every 2 carbon atoms of the SWCNTs, leading to a grafting density of 41.62 mmol·g^{-1} or 19 chains·nm^{-2} with an estimated specific surface area of the SWCNTs (or graphene sheet) of 1315 m^2·g^{-1}.[275] This maximum theoretical grafting density value can be calculated after the complete reaction of all unsaturated carbon double bonds with a PMMA-Cp polymer chain. In this model, one polymer chain is covalently linked with two carbon atoms, and – according to the graphene structure of the SWCNTs – the occupied surface can be approximated by a hexagon. By definition, the periodicity $\sigma_3 = 2$ leads to **Equation 4** and **5** (refer to **Equation 4.2**) using the same notation:

$$\sigma_1 = \frac{1315}{N_A \cdot A_{hexagon}} \ (mol \cdot g^{-1}) \qquad\qquad (Eq.\ 4)$$

$$\sigma_2 = \frac{1}{A_{hexagon}} \ (chain \cdot m^{-2}) \qquad\qquad (Eq.\ 5)$$

Equation 4.2. Equations determining the maximum theoretical grafting density for one polymer chain linked with one single carbon double bond. The employed terms refer to the equations **1** and **2** (see **Equation 4.1**).

These theoretical values are, however, somewhat unrealistic and do not take into account the steric demand of a polymer chain after the reaction onto the SWCNT surface. The ideal grafting density should take into account the morphology of the polymer chains and be based on the radius of gyration $\langle R_g \rangle$. For this, the Kuhn length b (17 Å) and the Flory coefficient C_∞ (9.0) were taken from literature[277] and applied to PMMA-Cp using the same formalism. The resulting approximation leads to a value of 5.71 monomer units (N). The mean-square radius of gyration and the radius of the corresponding disk are calculated according to **Equation 6** and **7** (refer to **Equation 4.3**), and delivered a theoretical radius of gyration $\langle R_g \rangle$ of 1.66 nm, which can be exploited to deliver more reasonable theoretical grafting densities.

$$\langle R_g^2 \rangle = \frac{N \cdot b^2}{6} \qquad\qquad \text{(Eq. 6)}$$

$$R_{disk}^2 = 2 \cdot \langle R_g^2 \rangle \qquad\qquad \text{(Eq. 7)}$$

Equation 4.3. Expression of the gyration radius as radius of the corresponding disk (polymer equivalent freely joined chain based on an interactions model) to determine a theoretical length of the PMMA-Cp polymer chain.

The surface of the disk (radius of 2.35 nm) can be subsequently substituted in the expressions of σ_1 and σ_3 to determine the maximum value of the theoretical grafting density for one polymer chain corresponding to the estimated grafting density σ_2 (0.058 chain·nm^{-2}). The values of σ_1 and σ_3 are determined employing **Equation 8** and **9** (refer to **Equation 4.4**):

$$\sigma_1 = \frac{1315}{N_A \cdot \pi \cdot R_{disk}^2} \ (\text{mol·g}^{-1}) \qquad\qquad \text{(Eq. 8)}$$

$$\sigma_3 = \frac{2 \cdot \pi \cdot R_{disk}^2}{A_{hexagon}} \ (\text{carbon atoms}) \qquad\qquad \text{(Eq. 9)}$$

Equation 4.4. Expressions determining the grafting density of an ideal polymer chain onto SWCNTs. The employed terms refer to **Equation 4.1**.

Consequently, the theoretical grafting ratio is evaluated to be as one polymer chain every 659 carbon atoms (0.126 mmol·g^{-1} or 0.058 chain·nm^{-2}) which is not far removed from the experimentally found values for the two studied samples (50 for **2a** and 67% for **2b** of the theoretical grafting density). The somewhat smaller grafting density obtained experimentally may be explained by the presence of SWCNT bundles not completely dispersed after ultrasonic dispersion before the functionalization with the polymer.

Elemental Analysis (EA)

In order to confirm the grafting density deduced via TGA, elemental analysis was performed on all the samples. With high accuracy, the results for PMMA-Cp are in excellent agreement with the stoichiometry of the polymer (see **Table 4.4**). The presence of other elements for non-modified SWCNTs indicates the presence of adsorbed molecules from the air and some impurities in the sample. Measurements of the sulphur content were performed, yet this element was not detected, since it is not involved in the synthetic procedure. The content of hydrogen for the carbon nanotubes based samples (**SWCNTs**, **2a** and **2b**) is very

low. For this reason, the elemental analysis leads to slight fluctuations in the carbon and oxygen content. Nevertheless, one can observe a significant presence of oxygen content in the functionalized SWCNTs.

Table 4.4 Elemental analysis results of non-modified **SWCNTs**, PMMA-Cp **1**, SWCNTs modified with PMMA-Cp (**2a**)[a] and (**2b**)[b].

	wt.-%			
	C	H	N	O
SWCNTs [c]	85.4	1.7	0.8	2.2
1	58.3	7.7	1.0	30.2
2a	74.6	1.8	1.8	7.0
2b	73.6	1.9	2.2	7.7

[a]at ambient temperature; [b]at 80 °C; [c]non-modified SWCNTs; [d]number of carbon atoms covered by one polymer chain grafted on the surface of SWCNTs.

The grafting ratio of polymer on the SWCNTs can be estimated from the ratio between carbon and oxygen atoms. The variable grafting densities (σ_1, σ_2 and σ_3) were determined by the same procedure as described above for the TGA. It should be noted that the key data for the grafting density calculation are the carbon and oxygen contents in **2a** and **2b**. Therefore, the calculated carbon (*C%*) and oxygen (*O%*) contents (excluding the nitrogen, sulphur and hydrogen contents) from non-modified SWCNTs and polymer PMMA-Cp were employed to calculate the grafting density (σ_{CO}) in *wt.-%*. According to the following **Equation 9** (refer to **Equation 4.5**), the results provide a slightly underestimated grafting density (σ_{CO}) for **2a** and **2b**, since the oxygen content (*O%*) from non-modified SWCNTs was directly used and not recalculated according to the composition of the sample. This leads to an error of close to 1% for (σ_{CO}).

$$\sigma_{CO} = \frac{O\%_{Sample} - O\%_{SWCNTs}}{O\%_{PMMA-Cp}} \cdot 100 \, (wt.\text{-}\%) \qquad \text{(Eq. 9)}$$

Equation 4.5. Equation for determining the grafting density from elemental analysis.

As the hydrogen content remains very low, the hydrogen contribution was estimated from the amount of polymer (based on the stoichiometry of the (methyl)methycrylate monomer unit) according to σ_{CO}. Taking into account the carbon, oxygen and theoretical hydrogen contents, a second value for the grafting density is subsequently delivered. From this value, the other grafting densities (σ_1, σ_2 and σ_3) can subsequently be expressed using

Equation 4.1. Therefore, the grafting density in *wt.-%* for the SWCNTs modified with PMMA-Cp at ambient temperature (**2a**) was calculated to be 19.2%, and at 80 °C (**2b**) 22.1% (see **Table 4.6** where all grafting data are compiled). Close inspection of the numbers collated in **Table 4.4** reveals two facts: *(i)* the order of magnitude for the grafting ratios is similar to those obtained via TGA and *(ii)* the same trends are observed with regard to the reaction conditions (0.025 chain·nm^{-2} (TGA) versus 0.038 chain·nm^{-2} (EA) for ambient temperature, and 0.040 chain·nm^{-2} (TGA) versus 0.045 chain·nm^{-2} (EA) for sample reacted at 80 °C).

X-Ray Photoelectron Spectroscopy (XPS)

Further investigations with XPS (see **Figure 4.6**) provide information about the elemental composition and chemical binding states of the samples in a non-destructive manner. For more clarity, the detailed C 1s spectra for each sample are reported in the column in the middle to display the deconvolution peaks for the C1s signal of the PMMA-Cp modified SWCNTs **2a** and **2b**.
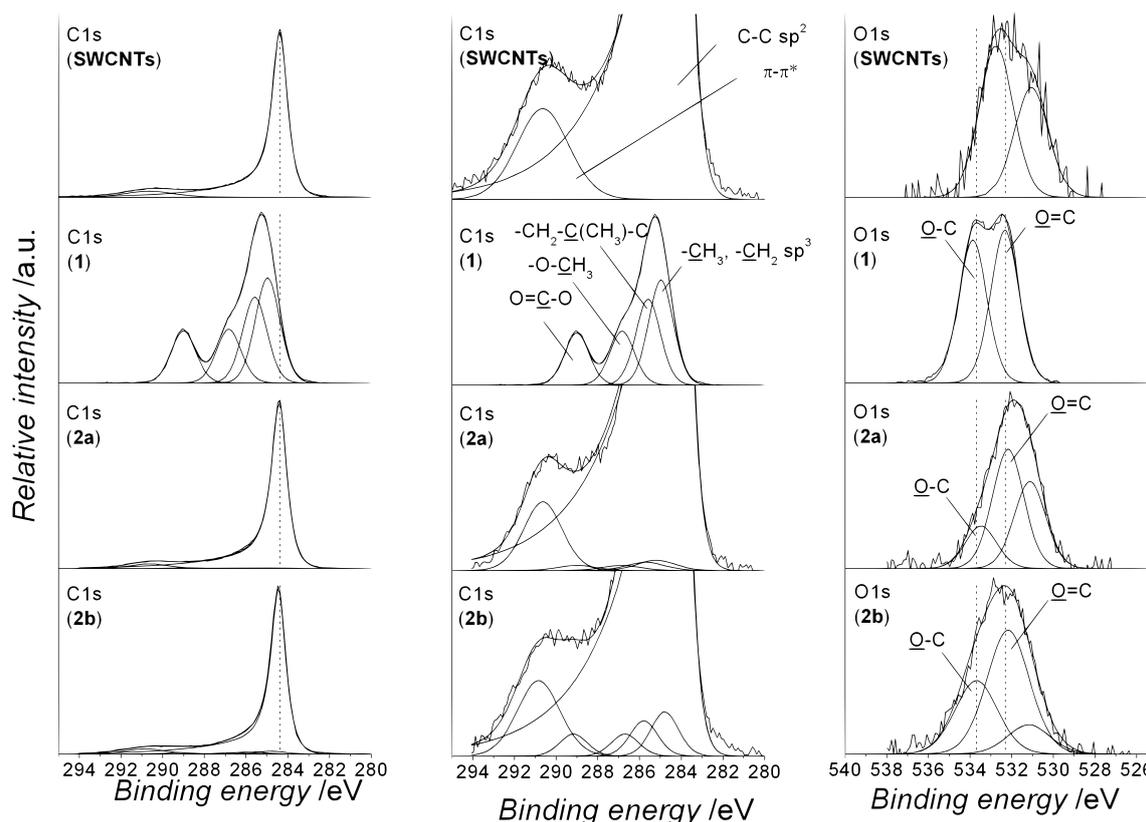
Figure 4.6. XPS spectra of non-modified **SWCNTs**, **1** PMMA-Cp, **2a** SWCNTs modified with PMMA-Cp at ambient temperature, **2b** SWCNTs modified with PMMA-Cp at 80 °C. The C 1s signal from modified SWCNTs (C-C sp^2 at 284.4 eV) is represented. The O 1s peaks at 532.3 eV (-O-C=$\underline{O}$) and 533.7 eV (-$\underline{O}$-CH$_3$) are attributed to PMMA and indicate the successful functionalization in **2a** and **2b**). The peak at 531.1 eV is probably due to surface contamination or reaction residuals (observable at 531.1 and 532.8 eV from **SWCNTs**). For more clarity, the detailed C 1s spectra for each sample are reported in the medium column.

The presence of O 1s peak components attributed to PMMA-Cp directly proves the successful functionalization of the SWCNTs. The XPS quantification together with the binding energy assignments are compiled in **Table 4.5**.

Table 4.5. Assignments of binding energy and comparison of atomic bond contribution after the deconvolution of the XPS spectra of non-modified **SWCNTs**, **1** PMMA-Cp, SWCNTs modified with PMMA-Cp **(2a)**[a] and **(2b)**[b].

Atom	B. E. /eV	at.-%				Entity
		SWCNTs[c]	1	2a	2b	
C 1s	284.4	85.9	-	83.8	80.2	C-C sp^2
	285.0	-	25.8	0.6	1.8	-$\underline{C}$H$_2$, -$\underline{C}$H$_3$ sp^3
	285.7	-	21.1	0.5	1.4	-CH$_2$-$\underline{C}$(CH$_3$)-COOCH$_3$
	286.8	-	13.2	0.3	0.9	-O$\underline{C}$H$_3$
	289.1	-	12.8	0.3	0.9	O=$\underline{C}$-OCH$_3$
	290.7	7.1	-	3.9	4.7	π-π*
O 1s	532.3	-	13.7	2.2	2.6	$\underline{O}$=C-OCH$_3$
	533.7	-	12.8	0.8	1.5	$\underline{O}$CH$_3$

[a]at ambient temperature; [b]at 80 °C; [c]non-modified **SWCNTs**. The C 1s peak at 531.1 eV for the PMMA-modified samples (**2a** with 1.6 *at.-%* and **2b** with 0.6 *at.-%*) is probably due to surface contamination (observable at 531.1 and 532.8 eV from SWCNTs, respectively 0.6 *at.-%* and 0.9 *at.-%*).

Non-modified SWCNTs as well as PMMA-Cp (sample **1**) were measured as reference samples in order to facilitate the interpretation of the XPS spectra obtained for the PMMA-Cp modified SWCNTs (**2a** and **2b**). The C 1s binding energy at 284.4 eV, as well as the peak shape found for the SWCNTs, are in a good agreement with literature[278,279] and is therefore used as a template to fit the C 1s spectra of the PMMA-Cp modified SWCNTs samples **2a** and **2b**. Additionally, the π-π* transition, well-known for graphitic and aromatic compounds (sp^2 hybridization), is found at 290.7 eV. A negligible amount of contamination is indicated by weak O 1s components (peaks at 531.1 and 532.8 eV, respectively 0.6 *at.-%* and 0.9 *at.-%*) and is due to atmospheric contact of the samples prior to the XPS measurements. In the case of PMMA-Cp (sample **1**), the C 1s spectrum shows four components consistent with the known structure of PMMA. Aliphatic carbon (-$\underline{C}$H$_2$, -$\underline{C}$H$_3$) with a C 1s signal at 285.0 eV, quaternary carbon (–CH$_2$-$\underline{C}$(CH$_3$)-COOCH$_3$) at 285.8 eV, methoxylic carbon (-O$\underline{C}$H$_3$) at 286.8 eV, and carboxylic carbon (O=$\underline{C}$-OCH$_3$, 289.1 eV) were identified. The corresponding O 1s components were measured at 532.3 eV ($\underline{O}$=C-OCH$_3$) and 533.1 eV (-$\underline{O}$CH$_3$). The binding energies as well as the stoichiometry correspond excellently with former measurements performed on PMMA.[280]

Considering these results, the deconvolution of the spectra of the modified SWCNTs samples **2a** and **2b** evidences that the reaction with PMMA-Cp through the formation of the norbornene entity at the surface of the SWCNTs occurred. However, the differentiation of C-C peaks from aliphatic carbons (primary, secondary and quaternary) of the polymer backbone remains difficult, since the tail of the SWCNT component dominates the high energy shape of the C 1s multiplet (see **Figure 4.6**). Consequently, the quantitative contribution of each identified entity cannot be employed to determine the grafting density. In contrast, the O 1s peaks (532.3 eV and 533.7 eV) indicate directly the uptake of PMMA-Cp as the respective O 1s components are not detectable in the spectra of non-modified SWCNTs. However, compared to the PMMA-Cp reference data, the intensity of the carboxylic component (peaks at 531.1 eV) for the PMMA-Cp modified SWCNTs samples **2a** and **2b** is higher and is probably due to atmospheric contamination as already observed for the non-modified SWCNTs.

The atomic amount of oxygen atoms estimated for the modified SWCNTs **2a** and **2b** (3 and 4.1 *at.-%* respectively) is sufficiently significant to conclude a successful functionalization of the SWCNTs with the polymer PMMA-Cp and to calculate the grafting density of the samples (see **Table 4.6**). Based on the same consideration as for TGA measurements with the specific area of the SWCNTs, the grafting ratio was calculated according to the increase of oxygen content of the modified SWCNTs compared to the non-modified ones. The grafting densities (σ_1, σ_2 and σ_3) were determined by the same procedure as employed for the thermogravimetric results. As for the elemental analysis, the grafting density (σ) was firstly expressed in *at.-%* and subsequently converted into *wt.-%.* The different signals for oxygen and for carbon were respectively summed up to yield the atomic content in oxygen and in carbon to be treated separately according to the signal assignment. The result was subsequently converted into *wt.-%* after adding the contribution of hydrogen from the polymer based on the stoichiometry of the (methyl)methycrylate monomer unit and the oxygen signals of the samples identical to PMMA-Cp reference spectrum. Based on the grafting density (σ) in *wt.-%*, the other grafting densities (σ_1, σ_2 and σ_3) can be expressed using the **Equation 4.1**.

Pleasingly, the same order of magnitude for the grafting ratios observed by XPS as for TGA and EA measurements evidences a successful functionalization of SWCNTs with cyclopentadienyl end-capped poly(methyl methacrylate) through [4+2] DA cycloaddition. To allow a better comparability of all results, **Table 4.6** summarizes the grafting ratios and densities obtained by the three independent techniques, as well as provides average values.

However – as discussed above – the quantitative grafting ratios obtained via XPS appears to be the most reliable.

Table 4.6. Grafting densities of PMMA-Cp functional SWCNTs (**2a**)[a] and (**2b**)[b] based on TGA, EA and XPS results for C and O atomic content.[c]

		Grafting density			
		wt.-% of polymer	mmol·g^{-1}	chain·nm^{-2}	Periodicity [d]
2a	TGA	12.3	0.055	0.025	1523
	EA	19.2	0.082	0.038	1015
	XPS	13.0	0.052	0.024	1615
	Average	**14.8**	**0.064**	**0.029**	**1384**
2b	TGA	18.2	0.086	0.040	968
	EA	22.1	0.098	0.045	850
	XPS	17.9	0.075	0.034	1108
	Average	**20.1**	**0.086**	**0.039**	**975**

[a]at ambient temperature; [b]at 80 °C; [c]the calculation proceeded by considering the reference (non-modified SWCNTs), the polymer (PMMA-Cp), and the theoretical graphene sheet specific surface area (1315 g·m^{-2}); [d]number of carbon atoms covered by one polymer chain grafted on the surface of SWCNTs.

High Resolution Transmission Electron Microscopy (HRTEM)

In order to further support the above quantitative results of the described chemical and physical analysis, HRTEM was performed on the modified and non-modified samples. The HRTEM observations of the functionalized SWCNTs (see **Figure 4.7**) reveals the presence of an approximately 3 nm thick uniform surrounding layer on the surface of the SWCNTs with a diameter of 1 nm, whereas no comparable structure was observed for the non-modified SWCNTs, macroscopically underpinning the functionalization of SWCNTs with PMMA-Cp evidenced by the above quantitative methods. HRTEM observations also enable to justify the comparison of XPS quantification with the results observed by elemental analysis, since an overall 6.8 nm diameter for the covalently modified SWCNTs is observed and corresponds to the XPS sampling depth of 5–10 nm. From the theoretical value obtained by approximating the polymer chain with a disk of radius 2.35 nm, it can be postulated that the polymer chains wrap the cylindrical surface of the SWNCTs and do not stand as rods at the surface.
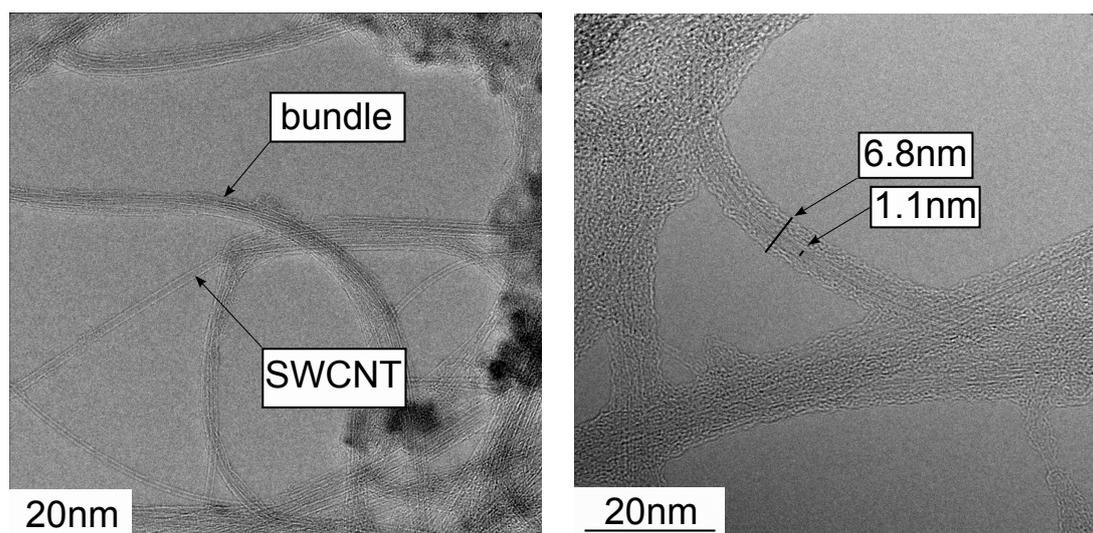
Figure 4.7. HRTEM pictures of non-modified **SWCNTs** (left) and **2b** SWCNTs modified with PMMA-Cp at 80 °C (right).

4.3.3. Conclusions

The [4+2] cycloaddition of Cp end-capped PMMA to SWCNTs was performed under mild conditions, without catalyst and at ambient temperature as well as at 80 °C. The chain-end fidelity of the polymer chains was guaranteed initially via the synthesis of well-defined bromine terminated PMMA-Br polymer strands via ATRP. The facile access to well-defined and quantitatively Cp capped macromolecules via an efficient bromine to cyclopentadiene switch makes the method especially appealing. The functional polymer PMMA-Cp was characterized via ^{1}H NMR spectroscopy and mass spectrometry (ESI-MS) and the presence of the Cp terminus at the chain-end evidenced. The grafting reaction was quantitatively evidenced by macroscopic measurements (TGA, EA), with spectroscopic tools (XPS) and observed at the nanoscopic scale (HRTEM). The grafting density of the polymer chains at the surface of the SWCTNs was estimated on the non pre-treated SWCNTs via the above three independent methods (average grafting density of 0.064 mmol·g^{-1} (0.029 chain nm^{-2}) for samples reacted at ambient temperature and 0.086 mmol·g^{-1} (0.039 chain nm^{-2}) for samples reacted at 80 °C). In addition, HRTEM images confirmed the presence of an amorphous polymer layer (~3 nm) around the SWCNTs after functionalization.

Based on these first successful investigations, it was possible to evidence that the DA reaction between the Cp capped PMMA polymer chains and the SWCNTs occurred, and to determine the grafting density via three independent methods. Based on these very encouraging results, an alternative monomer (*N*-isopropylacrylamide, NIPAM) was chosen to conduct the same DA ligation for the functionalization of SWCNTs and to equip them with

specific properties, especially of a thermo-responsive nature (see Chapter 5).

Chapter 5 – SWCNTs functionalization with thermo-responsive cyclopentadienyl end-capped poly(*N*-isopropylacrylamide)
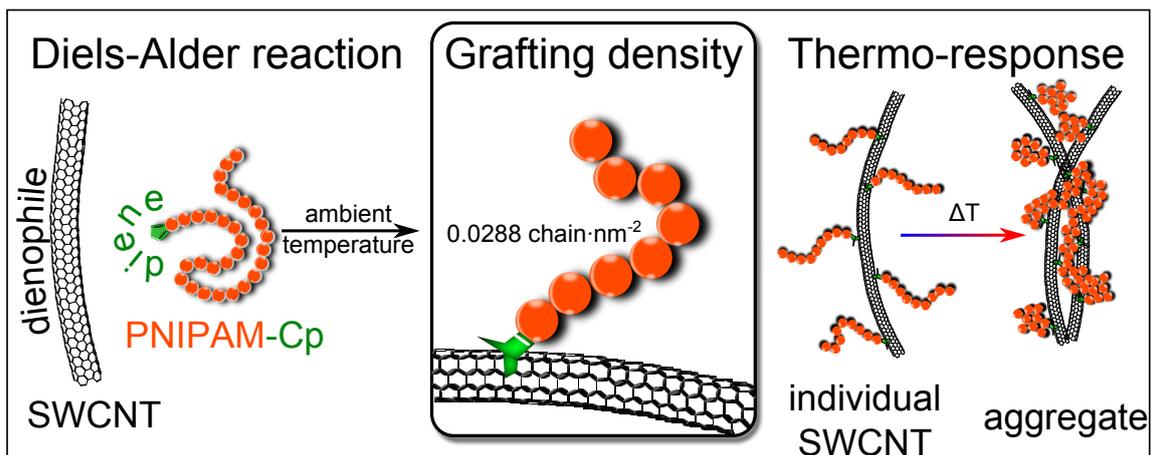
5.1. Introduction

Chapter 5 focuses on the functionalization of SWCNTs via ambient temperature DA chemistry with PNIPAM as stimuli-responsive polymer, to afford water dispersible SWCNTs with thermo-responsive properties, potentially suitable for carbon nanotube dispersion in highly polar polymer matrices.

A range of articles describes the functionalization of SWCNTs or MWCNTs with PNIPAM or alternative thermo-responsive polymers, underlining the importance of combining CNTs with stimuli-responsive materials. Indeed, enhancing the mechanical properties of materials via the incorporation of fillers or nano-fillers, such as CNTs, appears to be intertwined with the development of mechanically intelligent materials, as recently summarized by Hsu *et al.* on thermo-responsive and mechanically-adaptive polymer nanocomposites.[281] Being able to react to a thermal stimulus, the combination of PNIPAM and CNT composites opens new fields of application. For example, Zhang *et al.* developed a very impressive actuator, sensitive to heat, by enhancing the thermal response of PNIPAM hydrogels when mixed with MWCNTs.[282] The first study evidencing the properties of PNIPAM and CNTs appeared in 2004 from Kong *et al.* and was essentially focused on the covalent attachment of CNTs to PNIPAM.[283] After an acidic treatment of the MWCNTs, a *'grafting from'* approach was followed via the attachment of an atom transfer radical (ATRP) initiator to polymerize the monomer. Leading on from there, other research groups developed similar strategies,[284] including the reversible addition fragmentation chain transfer (RAFT) polymerization of monomers from CNT surfaces,[285,286,287] including the formation of block copolymer architectures.[288]

Despite these numerous examples, seldom are past studies describing a *'grafting to'* approach and − even more importantly − a non-destructive method for functionalizing CNTs with polymers, let alone with PNIPAM (see section 2.5.2). Adronov and co-workers performed a pseudo *'grafting to'* approach employing azide end-capped PNIPAM via a [3+2] Huisgen cycloaddition,[289] however the MWCNTs were pre-functionalized with an alkyne moiety. Only one article presents a *'grafting to'* approach of PNIPAM leaving the SWCNTs intact via a [2+1] nitrene cycloaddition.[290] The functionalization occurs by heating at 160 °C, and the relatively high temperature may cause the polymer to degrade. On the contrary, the *'grafting to'* method firstly enables a precise characterization of the synthetic polymer before being attached to the carbon material, as well as an efficient control of the grafting density: a detailed pre-characterization is not possible when employing the *'grafting from'* approach, since the grafted polymer strands remain inaccessible for detailed molecular analysis (unless

cleaved) and may even be interconnected and form a network when free radical polymerization is involved. Secondly, the main advantage of using the DA reaction remains, as noted earlier, in employing carbon nanotubes without any pre-treatment – the CNT surface acts as a dienophile (see section 2.5).

Preparing PNIPAM with a reactive diene end-group, e.g. Cp, requires exquisite control of the polymerization and efficient successive reactions leading to the desired chain termini. In terms of providing well-defined polymer structures with high end-group fidelity, RAFT polymerization has advantages over ATRP when polymerizing NIPAM. The polymerization of NIPAM by ATRP has raised the interest of polymer chemists since 1999.[291] The main difficulty in maintaining the living character during the polymerization of NIPAM or (meth)acrylamide based monomers in general via ATRP is associated with a cyclization reaction due to the elimination of the bromine end-group. Many strategies were developed to overcome the elimination issue. Firstly, a halide exchange strategy enables the incorporation of a chlorine atom as end-group, instead of a bromine atom, leading to a stronger halogen-carbon bond, minimizing the risk of cyclization and elimination.[292] Secondly, the use of an alternative ligand such Me$_6$TREN enabled the control of the polymerization up to reasonable conversions.[293,294] Yet all of these techniques involve a terminal chlorine atom, which is less labile than a bromine atom, thus leading to less intramolecular cyclization.[295] The most efficient route to introduce Cp at the terminus of a polymer chain is via the substitution of a bromine atom using nickelocene.[274] A chlorine atom cannot be employed in this procedure, thus disallowing the use chlorine based ATRP as a base material for the Cp-capped PNIPAM.

Thus, an alternative approach for the preparation of high end fidelity PNIPAM-Cp had to be identified. Although halides are not being introduced during the polymerization, the RAFT process of (meth)acrylamide based monomers is well-developed and modular strategies enable the modification of the introduced end-group.[296] These advantages led to perform the sequence described in **Scheme 5.1** to synthesize a Cp-capped PNIPAM. Initially, PNIPAM with an azide end-group (**P1**) is synthesized, subsequently conjugated with a bromine functional alkyne (2-propynyl 2-bromo-2-methylpropanoate) to afford the brominated polymer (**P2**). Next, **P2** is subjected to a nucleophilic substitution via the nickelocene-process[274] to yield the desired Cp end-capped PNIPAM (**P3**). The synthesized Cp-terminal PNIPAM polymer is subsequently dissolved in a dispersion of SWCNTs at ambient temperature (condition *a*) or 80 °C (condition *b*) to lead to the PNIPAM-functionalized SWCNTs (**P3a-SWCNT** and **P3b-SWCNT**).
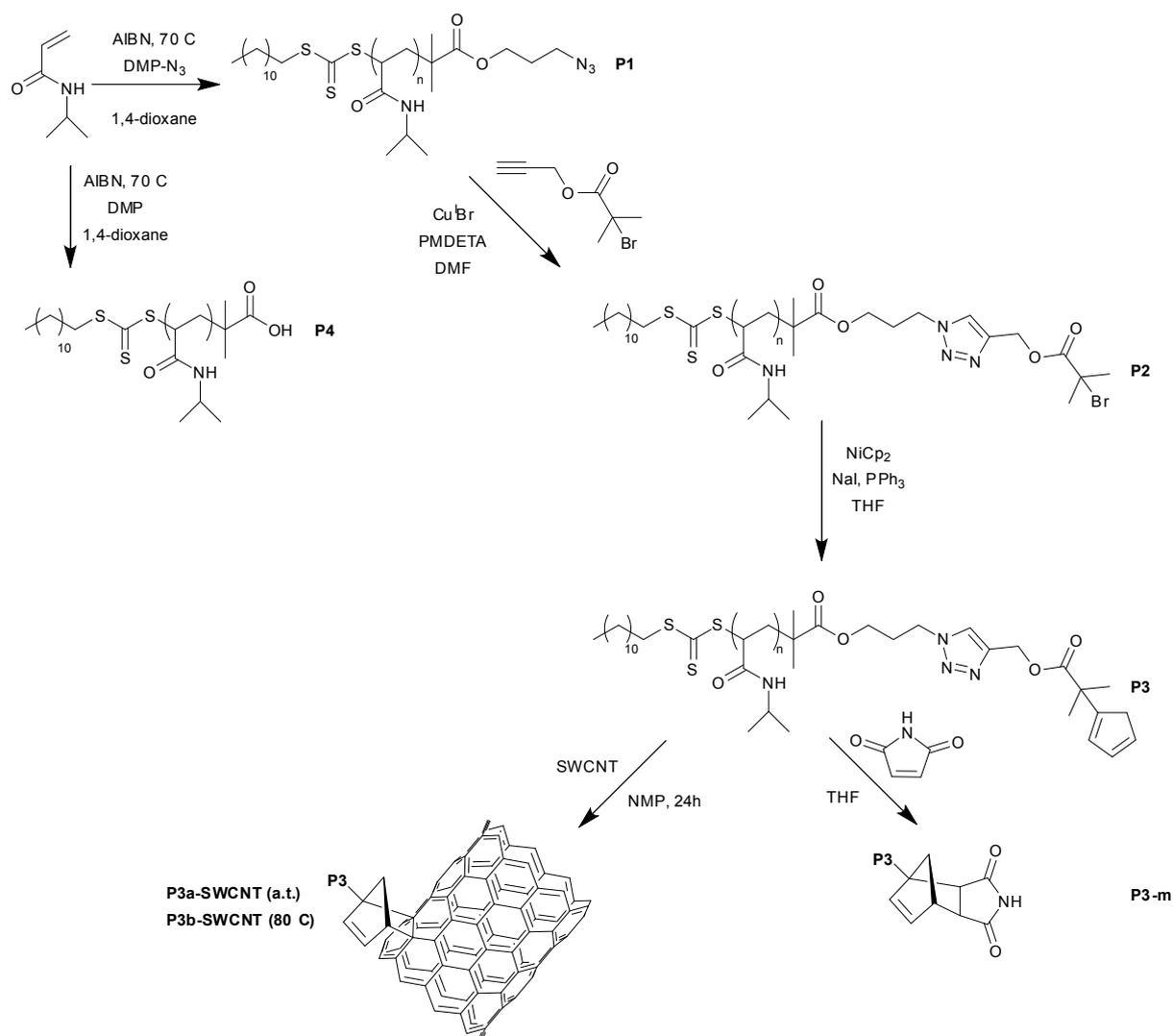
Scheme 5.1. Synthetic route to cyclopentadienyl end-capped PNIPAM (**P3**) and its intermediates carrying azide (**P1**) and bromine (**P2**) end-groups. PNIPAM with an acidic end-group is employed as reference (**P4**). The functionality of **P3** was assessed with *N*-maleimide leading to **P3-m**. **P3a-SWCNT** and **P3b-SWCNT** were reacted with **P3** in *N*-methylpyrrolidone (NMP) at ambient temperature (a.t.) and at 80 °C, respectively.

After each synthetic step, the successive PNIPAM (**P1-3**) as well as the non-DA reactive PNIPAM (**P4**) were characterized via ^{1}H NMR spectroscopy, SEC, ESI-MS and FTIR spectroscopy (section 5.2). The diene character of the polymer **P3** was further verified via ESI-MS by reacting with *N*-maleimide (**P3-m**) in section 5.2.3. The PNIPAM functionalized SWCNTs were characterized via TGA, EA and XPS to quantify the grafting density, and compared with a reference (**P4-SWCNT**), as well the synthesized polymers to ease the interpretation and the grafting density evaluation (refer to section 5.3). Finally, in section 5.3.3, the thermo-sensitive product **P3a-SWCNT** was characterized via ultraviolet (UV) turbidity measurements to determine the thermo-responsive nature of the dispersion, as

well as via DLS to evaluate the hydrodynamic diameter of the hybrid materials as a function of temperature.

5.2. Synthesis and characterization of PNIPAM-Cp

5.2.1. Polymerization and end-group transformation

The list of the employed materials can be found in Chapter 3 (section 3.12.2). The details of synthesis and characterization of 2-dodecylsulfanylthiocarbonylsulfanyl-2-methylpropionic acid (DMP), 2-dodecylsulfanylthio-carbonylsulfanyl-2-methylpropionic acid 3-azidopropyl ester (DMP-N$_3$), synthesized according to literature,[297,298] and 2-propynyl 2-bromo-2-methylpropanoate[299] can be found in the appendix section (**Synthesis A1.**).

Synthesis of NIPAM with azide end-group (P1)

NIPAM (12 g, 0.106 mol), DMP-N$_3$ (0.711 g, $1.59 \cdot 10^{-4}$ mol) and AIBN (26.1 mg, $1.58 \cdot 10^{-4}$ mol) were weighed in a 200 mL Schlenk flask. 57.6 mL of 1,4-dioxane was added and 0.1 mL of toluene added as marker for determining the conversion by ^{1}H NMR spectroscopy. The solution was subjected to five freeze-pump-thaw cycles prior to heating in an oil bath at 70 °C. The polymerization was stopped after 2 h at 70% conversion (determined by ^{1}H NMR spectroscopy) and the mixture dried under vacuum. The polymer was precipitated in cold ether three times, dried and dialyzed in water for three days in the dark with frequent changes of water. The residual solution was freeze-dried for 48 h in the dark (M_n(target) = 5800 g·mol^{-1}, M_n(NMR) = 5300 g·mol^{-1}, M_n(SEC) = 5100 g·mol^{-1}, $Đ$ = 1.11, see **Figure 5.1**).

Synthesis of PNIPAM with bromine end-group (P2)

1.2 g (0.226 mmol, 1.0 eq) of dry **P1** was dissolved in 5 mL dry DMF, with PMDETA (19.6 mg, 0.113 mmol, 0.5 eq) and 2-propynyl 2-bromo-2-methylpropanoate (60.3 mg, 0.294 mmol, 1.3 eq) and purged with nitrogen for 30 min. The solution was transferred via canula to Cu(I)Br (16.2 mg, 0.113 mmol, 0.5 eq) under a nitrogen atmosphere. The reaction was stirred for 24 h at ambient temperature. Once dried under vacuum, the residue was precipitated in cold ether and dialyzed for three days to eliminate the copper. The solution was freeze-dried for 48 h yielding a white powder. (M_n(SEC) = 5400 g·mol^{-1}, $Đ$ = 1.11, see **Figure 5.1**).

Synthesis of PNIPAM with Cp end-group (P3)

Immediately after freeze-drying, 1.0 g (0.189 mmol, 1 eq) of **P2** was weighed into a Schlenk flask and PPh$_3$ (99.0 mg, 0.377 mmol, 2 eq) and NaI (169.7 mg, 0.754 mmol, 6 eq) were added and evacuated overnight. The mixture was dissolved in 5 mL of dry THF and NiCp$_2$ (142.5 mg, 0.252 mmol, 4 eq) was subsequently transferred to the **P2** mixture via canula after dissolution in dry THF under a nitrogen atmosphere. The reaction was left overnight until the solution turned purple. The solution was passed over a short column of neutral alumina, precipitated in cold ether and dialyzed for three days. The residual solution was freeze-dried for 48 h (M_n(SEC) = 5400 g·mol^{-1}, $Đ$ = 1.13, see **Figure 5.1**).

Synthesis of PNIPAM with DMP (P4)

The polymerization of NIPAM was performed with DMP as described for **P1** and was conducted to 70% of conversion (determined by ^{1}H NMR spectroscopy) to a similar molecular weight as **P1** (M_n(NMR) = 6200 g·mol^{-1}, M_n(SEC) = 5800 g·mol^{-1}, $Đ$ = 1.15, see **Figure 5.1**).

Measurements performed via SEC on the different polymers enable to determine the polydispersity and indicate the molecular weight of the synthesized polymers. However, the overlay of the SEC traces **Figure 5.1**, show a slight evolution in the retention time from the successive end-group transformation from PNIPAM **P1** (azide end-group), **P2** (bromine terminated), finally **P3** (Cp-terminated).

An increase in retention time corresponds to an increase in the hydrodynamic volume of the polymer, caused by the introduction of the 2-propynyl 2-bromo-2-methylpropanoate moiety and by a probable gain of rigidity at the end-chain from the introduced triazole group. These first observed shifts in retention time support the transformation from **P1** to **P2** (see **Figure 5.1**), which is fully confirmed by the ^{1}H NMR spectroscopy and ESI-MS characterization (section 5.2.2). The polydispersity index ($Đ$) remains almost unchanged when going from **P1** to **P3**. The reference polymer with the acidic end-group **P4** was synthesized with similar molecular weight and $Đ$. The molecular weight of the starting polymer **P1** and the reference polymer **P4** can also be determined via ^{1}H NMR spectroscopy and the analysis of the spectra returns similar values as those obtained via SEC (M_n(NMR) = 5300 g·mol^{-1} and M_n(SEC) = 5100 g·mol^{-1} for **P1**, M_n(NMR) = 6200 g·mol^{-1} and M_n(SEC) = 5800 g·mol^{-1} for **P4**). The NMR molecular weight was determined considering the ratio of the integral signal of the protons of the methyl end-group (denoted *g* in **P1**, see **Figure 5.2**) to the

methyl proton associated with the polymer chain (denoted k in **P1**, see **Figure 5.2**). The ^{1}H NMR spectrum of **P4** is depicted in **Figure 5.3** and the estimation of the molecular weight was carried out in a similar fashion (with protons denoted i and e).
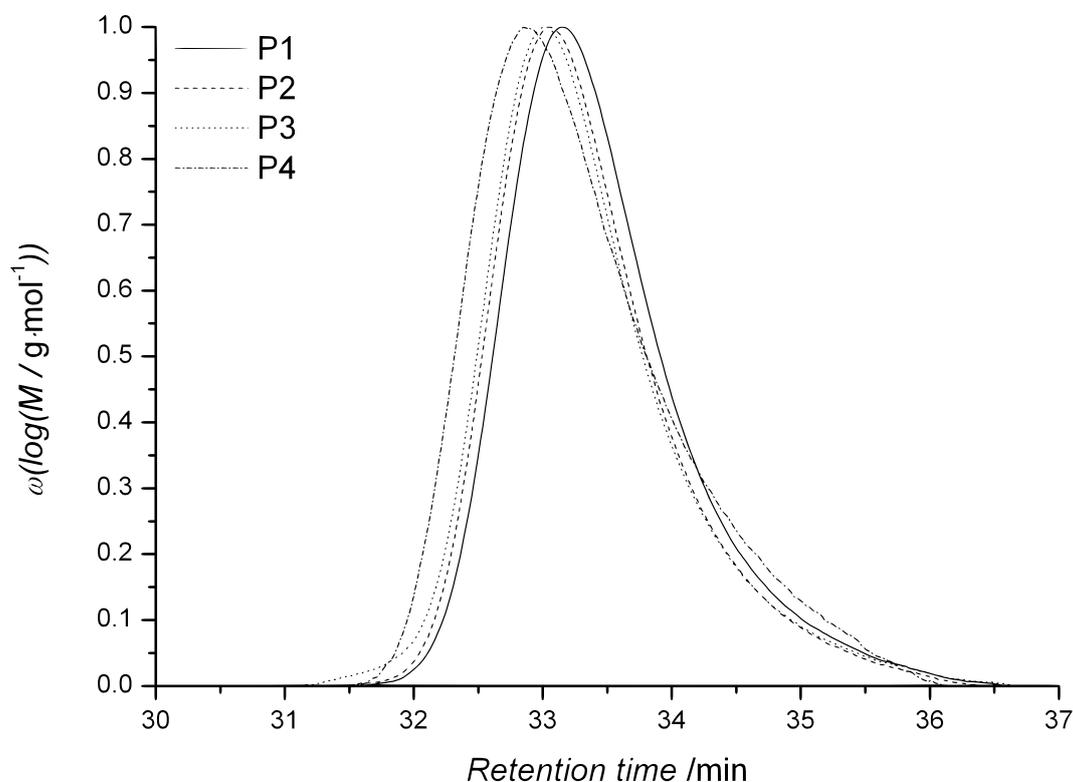
Figure 5.1. SEC traces of PNIPAM with different end-group (azide, **P1**, straight line), (bromine, **P2**, dashed line), (Cp, **P3**, dotted line), and (acidic, **P4**, dash-dotted line) in THF.

5.2.2. Chain-end fidelity

^{1}H Nuclear Magnetic Resonance spectroscopy (NMR)

As previously mentioned, the main advantage of the *'grafting to'* approach is the ability to characterize the polymer, and in particular its sequential end-group modification. The additional peaks of species, observed in the ^{1}H NMR spectra for each synthetic step, confirm the success of the end-modification. From **Figure 5.2**, the signal of the aliphatic protons a and c proves that the expected azide end-group of **P1** is present (**Figure 5.2**, top). For **P2** (**Figure 5.2**, middle), the appearance of the new signals from the protons denoted m, n and o confirms the attachment of the 2-propynyl 2-bromo-2-methylpropanoate. The success of the final reaction to synthesize the desired Cp-capped PNIPAM **P3** is confirmed by the presence of the p and q protons associated with the cyclopentadienyl group (**Figure 5.2**, bottom). The ^{1}H NMR spectrum of **P4** is depicted in **Figure 5.3**, the estimation of the molecular weight was carried out in a similar fashion (with protons denoted i and e).
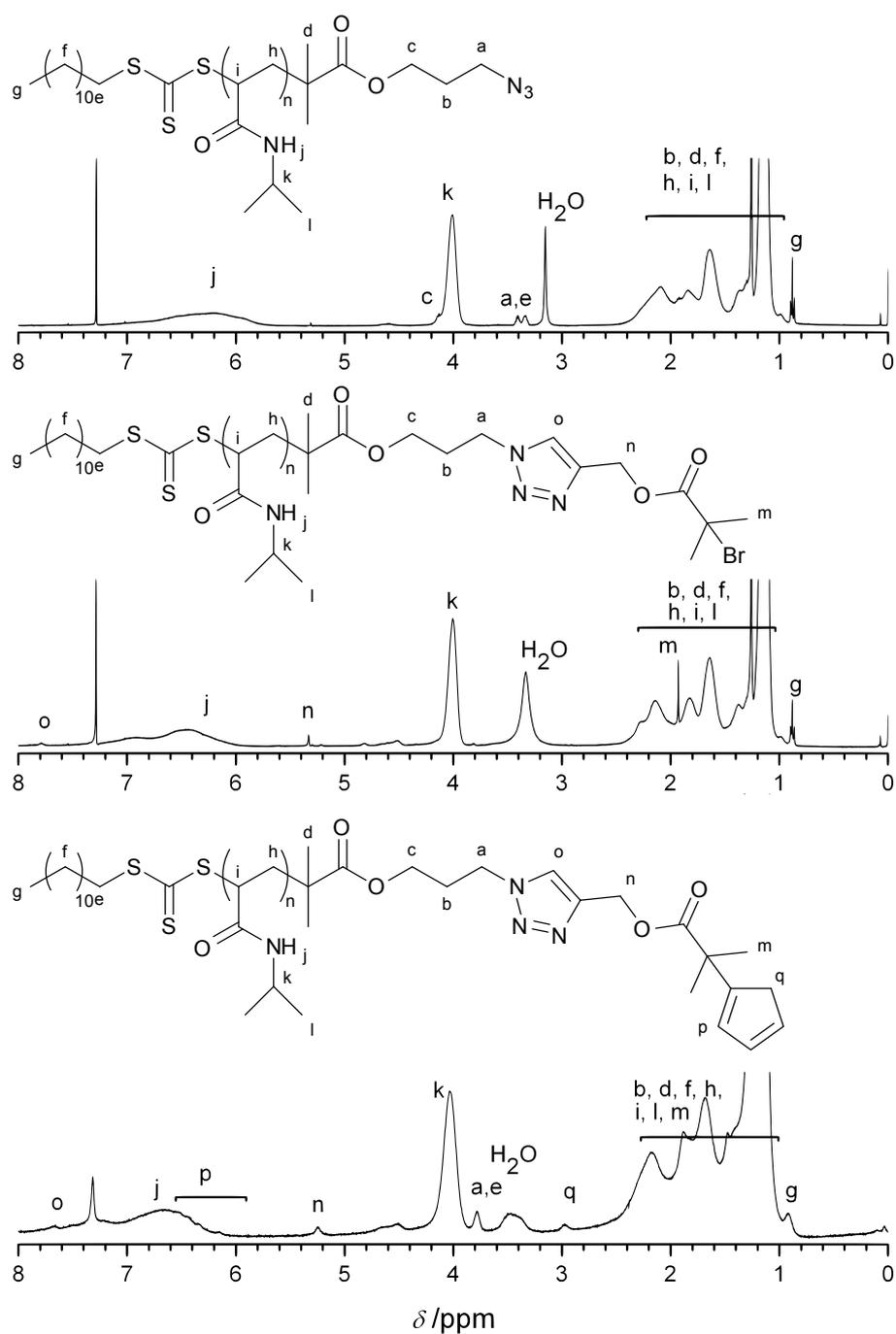
Figure 5.2. ^{1}H NMR spectra of PNIPAM with different end-groups (azide, **P1**, top), (bromine, **P2**, middle), and (Cp, **P3**, bottom).
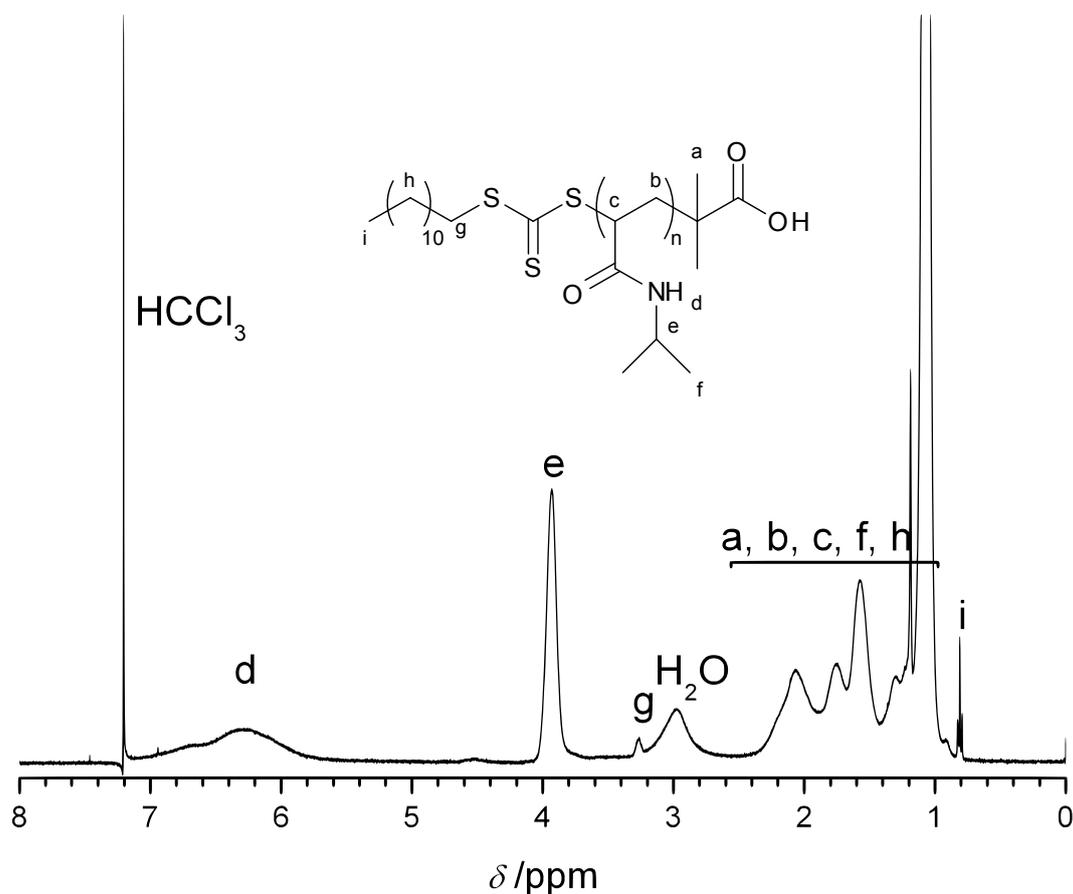
Figure 5.3. ^{1}H NMR overview spectrum of PNIPAM **P4**.

Fourier Transform Infrared spectroscopy (FTIR)

Furthermore, FTIR spectra additionally evidence the disappearance of the azide end-group from **P1** when ligated with the alkyne to generate **P2** (**Figure 5.4**). The FTIR spectrum of **P3** was also recorded, yet no particular change in the spectrum compared to **P2** was observed. The FTIR spectrum of **P4** is shown in the appendix section (**Figure A1**).
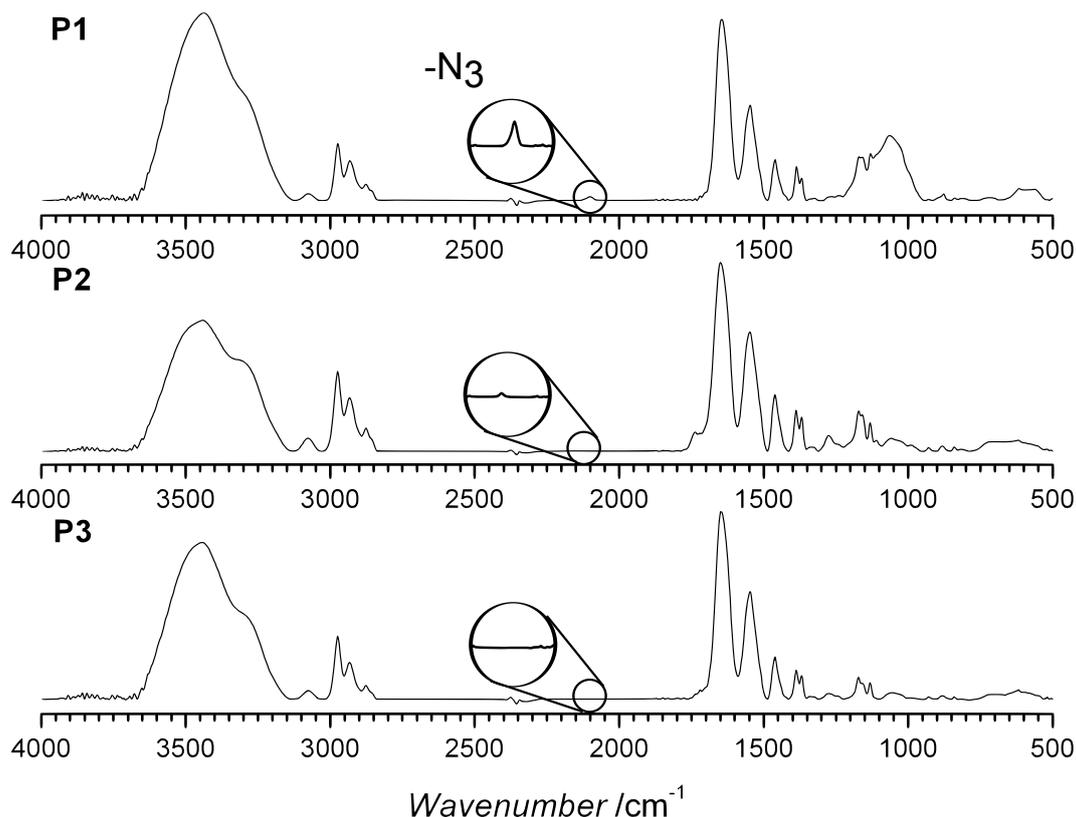
Figure 5.4. FTIR spectra of PNIPAM with different end-group (azide, **P1**), (bromine, **P2**), and (Cp, **P3**) in KBr pellets with recognizable azide peak for **P1** at 2096 cm^{-1} (zoomed part of the spectra).

Mass Spectrometry (ESI-MS)

A final characterization of the synthesized polymers was performed via ESI-MS. The spectra depicted in **Figure 5.5** display the change of the *m/z* ratio for the polymers **P1**, **P2** and **P3**.

The peaks from the ESI-MS spectrum of **P1** (**Figure 5.5**, top) are separated by 56.54 *m/z* corresponding to the monomer unit of the polymer in its doubly charged state (single charge 113.08 *m/z*). **Table 5.1** summarizes the theoretical *m/z* values expected for the doubly charged polymer species with an indication of the number of monomer units incorporated into the polymer chain, as well as the obtained experimental values.

The difference between the theoretical and the experimental values (Δ) remains below 0.24 *m/z* proving that the structure of polymer **P1** is the same as in **Scheme 5.1**. The isotopic pattern with a high resolution and the corresponding simulation are depicted in **Figure 5.6** (spectra top left) at 2960.54 *m/z*. The *m/z* shift observed for **P2** (**Figure 5.5**, middle) of 101.99 corresponds exactly to the addition of 2-propynyl 2-bromo-2-methylpropanoate doubly charged (203.98 *m/z* single charged). The comparison between the experimental and

theoretical *m/z* values is also within an acceptable error range (Δ below 0.34, see **Table 5.1**).
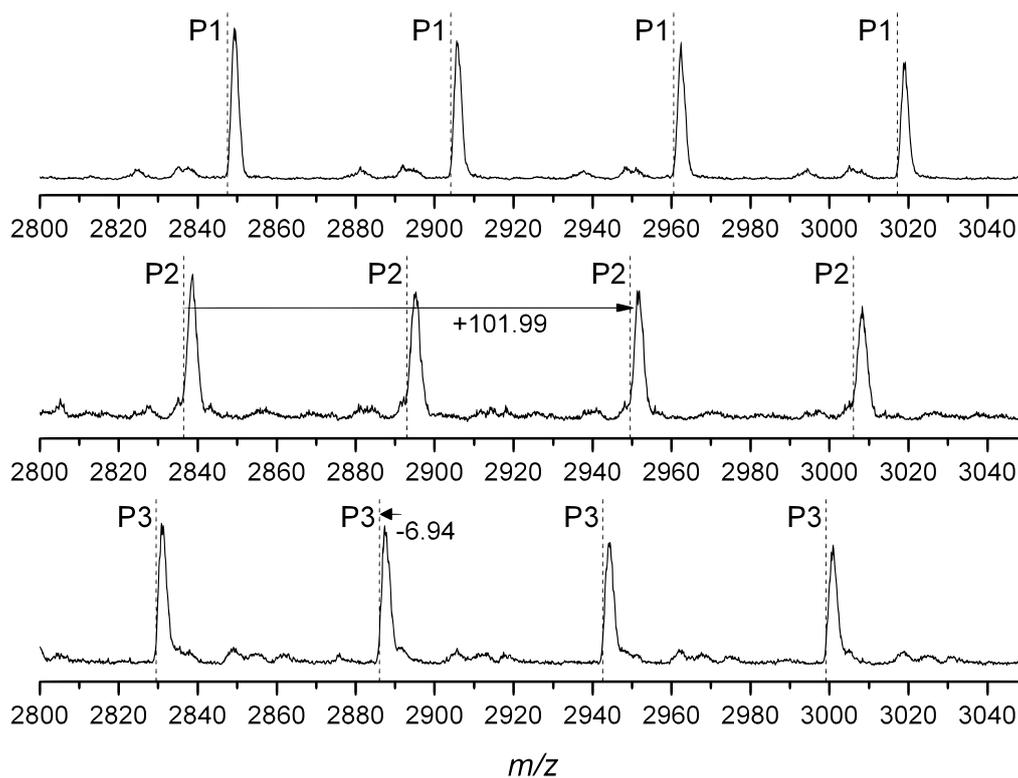
Figure 5.5. ESI-MS spectra of doubly charged PNIPAM with different end-groups (azide, **P1**), (bromine, **P2**), and (Cp, **P3**). All spectra are recorded via direct infusion.

In **Figure 5.6** (spectra top right), the detailed isotopic pattern at 2949.54 *m/z* and the simulated signal are represented, being in excellent agreement with each other. Finally, the success of the last reaction for exchanging the bromine end-group to Cp is observed in the ESI-MS spectrum of **P3** (**Figure 5.5**, bottom) by a negative *m/z* shift of -6.94. Calculating the replacement of a bromine (78.92 *m/z*) to a Cp (C_5H_5, 66.05 *m/z*), the *m/z* shift for single charged species should be -12.87 *m/z*, and for doubly charged species -6.44 *m/z*. The difference of 0.5 *m/z* between the experimental and theoretical values is acceptable, considering the deviation observed earlier (Δ = 0.25 for **P1**, or 0.34 for **P2**). Considering the theoretical and experimental *m/z* values, the deviation remains below 0.40 *m/z*, indicating that the transformation of **P2** to **P3** is successful. Moreover, the simulation of the isotopic pattern at 2942.66 *m/z* for **P3** is in accordance with the detailed spectrum obtained in the same range (see **Figure 5.6**, spectra down left).

A similar study was conducted for **P4**, and the ESI-MS spectra as well as the summarizing table can be found in **Figure A2** and **Table A1** in the appendix section respectively. The detailed zoom ESI-MS spectrum **Figure 5.6** (observed and simulated spectra bottom right) depicts the accuracy of ESI-MS as a very effective mass spectrometry

method to characterize the different PNIPAM polymer chains.

Table 5.1. Summary of ESI-MS data for PNIPAM with different end-groups (azide, **P1**), (bromine, **P2**), and (Cp, **P3**). All spectra are recorded via direct infusion and the detected species are doubly charged.

Species	n [a]	Formula	m/z		
			th.	exp.	Δ
P1	46	$[C_{296}H_{543}N_{49}O_{48}S_3Na_2]^{2+}$	2847.53	2847.45	0.08
	47	$[C_{302}H_{544}N_{50}O_{49}S_3Na_2]^{2+}$	2904.07	2903.82	0.25
	48	$[C_{308}H_{555}N_{51}O_{50}S_3Na_2]^{2+}$	2960.61	2960.54	0.07
	49	$[C_{314}H_{566}N_{52}O_{51}S_3Na_2]^{2+}$	3017.15	3016.91	0.24
P2	44	$[C_{291}H_{530}N_{47}O_{48}S_3BrNa_2]^{2+}$	2836.43	2836.09	0.34
	45	$[C_{297}H_{541}N_{48}O_{49}S_3BrNa_2]^{2+}$	2892.97	2892.91	0.06
	46	$[C_{303}H_{552}N_{49}O_{50}S_3BrNa_2]^{2+}$	2949.51	2949.54	0.03
	47	$[C_{309}H_{563}N_{50}O_{51}S_3BrNa_2]^{2+}$	3006.06	3006.00	0.06
P3	44	$[C_{296}H_{535}N_{47}O_{48}S_3Na_2]^{2+}$	2829.49	2829.09	0.40
	45	$[C_{302}H_{546}N_{48}O_{49}S_3Na_2]^{2+}$	2886.03	2885.91	0.12
	46	$[C_{308}H_{557}N_{49}O_{50}S_3Na_2]^{2+}$	2942.58	2942.66	0.08
	47	$[C_{314}H_{568}N_{50}O_{51}S_3Na_2]^{2+}$	2999.12	2998.82	0.30

[a] number of monomer units.
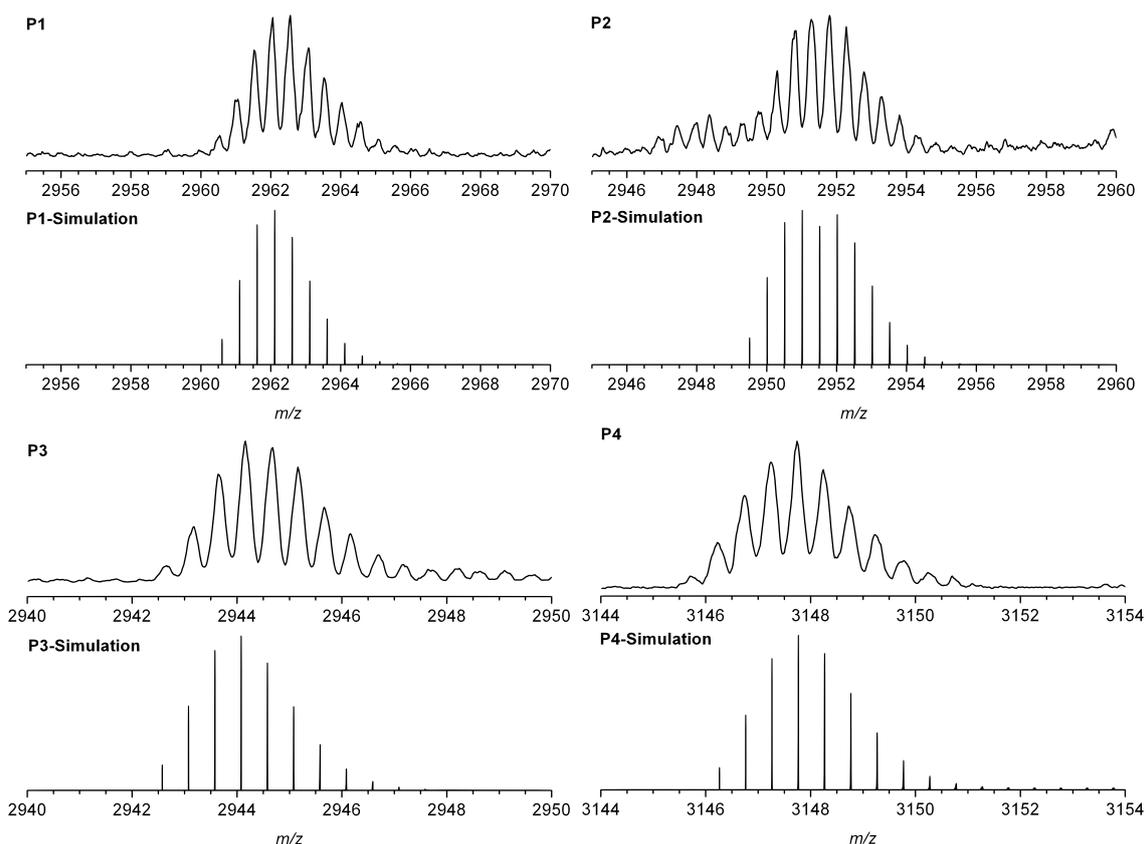
Figure 5.6. ESI-MS isotopic pattern of doubly charged PNIPAM with different end-groups (upper spectra) and the respective simulated isotopic pattern (lower spectra): **P1** (azide, top left spectra), **P2** (bromine, top right), **P3** (Cp, bottom left) and **P4** (acidic end-group, bottom right). The spectra are recorded via direct infusion.

5.2.3. Model ligation of PNIPAM-Cp with *N*-maleimide (ESI-MS)

Ligation of P3 with N-maleimide (P3-m)

1 mg of **P3** (0.1886 μmol, 1.0 eq) was dissolved in an excess of *N*-maleimide (0.1 mg, 1.03 μmol, 10 eq) in dry THF and left to react at ambient temperature for 2 h. The mixture was subsequently dried and analyzed directly via ESI-MS.

The final proof evidencing the ability of Cp-capped PNIPAM **P3** to react in a DA reaction can be found in the ESI-MS spectrum of the obtained product when reacting **P3** with *N*-maleimide (**P3-m**. see **Figure 5.7**, spectrum at the bottom). The diene capped polymer (**P3**) reacts with the dienophile (*N*-maleimide), leading to a positive shift of 97.02 *m/z* (single charged species, 48.51 for doubly charged species). The observed *m/z* shift is, however, 48.00 *m/z* probably due to experimental error (Δ below 0.25, see **Table 5.2**) or the elimination of one maleimide proton.
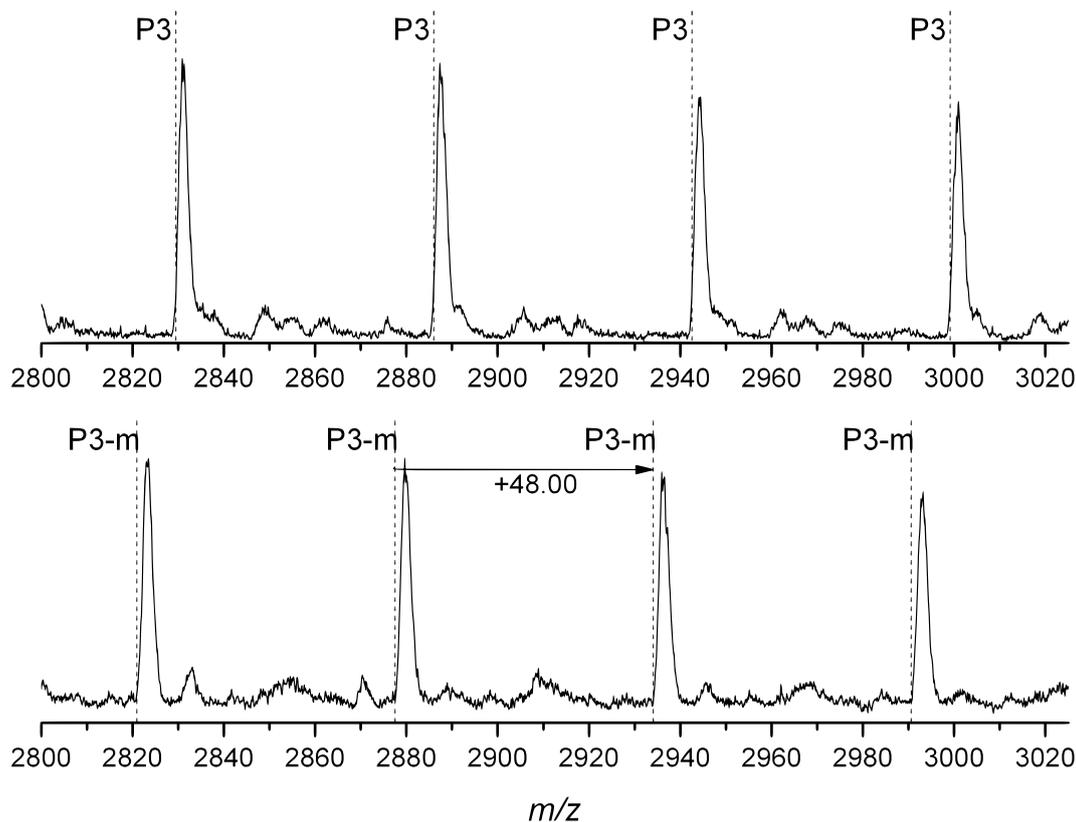
Figure 5.7. ESI-MS spectra of doubly charged PNIPAM with Cp end-group conjugated with *N*-maleimide (**P3-m**) in THF. All spectra are recorded via direct infusion.

Table 5.2. Summary of ESI-MS data for PNIPAM with Cp end-group clicked with *N*-maleimide (**P3-m**).

Species	n[a]	Formula	m/z		
			th.	exp.	Δ
	42	$[C_{288}H_{516}N_{46}O_{48}S_3Na_2]^{2+}$	2764.91	2765.16	0.25
	43	$[C_{294}H_{527}N_{47}O_{49}S_3Na_2]^{2+}$	2820.95	2820.91	0.04
P3-m	44	$[C_{300}H_{538}N_{48}O_{50}S_3Na_2]^{2+}$	2877.50	2877.55	0.05
	45	$[C_{306}H_{549}N_{49}O_{51}S_3Na_2]^{2+}$	2934.04	2934.00	0.04
	46	$[C_{312}H_{560}N_{50}O_{52}S_3Na_2]^{2+}$	2990.58	2990.82	0.24

[a] number of monomer units.

According to the characterization performed via ^{1}H NMR spectroscopy and ESI-MS, the modification of the end-groups from **P1** to **P3** is successful, and the diene character of the Cp-capped PNIPAM **P3** is proven. The reaction with *N*-maleimide is similar to the functionalization performed on the SWCNTs surface reacting as dienophile, and the Cp-capped PNIPAM as diene. The results described below describe and quantify the grafting of

P3 onto the surface of untreated SWCNTs under very mild conditions, e.g. in solution, at ambient temperature and without catalyst.

5.3. Characterization of functionalized PNIPAM-Cp SWCNTs

5.3.1. Synthesis

Functionalization of SWCNTs (P3a-SWCNT and P3b-SWCNT)

30 mg of SWCNTs were dispersed in 300 mL NMP in an ultrasonic bath and purged with nitrogen for 1 h. 300 mg of Cp-terminated PNIPAM (**P3**) was added. The mixture was stirred at ambient temperature (**P3a-SWCNT**) for 24 h under a nitrogen atmosphere. The dispersion was filtered over a PFTE 0.2 μm membrane, rinsed with 100 mL THF and dried under vacuum. The same procedure is performed to generate **P3b-SWNCT** at 80 °C instead of ambient temperature.

Preparation of SWCNT reference (P4-SWCNT)

The same procedure as **P3a-SWCNT** was followed, with **P4** instead of Cp terminated PNIPAM (**P3**).

The reaction between the Cp-capped PNIPAM (**P3**) and the SWCNTs was conducted after dispersion of the SWCNTs in *N*-methylpyrrolidone, at ambient temperature and at 80 °C, leading to the products **P3a-SWCNT** and **P3b-SWCNT** respectively. These two products were characterized via TGA, EA and XPS to determine the grafting density. The same characterization was performed for the SWCNTs treated under the same conditions as **P3a-SWCNT** (ambient temperature) with **P4**, which does not feature a Cp-function (product denoted **P4-SWCNT**). For each method, the polymers **P1**, **P2**, **P3** and **P4**, the pristine SWCNTs (**p-SWCNT**), the treated SWCNTs with **P3** (**P3a-SWCNT** and **P3b-SWCNT**), and the reference sample **P4-SWCNT** were characterized.

5.3.2. Results and discussion

Thermogravimetric Analysis (TGA)

Figure 5.8 depicts the thermogravimetric profiles of all samples (except the polymer **P2** for clarity). The thermogravimetric profile of **P2** can be found in the appendix (**Figure A3**), as well as the derivative curves obtained from the TGA traces for the rest of the samples (**Figure A4**). The same procedure for analysis was carried out as in Chapter 4 (section 4.3.2). The summary of the identified degradation points for the polymers and for the SWCNTs can be found in the appendix (**Table A2** and **Table A3**).
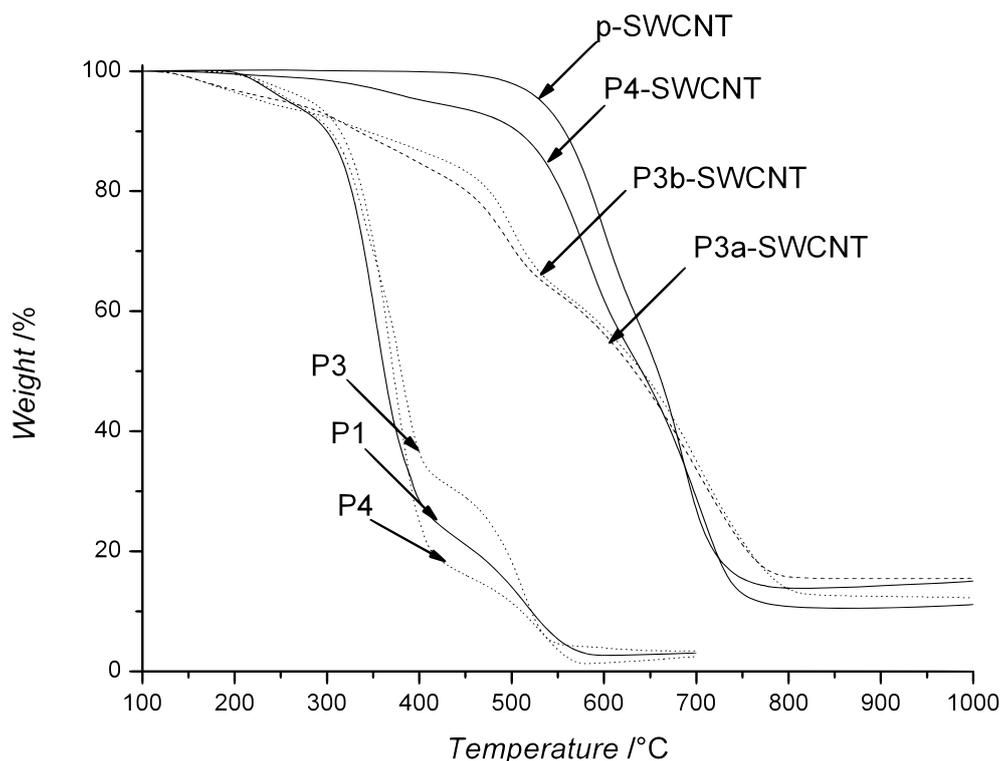
Figure 5.8. Thermogravimetric profiles of PNIPAM with different end-groups (azide, **P1**), (Cp, **P3**) and (acid, **P4**), as well as pristine SWCNTs (**p-SWCNT**), functionalized with Cp-terminated PNIPAM at ambient temperature (**P3a-SWCNT**), and at 80 °C (**P3b-SWCNT**). All samples are measured in air atmosphere with a heat flow of 10 °C·min^{-1}, undergoing a preliminary isothermal step at 100 °C for 30 minutes.

The degradation profiles for the polymers **P1**, **P3** and **P4** are similar: their degradation occurs at approximatively the same temperatures. For **P3**, the successive temperatures of maximal degradation T_m obtained from the derivative of the thermogravimetric profile are 245, 345, 380 and 510 °C. For **P4**, only three temperatures of maximal degradation (T_m) can be identified at 235, 375 and 540 °C. One should note that the penultimate degradation finishes between 425–440 °C for all polymers. At these temperatures **p-SWCNT** starts to decompose (T_m = 685 °C for the first transformation). At higher temperatures, a residue of 13 *wt.-%* is observed, probably due to catalyst residues. When considering the treated SWCNTs, one can observe that degradations occur below 430 °C, implying that organics are present. At higher temperature, for **P3a-SWCNT**, **P3b-SWCNT** and **P4-SWCNT**, a degradation at similar T_m (respectively 390, 395 and 375 °C) as for **P3** (T_m = 380 °C) is observed, due to the presence of the polymer. Then, above the temperature range of 545–580 °C, the last degradation (T_m = 700 °C) occurs as for **p-SWCNT**. These first observations via TGA reveal the presence of polymer in the three samples of SWCNTs treated with the polymers **P3** and **P4**, yet the quantity (*wt.-%*) of polymer present in the different samples

varies as depicted in **Table 5.3**.

Table 5.3. Determination of the grafting density based on the thermogravimetric analysis of SWCNTs functionalized with Cp-end-capped PNIPAM (**P3**) at ambient temperature (**P3a-SWCNT**), at 80 °C (**P3b-SWCNT**) and SWCNTs mixed with PNIPAM with acidic end-group (**P4-SWCNT**).

Sample	$wt.\text{-}\%$ at T_f^a	Grafting density		
		mmol·g^{-1}	molecule·nm^{-2}	Periodicity^e
P3a-SWCNT	83.9^b	0.0601	0.0275	1384
P3b-SWCNT	86.2^c	0.0515	0.0236	1616
P4-SWCNT	94.6^d	0.0215	9.83·10^{-3}	3880

^{a}weight percentage before the final degradation temperature T_f; ^bT_f = 410 °C; ^cT_f = 410 °C; ^dT_f = 420 °C; ^{e}number of C atoms of the SWCNTs surrounded by a polymer chain.

The grafting density is calculated by considering the quantity of sample that degrades below T_f in the range 410–420 °C (final degradation temperature of the penultimate degradation of the considered samples). For **P3a-SWCNT** and **P3b-SWCNT**, the residual weight percentage due to the polymer degradation is close to 83.9 and 86.2%, respectively. For the reference sample **P4-SWCNT**, the weight percentage is 94.6%: as expected, a very low amount of polymer on the surface of the SWCNTs is observed, probably due to polymer chains adsorbed at the SWCNTs' surface. For a better understanding, the grafting density can be expressed in alternative units (see **Table 5.3**). The grafting density expressed in molecule·nm^{-2} corresponds to the number of polymer chains present at the surface of the SWCNT and the periodicity represents the number of carbon atoms the polymer chains are (on average) separated from each other. The periodicity is related to the surface of one hexagon (6/3 = 2 carbons) of the honeycomb constituting the tubes. From these grafting density values, it is obvious that the presence of functional polymer is three times higher than for the reference sample (for details for grafting density calculations, refer to Chapter 4)

Elemental Analysis (EA)

In addition, EA was performed on the samples (refer to **Table 5.4**) to evaluate the composition of the polymers (**P1**, **P3** and **P4**), and the SWCNT samples (**p-SWCNT**, **P3a-SWCNT**, **P3b-SWCNT** and **P4-SWCNT**).

Table 5.4. Elemental analysis results for PNIPAM with different end-groups (azide, **P1**), (Cp, **P3**), (acid, **P4**), and pristine SWCNTs (**p-SWCNT**), SWCNTs functionalized with **P3** at ambient temperature (**P3a-SWCNT**), at 80 °C (**P3b-SWCNT**), and mixed with **P4** (**P4-SWCNT**).

Sample	*wt.-%*				
	C	H	N	O	S
P1	55.04	9.17	10.13	11.94	1.98
P3	51.28	7.80	9.19	10.22	2.10
P4	59.86	10.25	10.57	16.54	1.25
p-SWCNT	79.14	0.55	0.58	4.14	0.00
P3a-SWCNT	75.30	5.34	2.30	5.74	0.87
P3b-SWCNT	78.19	5.10	2.09	4.57	0.37
P4-SWCNT	84.99	0.4	0.41	0.11	0.85

The untreated **p-SWCNT** sample contains some oxygen, hydrogen and nitrogen, which may originate from the air, from the amorphous carbon or catalyst residues. Because of these impurities, the mass balance is 84.14% for **p-SWCNT**, and for all the treated SWCNT samples within the same approximate range. The significant increase of the hydrogen, nitrogen, oxygen and sulfur content for **P3a-SWCNT** and **P3b-SWCNT** reveals the presence of PNIPAM. The reference sample **P4-SWCNT** displays an increase of the sulfur content, yet a very low level of hydrogen, nitrogen and oxygen. This discrepancy might be due to the ability of the polymer **P4** to attach to impurities and remove them from the sample. The low content of the other atoms, the same order as for **p-SWCNT**, leads to the conclusion that no polymer is detectable in the reference graft sample − a very gratifying result. Therefore, only the grafting density for **P3a-SWCNT** and **P3b-SWCNT** can be calculated (see **Table 5.5**).

Table 5.5. Determination of the grafting density based on elemental analysis of SWCNTs functionalized with Cp-end-capped PNIPAM (**P3**), at ambient temperature (**P3a-SWCNT**) and at 80 °C (**P3b-SWCNT**).

Sample			*Grafting density*		
	wt.-%	*x.-%*	mmol·g^{-1}	chain·nm^{-2}	Periodicity[a]
P3a-SWCNT	23.17	27.78	0.0628	0.0288	1324
P3b-SWCNT	20.27	25.30	0.0520	0.0238	1602

[a]number of C atoms of the SWCNTS surrounded by a polymer chain.

The nitrogen content was employed to estimate the grafting density in a similar fashion as described in Chapter 4 (refer to section 4.3.2). The sulfur content is too low in the samples

and would lead to some uncertainty, as for oxygen, since this element is already present in the pristine SWCNTs due to impurities. The grafting density obtained from the nitrogen content is very similar to the values deduced via TGA. The weight content via TGA may be less accurate than the EA, since the degradation of the polymer occurs in two steps as observed above (see **Figure 5.8**). An interesting tendency is observed while comparing these two methods. For **P3a-SWCNT** (reaction at ambient temperature), the grafting density seems to be slightly higher than for **P3b-SWCNT** (reaction at 80 °C). In fact, one could expect the reverse, as the temperature would displace the DA equilibrium to the products. However, PNIPAM is thermo-responsive and will collapse in the solvent (NMP) below this temperature, thus decreasing the possibility for the polymer chain to diffuse to the surface of the SWCNTs.

X-Ray Photoelectron Spectroscopy (XPS)

Complementary to bulk characterization methods such as TGA and EA, XPS was employed to characterize the surface of the SWCNTs. XPS enables the characterization of surfaces to a depth of approximatively 10 nm. Thus, no perturbation from impurities, e.g. catalyst used to generate the SWCNTs, occurs and the elemental composition at the surface of the SWCNTs can be accurately determined. The XPS-spectra of **P3a-SWCNT** (see **Figure 5.9**, third spectrum from the top) and **P3b-SWCNT** (see **Figure 5.9**, fourth spectrum from the bottom) reveal the presence of nitrogen, which is not present in pristine **p-SWCNT** (see **Figure 5.9**, top) at the same binding energy (399.8 eV) as for the PNIPAM **P3** (see **Figure 5.9** second spectra from the top), indicating that the polymer is located at the surface of the SWCNTs.

Small quantities of nitrogen (in a noisy signal) are detected for **P4-SWCNT** (see **Figure 5.9**, bottom) confirming, as in TGA and EA, the presence of only very limited amounts of **P4** adsorbed at SWCNTs' surface. The binding energy assignment for the different chemical groups and the quantification of each sample represented in **Figure 5.9** are depicted in **Table 5.6**. XPS-spectra of the polymers **P1**, **P2** and **P4** can be found in the appendix (**Figure A5**) and each atom (except hydrogen) constituting the polymer was identified at the corresponding binding energy already referenced in the literature[300] as for **P3**. The deconvolution of the C 1s signal for the SWCNT based samples was performed in a similar fashion as in the XPS measurements in Chapter 4 (section 4.3.2). The relative abundance of each atom was quantified also for these polymers (see appendix, **Table A4**). The data for those three polymers are similar to the data obtained for **P3**.
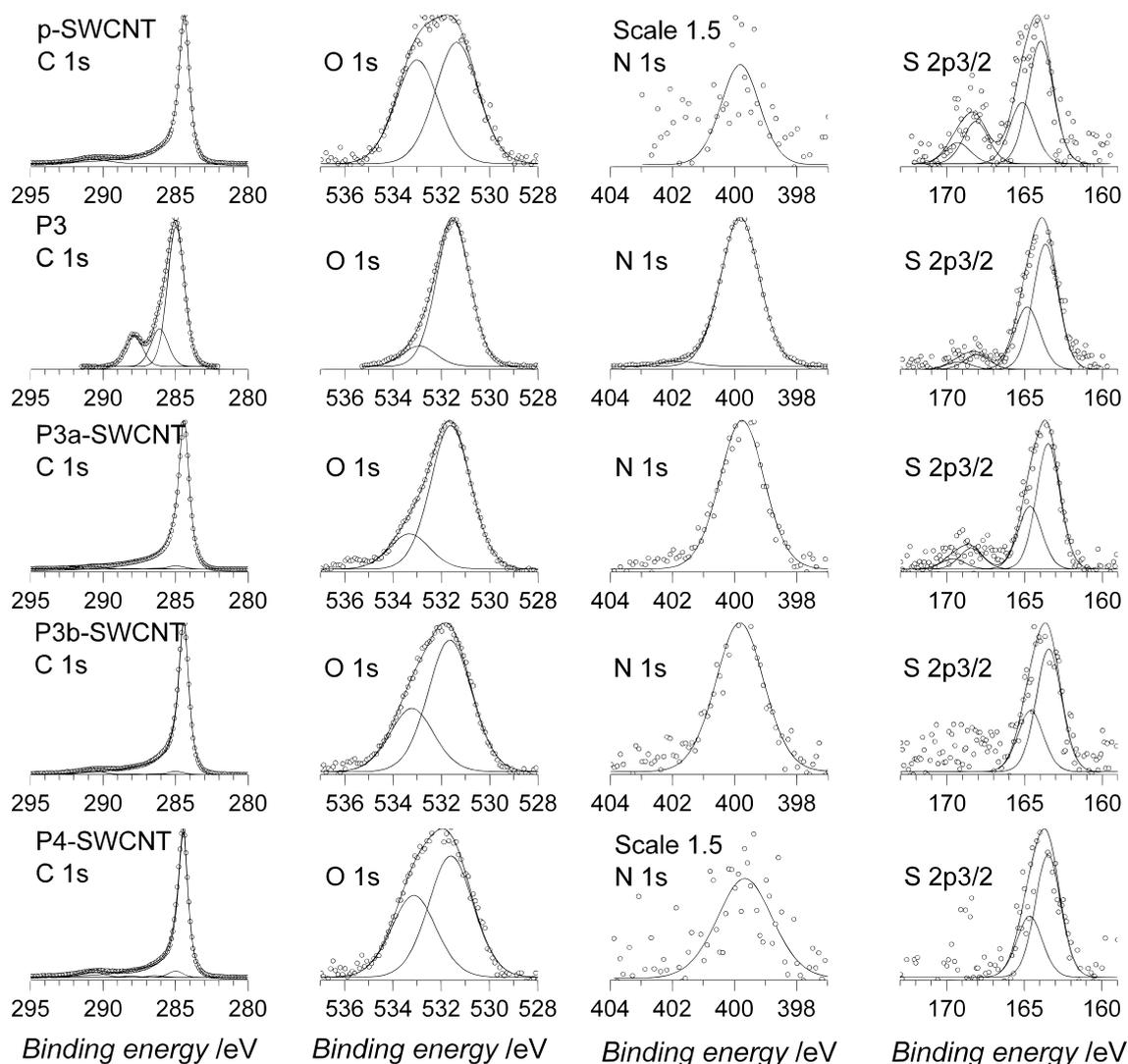
Figure 5.9. XPS spectra of pristine SWCNTs (**p-SWCNT**, top), Cp end-capped PNIPAM (**P3**, second spectra from the top), functionalized SWCNTs at ambient temperature (**P3a-SWCNT**, third spectra from the top) and at 80 °C (**P3b-SWCNT**, fourth spectra from the top), and the reference sample with non functional PNIPAM (**P4-SWCNT**, bottom) for each characteristic atom (carbon, oxygen, nitrogen and sulfur). For a better visualization, all spectra were normalized to maximal intensity.

The increase in the nitrogen signal can be employed to estimate the grafting density of the samples **P3a-SWCNT**, **P3b-SWCNT** and the reference **P4-SWCNT**, since nitrogen is not detected in the non modified **p-SWCNT**, in contrast to oxygen. Nevertheless, the increase of oxygen is very significant for the samples **P3a-SWCNT** and **P3b-SWCNT** compared to the references **p-SWCNT** and **P4-SWCNT**, confirming the presence of PNIPAM. The higher amount of oxygen for **P3a-SWCNT** than for **P3b-SWCNT** confirms the result from the nitrogen amount, e.g. a higher grafting density for **P3a-SWCNT** is observed. Since hydrogen cannot be identified by XPS, the content of carbon, oxygen and sulfur in the sample attributed from the polymer were firstly determined, according to the results obtained for **P3** by XPS

(see **Table 5.6**).

Table 5.6. Assignment of binding energy and comparison of the bond contribution after the deconvolution of the XPS spectra of pristine SWCNTs (**p-SWCNT**), Cp end-capped PNIPAM (**P3**), functionalized SWCNTs at ambient temperature (**P3a-SWCNT**) and at 80 °C (**P3b-SWCNT**), and the reference **P4-SWCNT** (non functional PNIPAM).

Peak	B. E.[a] /eV	at.-%					Entity
		p-SWCNT	P3	P3a-SWCNT	P3b-SWCNT	P4-SWCNT	
S $2p_{3/2}$	163.5	0.15	0.60	0.50	0.22	0.17	$\underline{S}$-C
	168.5	0.05	0.07	0.08	-	-	$\underline{S}$=C
C 1s	284.4	92.0	-	85.2	87.1	86.7	C-C sp^2
	285.0	-	50.1	2.00	2.00	3.5	$\underline{C}H_2$, $\underline{C}H_3$ sp^3
	286.1	-	13.5	0.5	0.5	1.0	$\underline{C}$-N, $\underline{C}$-O
	287.9	-	11.0	0.4	0.4	0.8	$\underline{C}$=O
	290.0	5.5	-	2.3	3.2	4.8	π-π*
N 1s	399.8	-	10.1	1.1	1.0	0.3	$\underline{N}$-C
	401.9	-	0.4	-	-	-	$\underline{N}^+$-H
O 1s	531.4	1.2	11.7	4.5	3.2	1.4	$\underline{O}$-C
	533.3	1.0	1.7	1.1	1.5	1.0	$\underline{O}$=C

[a]binding energy.

The hydrogen content was subsequently calculated from the composition of the monomer, based on the atomic composition attributed to the polymer and to the SWCNTs. From the atomic percent, the grafting density was deduced in the already defined units (see **Table 5.7**). From the atomic content, the amount of **P3** present at the surface of the SWCNT is slightly higher when the reaction is performed at ambient temperature (**P3a-SWCNT**) than at 80 °C (**P3b-SWCNT**, respectively 23.49 and 22.50 *at.-%*) confirming the results obtained by TGA and EA. Gratifyingly, the content of PNIPAM in the reference sample remains extremely low (0.3 *at.-%*, or 0.0167 mmol·g^{-1}). In contrast to TGA and EA, lower grafting densities are obtained via XPS, yet are of the same magnitude. For TGA and EA, for which very similar grafting densities are observed, the quantitative combustion of the sample (necessary for these two methods) may be influenced by the presence of impurities, leading to fluctuation in the composition. The weight content of polymer in the sample is strongly dependent on the amount of residue after the combustion. In contrast, due to its specificity, XPS delivers values not affected by the presence of impurities, yet may be associated with a larger error for quantification. The presence of the PNIPAM on the surface of the SWCNTs

was also evidenced by the thermo-sensitive behavior of the functionalized SWCNTs, which is discussed below.

Table 5.7. Summary of calculated grafting densities from TGA, EA and XPS for grafting experiments carried out at ambient temperature (**P3a-SWCNT**) and 80 °C (**P3b-SWCNT**) without the presence of any catalyst.

Sample	Method	Grafting density				
		wt.-%	*x.-%*	mmol·g^{-1}	chain·nm^{-2}	Periodicity ^{b}
P3a-SWCNT	TGA	18.6	-	0.0601	0.0275	1384
	EA	23.17	27.78	0.0628	0.0288	1324
	XPS	*15.23*	*23.49*	*0.0372*	*0.0171*	*2235*
P3b-SWCNT	TGA	15.7	-	0.0515	0.0236	1616
	EA	20.27	25.30	0.0520	0.0238	1602
	XPS	*13.91*	*22.50*	*0.0305*	*0.0140*	*2730*

^{a}number of C atoms of the SWCNTs surrounded by a polymer chain.

### 5.3.3. Thermo-response of PNIPAM-Cp functionalized SWCNTs

UV-Absorbance

The evaluation of the Lower Critical Solution Temperature (LCST) of aqueous solutions of **P1** and **P3** (0.1 mg·mL^{-1}), and the behavior of **p-SWCNT** and **P3a-SWCNT** based dispersions (0.01 mg·mL^{-1}) was employed by following their absorption at 600 nm while increasing the temperature (**Figure 5.10**).

The upper part of **Figure 5.10** depicts the turbidity curves for **P1** and **P3** as a function of temperature within a heating/cooling cycle. A more significant hysteresis between the heating and the cooling cycle is observed for **P3** than for **P1**. The presence of a longer organic section in **P3** may induce the delay in returning to a clear solution. Moreover, while the LCST of PNIPAM is typically close to 32 °C,[301] **P1** and **P3** display a lower LCST at close to 29 °C, probably due to the dodecyl end-chain.[302,303]

The most important information from **Figure 5.10**, however, comes from the comparison between the **p-SWCNT** and **P3a-SWCNT** dispersions, where the thermo-responsive behavior the PNIPAM modified SWCNTs is evidenced. After sonication, the **p-SWCNT** dispersion is instable, as microscopic particles are optically recognizable within 5 min and these sediment to the bottom of the flask. While varying the temperature, no evolution of the relative absorption is observed. On the contrary, the **P3a-SWCNT** dispersion leads to a stable, clear and gray dispersion when kept within the confines of an ice-bath (over

24 h, see DLS section). Once the temperature increases, the solution becomes increasingly more transparent, which is also evident by inspecting the images embedded within the graph.
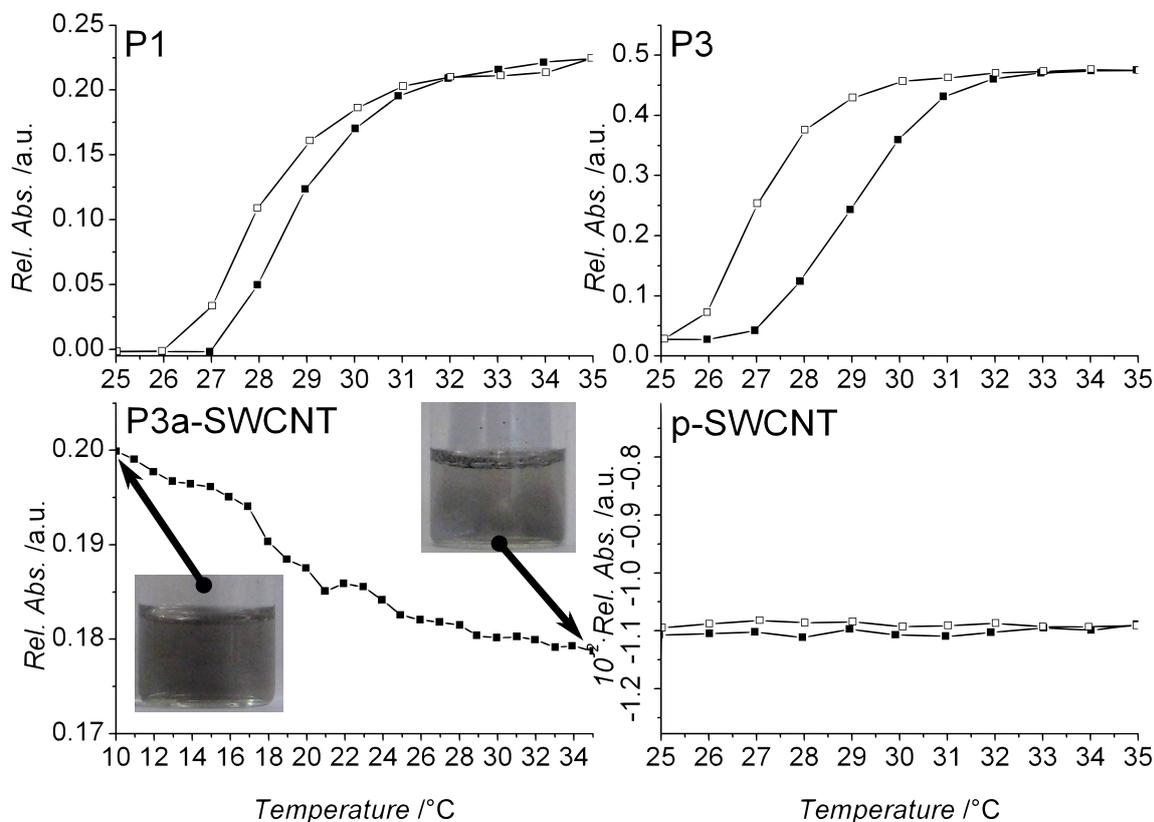
Figure 5.10. Evolution of absorbance with the temperature at 600 nm of PNIPAM with different end-group (azide, **P1**), (Cp, **P3**) dissolved in water (0.1 mg·mL^{-1}), functionalized SWCNTs with Cp-terminated PNIPAM at ambient temperature (**P3a-SWCNT**), and non-modified pristine SWCNTs (**p-SWCNT**) dispersed in water (0.01 mg·mL^{-1}). Heating (full squares) and cooling (empty squares) cycles at 0.1 °C·min^{-1}.

The pictures of the dispersion after sonication (picture on the left) and at 35 °C (picture on the right) demonstrate the macroscopic effect of the functionalization, namely as the temperature increases, the polymer chains collapse onto the CNTs surface and the dispersion is destabilized, leading to the aggregation of the functionalized SWCNTs, recognizable by their flotation at the air interface. The overall effect is a clearer solution. An identical behavior involving PNIPAM functionalized nano- and micro-objects, including microspheres[304,305] and CNTs[306] has been reported previously in excellent agreement with the current results.

Dynamic Light Scattering (DLS)

Dynamic Light Scattering (DLS) and Static Light Scattering (SLS) are frequently employed for the evaluation of aqueous CNT dispersions, e.g. to assess the influence of the sonication,[307] of wrapped polymer,[308] of surfactant,[309] or of the solvent.[310] The combination of

both methods enables the evaluation of the length of the CNTs via the relation between hydrodynamic radius and the radius of gyration.[311,312] Specifically the work of Gigault *et al.* features a complete study of SWCNT dispersions in water, stabilized with a surfactant, by selectively dissociating individual SWCNTs from aggregates via field-flow fractionation coupled with DLS and SLS.[313] In here, a similar rationale is followed for evaluating the thermo-responsive behavior PNIPAM/SWCNT hybrids via DLS.

Due to the instability of the **p-SWCNT** and **P4-SWCNT** dispersion (see previous UV-spectroscopy section), the samples could not be assessed via DLS. The visual recognition of parts in the clear solution just after sonication already suggests the presence of microscopic particles which very significantly scatter light and saturate the DLS system. Even diluted, the dispersion could not be characterized. However, the PNIPAM functional SWCNTs could be readily assessed. **Figure 5.11** depicts the evolution of the hydrodynamic diameter (D_h) of two populations of particles observed in the dispersion based on **P3a-SWCNT** (0.01 mg·mL^{-1}).
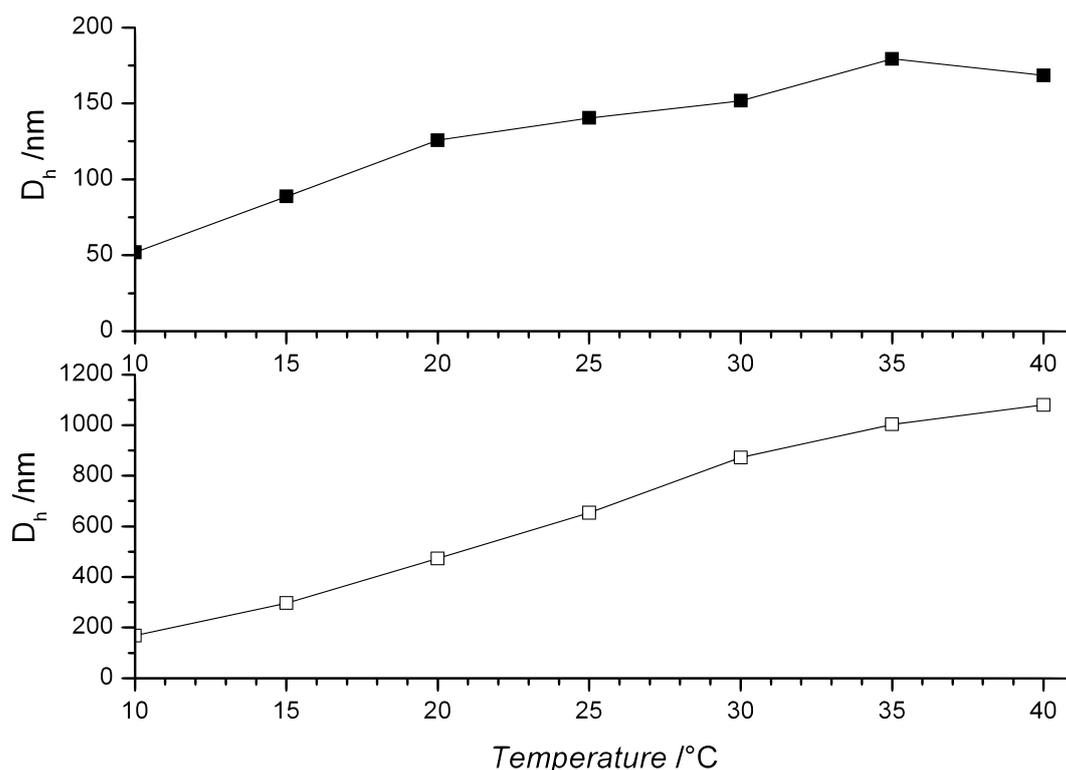
Figure 5.11. Evolution of the hydrodynamic diameter (D_h) of individually dispersed SWCNTs (top) and aggregates (bottom) population from **P3a-SWCNT** dispersion in water (0.01 mg·mL^{-1}) with the temperature via DLS.

Comparable results to those of Gigault *et al.* are obtained since two populations of particles are observed. The mild sonication methods employed in the present study (ultrasonic bath for the functionalization and a sonifier for the dispersion) contribute to this dispersion state. A total exfoliation of the SWCNTs would require more mechanical energy, which

would not guarantee the absence of degradation of the SWCNTs (shortening).[307] The diameter of both populations is comparable to the values obtained in the literature, e.g. individual SWCNTs and aggregates are recognizable at 52 nm and 169 nm, respectively, after sonication at 10 °C. For comparison, the dispersion measured over 7 h at 10 °C, such as the 24 h dispersion (also measured for 7 h at 10 °C) used for references, returns D_h-values between 50 and 90 nm for the smaller population, and 200 and 300 nm for the aggregates. These fluctuations are due to the difficulty to sonicate the samples at exactly the same energy and experimental error (10%). The values obtained at 15 °C for the **P3a-SWCNT** dispersion (89 and 297 nm) are within this range. However, as the temperature is increasing from 20 °C to 40 °C, the hydrodynamic diameter for both populations increases steadily to 152–169 nm and 0.9–1 μm, respectively. The volume weighted quantification of the two populations (see **Figure 5.12**) reveals an inversion of the population from 60% of individual SWCNTs at 10–15 °C to 30% at 35–40 °C (respectively 40% to 70% for aggregates).
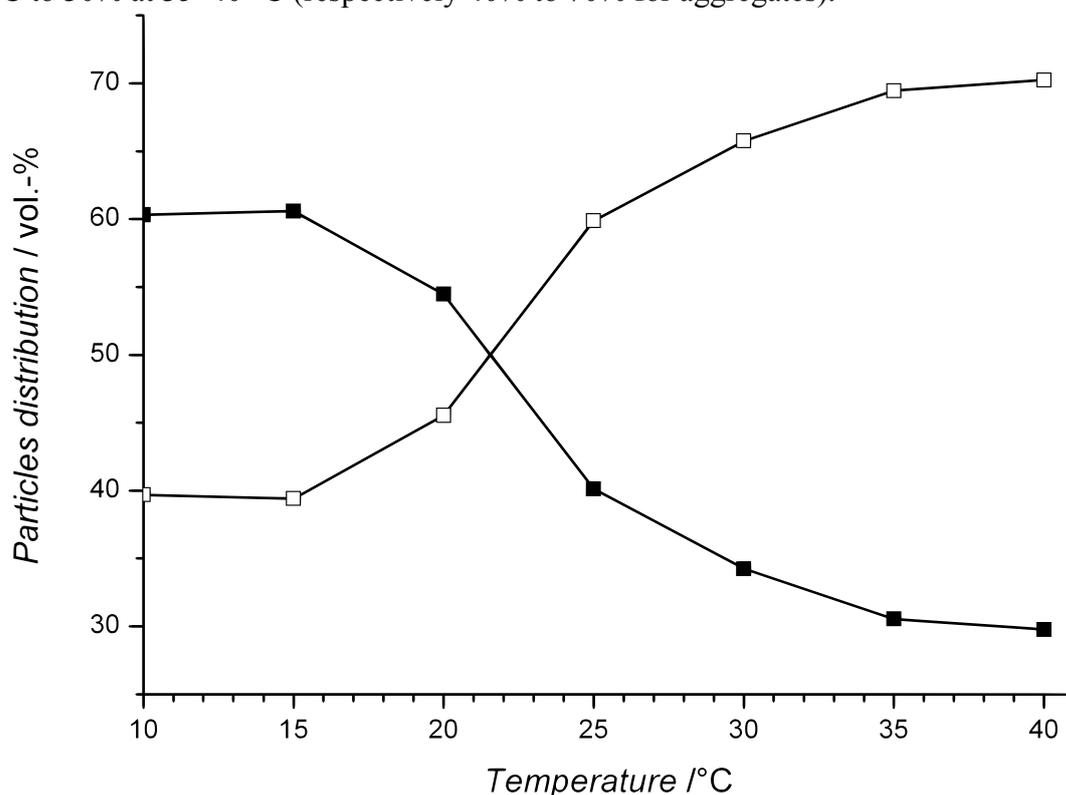
Figure 5.12. Evolution of the population in volume percent of individual SWCNTs (filled squares) and aggregates (white squares) with temperature from the 0.01 mg·mL^{-1} water dispersion of PNIPAM functionalized SWCNTs (**P3a-SWCNT** sample).

Individual SWCNTs aggregate to larger particles at 20 °C, before the LCST of **P3** is reached, and already present aggregates of microscopic particles, revealing the presence of PNIPAM (**P3**) at the surface of the SWCNTs. Moreover, the presence of individual **P3** could not be observed due to complete covalent attachment of the polymer to the SWCNTs. The

hydrodynamic diameter of **P3** was evaluated to vary from 5 nm to 120 nm, with a transition between 25 and 30 °C. These observed phenomena are in good agreement with the UV-spectroscopic results, for which the LCST of **P3** was determined at 29 °C and the aggregation of the **P3a-SWCNT** in dispersion starting over 20 °C, which is in accordance with the observation from the UV-measurements.

5.3.4. Conclusions

The synthesis of Cp end-capped PNIPAM was successfully performed via the combination of a RAFT process and a copper catalyzed alkyne/azide ligation reaction. The analytic methods employed evidenced a high end-group fidelity of the diene functional thermo-responsive polymers, able to undergo an efficient DA ligation: the Cp-functional PNIPAM displayed a diene character while reacting with a dienophile (*N*-maleimide). The functionalization of SWCNTs with the diene-functional PNIPAM occurred via a DA reaction, and the presence of polymer at the surface was evidenced via three methods (TGA, EA and XPS). The grafting density was estimated to be closed to 0.0628 mmol·g^{-1} (0.0288 chain·nm^2, or one chain every 1384 carbon atoms). The functionalized SWCNTs displayed thermo-responsive behavior and precipitated at 20 °C in aqueous dispersion. The evolution of the dispersion was followed via DLS, showing individual SWCNTs (50–90 nm hydrodynamic diameter) and aggregates (200–300 nm diameter). Over 20 °C, the individual SWCNTs aggregated to 152–169 nm diameter particles, and even larger aggregates (microscopic particles).

The herein demonstrated functionalization of SWCNTs is the method of choice to modify SWCNTs under very mild conditions (ambient temperature, no catalyst) and offers the possibility to transform end-groups from RAFT-polymers in a very simple manner. The current study proved the efficiency of Cp end-capped polymers (PNIPAM) to react with SWCNTs and provide SWCNTs with macroscopic observable properties, thermo-response.

Chapter 6 – SWCNT functionalization with conjugated cyclopentadienyl end-capped poly(3-hexylthiophene)
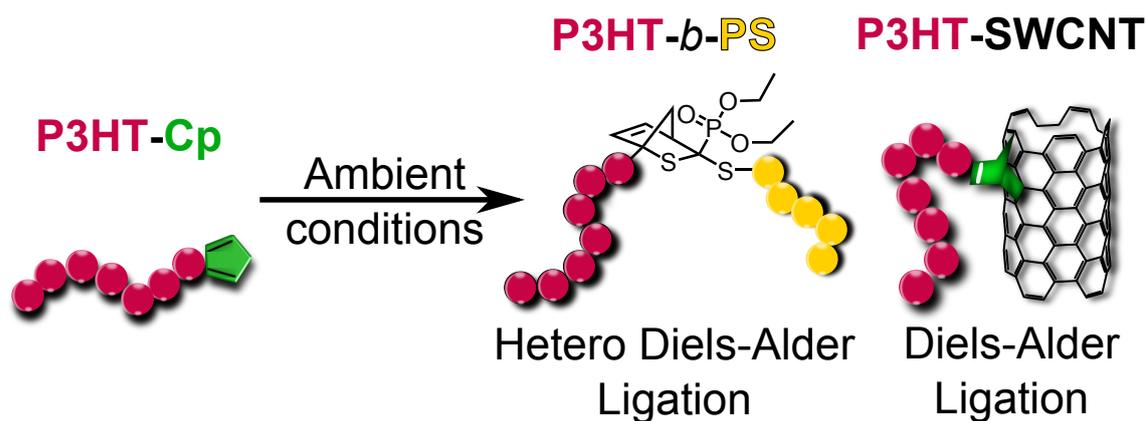
6.1. Introduction

Organic optolectronics/solar cells,[314] offering low cost, easy to process, light weight, flexible, reliable and environmentally benign energy production technology, is one area where the optoelectronic properties of CNTs are set to play a vital role.[315] On the other hand, the development of conducting polymers for electronic and photovoltaic devices is being extensively explored.[316] These semiconductor devices function are based on the photovoltaic effect, which involves the generation of excitons (electron-hole pairs) after photon absorption and their dissociation for current collection. In conducting polymers, the excitons are short lived and tend to recombine before the charge collection at the electrodes.[317] The dissociation of excitons can be promoted at the interface of a heterojunction between semiconductor materials of different electron affinities.[318] Conducting polymers (electron donor - D) and fullerenes (electron acceptor - A) are extensively employed to generate heterojunctions.[319] However, the desired optimum morphology for the active layer of the photovoltaic cells is predicted to be an interpenetrating network containing vertically aligned domains carrying the charges to the electrodes,[320] making CNTs a natural choice and holding promise for improving photovoltaic effects. On the part of conducting polymers, the highly fluorescent P3HT is one of the most widely studied materials in the context of conducting polymers/CNTs bulk heterojunction (BHJ) systems. Several studies in recent years have predicted an improvement of charge separation efficiency for P3HT/CNT based BHJ systems as compared to fullerene based systems (refer to Chapter 2, section 2.4.2).[321] However, this improvement remained naturally connected to the de-bundling of CNTs allowing a better contact between P3HT (D) and the CNTs (A) surface. A rationally designed surface functionalization of CNTs is key to provide the required BHJ systems. Both non-covalent supramolecular interaction and covalent functionalization are being explored in this field. The non-covalent CNTs surface functionalization strategies exploit the Van der Waals/π-π interactions[322] resulting in physical adsorption of conducting polymers at the surface of CNTs, whereas the covalent functionalization strategies exploit various surface chemical reactions to covalently graft chemical moieties at the surface of CNTs.[138,315] Due to its chemical robustness, covalent functionalization is generally preferred over non-covalent adsorption which is prone to desorption under stress. Kuila et al.[323] have reported an improved photovoltaic cell performance when P3HT was covalently functionalized at the surface of CNTs. Similarly, the studies of Kumar et al.,[324] Boon,[325] Niu et al.,[326] Sadhu et al.,[327] and Le et al.[328] have reported the improved photovoltaic characteristics achieved by the functionalization of CNT surfaces with P3HT. In all these examples the P3HT chains are

grafted onto the surface of pre-functionalized CNTs via intricate, multi-step pre-functionalization treatments, involving the oxidation of CNTs often under extremely aggressive conditions.

The former investigations in Chapter 4 and 5 provide substantial and unambiguous evidence that the DA reaction with Cp end-capped PMMA and PNIPAM efficiently occurred on non-modified SWCNTs under mild conditions. Alongside the in-depth characterization of the SWCNT/hybrid material, the thermo-response of such a material reveals additional properties the polymer chains impart onto the SWCNTs. Thus, the aim of the present section is to design an unprecedented conducting polymer with a highly reactive diene Cp end-group suitable for subsequent direct ligation with non-modified SWCNTs, and for a long term perspective to introduce an important new aspect to the design of CNT/conducting polymer based photovoltaic units at lower costs and via simplified production.

In collaboration with Dr. Basit Yameen (KIT), a novel Cp end-capped P3HT via an *in situ* chain end-capping strategy was synthesized and characterized developed by McCullough *et al*.[208,239,329] The Cp end-capped P3HT was fully characterized employing ^{1}H NMR spectroscopy and MALDI-ToF mass spectrometry. The reactivity of the Cp end-groups was demonstrated by synthesizing P3HT-*b*-PS block copolymers via HDA ligation (section 6.2).

Exploiting the DA reactivity of SWCNTs towards dienes, the new Cp end-capped P3HT was directly covalently grafted onto the surface of pristine SWCNTs and the resulting P3HT functionalized SWCNTs were fully characterized via TGA, EA, XPS and HRTEM (refer to section 6.3) as already described in Chapter 4 and 5. The results reported here are of paramount importance, on the one hand in the context of pioneering the synthetic design of Cp capped conducting polymers which are highly suitable for DA based modular ligation, and on the other hand for the direct ligation of conducting polymer onto the surface of pristine SWCNTs.

6.2. Synthesis and characterization of P3HT-Cp

The synthetic strategy employed to generate the Cp-capped P3HT conducting polymer was based on the *in situ* end functionalization using the GRIM polymerization developed by McCullough *et al*.[208,239,329] The GRIM method generally yields region-regular head-to-tail coupled P3HT with a predominant chain-end composition of H/Br. Exploiting the chain growth mechanism of GRIM polymerization, McCullough *et al*. have further developed a simple route to various end-capped P3HT polymers simply by adding a pertinent Grignard reagent (RMgX), leading to P3HT with a predominant chain-end composition of Br/R with a small fraction of an H/R combination. In the present section (refer to **Scheme 6.1**), P3HT with

a Br/Vinyl chain-end combination (**P-Vinyl**) was prepared by adding vinylmagnesium bromide at the end of the polymerization. The terminal vinyl groups were transformed into hydroxyl ethyl groups by subjecting them to hydroboration using 9-BBN followed by oxidation with H_2O_2 in the presence of NaOH. The hydroxyl end-capped P3HT (**P-OH**) was subsequently reacted with 2-bromopropionyl bromide to give **P-Br** with a chain-end constitution of aromatic-Br/aliphatic-Br.[208] Capitalizing on the $NiCp_2$ assisted ambient temperature transformation of aliphatic bromo to Cp groups,[274] the terminal aliphatic-Br groups of **P-Br** were quantitatively transformed into Cp groups (**Scheme 6.1**, route A, although the transformation leads to a mixture of 1-, 2-, and 5-substituted cyclopentadienes, only the chemical structure for the 1-isomer is presented for reasons of brevity). For the sake of comparison, a P3HT polymer with a chain-end constitution of Br/H (**P-0**) was additionally prepared employing the same GRIM method (**Scheme 6.1**, route **B**).
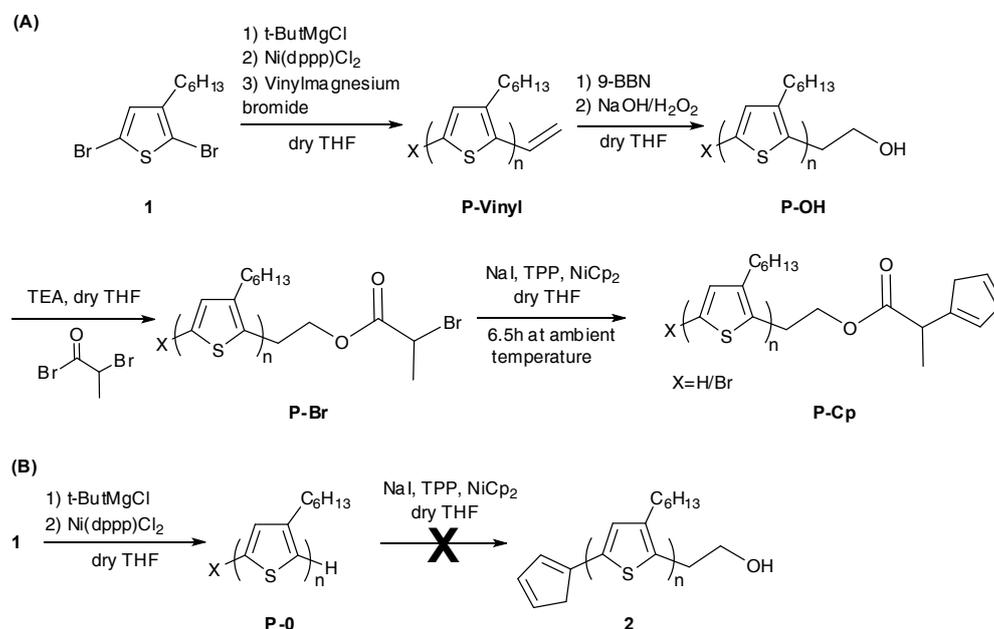
Scheme 6.1. (A) Synthesis of Cp end-capped P3HT (**P-Cp**) by a combination of *in situ* end functionalization employing GRIM polymerization and $NiCp_2$ assisted transformation of the terminal aliphatic bromo group into a Cp group. (B) Synthesis of a reference P3HT sample (**P-0**). The terminal bromo groups of the **P-0** remained inert during reaction with $NiCp_2$.

For clarity, the synthesis and the results obtained from ^1H NMR spectroscopy and MALDI-ToF mass spectrometry are detailed for the last synthetic step transforming the bromine terminated polymer chains **P-Br** into the Cp end-capped polymer chains **P-Cp**. The synthesis of **P-Vinyl** and **P-OH** have previously been reported in the literature, and thus the results of their characterization are reported in the appendix, e.g. the detailed ^1H NMR spectra in **Figure A6** and the mass spectra in **Figure A7**. For the same reason, the synthesis and the results for the reference sample **P-0** are reported in the appendix (refer to **Figure A8** for the

^{1}H NMR spectrum, and **Figure A9** for the MALDI-ToF spectrum).

6.2.1. Polymerization and end-group transformations

The list of the employed materials can be found in Chapter 3 (section 3.12.3).

Synthesis of vinyl terminated P3HT (P-Vinyl) and the reference polymer (P-0)

4 g (12.3 mmol) of 2,5-dibromo-3-hexylthiophene was dissolved in 120 mL of dry THF under N_2(g) atmosphere. To this solution 6.12 mL (12.2 mmol) of a 2 M ether solution of *tert*-butylmagnesium chloride was added and the reaction mixture was stirred under reflux for 90 min in a N_2(g) atmosphere. The reaction mixture was subsequently cooled to ambient temperature and 332.4 mg (0.613 mmol) of Ni(dppp)Cl$_2$ were added. The polymerization was allowed to proceed for 10 min followed by the addition of 2.46 mL (2.46 mmol) of 1 M THF solution of vinylmagnesium bromide. The polymerization reaction was further stirred for 5 min before it was poured into methanol to precipitate the polymer. The precipitated polymer was collected and subjected to sequential Soxhlet extractions with methanol, hexanes and chloroform. **P-Vinyl** (M_n = 5700 g·mol^{-1}, $Đ$ = 1.1) was collected from the chloroform extract by evaporation of chloroform via a rotary evaporator and drying overnight under vacuum at ambient temperature. A reference P3HT sample referred to as **P-0** was prepared in a similar fashion without the end-capping with vinylmagnesium bromide (M_n = 6200 g·mol^{-1}, $Đ$ = 1.09). The **P-0** polymer was used to prepare the reference sample blends of P3HT/SWCNT for comparison.

Synthesis of hydroxyl terminated P3HT (P-OH)

680 mg (0.119 mmol) of **P-Vinyl** was dissolved in 80 mL of dry THF under N_2(g) atmosphere. To this solution 4.75 mL of 0.5 M THF solution of 9-BBN were added. The reaction mixture was stirred at 40 °C for 24 h. Subsequently, 1.2 mL of 6 M aq. NaOH solution were added. The reaction mixture was cooled to ambient temperature followed by the addition of 1.2 mL of 35% aq. H_2O_2 solution and was stirred for a further 24 h at 40 °C. At the end of the reaction the polymer was recovered by precipitation in a methanol water mixture (2.5:1). The precipitates were filtered, washed with water and subjected to Soxhlet extraction with methanol for 24 h. **P-OH** (M_n = 6400 g·mol^{-1}, $Đ$ = 1.1) was collected by extraction in chloroform.

Synthesis of aliphatic bromo terminated P3HT (P-Br)

540 mg of **P-OH** (0.085 mmol) was dissolved in 50 mL of dry THF and stirred at 40 °C

for 15 min. To this solution 3.91 mL (28.05 mmol) of TEA were added followed by the dropwise addition of 2.67 mL (25.5 mmol) of 2-bromopropionyl bromide at 40 °C. The reaction mixture was stirred at 40 °C for 24 h after which it was cooled to ambient temperature and filtered. The filtrate was concentrated and precipitated in methanol. The precipitates were collected and subjected to Soxhlet extraction with methanol for 24 h. The **P-Br** was collected by extraction with chloroform and the chloroform was removed on a rotary evaporator. The obtained **P-Br** (M_n = 6500 g·mol^{-1}, $Đ$ = 1.1) was subsequently dried under vacuum at ambient temperature.

Synthesis of Cp terminated P3HT (P-Cp)

The synthesis of **P-Cp** was adapted from the method developed by Inglis *et al.*[274] and a representative synthesis is described here. The reaction was performed at ambient temperature in a dry glove box under N_2(g) atmosphere. 527 mg (0.081 mmol) of **P-Br** (M_n = 6500 g·mol^{-1}, $Đ$ = 1.15) was dissolved in 21 mL of dry THF. To this solution, 72.74 mg (0.485 mmol) NaI and 42.43 (0.162 mmol) of TPP were added and the solution was stirred for 5 min. 61.11 mg (0.324 mmol) of NiCp$_2$ was separately dissolved in 1.8 mL of THF and was transferred to the solution of **P-Br** containing NaI and PPh$_3$. The reaction was stirred at ambient temperature for 6.5 h. The reaction mixture was subsequently passed through a short basic alumina column, concentrated and precipitated in methanol. The precipitates were collected by centrifugation and were dissolved in chloroform. The chloroform mixture was washed three times with water, concentrated and precipitated in methanol. The precipitates were collected by centrifugation and dried overnight under vacuum at ambient temperature to give **P-Cp** (M_n = 6500 g·mol^{-1}, $Đ$ = 1.2).

Synthesis of P3HT-b-PS via HDA Ligation

24.8 mg (M_n = 6500 g·mol^{-1}, $Đ$ = 1.2, 3.8·10^{-3} mmol) of **P-Cp**, 11.86 mg (M_n = 3100 g·mol^{-1}, $Đ$ = 1.1, 3.8·10^{-3} mmol) of RAFT polymerized **PS** and 1.2 equivalent of ZnCl$_2$ were dissolved in 70 µL of THF. The solution was stirred at 50 °C for 24 h. The reaction was cooled to ambient temperature and the polymer was recovered by precipitation in methanol. The obtained block copolymer was dissolved several times in the minimum volume of THF and precipitated in acetone. The precipitates were collected via centrifugation and dried under vacuum at ambient temperature.

An overlay of the SEC traces of **P-Br** and **P-Cp** is depicted in **Figure 6.1**. The two

chromatograms and are essentially identical except a very small shoulder that appeared on the higher molecular weight side for **P-Cp**. The small shoulder can be attributed to the DA coupling reaction between the Cp end-groups of **P-Cp**. The overall SEC data for **P-Br** (M_n = 6500 g·mol^{-1}, Đ = 1.1) and **P-Cp** (M_n = 6500 g·mol^{-1}, Đ = 1.2) are almost identical and both polymers have narrow dispersities.
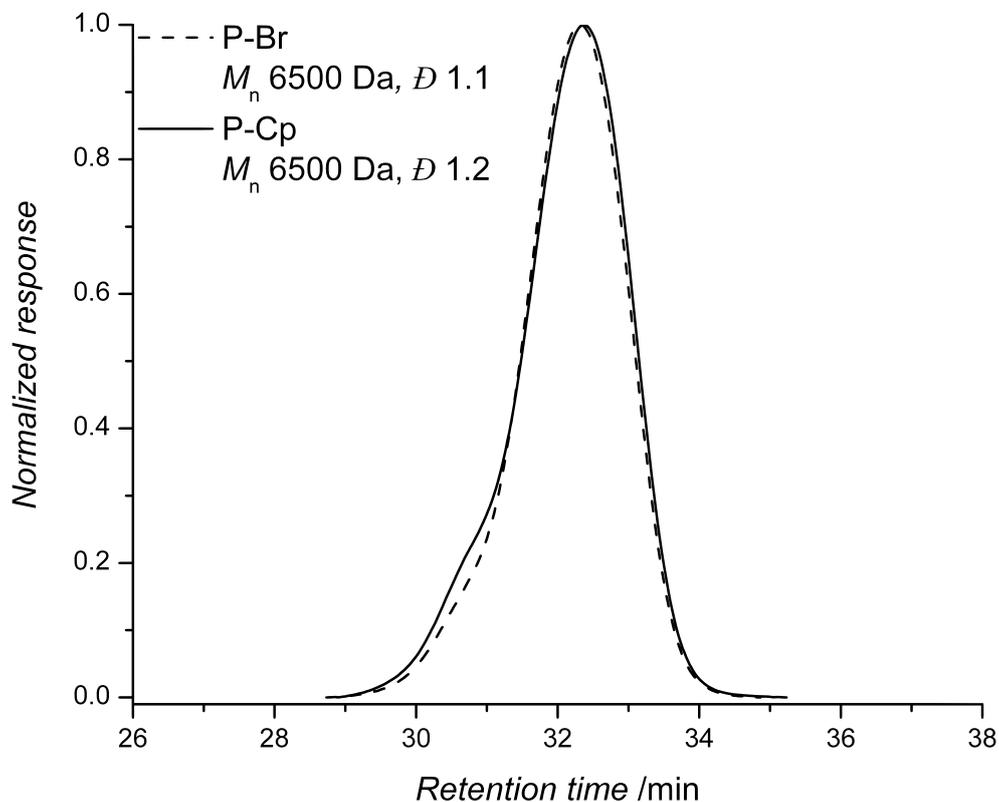

Figure 6.1. Overlay of SEC traces of **P-Br** and **P-Cp**.

6.2.2. Chain-end fidelity

^{1}H Nuclear Magnetic Resonance spectroscopy (NMR)

The ^{1}H NMR data for the transformation steps leading to the **P-Br** stage were in complete agreement with those reported in the literature[208] (refer to **Figure A6** in the appendix for the ^{1}H NMR spectra of **P-Vinyl** and **P-OH**). The successful transformation of the aliphatic-Br of **P-Br** to Cp end-groups was evidenced by the appearance of proton resonances characteristics of the Cp group[274] at 6.0–6.5 ppm and 2.9 ppm in the ^{1}H NMR spectrum of **P-Cp**. The resonance for the proton at the α-position to the aliphatic-Br group was also shifted from 4.3 ppm in **P-Br** to 3.5 ppm in **P-Cp**. Additionally, the doublet for the methyl protons at β-position to aliphatic-Br group was shifted up-field, being obscured by the aliphatic signals from the hexyl substituents of P3HT. The ^{1}H NMR data thus fully corroborate the successful end-group transformation (refer to **Figure 6.2**). The presence of

distinguishable end-groups enabled the estimation of M_n values by the NMR end-group analysis. The consistent M_n values of **P-Vinyl** (7800 g·mol^{-1}), **P-OH** (8100 g·mol^{-1}), **P-Br** (8000 g·mol^{-1}), and **P-Cp** (8600 g·mol^{-1}) reflect a high end-group fidelity during the end-group transformation depicted in **Scheme 6.1**.
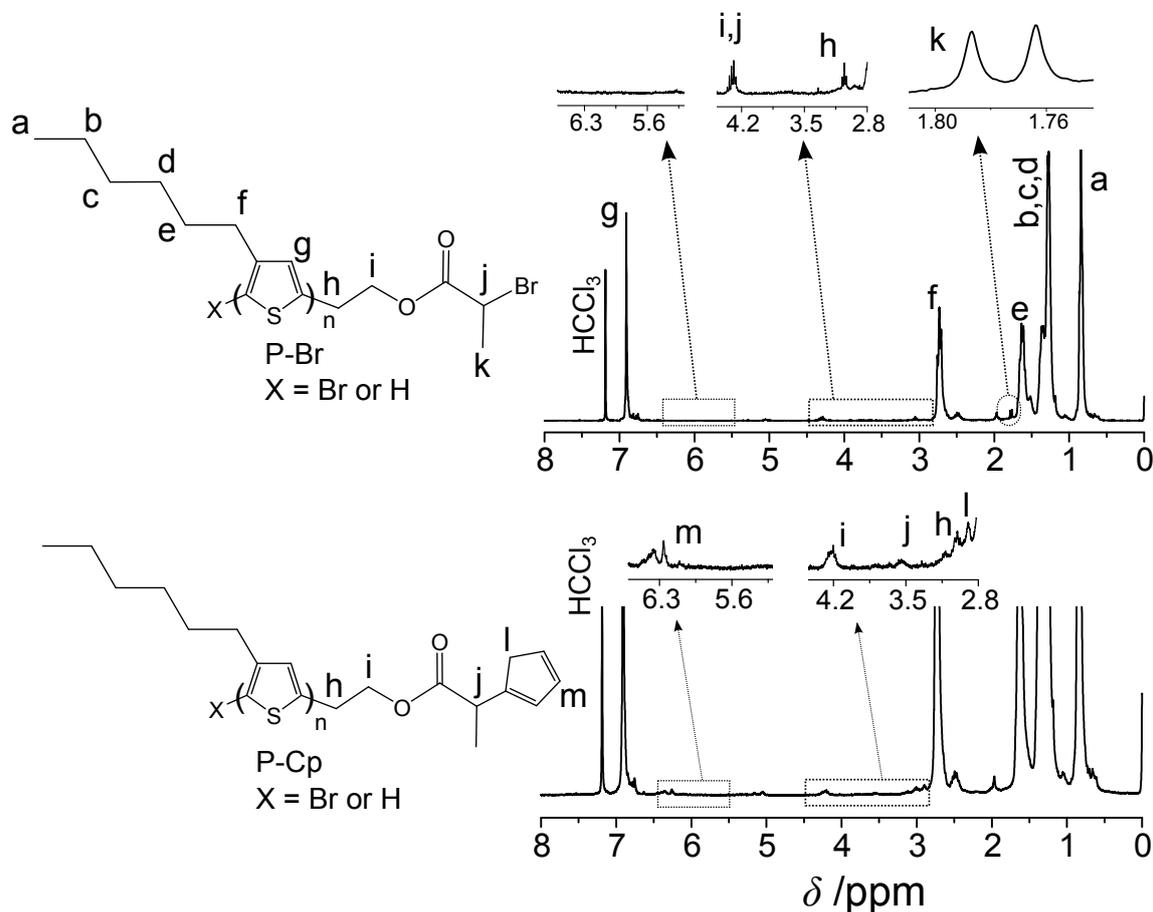
Figure 6.2. ^{1}H NMR spectra of **P-Br** (top) and **P-Cp** (bottom) with resonance assignment to the respective protons revealing the successful transformation of the terminal aliphatic bromo group into a Cp group.

Mass Spectrometry (MALDI-ToF)

In addition to ^{1}H NMR spectroscopy, MALDI-ToF mass spectrometry analysis additionally confirms the quantitative end-group transformation. An overlay of the MALDI-ToF mass spectra of **P-Vinyl**, **P-OH**, and **P-Br** is provided in the appendix (refer to **Figure A7**). The MALDI-ToF mass spectrum for the **P-Cp** is depicted in the **Figure 6.3**.

The *m/z* values for the major peak series in **Figure 6.3** correspond to the **P-Cp** molecules as expected (refer to **Scheme 6.1**, route A) with a Cp group at one end of the chain, while the other end of the chain is capped with the bromo group. It is worthwhile noting that only the aliphatic-Br end-groups of **P-Br** were transformed into the Cp groups while the bromo groups directly attached to the thiophene ring did not react with the NiCp$_2$. The

transformation of the bromo end-groups of the **P-0** (M_n = 4000 g·mol^{-1}, Đ = 1.1) into a Cp group under similar conditions did not occur (product **2**) which evidences the inertness of bromo groups directly attached to thiophene rings towards NiCp$_2$ under the applied condition.
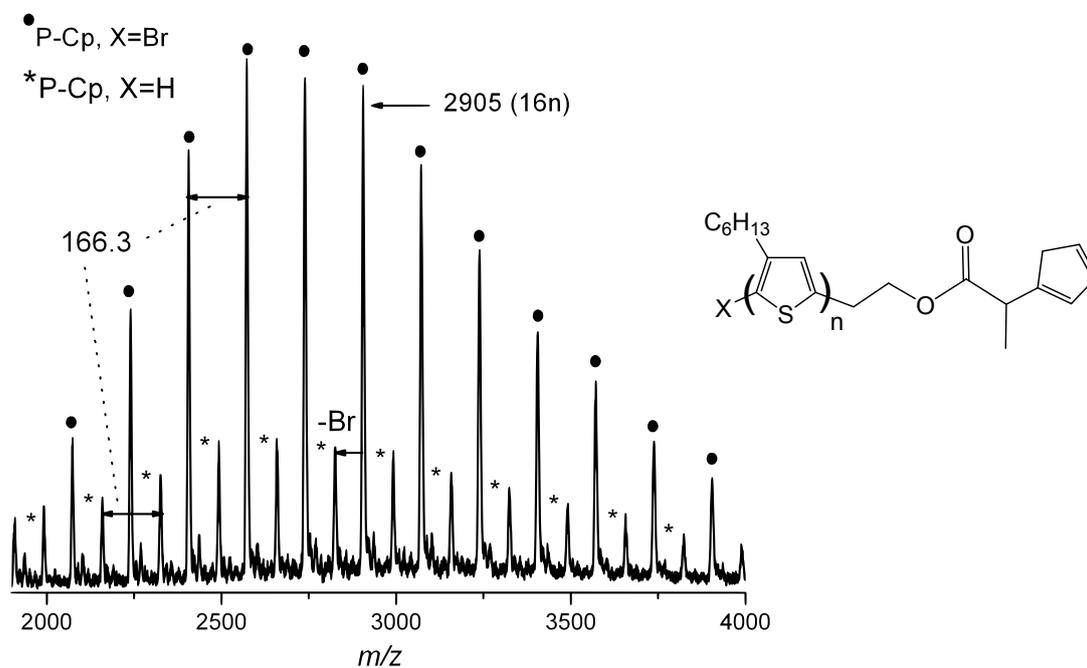

Figure 6.3. MALDI-ToF mass spectrum of **P-Cp**. The major peak series corresponds to **P-Cp** with X=Br while the minor peak series represents **P-Cp** with X=H. For both series the difference between two consecutive peaks matches the mass of P3HT repeat units. For a detailed peak assignment refer to **Table 6.1**.

In the MALDI-ToF mass spectrum of **P-Cp**, as depicted in **Figure 6.3**, the difference of 166.3 Da between the consecutive major peaks (marked with a point •) matches the mass of the P3HT repeat units well. In addition to the major peak series, a minor peak series, as marked by the asterisks in **Figure 6.3**, was observed. A difference of 166.3 Da between the consecutive minor peaks confirmed that they also originated from P3HT molecules and the mass difference between the consecutive minor and major peaks matched the mass of a bromine atom which reflected on the **P-Cp** molecules with H/Cp chain-ends constitution. This is in accord with the results reported by the McCullough *et al.*, where quenching the GRIM polymerization with vinylmagnesium bromide results in P3HT with majority chain-ends constitution of Br/Vinyl and a minor fraction of H/Vinyl chains end constitution.[208,239,329] The combination of the chain-end constitutions is subsequently carried over into all the end-group transformations as depicted in **Scheme 6.1** (route A).

A comparison of MALDI-ToF mass spectra of **P-Br** and **P-Cp** is presented in **Figure 6.4** along with the chemical structures of the **P-Br** (**P-Br**$^{\text{Br}}$ refers to Br/Br and **P-Br**$^{\text{H}}$

refers to H/Br chain-end constitution) and **P-Cp** (**P-Cp^{Br}** refers to Br/Cp and **P-Cp^{H}** refers to H/Cp chain-end constitution) polymers.
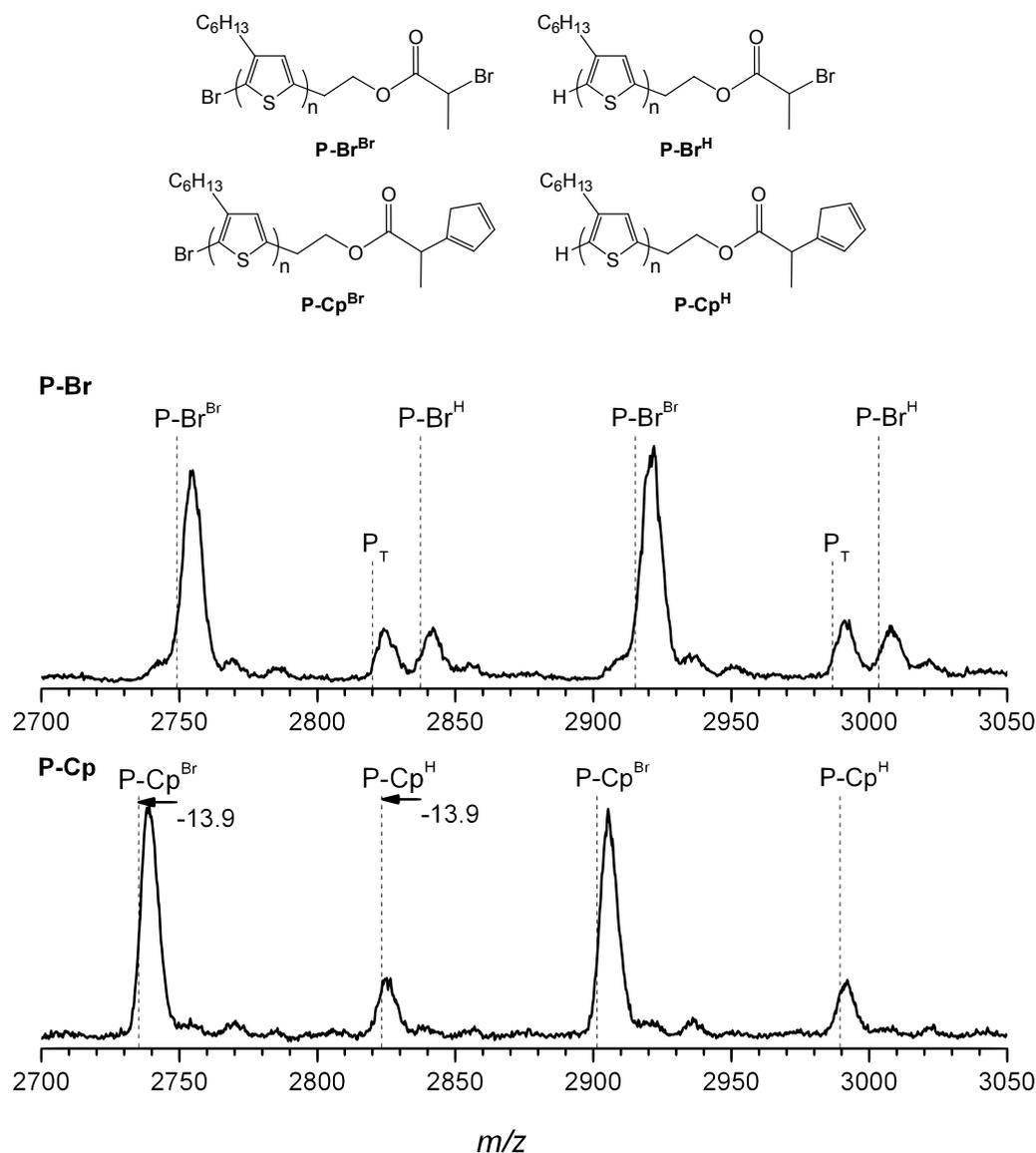
Figure 6.4. Top: Chemical structures of the **P-Br** (**P-Br^{Br}** refers to Br/Br and **P-Br^{H}** refers to H/Br chain-end constitution) and **P-Cp** (**P-Cp^{Br}** refers to Br/Cp and **P-Cp^{H}** refers to H/Cp chain-end constitution) polymers. Bottom: MALDI-ToF mass spectra of **P-Br** and **P-Cp**. A shift of peaks by -13.88 Da (78.92 (*Br*) – 65.04 (*C$_5$H$_5$*) = 13.88 Da) confirms the quantitative transformation of the terminal aliphatic bromo group to a Cp group.

The absence of **P-Br^{Br}** species in the **P-Cp** MALDI-ToF mass spectrum and a shift of the peaks by -13.9 Da (78.92 (*Br*) – 65.04 (*C$_5$H$_5$*) = 13.88 Da) confirmed the quantitative transformation of only the terminal aliphatic bromo groups of **P-Br^{Br}** into the Cp groups. The transformation is clearly observable for **P-Br^{Br}** species, however, in the case of the transformation of the **P-Br^{H}** species, the **P-Cp^{H}** peaks overlaps with a small peak (marked as

P_T) already present in the **P-Br** mass spectrum in the same region. A 166.3 Da difference between consecutive P_T peaks shows their origin from the P3HT, however, the exact end-group nature of the P_T is unclear at this stage. Nevertheless, one can clearly observe the disappearance of the **P-Br^H** peaks, confirming their quantitative transformation. Furthermore, the peak shift of -13.9 Da during the transformation of **P-Br** to **P-Cp** confirms the inertness of the bromo group which is directly attached to the thiophene ring towards the NiCp$_2$ transformation procedure under the applied conditions. The MALDI-ToF mass spectrum data for **P-Br** and **P-Cp** are summarized in **Table 6.1**.

Table 6.1. A summary of MALDI-ToF mass spectrometry data for different chain-end constitutions of **P-Br** and **P-Cp**.

Species	n^a	Formula	m/z th.	m/z exp.	$\Delta\ m/z$
P-Br^{Br}	15	$[C_{155}H_{218}Br_2O_2S_{15}]^+$	2749.11	2749.41	0.30
P-Br^H	16	$[C_{165}H_{233}BrO_2S_{16}]^+$	2837.28	2837.63	0.35
P-Br^{Br}	16	$[C_{165}H_{232}Br_2O_2S_{16}]^+$	2915.20	2915.30	0.1
P-Br^H	17	$[C_{175}H_{247}BrO_2S_{17}]^+$	3003.37	3003.77	0.40
P-Cp^H	15	$[C_{160}H_{223}BrO_2S_{15}]^+$	2735.23	2735.27	0.04
P-Cp^{Br}	16	$[C_{170}H_{238}O_2S_{16}]^+$	2823.41	2823.59	0.18
P-Cp^H	16	$[C_{170}H_{237}BrO_2S_{16}]^+$	2901.32	2901.40	0.08
P-Cp^{Br}	17	$[C_{180}H_{252}O_2S_{17}]^+$	2989.49	2988.99	0.50

^{a} number of monomer unit

A close agreement between the theoretical and the experimental m/z values fully corroborates the chain-end constitution (refer to **Figure 6.5** and **Figure 6.6**, showing close agreement between the experimentally measured MALDI-ToF and the simulated mass spectra for **P-Br** and **P-Cp**). To avoid any interference from P_T and considering the quantitative nature of the **P-Br** to **P-Cp** transformation, the end-group fidelity was estimated at the **P-Br** stage. A comparison of area under the peaks associated with **P-Br^{Br}**, **P-Br^H**, and P_T in the MALDI-ToF mass spectrum of **P-Br** revealed an end-group fidelity of 90%. These data – jointly with NMR data – evidence the efficacy of the synthetic approach for the introduction of a Cp moiety at the terminus of a P3HT chain.
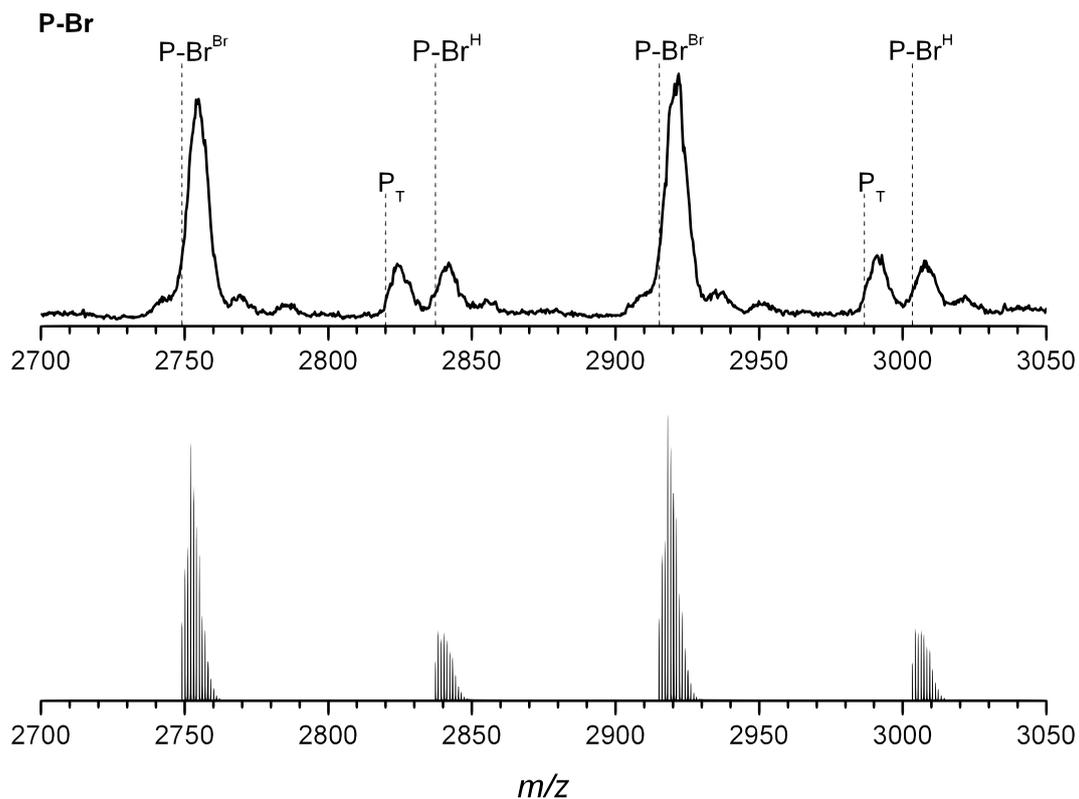
Figure 6.5. Comparison between the experimentally measured and the simulated mass spectrum of **P-Br**.
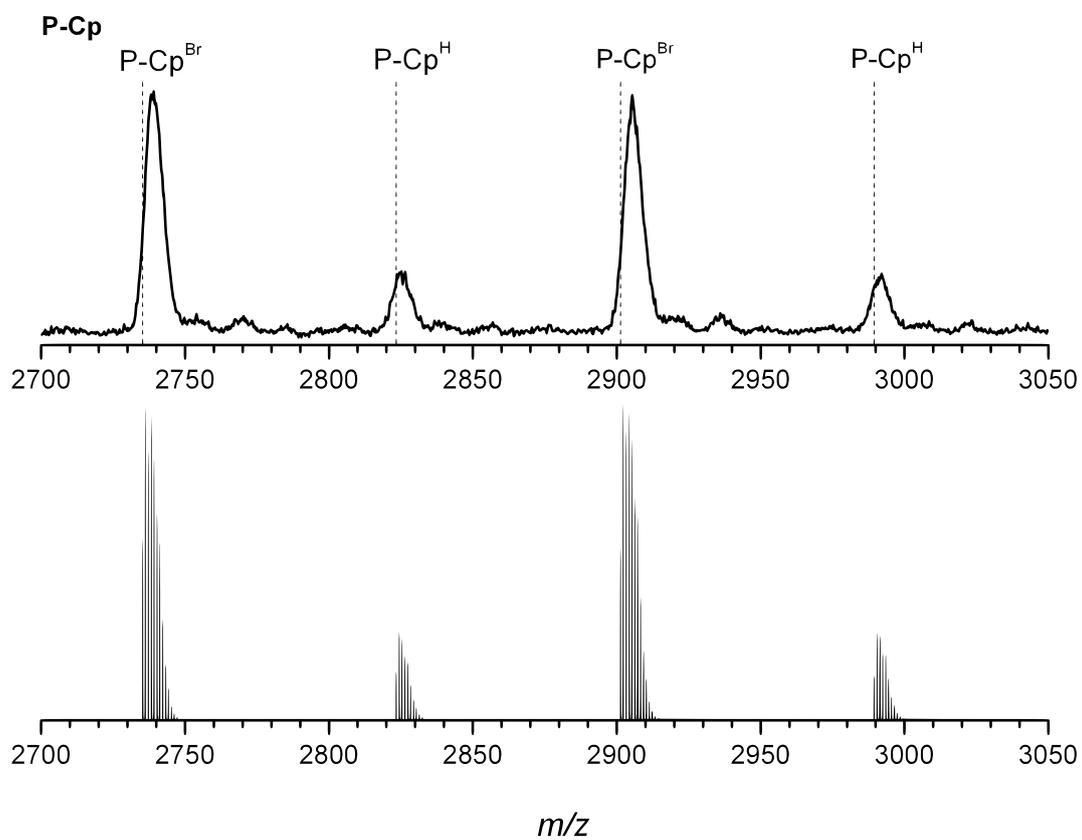
Figure 6.6. Comparison between the experimentally measured and the simulated mass spectrum of **P-Cp**.

After characterizing the **P-Cp** polymer and ascertaining the nature of the end-groups, the reactivity of the Cp end-groups as a diene in a DA reaction was demonstrated. For this purpose, **PS** carrying dithioester based electron deficient dienophile end-groups was synthesized by employing benzyl (diethoxyphosphoryl)dithioformate as chain transfer agent according to the RAFT procedure previously established.[86] The suitability of electron-deficient dithioester end-capped polymers for block copolymer synthesis via [4+2] HDA cycloaddition reactions has been previously established (refer to section 2.2).[85,86] The HDA cycloaddition coupling reaction was performed between Cp (diene) end-capped P3HT **P-Cp** and RAFT polymerized electron deficient dithioester (dienophile) end-capped **PS** (refer to **Scheme 6.2**). The reaction was performed in THF in the presence of $ZnCl_2$ at 50 °C for 24 h.
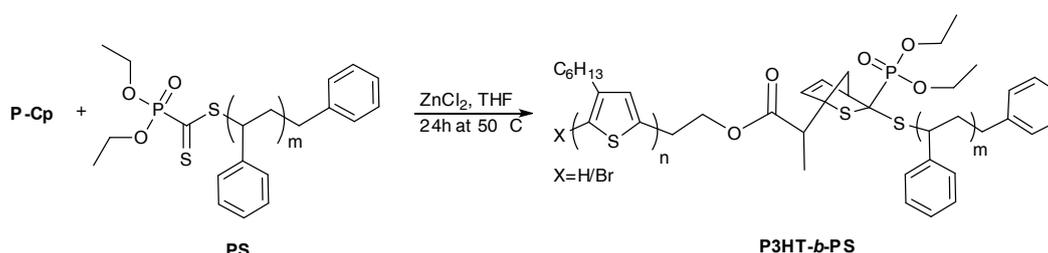
Scheme 6.2. Schematic representation of the **P3HT-*b*-PS** synthesis via HDA ligation.

The SEC analysis of the reaction mixture clearly showed the formation of block copolymer. The corresponding SEC traces of reacting polymers and formed block copolymer are depicted in **Figure 6.7** and their molecular weights are collated in **Table 6.2**.

Table 6.2. SEC data for the **P-Cp**, RAFT synthesized **PS** with dithioester end-groups, **P3HT-*b*-PS** synthesized via HDA ligation.

Sample	M_p /g·mol^{-1}	M_n /g·mol^{-1}	M_w /g·mol^{-1}	$Đ$
P-Cp	6300	6500	7600	1.2
PS	3300	3100	3500	1.1
P3HT-*b*-PS	8700	7800	9100	1.2

The resulting block copolymer was also characterized by ^{1}H NMR spectroscopy. Before the ^{1}H NMR spectroscopic analysis, the block copolymer sample was repeatedly precipitated from its THF solution into acetone. Such a procedure removed any traces of unreacted PS which is readily soluble in acetone. The ^{1}H NMR spectrum of the purified P3HT-*b*-PS formed by the [4+2] HDA cycloaddition reaction clearly showed the signals for the aromatic proton resonances originating from the PS block (refer to **Figure A10** in the appendix). These results support the suitability of the terminal Cp groups of P-Cp to undergo DA reactions.
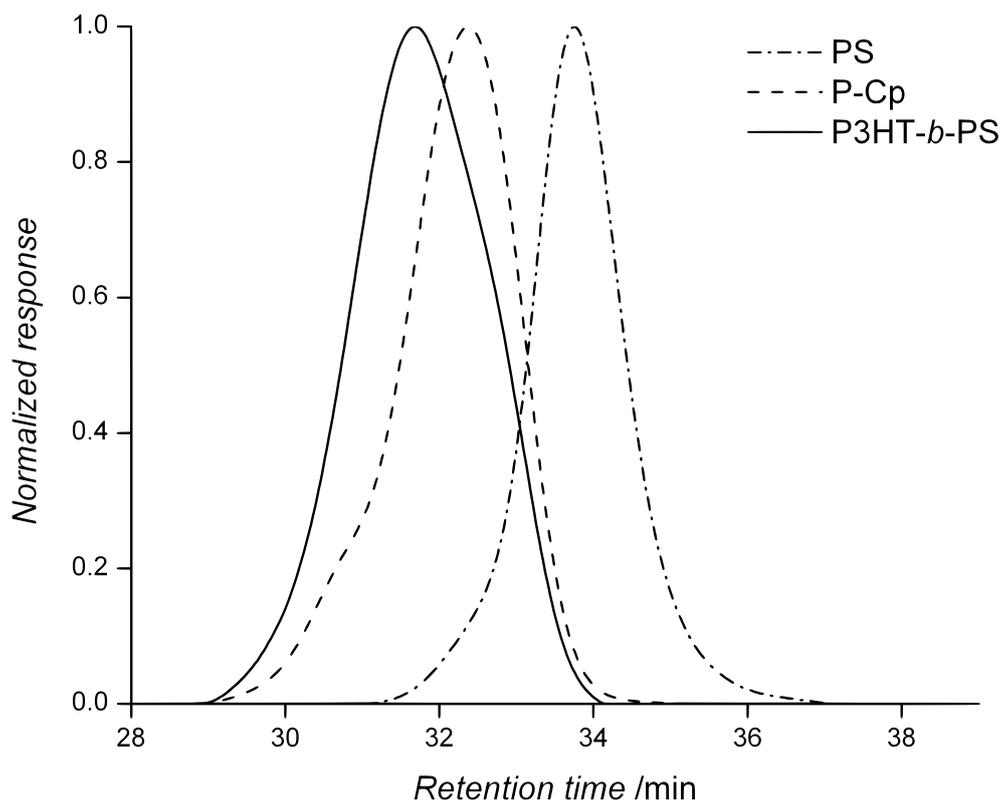
Figure 6.7. Overlay of SEC traces of **P-Cp**, RAFT synthesized **PS** with dithioester end-groups, and **P3HT-*b*-PS** synthesized via HDA ligation.

The so far discussed characterization data for the **P-Cp** augmented by the example of block copolymer formation clearly evidences the presence of DA active Cp groups at the end of P3HT chains. The **P-Cp** was subsequently reacted with pristine SWCNTs (**SWCNT-1**) in order to demonstrate the unprecedented one-step facile and direct surface functionalization of pristine SWCNTs with P3HT via DA ligation. The surface DA ligation was carried out at 80 °C for 24 h. For the purpose of comparison, a reference sample (**SWCNT-0**) was prepared by mixing **P-0** – P3HT lacking a Cp end-group – with the **p-SWCNT** under the identical conditions. Both the **SWCNT-1** and **SWCNT-0** samples were extensively washed with THF – until the washings were colorless – before the characterization. The resulting P3HT/SWCNTs covalent hybrid materials were successfully characterized by employing TGA, EA, XPS, and HRTEM.

6.3. Characterization of P3HT-Cp functionalized SWCNTs

6.3.1. Synthesis

Ligation of cyclopentadienyl end-capped P3HT with SWCNTs and reference sample (SWCNT-0 and SWCNT-1)

35 mg of pristine SWCNTs (**p-SWCNT**) were dispersed in 350 mL NMP in an

ultrasonic bath and nitrogen purging for 1 h. 350 mg of Cp end-capped P3HT (**P-Cp**) were added to the mixture and degassed for 15 minutes. The mixture was allowed to stir at ambient temperature for 24 h under inert atmosphere at 80 °C to generate the sample **SWCNT-1**. The reference sample (**SWCNT-0**) was prepared by mixing of SWCNTs and non-functional P3HT (**P-0**) under the identical conditions.

6.3.2. Results and discussion

Thermogravimetric Analysis (TGA)

The thermogravimetric profiles of the SWCNT based samples (**p-SWCNT**, **SWCNT-0** and **SWCNT-1**), cyclopentadienyl end-capped P3HT (**P-Cp**) and the non-functional P3HT (**P-0**) are depicted in **Figure 6.8**.
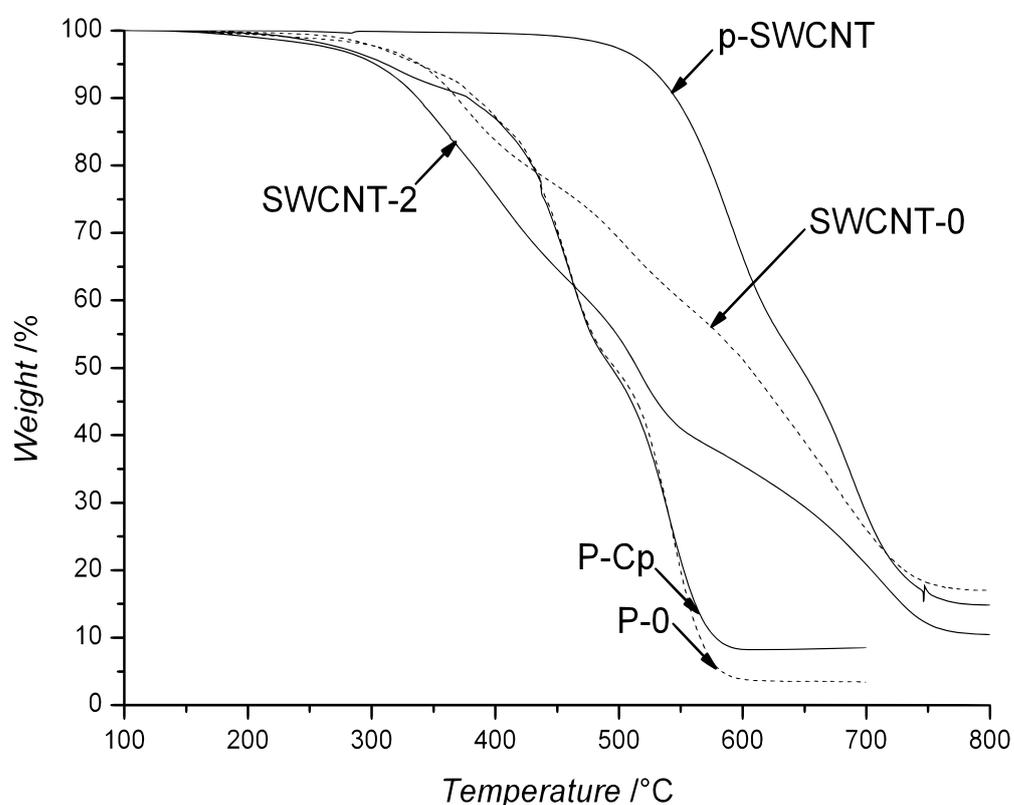
Figure 6.8. Thermogravimetric profiles of non-modified SWCNTs (**p-SWCNT**), cyclopentadienyl end-capped P3HT (**P-Cp**) and functionalized SWCNTs with **P-Cp** (**SWCNT-1**). Profiles of the non-functional P3HT (**P-0**) and the reference sample SWCNTs mixed with **P-0** (**SWCNT-0**) are also shown. A heating rate of 10 °C·min^{-1} was applied, following a 30 minutes isothermal step at 100 °C.

The analysis of the TGA data was performed using the first derivative profiles to identify the successive degradation of the samples (same procedure as described in Chapter 4, section 4.3.2). Each degradation is characterized by an initial temperature (T_i), a final

temperature (T_f), and a temperature corresponding to the maximum rate of weight loss (T_m). In the appendix, the derived profiles are depicted in **Figure A11** and a summary of the degradation characteristics is available in **Table A5**. The non-modified SWCNTs (**p-SWCNT**) start to decompose at 440 °C until a weight of 14.6% (catalytic residue) at 820 °C. The polymer samples (**P-Cp** and **P-0**) displayed decomposition from 100 °C to 630 °C in several steps in a similar fashion. At 410 °C, a residual weight of 85.0% for the **P-Cp**, and 85.4% for the **P-0** was observed. A subsequent degradation until 495 °C led both polymers to a similar residual weight percentage, 49.7% for **P-Cp** and 50.4% for **P-0**, before further degradation occurred at higher temperature. The fact that the polymers are not completely degraded before the SWCNTs have started to degrade (T_i = 440 °C) made it difficult to precisely quantify the functionalization of the SWCNTs bonded to P3HT polymer chains. The TGA profiles of the SWCNTs functionalized with the polymer (including the reference sample) revealed the onset of degradation for all the samples at temperatures below T_i (440 °C) of the pristine SWCNTs, evidencing the presence of the polymer in all polymer/SWCNT based samples. Comparing the TGA thermograms of **SWCNT-0** and **SWCNT-1**, one can clearly notice a higher overall weight loss in the case of **SWCNT-1**. The TGA thermograms of the SWCNTs modified with **P-Cp** (**SWCNT-1**), showed a significantly higher degradation when heated to 440 °C (T_i for pristine SWCNTs). For **SWCNT-1**, a weight loss of 37.2% was observed at 440 °C, while at the same temperature a lower weight loss of 21.8% was observed for the **SWCNT-0**. The wrapping of SWCNTs with the P3HT via Van der Waals/π-π interaction accounts for the presence of polymer in **SWCNT-0** sample and most of the P3HT/CNTs hybrid materials reported in literature are based on this physical interaction.[330,331,332] The onset of SWCNTs degradation before the complete degradation of P3HT made quantification of grafting density impossible. Nevertheless, the TGA experiments clearly evidenced a higher amount of polymer in case SWCNTs functionalized with Cp end-capped P3HT.

Elemental Analysis (EA)

In order to provide complementary information regarding the presence of the polymer chains for the SWCNTs functionalized or mixed with P3HT, their elemental composition was determined for carbon, hydrogen, nitrogen, oxygen and sulfur. The results of the elemental analysis are collated in **Table 6.3**.

Table 6.3. Elemental composition of non-modified SWCNTs (**p-SWCNT**), cyclopentadienyl end-capped P3HT (**P-Cp**), functionalized SWCNTs with **P-Cp** (**SWCNT-1**), and the reference samples: non-functional P3HT (**P-0**) and the SWCNTs mixed with **P-0** (**SWCNT-0**). The amount of P3HT incorporated in the hybrid samples expressed as grafting density in *wt.-%* is indicated.

Sample	C	H	N	O	S	Grafting density /wt.-%
p-SWCNT	79.1	0.6	0.6	4.1	0	-
P-Cp	69.5	8.2	0.3	0.9	14.3	-
P-0	67.2	7.7	0.4	1.1	14.6	-
SWCNT-1	70.1	2.3	0.9	3.7	3.9	27.3
SWCNT-0	50.9	1.4	0.7	6.9	0.8	8.1

For the **p-SWCNT**, the carbon content was found to be 79.1 *wt.-%* of the composition. Beside carbon, some oxygen (4.1 *wt.-%*) was also detected. The mass balance was not complete which was attributed to some catalytic residue present in the sample from its production process. The elemental compositions of **P-Cp** and **P-0** reflected a difference mainly between the carbon, hydrogen and sulfur atoms, whereas the nitrogen and oxygen contents are not relevant and may be due to air contamination. The compositions did also not exactly correspond to the expected theoretical values. The sulfur content is about 5 *wt.-%* lower than the theoretical value (see **Table 6.4**).

Table 6.4. Comparison of the theoretical elemental composition of cyclopentadienyl end-capped P3HT (**P-Cp**) and non-functional P3HT (**P-0**) with the experimentally obtained values via EA.

Sample		at.-%			wt.-%		
		C	H	S	C	H	S
P-Cp	Experimental	40.5	55.5	4.0	72.6	8.4	19.0
	Theoretical	40.3	56.6	3.1	75.6	8.9	15.5
P-0	Experimental	55.5	39.0	5.5	75.4	4.5	20.1
	Theoretical	41.1	55.6	3.3	75.1	8.6	16.3

For **P-0** and **P-Cp**, the mass balance was not closed. The presence of bromine atoms at the chain-end, as evident in MALDI-ToF mass spectrometry data discussed earlier, explains the deviation of the experimental EA results from the theoretical values. Bromine, as other halogens, acted as a combustion inhibitor, leading to an incomplete combustion of the sample and to errors in the elemental composition. Quantifying the amount of P3HT polymer chains

for **SWCNT-1** and **SWCNT-0** was thus not reliable. However, the analysis of the EA data corroborated the same trend as observed in TGA. Firstly, the sulfur and hydrogen contents increased unambiguously after functionalization with **P-Cp**. The **SWCNT-1** showed sulfur and hydrogen contents of 3.9 and 2.3 *wt.-%*, respectively. The presence of P3HT was also observed in **SWCNT-0**, yet in a smaller amount than **SWCNT-1**. The grafting densities in weight percentage (*wt.-%*) for the **SWCNT-0** and **SWCNT-1** based samples are presented in the **Table 6.3**. Keeping in mind the limitations discussed above (mass balance not complete, presence of bromine as combustion inhibitor) these values must be handled with care. However, one can qualitatively conclude a higher grafting density in case of SWCNTs functionalized with Cp end-capped P3HT as compared to the reference sample where P3HT was physically adsorbed at the surface of the SWCNTs.

X-Ray Photoelectron Spectroscopy (XPS)

Contrary to TGA and EA, which are bulk characterization techniques, XPS offers the possibility to characterize the surface of a sample. Complementary to EA, the elemental composition can also be assessed via XPS. In addition, the same element present in different chemical environments can also be detected. **Figure 6.9** depicts the high resolution XPS scans for the carbon (C1s), sulfur (S2p) and bromine (Br3d) signals obtained for the **p-SWCNT**, **P-Cp**, **SWCNT-1**, **P-0**, and **SWCNT-0**.

The C1s carbon signal at 284.4 eV is representative the graphitic carbon atoms of **p-SWCNT** (refer to the XPS measurement performed in section 4.3.2 and 5.3.2). A small amount of sulfur (0.2 *at.-%*) was also detected in the case of **p-SWCNT** (refer to **Table 6.5**).

XPS spectra for both polymers (**P-Cp** and **P-0**) showed the presence of bromine. Via the Br3d$_{3/2}$ signal at 70.3 eV,[333,334] originating from the bromo end-groups of **P-Cp** and **P-0**. The presence of sulfur signals (S2p$_{3/2}$ signal at 163.9 eV)[335] and the signal for the carbon atoms from hydrocarbon (C1s signal at 285.0 eV)[336] correlate with the composition of the repeat unit for **P-Cp** and **P-0** (3-hexylthiophene-2,5-diyl). A small fraction of the deconvoluted C 1s signal represented by the peak located at 287.0 eV have been assigned to C-Br and C-O.[334] Another small constituting peak of deconvoluted C1s signal at 283.8 eV could not be attributed unambiguously, however, such a signal may be attributable to carbide species which may have originated from contamination.[337] The atomic composition for the carbon, sulfur and bromine contents as determined by XPS are in complete agreement with the theoretical composition for both the polymers (**P-Cp** and **P-0**), reflecting on the higher accuracy of XPS analysis than EA (refer to **Table 6.6**).
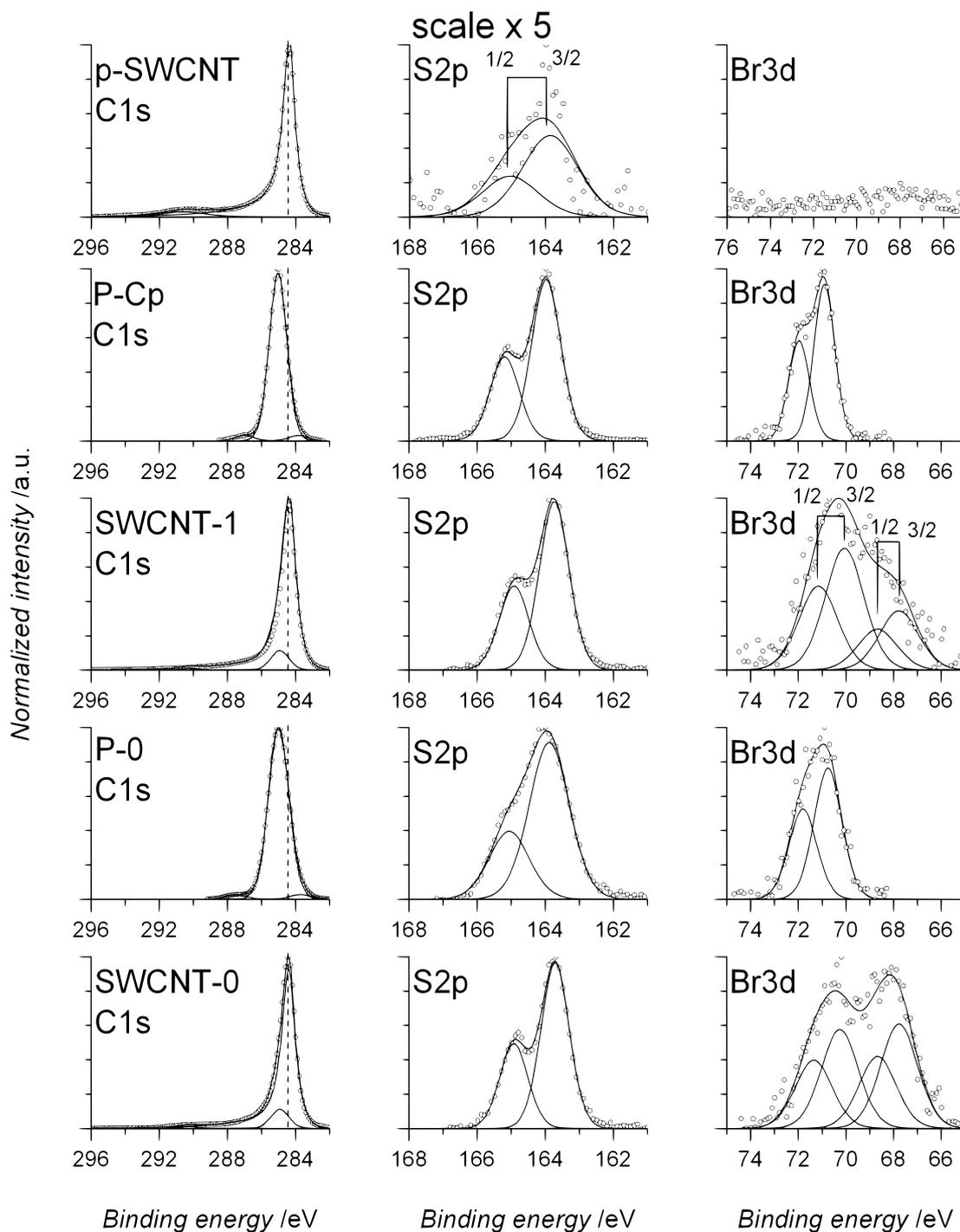
Figure 6.9. XPS spectra of non-modified SWCNTs (**p-SWCNT**), cyclopentadienyl end-capped P3HT (**P-Cp**), functionalized SWCNTs with **P-Cp** (**SWCNT-1**). The reference samples, non-functional P3HT (**P-0**) and the SWCNTs mixed with **P-0** (**SWCNT-0**) are depicted. For a better visualization all spectra are normalized to the maximum intensity, and the signal S2p for **p-SWCNT** is enlarged by a factor of 5.

Table 6.5. Assignment of binding energies and comparison of the bond contribution after the deconvolution of the XPS spectra of non-modified SWCNTs (**p-SWCNT**), cyclopentadienyl end-capped P3HT (**P-Cp**), functionalized SWCNTs with **P-Cp** (**SWCNT-1**), and reference samples: non-functional P3HT (**P-0**), and the SWCNTs mixed with **P-0** (**SWCNT-0**) are represented.

Peak	$B.\ E.^a$ /eV	at.-%					Entity
		p-SWCNT	P-Cp	P-0	SWCNT-1	SWCNT-0	
Br3d$_{5/2}$	67.7	-	-	-	0.1	0.2	$\underline{Br}^-$
Br3d$_{3/2}$	70.3	-	0.3	0.2	0.2	0.2	$\underline{Br}$-C
S2p$_{3/2}$	163.9	0.2	8.5	9.2	3.7	2.8	$\underline{S}$-C
C1s	283.8	-	2.8	2.4	-	-	C$_{carbide}$
	284.4	93.3	-	-	85.2	85.6	C-C$_{graphite}$
	285.0	-	85.5	85.4	9.9	10.2	C-C, $\underline{C}$-H
	287.0	-	2.9	2.8	-	-	$\underline{C}$-O, $\underline{C}$-Br
	290.6	6.5	-	-	0.9	1.0	π-π^*

^{a}binding energy.

Like **p-SWCNT**, the C1s signal for **SWCNT-0** and **SWCNT-1** is dominated by the peak for graphitic carbon at 284.4 eV. The presence of hydrocarbons signals at 285.0 eV reflects on the presence of the P3HT polymer chains in **SWCNT-0** and **SWCNT-1** samples. However, the presence of P3HT in both samples, **SWCNT-1** and **SWCNT-0**, is more evident by the appearance of the signals for sulfur and bromine atoms at the characteristic binding energies of 163.9 eV for S2p$_{3/2}$, and at 67.7 and 70.3 eV for Br3d$_{5/2}$ and Br3d$_{3/2}$ respectively.

Table 6.6. Comparison of the theoretical elemental composition of cyclopentadienyl end-capped P3HT (**P3HT-Cp**) and non-functional P3HT (**P-0**) with the experimental values obtained via XPS.

Sample		at.-%		
		Br	S	C
P-Cp	Experimental	0.3	8.5	91.2
	Theoretical	0.2	8.9	90.9
P-0	Experimental	0.2	9.2	90.6
	Theoretical	0.1	9.1	90.8

The sulfur content was found to be 3.7 *at.-%* for **SWCNT-1**, whereas the sulfur content for **SWCNT-0** was 2.8 *at.-%*. The detection of the signal located at 67.7 eV for the Br3d$_{5/2}$ peak may be associated with the formation of bromide ions (Br⁻) via decomposition during the

XPS analysis.[338] Based on similar considerations as in Chapter 4 (section 4.3.2) for the grafting density via XPS, the amount of atoms (C, H, O, S) introduced from the P3HT polymer chains to the SWCNTs was estimated from the respective atomic percentages (*at.-%*). The known molecular weights (M_n) of the polymer samples (**P-Cp** and **P-0**) enabled the estimation of loading capacity in mmol·g^{-1}. From the theoretical specific area of the SWCNTs (identical to a graphene sheet), the area occupied by the polymer chain at the SWCNT surface can be evaluated in chain·nm^{-2}. The periodicity, i.e. the average number of carbon atoms at the SWCNTs surface per polymer chain, was determined by considering the surface of a hexagonal ring constituted by 2 residual carbon atoms (each carbon atom being shared between three rings, 6/3 = 2). **Table 6.7** summarizes the grafting density expressed in three different units for **SWCNT-1**. The amount of polymer physically adsorbed at the surface of the reference sample (**SWCNT-0**) is also included as mmol·g^{-1} (loading capacity).

Table 6.7. Grafting density estimated via XPS for the modified SWCNTs with cyclopentadienyl end-capped P3HT (**SWCNT-1**), and the reference sample (SWCNTs mixed with non-functional P3HT **SWCNT-0**).

Sample	*at.-%*	*wt.-%*	*Grafting density*		
			mmol·g^{-1}	chain·nm^{-2}	Periodicity[a]
SWCNT-1	39.2	46.2	0.111	0.0510	748
SWCNT-0	28.4	32.2	0.0617	-	-

[a] Number of carbon atoms per polymer chain.

As already observed via TGA and EA, the reaction of **P-Cp** with the SWCNTs via DA reaction led to a higher amount of polymer grafted at the surface of SWCNTs. In the **SWCNT-1** sample, the estimated atomic percentage due to the elemental composition of the P3HT chain determined via XPS reads 39.2% and corresponds to a 46.2 *wt.-%* of polymer in the sample. The obtained grafting density can be calculated in alternative units, leading to 0.111 mmol·g^{-1} which is equivalent to 0.0510 chain·nm^{-2}. These numbers led to a periodicity of one polymer chain every 748 carbon atoms for **SWCNT-1**. The calculation of such numbers is irrelevant in the case of **SWCNT-0** as the P3HT is only physically adsorbed at the surface of SWCNTs. However, the amount of P3HT adsorbed at the surface of SWCNTs in case of **SWCNT-0** is reported in **Table 6.7** as mmol of P3HT per gram of SWCNTs. A comparison of the data provided in **Table 6.7** revealed that the amount of polymer in **SWCNT-1** sample was 2 times higher than the reference sample **SWCNT-0**. The analysis thus confirmed the efficient grafting of P3HT at the surface of SWCNTs via a DA reaction

employing Cp end-capped P3HT polymer compared to the physical wrapping effect in case of the reference sample. Compared to the grafting densities obtained for the SWCNTs surface functionalization with the Cp end-capped PMMA (0.064 to 0.086 mmol·g^{-1} for M_n = 2900 g·mol^{-1}) in Chapter 4, and PNIPAM (0.0520 to 0. 0628 mmol·g^{-1} for M_n = 5400 g·mol^{-1}) in Chapter 5, the grafting density observed for **P-Cp** is 2 times higher (0.111 mmol·g^{-1}). A comparatively higher supramolecular affinity between P3HT and SWCNTs can lead to an enhanced proximity of reactive Cp end-groups on the surface of SWCNTs which may account for the higher grafting density in case of **P-Cp**.

In order to further characterize and differentiate the reference sample **SWCNT-0** from **SWCNT-1**, the samples were analyzed with HRTEM.

High Resolution Transmission Electron Microscopy (HRTEM)

Figure 6.10 depicts representative HRTEM images of the non-modified SWCNTs (top, left side, **p-SWCNT**), the SWCNTs functionalized with Cp end-capped P3HT (top, right side, **SWCNT-1**) and the reference sample (SWCNTs mixed with non functional P3HT, bottom, **SWCNT-0**).

The single-walled nature of the SWCNTs was observed in all cases, with a tube diameter ranging between 1.0 and 1.6 nm. The **p-SWCNT** expectedly exhibited a surface free from any amorphous carbon. In the case of **SWCNT-1**, the surface of the individual SWCNTs was covered by an amorphous layer (thickness estimated by 2.1 nm) of P3HT polymer. The amorphous layer of P3HT was also found wrapping the SWCNTs in the reference sample **SWCNT-0**; however, in case of the **SWCNT-0** the sample was predominantly constituted by bundles of SWCNTs wrapped by the amorphous P3HT. On the other hand, microscopic agglomerates were detected in **SWCNT-0** which appeared to be coated with the polymer film (refer to **Figure A12** in the appendix). Beside those aggregates the polymer layer also appeared to have covered the entire copper grid, which led to critical conditions for the HRTEM experiments. Such a behavior of the reference sample suggests that the non-functional P3HT may be initially physisorbed at the surface of the SWCNTs, such the subsequent ultrasonic treatment for the HRTEM sample preparation resulted in the desorption of the polymer chains from the surface of the SWCNTs, leading to a polymer film covering the copper grid.
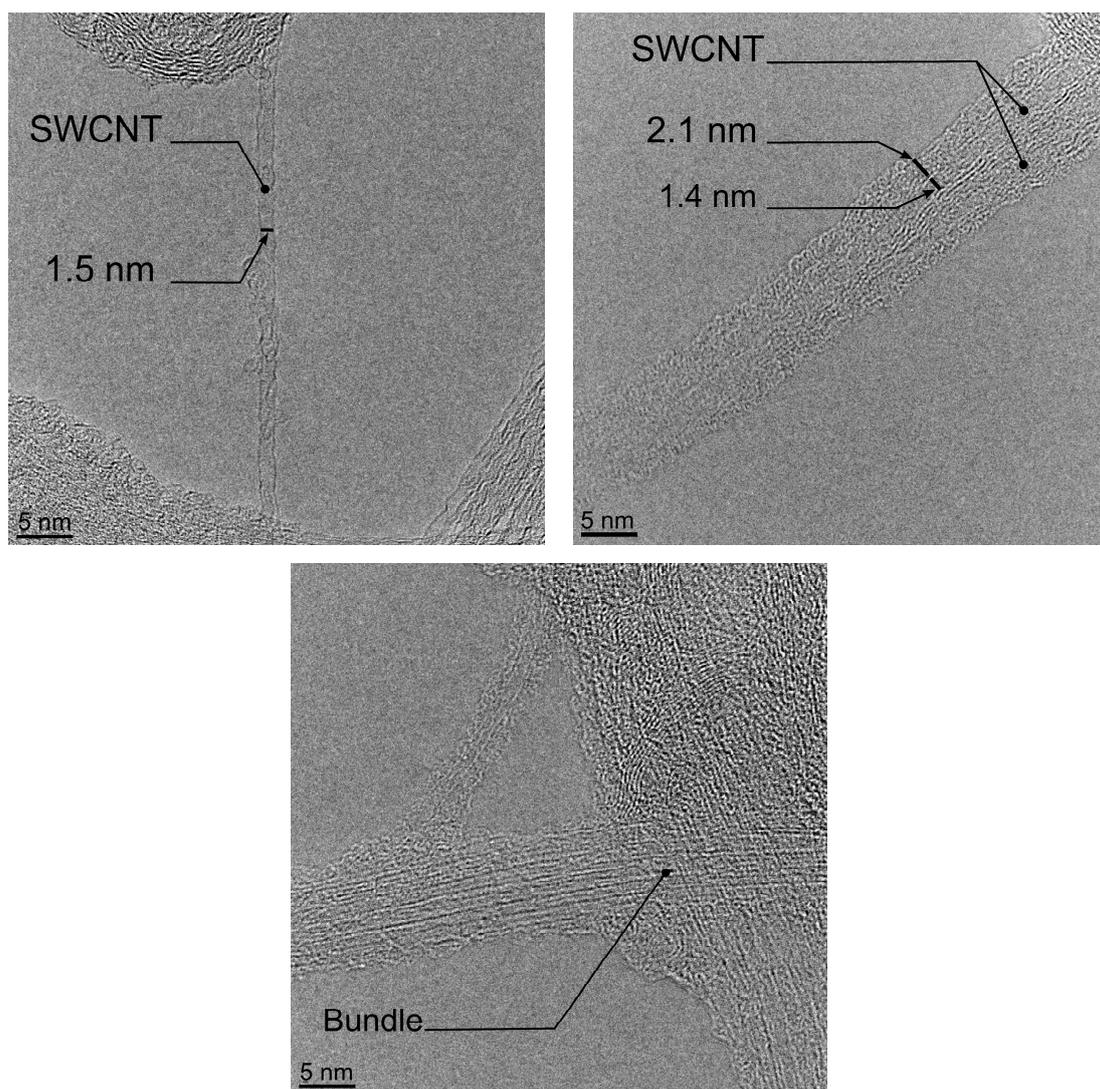
Figure 6.10. HRTEM images of non-modified SWCNTs (**p-SWCNT**, top, left), SWCNTs functionalized with **P-Cp** (**SWCNT-1**, top right side), and the reference sample of SWCNTs mixed with non-functional P3HT **P-0** (**SWCNT-0**, bottom).

A UV-VIS spectroscopic analysis of the chloroform extract after ultrasonication of both samples (**SWCNT-0** and **SWCNT-1**) underpins the covalently bound nature of the P3HT in **SWCNT-1**, as substantial amounts of P3HT leached from the **SWCNT-0** and only limited P3HT leaching was observed in the chloroform extract of **SWCNT-1**. The UV-VIS absorption spectra after sonification evidence that the amount of detached P3HT is substantially lower in the **SWCNT-1** sonicated sample compared to the **SWCNT-0** sample (refer to **Figure A13** in the appendix). A combination of limited ultrasound assisted retro DA reaction[339] and slight physisorption of polymer in addition to the covalent grafting accounts for the P3HT observed in the chloroform extract of **SWCNT-1**. Contrary to the **SWCNT-0** sample, the **SWCNT-1** sample did not display any aggregation during the HRTEM analysis, highlighting the effective de-bundling of SWCNTs by covalent grafting of polymer chains at

the surfaces of the SWCNTs via the DA reaction between the Cp terminus of the P3HT polymer and surface of the SWCNTs. Furthermore, the covalent attachment resulted in a stable dispersion of **SWCNT-1** in chloroform without any sign of aggregation over a period of 5 days whereas the dispersion of **SWCNT-0** in chloroform showed a clear aggregation after 12 h (refer to **Figure A14** in the appendix).

6.3.3. Conclusions

For the first time, the scope of the DA reaction was demonstrated between Cp-capped P3HT and SWCNTs' surface as a facile mean for the covalent functionalization of SWCNTs with conducting P3HT polymer. *In situ* end-group capping using the GRIM method and subsequent end-group transformations led to the unprecedented Cp-capped P3HT. The reaction of an aliphatic bromo group terminated P3HT with $NiCp_2$ selectively and quantitative transformed only the terminal aliphatic bromo group into the Cp group. The inertness of bromo groups directly attached to the thiophene ring exclusively led to P3HT with Cp groups only at one end of polymer chain. The terminal Cp groups were reactive towards dithioester based dienophiles under HDA reaction conditions which was demonstrated by the preparation of a P3HT-*b*-PS block copolymer. The DA ligation of Cp-terminated P3HT produced P3HT/SWCNTs molecular hybrid materials, where individual SWCNTs were functionalized with P3HT, thus addressing the bundling issue intrinsically associated with CNTs. The synthesized SWCNT/P3HT hybrid material was found to contain 2 times more P3HT than the reference sample featuring a grafting density of the polymer chains at the surface of the SWCNTs to be close to 0.111 mmol·g^{-1}, in other units, 0.0510 chain·nm^{-2} and a periodicity of 1 P3HT chain per 748 carbon atoms of SWCNTs. HRTEM revealed individual SWCNTs wrapped with P3HT whereas in the reference sample P3HT was adsorbed on the bundles of the SWCNTs.

# Chapter 7 – Tuning the polymer grafting density on SWCNTs via hetero Diels-Alder ligation
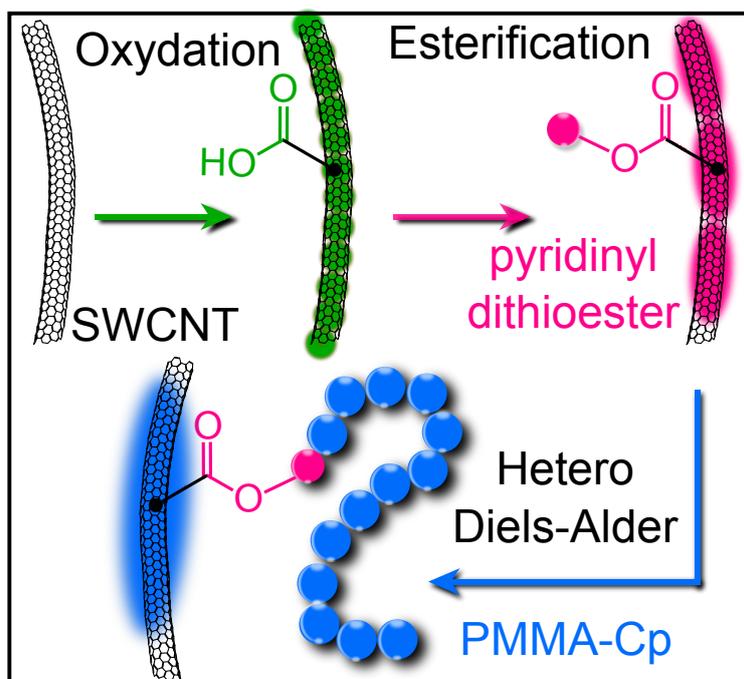
7.1. Introduction

The ligation of SWCNTs via DA reactions with Cp end-capped PMMA polymer chains, featuring molecular weights (M_n) of close 3000 g·mol^{-1}, the grafting densities evaluated via TGA, EA and XPS, gave similar values, congruent with those observed in the literature.[340] Recently, the Adronov group evidenced for the first time that the molecular weight of the polymer strands governs the grafting density of pre-functionalized SWCNTs by a power of law.[341] In their study, SWCNTs were pre-functionalized with an alkyne moiety precursor and the degree of functionalization evaluated to be close to one functional group every 150 carbon atoms. The ligation of the pre-functionalized SWCNTs occurred via a 1,3-cycloaddition with azide terminated poly(styrene) strands synthesized via ARGET polymerization. The living character of the polymerization delivered well-defined polymer strands with molecular weights (M_w) varying from 2000 g·mol^{-1} to 176 000 g·mol^{-1}, and the grafting densities of the modified SWCNTs were determined via thermogravimetry. For the studied system, a power law expressing the grafting density as a function of the molecular weight was established. The molecular weight of selected polymer strands is a limiting factor for grafting SWCNTs due to steric hindrance.

The investigations conducted in this chapter demonstrate that a pre-functionalization of SWCNTs with DA reactive groups leads to an increase in the grafting density of the polymer strands of a given molecular weight (PMMA, M_n = 2700 g·mol^{-1}), compared to the direct grafting systems studied in the previous chapters. However – and importantly – such a strategy involves an at least partly destructive step compared to the previous direct functionalization route employing virgin SWCNT material. In the current section, the synthetic route is depicted in **Scheme 7.1** in which the polymer strands react with pre-functionalized SWCNTs via a HDA reaction under similar conditions.

The mild acidic treatment employed was inspired by numerous studies considering the purification[342] and functionalization[32,343] of the SWCNTs for their better dispersibility in solvents[344] or compatibility in thermoplastic matrices.[345] Yet the main disadvantage of such a preliminary treatment remains the destruction of the SWCNTs (shortening),[346] the loss of the SWCNTs intrinsic properties (mechanical and electrical)[279,347] and the difficulty to implement such a treatment (multiple filtration – centrifugation – neutralization cycles) on a larger scale. In the present chapter, oxidized SWCNTs (**o-SWCNT**) were esterified with a pyridinyl based dithioester (**Dithio-OH**) employed as a dienophile. The reactivity of the dithioester for a HDA-reaction with a cyclopentadienyl end-capped PMMA (**PMMA-Cp**) was performed as a model reaction in solution, and subsequently translated to the esterified SWCNTs

(**1-SWCNT**) with **Dithio-OH** to lead to polymer functionalized SWCNTs via a HDA-reaction (**2-SWCNT**) after the addition of **PMMA-Cp**.
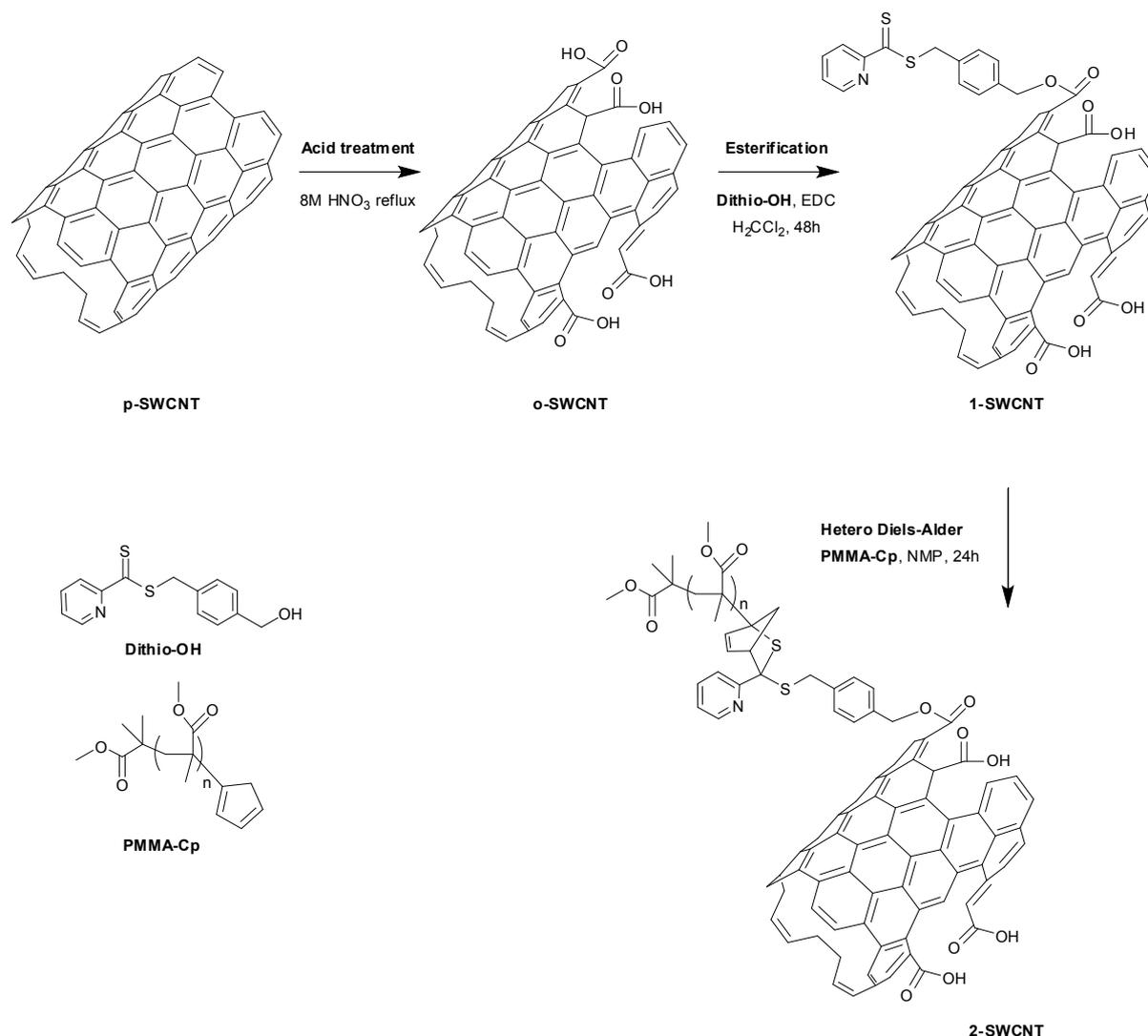
Scheme 7.1. Functionalization of SWCNTs (**p-SWCNT**) with **PMMA-Cp** via a HDA reaction. Oxidized SWCNTs (**o-SWCNT**) are esterified with a pyridine based dithioester (dienophile, **Dithio-OH**) affording **1-SWCNT**, reacting in a HDA reaction with a cyclopentadienyl end-capped polymer (diene, **PMMA-Cp**) and generating **2-SWCNT**.

The oxidation of the SWNTs was initially characterized via Raman spectroscopy. To determine the grafting density, the characterization of the SWCNTs after each synthetic step was performed via FTIR spectroscopy, TGA, EA, and finally via XPS. The end-group characterization of the polymer (**PMMA-Cp**), and the resulting product (**PMMA-HDA**) after the HDA-reaction with the dithioester (**Dithio-OH**) was carried out via ESI-MS.

7.2. Synthesis and characterization of pyridine based dithioester

The list of the employed materials is summarized in Chapter 3 (section 3.12.4). The synthetic route defined above requires the synthesis of **Dithio-OH**, a new pyridine based dithioester featuring a hydroxy group.

Synthesis of 2-picolyl phenyl sulfone

The synthesis was performed as described in the literature.[348,349] A mixture of picolylchloride (6.60 g, 40 mmol, 1 eq), phenylsulfinate sodium (9.86 g, 60 mmol, 1.5 eq), DBU (6.08 g, 40 mmol, 1 eq) and tetrapropylammoniumbromide (2.14 g, 8 mmol, 0.2 eq) was refluxed overnight in 40 mL acetonitrile, and subsequently dried under vacuum. The mixture was dissolved in dichloromethane (40 mL) and washed with brine (100 mL). The organic phase was dried over $MgSO_4$ and under vacuum affording a brown solid. *Yield* 66%. ^{1}H NMR (400 MHz, $CDCl_3$, δ): 8.39–8.35 (ddd, J = 4.88, 1.83, 0.92 Hz, 1H), 7.75–7.59 (m, 3H), 7.59–7.51 (tt, J = 7.30, 2.14 Hz, 1H), 7.48–7.36 (m, 3H), 7.27–7.18 (ddd, J = 7.50, 5.00, 1.20 Hz, 1H), 4.52–4.56 (s, 2H, CH-SO_2).

Synthesis of p-bromomethylbenzoic methylester and p-bromomethylbenzyl alcohol

The synthesis of the title compounds was performed according to a modified literature procedure.[350] *p*-Bromomethylbenzoic acid (5 g, 23.0 mmol, 1 eq) and sulfuric acid (1.4 mL) were mixed in methanol (56 mL) and refluxed for 5 h. After drying under vacuum, ice water (200 mL) was carefully added and filtered. The residue was washed with 200 mL ice water and extracted in a diethylether : ethyl acetate (1:1) solution (100 mL), neutralized with a saturated solution of sodium carbonate (100 mL) and dried over Na_2SO_4. A yellowish oil was collected after drying under vacuum and identified as *p*-bromomethylbenzoic methylester. *Yield* 81%. ^{1}H NMR (400 MHz, $CDCl_3$, δ): 8.00–7.28 (m, 4H, Ar H), 4.56–4.31 (s, 2H, CH_2-Br), 3.87–3.80 (s, 3H, O-CH_3). To an ice cooled solution of DIBAL-H (25%) in *n*-hexane (50 mL, 2.7 eq), dry toluene (8 mL) was added under inert atmosphere. A solution of *p*-bromomethylbenzoic methylester (3.04 g, 13.4 mmol, 1 eq) in dry toluene (35 mL) was slowly added to the DIBAL-H solution. The mixture was allowed to react for 4 h in an ice bath (0 °C). Water was carefully added and the solution was filtered. The organic phase was separated, diluted with 100 mL dichloromethane and extracted twice with 100 mL water. After drying over $MgSO_4$ and under vacuum, the organic phase led to brownish white crystals. The solid was recrystallized from *n*-hexane until white crystals formed. *Yield* 27%. ^{1}H NMR (400 MHz, $CDCl_3$, δ): 7.47–7.21 (m, 4H, Ar H), 4.73–4.58 (s, 2H, CH_2-(OH)),

4.48–4.41 (s, 2H, CH_2-Br), 1.63–1.47 (broad, 1H, OH).

*Synthesis of 4-((pyridine-2-carbonothioylthio)methyl) benzyl alcohol (Dithio-OH)*

A mixture of 2-picolyl phenyl sulfone (1.00 g, 4.29 mmol, 1 eq), elemental sulfur (S_8, 0.43 g, 12.93 mmol, 3 eq) and THF (5 mL) was cooled with an ice bath at 0 °C. Potassium *tert*-butanolate (1.45 g, 12.93 mmol, 3 eq) was added, the solution turned red and was stirred overnight. A solution of *p*-bromomethylbenzyl alcohol (2.58 g, 12.93 mmol, 3 eq) dissolved in THF (9 mL) was added, and the mixture stirred for a subsequent 6 h. The solution was dried and dissolved in 45 mL from a THF : HCl (2 mol·L^{-1}) (1:1) solution, and 125 mL of dichloromethane. The organic phase was washed five times with water (50 mL) until the aqueous phase remained slightly yellowish. After being dried over Na_2SO_4 and evaporated under vacuum, a red oil was obtained. A small amount of cold dichloromethane (5 mL) was added and the solution filtered to separate a yellowish solid residue. The solution was passed over silicagel mixed with a dichloromethane : diethylether (6:1) solution and a reddish solution was collected and dried under vacuum. A silicagel column (*n*-hexane : diethylether 1:6) enabled to separate a pink colored solid appearing with an appearance as cotton wool. *Yield* 21%. ^{1}H NMR (400 MHz, CDCl$_3$, δ): 8.56–8.49 (ddd, J = 4.73, 1.68, 0.83 Hz, 1H, Py Hα), 8.27–8.21 (dt, 8.1, 1 Hz, 1H, Py Hγ), 7.76–7.69 (td, J = 7.83, 1.77 Hz, 1H, Py Hβ), 7.43–7.37 (ddd, J = 7.58, 4.67, 1.14 Hz, 1H. Py Hδ), 7.34–7.21 (m, 4H, Ar H), 4.61–4.58 (s, 2H, CH_2), 4.47–4.44 (s, 2H, CH_2), 2.06–1.78 (t, J = 14.61 Hz, 1H, OH); ^{13}C NMR (100 MHz, CDCl$_3$, δ): 224.8 (C=S), 155.3 (Py Cε), 146.8 (Py Cα), 139.3 (Ar C4-(CO)), 136.0 (Py Cγ), 133.4 (Ar C1-(CS)), 128.6 (2 Ar C2), 126.2 (2 Ar C3), 125.8 (Ar Cβ) 121.3 (Py Cδ), 64.0 (C-OH), 40.2 (C-S); IR (KBr): v = 3286 - 3000 (OH, v), 2908 (m), 2856 (v_s(OCH$_2$); m), 1666, 1577, 1515, 1454, 1429, 1429, 1419, 1394, 1353, 1290, 1267, 1243, 1211, 1147, 1106, 1060, 1010, 991, 927, 892, 840, 827, 781, 727, 713, 692, 669 cm^{-1}. Anal. calcd for $C_{14}H_{13}NOS_2$: C 61.1, H 4.8, N 5.1, O 5.8, S 23.3; found: C 61.3, H 4.9, N 4.9, O 5.5, S 22.7.

7.3. Model for HDA reaction with PMMA-Cp (ESI-MS)

Synthesis of PMMA-Cp and ligation with Dithio-OH (PMMA-HDA)

The synthesis of **PMMA-Cp** was performed as already described in the literature[274] from ATRP synthesized PMMA (bromine terminated, **PMMA-Br**) and Chapter 4 (M_n = 2700 g·mol^{-1}, *Đ* = 1.2 from SEC in THF, see **Figure A15** in the appendix). 200 mg of **PMMA-Cp** (74 μmol, 1 eq) and 21.1 mg of **Dithio-OH** (81.4 μmol, 1.1 eq) were dissolved in chloroform and purged with nitrogen. 5 μL (65 μmol, 1.1 eq) of TFA was added and the reacting mixture turned brown. The solution stirred for 24 h. The synthetic sequence is

illustrated in **Scheme 7.2**.
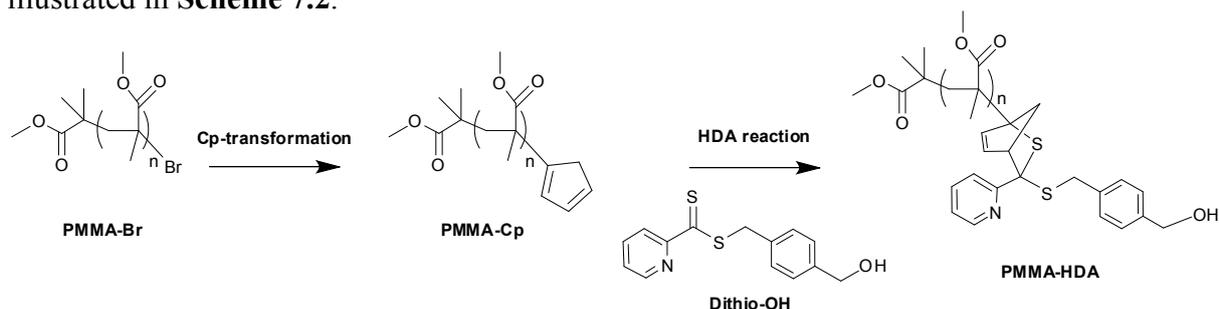
Scheme 7.2. Representation of the synthesis of **PMMA-HDA** via HDA reaction between **PMMA-Cp** and **Dithio-OH**.

The ligated **PMMA-HDA** was characterized via ESI-MS to verify the dienophilic character of the pyridine based hydroxy dithioester with the Cp end-capped PMMA. **Scheme 7.3** depicts the chemical structures of the identified molecules in the ESI-MS spectrum (**Figure 7.1**).
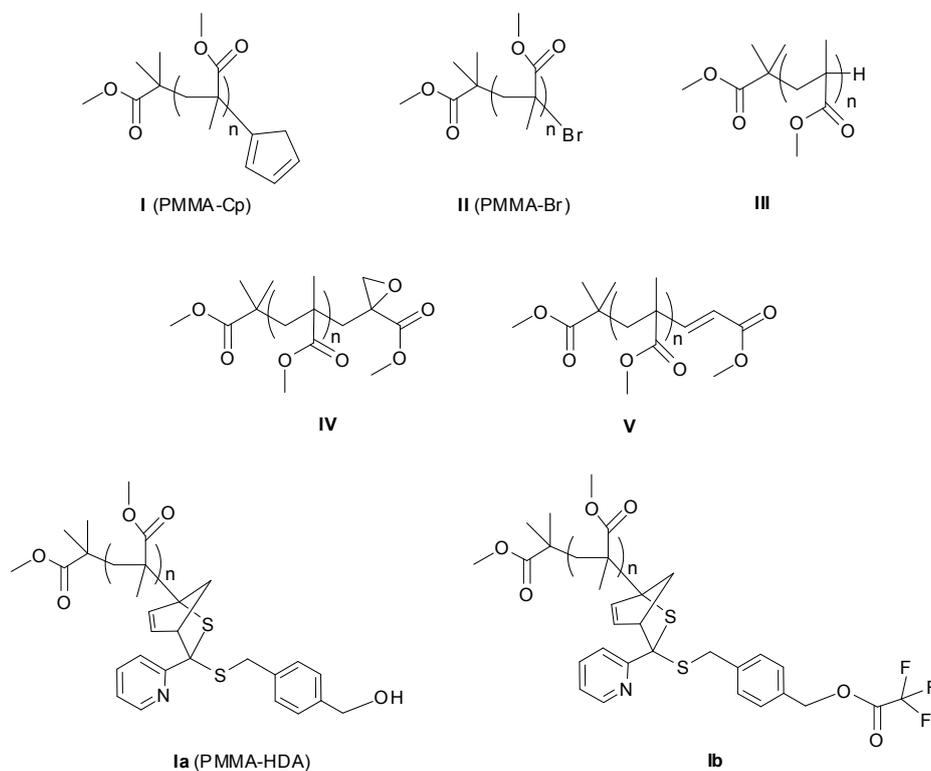
Scheme 7.3. Identified species via ESI-MS in the **PMMA-Cp** spectrum (I-V), and in the **PMMA-HDA** spectrum (Ia, Ib, III and V) based on the synthetic route depicted in **Scheme 7.2**.

The preliminary characterization of **PMMA-Br** and **PMMA-Cp** was conducted in a similar fashion as described in Chapter 4 (section 4.2.2). The Cp end-capped **PMMA-Cp** is clearly identified in the ESI-MS spectrum (see **Figure 7.1**, top) via the presence of singly charged (peaks noted I) and doubly charged (peaks noted I[*]) species. Side products from the polymerization process are also identified (peaks II, III, IV and V). Similarly to the study

conducted in Chapter 4 (section 4.2.2), the assignment of peaks according to their *m/z* is summarized in **Table A6** for the singly charged species and in **Table A7** for the doubly charged species in the appendix.
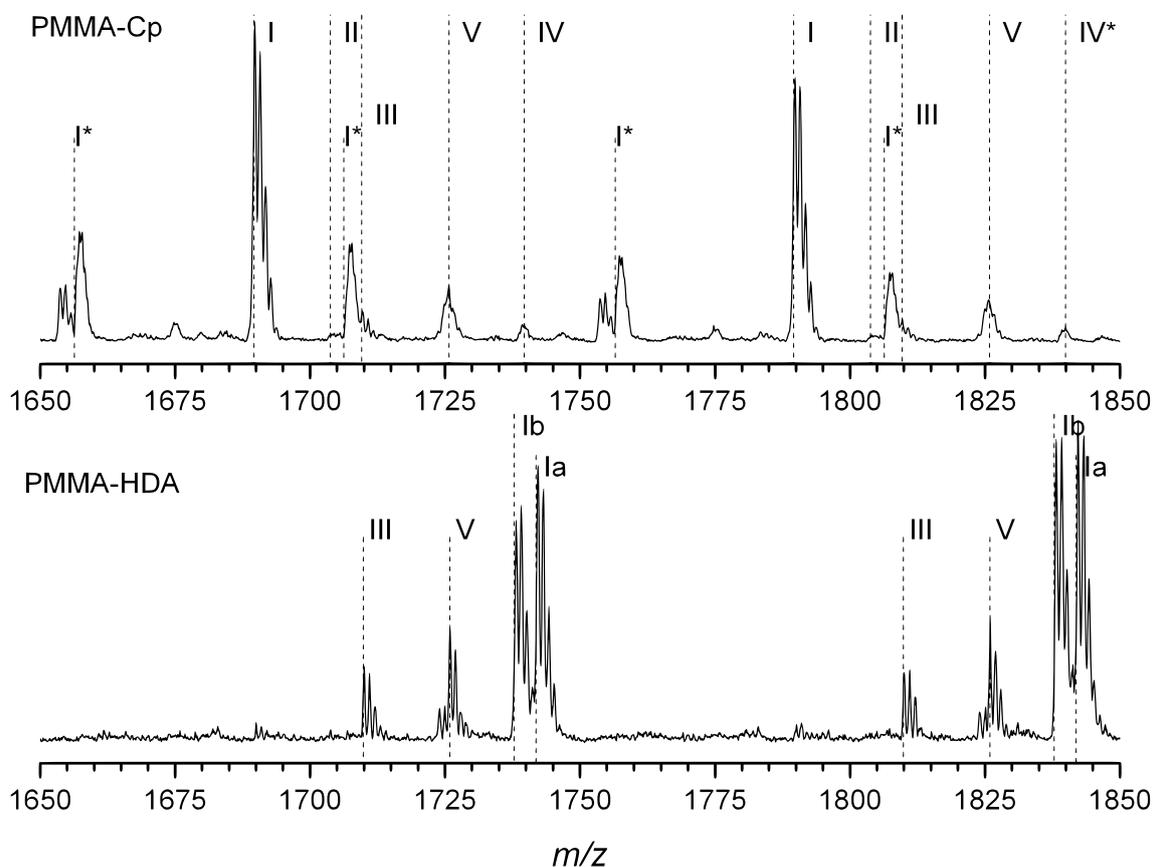

Figure 7.1. ESI-MS spectra of **PMMA-Cp** (top), after its HDA reaction with **Dithio-OH** (**PMMA-HDA**, bottom). The *m/z* shift results from the successful reaction between **PMMA-Cp** and **Dithio-OH** (with a loss of one sodium ion). The resulting product **PMMA-HDA** (Ia, bottom) is able to esterify with trifluoroacetic acid employed for ionization (Ib, bottom).

From the ESI-MS spectrum of **PMMA-HDA** (see **Figure 7.1**, bottom), a shift of + 252.7 *m/z* is observed. While the molecular weight of the dithioester (**Dithio-OH**) is 275.04 g·mol^{-1}, the ionization does not occur via a sodium ion adduct but proceeds via the protonated form of the pyridine moiety (peak Ia). A resulting *m/z* shift (+ 275.39 − 22.99 (sodium adduct) + 1.01 (proton) = 253.41 *m/z*) is subsequently obtained, leading to an experimental error of Δ*m/z* = 0.71. An esterification of the alcohol end-group occurs with trifluoroacetic acid and shifts the *m/z* values to 96.99 *m/z* (+ 113.99 − 17.00 = 96.99 *m/z*) with the loss of one water molecule (refer to the corresponding structures in **Scheme 7.3** and the assignment of the peaks in **Table 7.1**). The corresponding peak (Ib) is identical to the Ia species, i.e. a protonated species, yet not a sodium adduct. The reaction in chloroform is

modeling the reaction that occurs at the surface of the pre-functionalized **1-SWCNT** in the presence of **PMMA-Cp**. The main advantage of performing such a test reaction is the possibility to isolate the ligated polymer chains from chloroform, since the SWCNT ligation conditions involve NMP featuring a high boiling temperature (202 °C). At this temperature, even under vacuum distillation condition, the product would be affecting and possibly destroyed.

Table 7.1. Summary of the identified species in the ESI-MS spectrum of **PMMA-HDA** spectrum (Ia, Ib).

Species	n^a	Formula	m/z exp.	m/z th.	$\Delta m/z$
Ia	12	$[C_{84}H_{124}O_{27}NS_2]^+$	1642.36	1642.78	0.42
	13	$[C_{89}H_{132}O_{29}NS_2]^+$	1742.36	1742.83	0.47
	14	$[C_{94}H_{140}O_{31}NS_2]^+$	1842.27	1842.89	0.53
	15	$[C_{99}H_{148}O_{33}NS_2]^+$	1942.27	1942.94	0.67
Ib	12	$[C_{86}H_{123}O_{28}NS_2F_3]^+$	1738.27	1738.77	0.50
	13	$[C_{91}H_{131}O_{30}NS_2F_3]^+$	1838.27	1838.81	0.54
	14	$[C_{96}H_{139}O_{32}NS_2F_3]^+$	1938.36	1938.87	0.51

^{a}number of monomer units

The ligation between **Dithio-OH** and **PMMA-Cp** being evidenced by ESI-MS, the pristine SWCNTs (**p-SWCNT**) were pre-functionalized in two steps, firstly via oxidation (**o-SWCNT**), secondly via esterification with **Dithio-OH** to form the SWCNT-precursor **2-SWCNT**.

7.4. Two step functionalization of oxidized SWCNTs

7.4.1. Synthesis

Oxidation of SWCNTs (o-SWCNT)

In 200 mL nitric acid (8 mol·L^{-1}), 100 mg of SWCNTs were dispersed in an ultrasonic bath for 1 h, before being heated under reflux for 8 h. After cooling, the solution was diluted in deionized water before centrifugation. The clear supernatant was removed and the residue dispersed again in water. The operation was repeated four times, until the pH of the solution reached 6. The dispersion was subsequently filtered over a PTFE membrane and rinsed with deionized water, and the solid residue dried under vacuum, leading to **o-SWCNT**. The oxidation process was followed via Raman spectroscopy (refer to section 7.4.2).

Esterification of o-SWCNT with Dithio-OH (1-SWCNT)

75 mg **o-SWCNT** were dispersed via an ultrasonic bath in 750 mL freshly distilled dicholoromethane and purged with nitrogen. 429.6 mg of **Dithio-OH** (1.56 mmol, 1 eq), 299.5 mg EDC (1.56 mmol, 1 eq) and 19.1 mg DMAP (0.156 mmol, 0.1 eq) were added under a nitrogen atmosphere and the mixture was stirred for 2 days. The dispersion was filtered over a PTFE membrane, the solid residue rinsed with 100 mL dichloromethane and dried under vacuum. The quantity of **Dithio-OH** was evaluated (after analysis of the sample **o-SWCNT**) and 10 eq of **Dithio-OH** relative to the COOH groups present at the surface of the SWCNTs were employed.

Ligation of PMMA-Cp with Dithio-OH functionalized SWCNT (2-SWCNT)

35 mg of freshly synthesized **1-SWCNT** were dispersed in 350 mL freshly distilled NMP in an ultrasonic bath and purged with nitrogen. 1.97 g of **PMMA-Cp** (0.73 mmol, 1 eq) and 61 μL of TFA (0.80 mol, 1.1 eq) were added under nitrogen atmosphere. The dispersion was stirred for 24 h, filtered over a PTFE membrane and rinsed with 100 mL of THF, and the residual black solid dried under vacuum.

7.4.2. Results and discussion

The characterization of the different SWCNT based materials was conducted in a similar fashion as in the previous chapters, by employing TGA, EA and XPS. Additionally, FTIR measurements were additionally conducted to characterize the intermediate products. Raman spectroscopy was performed, especially to determine the degree of oxidation of the SWCNTs in a very convenient way, preliminary to any further characterization.

Raman spectroscopy

Typical Raman spectra[351] were obtained from the SWCNTs at different time of the oxidation process (refer to the appendix section, **Figure A16** and **Figure A17**), and several peaks could be identified.

From the first order resonance peaks (peak intensity not dependent on the laser power), the radial breathing mode (RBM, below 500 cm^{-1}) and the G-band (1500–1600 cm^{-1}) corresponding to tangential vibration modes were identified. The second order resonance peaks (dependent on the laser excitation) are represented by the D-band (defect band corresponding to sp^3-hybridization and the hexagonal structure, between 1250–1400 cm^{-1}), the G'-band (the overtone of the D-band, only representing the hexagonal deformation, close to 2600 cm^{-1}) and two minor peaks. The intermediate frequency modes (below 900 cm^{-1}) and

M-band (1700 cm^{-1}) and iTOLA (combination of optical and acoustic mode) band (1900 cm^{-1}) were also observed.

The evolution of the peak area of the D-band (noted ID) towards the G-band (noted IG) is representative of the defect induced by the acidic treatment.[32] The analysis was performed with two set-ups in order to carefully follow the evolution of the ID/IG ratio since the intensity of the D-band is dependent from the laser wavelength, and the SWCNTs present in the sample resonate differently according to the laser wavelength.[352] Consequently, the above cited wavenumber regions for the characteristic peaks (second order peaks and RBM modes), as well as their intensity, is varying with the laser excitation. The non-modified **p-SWCNT** sample displays in the solid state a very typical spectrum for SWCNTs (refer to **Figure A16**, at a laser wavelength of 1064 nm). **Figure A16** (1064 nm laser wavelength) and **Figure A17** (785 nm laser wavelength) also display the spectra obtained from the oxidized SWCNTs in dispersion with increasing reaction time. The ID/IG ratio was determined for each spectrum after a Lorentzian fitting of the G-band and the D-band (see **Figure 7.2**).
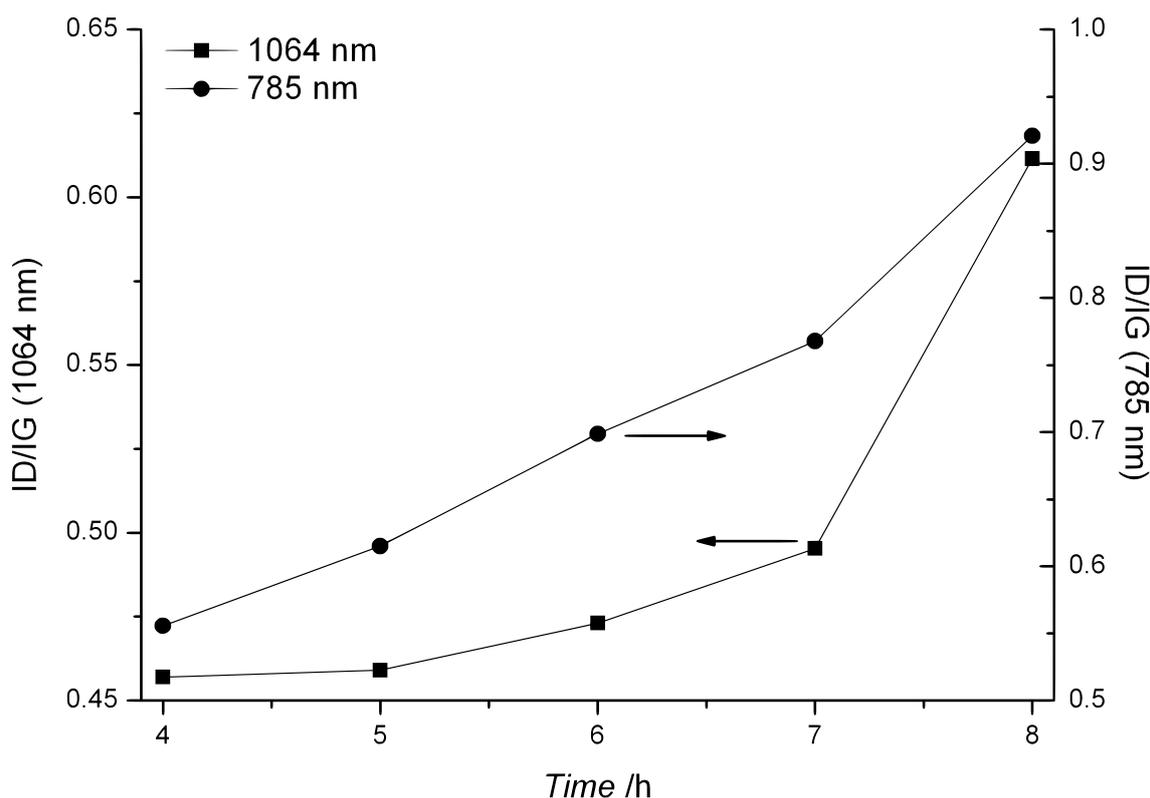
Figure 7.2. Evolution of the intensity ratio (ID/IG) of the defect D-band and G-band as a function of oxidation time with nitric acid. The values were obtained after Lorentzian fitting of the peaks for the dispersions in water with a 1064 nm (squares, scale on the left side) and 785 nm (circles, scale on the right side) laser excitation wavelength.

After only 4 h acidic treatment, the SWCNTs were dispersible in water and allowing the Raman spectra to be measured. From an ID/IG ratio evaluated in the solid state (1064 nm) for

the **p-SWCNT** at 0.50, the ID/IG ratio increased with the duration of the acidic treatment. (refer to **Figure 7.2**). After 8 h, the oxidation was stopped, indicating sufficient functionalization.

Since the preliminary oxidation of the SWCNTs was successful, further characterization and quantification of the different SWCNT hybrid materials was conducted.

Fourier Transform Infrared spectroscopy (FTIR)

From the recorded FTIR spectra of the pristine SWCNT (**p-SWCNT**, refer to the complete spectrum similar to spectra already published in the literature,[353] in the appendix, **Figure A18**) to the **PMMA-Cp** (see spectrum in the appendix, **Figure A19**) modified SWCNTs (**2-SWCNT**), the evolution of the C=O band at 1718 cm^{-1} compared to the normalized peak at 1631 cm^{-1} (corresponding to the aromatic deformation C=C stretch in a vibration within the benzene ring and the C-C stretching vibration as described in the literature[354]) is depicted in **Figure 7.3**.

Further evidence for the successful oxidation of **p-SWCNT** (**Figure 7.3**, top), complementary to Raman spectroscopy, is revealed by the increase of the C=O band (refer to **Figure 7.3**, second spectrum from the top) at 1724 cm^{-1}. A slight increase of the peak for **1-SWCNT** (**Figure 7.3**, third spectrum from the top) is observed after the esterification of **o-SWCNT** with **Dithio-OH**. After the HDA reaction with **PMMA-Cp**, for which the C=O band located at 1724 cm^{-1} is a predominant peak (see spectrum in the appendix, **Figure A19**), the band at 1718 cm^{-1} for the final product **2-SWCNT** increases significantly (refer to **Figure 7.3**, bottom) revealing the presence of PMMA at the surface of the SWCNTs.
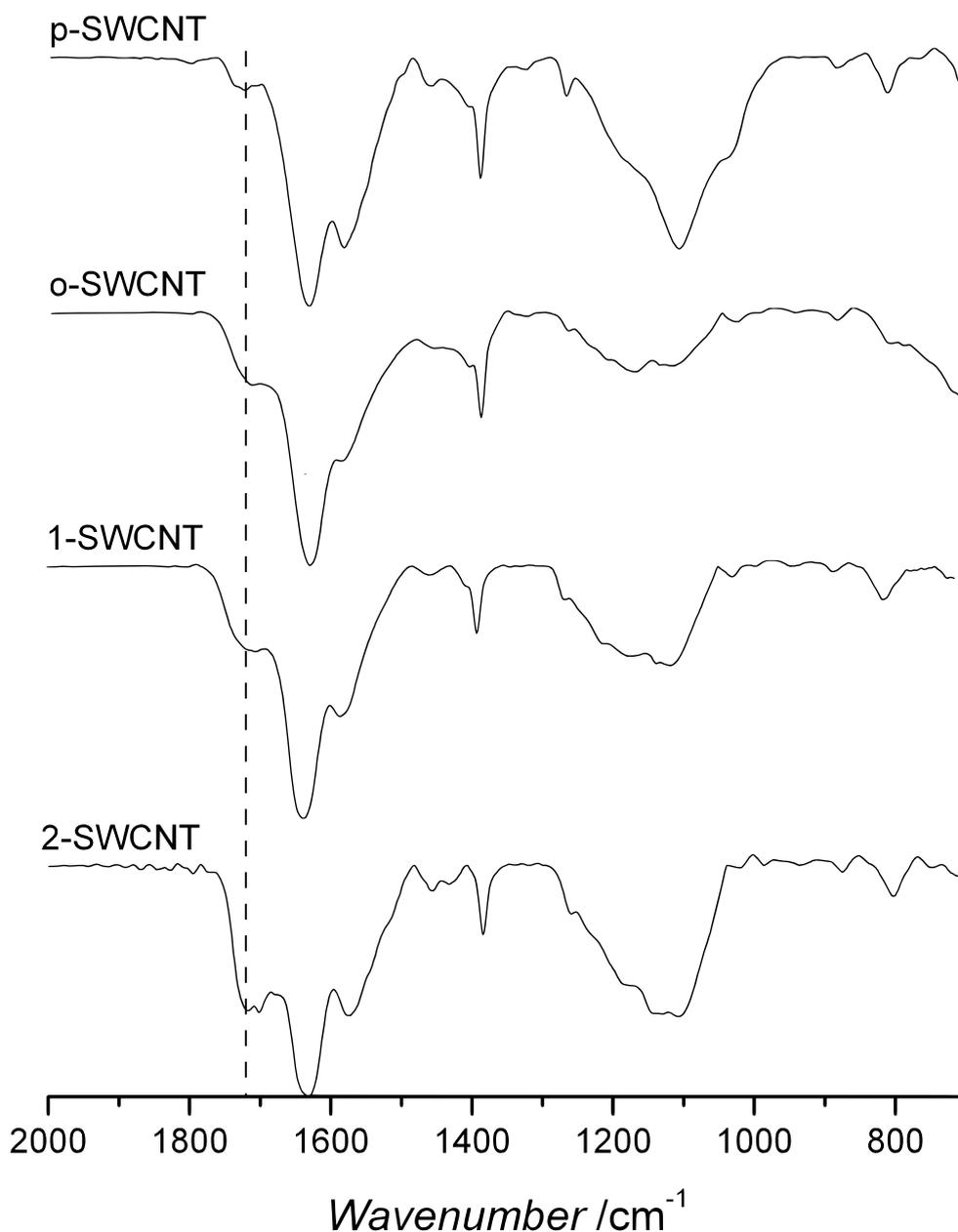
Figure 7.3. FTIR transmission spectra of pristine SWCNTs (**p-SWCNT**), after oxidation (**o-SWCNT**) and esterification (**1-SWCNT**) with the pyridine based **Dithio-OH** as well as after the HDA reaction (**2-SWCNT**) with **PMMA-Cp**. The increasing intensity of the peak at 1718 cm^{-1} supports the presence of the -C=O bond through the functionalization with **PMMA-Cp**.

Thermogravimetric Analysis (TGA)

In order to quantify the presence of the polymer strands, TGA was performed as in the precedent chapters, for each SWCNT based product as well as for **Dithio-OH** and **PMMA-Cp**. **Figure 7.4** depicts the temperature profiles recorded under air atmosphere for each sample. The pristine SWCNTs (**p-SWCNT**) start to degrade at 350 °C (T_i, initial temperature) until 600 °C (T_f, final temperature) with a maximum of degradation located at 545 °C (T_m) (all TGA data are collated in **Table A8** in the appendix). The associated

characteristic temperatures (T_i, T_m, T_f) and the corresponding weight loss were determined via the derivative profiles displayed in the appendix (refer to **Figure A20**).
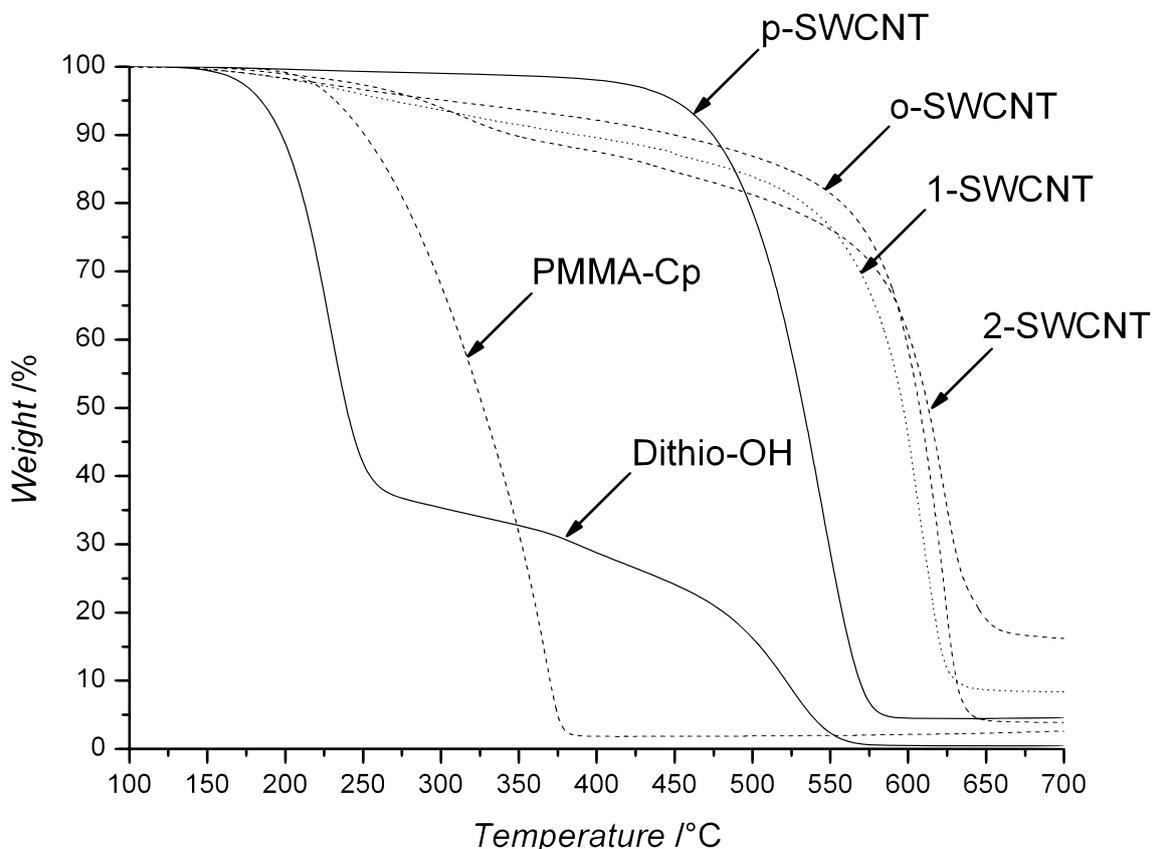

Figure 7.4. Thermogravimetric profiles of pristine SWCNTs (**p-SWCNT**), after oxidation (**o-SWCNT**) and esterification (**1-SWCNT**) with the pyridine based **Dithio-OH**, as well as after the HDA reaction (**2-SWCNT**) with **PMMA-Cp**. All samples are measured under air atmosphere, with a heat flow of 10 °C·min^{-1}, after an isothermal step at 100 °C for 30 minutes.

After oxidation, **o-SWCNT** initially degrades at a lower temperature ($T_m = 225$ °C) than **p-SWCNT**, revealing the presence of COOH groups (5.1 *wt.-%*) and confirming the results obtained via FTIR spectroscopy. Due to a second degradation at higher temperature than for **p-SWCNT** ($T_m = 610$ °C) and less amounts of residue (3.9 *wt.-%* for **o-SWCNT** instead of 4.5 *wt.-%* for **p-SWCNT**), the SWCNTs were evidently purified by the acidic treatment. The organic adducts (**Dithio-OH** and **PMMA-Cp**) degrade at lower temperature than the SWCNT based samples. For **PMMA-Cp**, the degradation is complete below 400 °C, and for **Dithio-OH** the degradation occurs in three steps ($T_m = 230$ °C for the first degradation, 460 °C for the second, 570 °C for the last degradation) and is complete at $T_f = 670$ °C (refer to the appendix, **Table A9**). The presence of **Dithio-OH** in **1-SWCNT** after the esterification of the oxidized SWCNTs is evidenced by additional degradation steps at temperatures below 350 °C and a weight loss of 10.1 *wt.-%* at 390 °C, which is higher than for **o-SWCNT**.

Considering the temperature profile of **2-SWCNT** (the HDA product of the reaction between **PMMA-Cp** and **1-SWCNT)**, a higher weight loss (16.1 *wt.-%* at 460 °C) than for **1-SWCNT** is observed, which can be attributed to the presence of **PMMA-Cp**. One could expect that the different chemical treatments (oxidation, esterification, HDA reaction) would be sequentially identifiable in the last sample via TGA. However, it is understandable that this cannot be the case since the different additional organic groups do not degrade separately at the surface of the SWCNTs, especially for **Dithio-OH**, which degradation is completed at higher temperatures than **PMMA-Cp** and the introduced COOH-groups on the **o-SWCNT**. Moreover, such a behavior does not enable any quantification of the different functional groups added towards the samples **p-SWCNT** and **o-SWCNT**, as the final degradation for **Dithio-OH** (T_f = 670 °C) occurs in the same range as for the SWCNT based samples (T_f included between 650–680 °C). Nevertheless, TGA provides unambiguous evidence that **PMMA-Cp** is present after the HDA-reaction with the modified SWCNTs, and thus it was employed to quantify the efficiency of the acidic treatment (see below).

Elemental Analysis (EA)

In order to characterize more precisely and quantify the grafting density of the final product (**2-SWCNT**), the characterization of the samples was carried out in bulk via EA and at the surface via XPS. Firstly, the composition by carbon, hydrogen, oxygen, sulfur and nitrogen was determined via EA and the results can be found in **Table 7.2** for the SWCNT based samples. The elemental compositions for **Dithio-OH** and **PMMA-Cp** are summarized in **Table A10** in the appendix.

Table 7.2. Elemental composition of pristine SWCNTs (**p-SWCNT**), after oxidation (**o-SWCNT**), the esterification with **Dithio-OH** (**1-SWCNT**) and after the HDA reaction with **PMMA-Cp** (**2-SWCNT**).

Sample	C /wt.-%	H /wt.-%	N /wt.-%	O /wt.-%	S /wt.-%
p-SWCNT	85.4	1.7	0.8	2.2	0
o-SWCNT	86.9	0.8	0.8	2.7	0
1-SWCNT	79.1	1.1	1.6	1.6	1.5
2-SWCNT	78.4	3.9	1.2	4.9	1.0

For **p-SWCNT**, the presence of hydrogen, nitrogen and oxygen can be interpreted as carbonaceous impurities in the sample. The presence of catalyst is revealed by the incomplete

mass balance of 90.1%. A slight increase of the O/C ratio for **o-SWCNT** (0.031 and 0.025 for **p-SWCNT**) confirms the success of the oxidation. The introduction of sulfur (1.5 *wt.-%*), and an increase of the nitrogen content evidences the presence of **Dithio-OH** in the sample **1-SWCNT** after the esterification. A most significant change in the content of oxygen and hydrogen towards the carbon content is observed for **2-SWCNT** and can be attributed to the presence of PMMA. It is noticeable that the sulfur content in **2-SWCNT** remains in the same order of magnitude as for **1-SWCNT**, proving that the dithioester is still present (i.e. no degradation via ultrasonic treatment or hydrolysis).

X-Ray Photoelectron Spectroscopy (XPS)

XPS enables to characterize more deeply the observations made via EA, since elements can be detected at low concentration and the different oxidation states of each element (in the present case carbon, oxygen, sulfur and nitrogen) can be determined. **Figure 7.5** depicts the XPS spectra obtained for the SWCNT based samples after the successive treatments. The XPS spectra of the pristine **p-SWCNT**, **Dithio-OH** and **PMMA-Cp** are depicted in **Figure 7.6**.
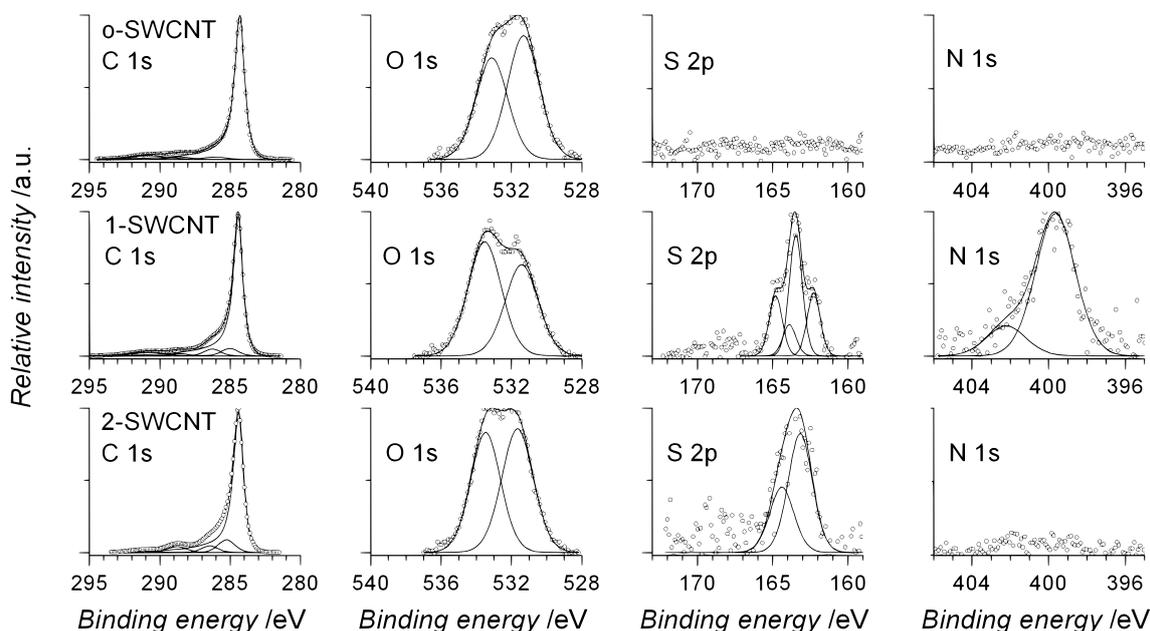
Figure 7.5. XPS spectra of SWCNTs after each functionalization step for each constituting atom (C, O, S and N): after oxidation (**o-SWCNT**, top), after esterification with **Dithio-OH** leading to **1-SWCNT** (middle), after HDA reaction with **PMMA-Cp** leading to **2-SWCNT** (bottom). For a better visualization, all spectra are normalized to maximal intensity.
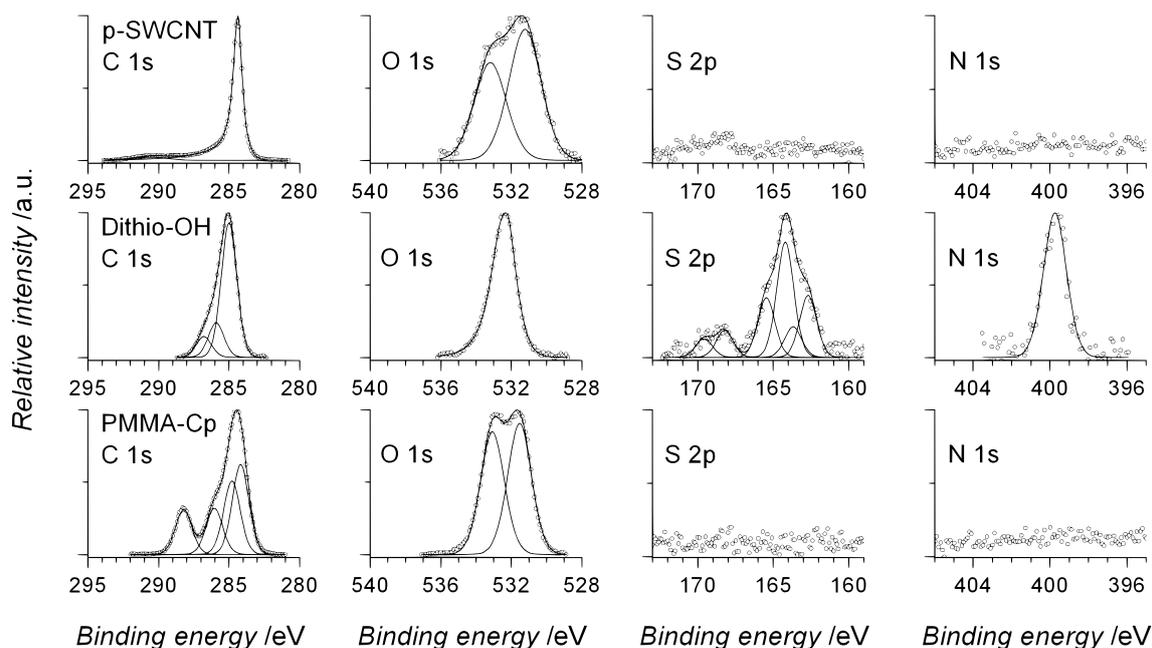
Figure 7.6. XPS spectra of reference materials for each constituting atom (C, O, S and N): pristine SWCNTs (**p-SWCNT**, top), **Dithio-OH** (middle), and **PMMA-Cp** (bottom). For a better visualization, all spectra are normalized to maximal intensity.

For the SWCNT based samples, similar peaks for C 1s were recorded and were identical to those reported in the literature.[279,355] The sequential chemical modifications are highlighted by the contribution of other elements (i.e. oxygen, sulfur and nitrogen). The O 1s spectrum for **p-SWCNT** reveals the presence of oxygen due to impurities (531.6 and 533.4 eV). A signal at similar energy is observed for **o-SWCNT**, whereas sulfur and nitrogen could not be detected. The detailed assignment and quantification for the SWCNT based samples is summarized in **Table 7.3**, and for **Dithio-OH** and **PMMA-Cp** (characterization performed in the same fashion as in Chapter 4, section 4.3.2) in **Table 7.4** and **Table A11** (in the appendix), respectively. As already determined by EA, the XPS measurements confirm that the oxygen content for the **o-SWCNT** sample is higher than for **p-SWCNT**. The binding energy observed for the O 1s peaks reveals the presence of COOH groups ($\underline{O}$=C at 531.6 eV, $\underline{O}$-C at 533.4 eV),[356,357] corroborated by the corresponding C 1s peak at a binding energy of 288.5 eV.

The characterization of **Dithio-OH** yields the expected chemical information regarding the present sulfur (162.7 eV for $\underline{S}$=C, 164.2 eV for $\underline{S}$-C)[336,358] and nitrogen from the pyridinyl group (399.7 eV).[359] Higher binding energies detected in the sulfur signal (167.2 eV) might be caused by a partial oxidation of the dithioester. The XPS spectra for **1-SWCNT** after esterification show similarities to the spectra obtained for **Dithio-OH**, as sulfur and nitrogen are detected.

Table 7.3. Assignment of binding energies and comparison of the band contribution after deconvolution of the XPS spectra of pristine SWCNTs (**p-SWCNT**), after oxidation (**o-SWCNT**) and esterification (**1-SWCNT**) with the pyridine based **Dithio-OH** as well as after the HDA reaction (**2-SWCNT**) with **PMMA-Cp**.

Peak	B.E.[a]	p-SWCNT	o-SWCNT	1-SWCNT	2-SWCNT	Entity
	/eV	/at.-%	/at.-%	/at.-%	/at.-%	
C1s	284.4	90.4	83.4	74.0	71.8	C-C sp^2
	285.0	-	-	5.0	6.2	$\underline{C}H_2/\underline{C}H_3$ sp^3
	286.2	-	-	4.6	-	$\underline{C}$-O/$\underline{C}$-N/$\underline{C}$-S
	286.4	-	2.1	-	4.2	$\underline{C}$-OH/$\underline{C}$-O
	288.5	-	2.3	1.6	5.4	$\underline{O}$=C-OH/$\underline{S}$=C-S
	290.7	5.0	5.8	5.1	2.1	π-π^*
O 1s	531.6	2.7	3.5	3.2	4.9	$\underline{O}$=C
	533.4	1.9	2.9	4.0	4.8	$\underline{O}$-C
S 2p$_{3/2}$	162.4	-	-	0.3	0.6	$\underline{S}$=C
	163.5	-	-	0.5		$\underline{S}$-C
N 1s	399.7	-	-	1.4	-	$\underline{N}$(pyridine)
	401.9	-	-	0.3	-	$\underline{N}^+$-H

[a]binding energy.

Table 7.4. Assignment of the binding energies and comparison of the band contribution after deconvolution of the XPS spectra of the pyridine based **Dithio-OH**. The spectra are referenced at 285.0 eV for C-C sp^3.

Peak	B.E.[a]	Dithio-OH	Entity
	/eV	/at.-%	
C1s	285.0	52.4	$\underline{C}$-H/$\underline{C}$-C sp^3
	286.0	13.6	$\underline{C}$-N/$\underline{C}$-S
	286.8	8.2	S=$\underline{C}$-S
O 1s	532.4	16.0	$\underline{O}$-C
S 2p$_{3/2}$	162.7	2.3	$\underline{S}$=C
	164.2	4.2	$\underline{S}$-C
	167.2	1.0	$\underline{S}$(oxidized)
N 1s	399.8	2.3	$\underline{N}$(pyridine)

[a]binding energy.

The appearance of protonated nitrogen is revealed by the peaks located at 401.9 eV. The significant increase of the oxygen contribution in the sample **2-SWCNT** is attributed to the

PMMA strands located at the surface of the SWCNTs, evidencing, as for FTIR spectroscopy, TGA and EA, the successful HDA-reaction with **Dithio-OH** functionalized SWCNTs. One should note that sulfur is still present in the sample, however represented in a much noisier signal as for **1-SWCNT**, probably due to the presence of a polymer layer at the surface of the SWCNTs. Therefore, the deconvolution of the S $2p_{3/2}$ signals was not exploitable to differentiate the S=C peak at 162.4 eV and the S-C peak at 163.5 eV. In the case of **2-SWCNT**, the weak nitrogen content is not quantifiable due to the insufficient XPS detection limit.

Evaluation of the grafting density

In order to precisely characterize the different synthetic steps as proposed in **Scheme 7.1**, the three described methods (TGA, EA, XPS) enabled to qualitatively evidence the success of the synthetic route. In the last part of the present chapter, the data are analyzed to estimate the grafting density after each chemical modification of the SWCNTs, compared, and the efficiency (conversion) of the HDA-reaction evaluated. From the different methods, a *wt.-%* or atomic concentration (*x.-%*) of the additional groups at the surface of the SWCNTs was determined. For TGA, a similar analysis was performed as already described in Chapter 4 (section 4.3.2). The oxidation of the SWCNTs was readily evaluated by the described method. Yet a further analysis for **1-SWCNT** and **2-SWCNT** was not possible due to an overlap of the temperature profiles with **Dithio-OH**. For EA and XPS, the contribution of oxygen for **o-SWCNT** towards **p-SWCNT** enables to evaluate the efficiency of the oxidation. The estimation of the carboxylic group content resulted in the same order of magnitude for the functionalization via the three employed analytical methods (one carboxylic group every 35–49 carbon atoms, refer to **Table 7.5**).

Table 7.5. Characterization data of SWCNTs after oxidation (**o-SWCNT**) and esterification with **Dithio-OH** (**1-SWCNT**) analyzed via TGA, XPS and EA.

Sample	Method	Grafting ratio				
		/wt.-%	/x.-%	/mmol·g^{-1}	/molecule·nm^{-2}	/C atoms
o-SWCNT	TGA	5.1	-	1.70	0.778	49
	EA	5.07	2.9	1.833	0.840	45
	XPS	8.3	6.4	2.070	0.948	40
1-SWCNT	TGA	-	-	-	-	-
	EA	7.18	9.21	0.299	0.137	278
	XPS	9.3	12.4	0.370	0.170	225

For **1-SWCNT**, the evolution of the sulfur content enabled the determination of the grafting density of **Dithio-OH** molecules located at the surface of the SWCNT via XPS and EA. The conversion of the esterification can be estimated to be close to 15%. The difficulty to disperse the SWCNTs in dichloromethane and perform the esterification under mild conditions (via EDC coupling) may explain the low conversion of the reaction.

However, XPS (0.370 mmol·g^{-1}) and EA (0.299 mmol·g^{-1}) deliver very similar results for the loading capacity. A further difficulty occurs while determining the grafting density of **2-SWCNT** as the introduced atoms (carbon, oxygen and hydrogen) from the PMMA strands are already present in the sample. However, based on the results for **1-SWCNT**, one can evaluate the elemental composition – and thus the grafting density – resulting for a complete (100% conversion) of the HDA reaction. The comparison between the experimental compositions and the theoretical values is illustrated in **Table 7.6**.

Table 7.6. Comparison between the experimental composition obtained via XPS and TGA, and the theoretical composition to be expected for the 100% grafting of **1-SWCNT** with **PMMA-Cp** via the HDA reaction.

Method	Source	C	H	N	O	S
XPS[a]	Experimental[c]	89.7	-	-	9.7	0.6
	Theoretical[d]	77.8	-	0.3	21.2	0.7
EA[b]	Experimental	87.7	4.3	1.4	5.5	1.1
	Theoretical	79.8	4.0	1.0	14.2	1.0

[a]in x.-%; [b]in wt.-%; [c]values obtained from **2-SWCNT**; [d]based on sulfur content and 100 % conversion of the HDA reaction.

Considering the oxygen content determined via XPS and EA, one can observe lower

values (approximately 45% from XPS, 39% for EA) obtained experimentally compared to the theoretically expected numbers. The uncertainty of EA originates in the hydrogen content, since the mass balance is not 100% (due to impurities) and thus may induce experimental errors. The fact that the HDA reaction does not occur in a complete fashion can be explained by dispersion issues of the SWCNTs (although well dispersible in NMP) and by the high dilution (and the localization) of the reagent **Dithio-OH** in the mixture. However, from the estimated conversion, the grafting density of polymer strands at the surface of SWCNTs is higher than the values obtained via the direct – no pre-treatment required – DA reaction between SWCNTs (dienophile) and **PMMA-Cp** (diene) at ambient temperature. In the first case, the grafting density can be evaluated via XPS characterization of being close to $0.169 \, \text{mmol·g}^{-1}$ ($0.115 \, \text{mmol·g}^{-1}$ from EA, average value XPS and EA $0.142 \, \text{mmol·g}^{-1}$), $0.0774 \, \text{chain·nm}^{-2}$ ($0.0527 \, \text{chain·nm}^{-2}$ from EA), or – in terms of the periodicity – one polymer chain every 493 carbon atoms (724 carbon atoms from EA). In the case of the direct reaction performed at ambient temperature between SWCNTs and **PMMA-Cp** (of identical molecular weight), the grafting densities are a factor of approximately 2 lower (average value $0.064 \, \text{mmol·g}^{-1}$, $0.029 \, \text{chain·nm}^{-2}$, one polymer chain every 1384 carbon atoms).

7.4.3. Conclusions

The HDA reaction with Cp terminal PMMA chains was performed on pre-functionalized SWCNTs decorated with an electron deficient pyridine based dithioester. The sample characterization via FTIR spectroscopy and TGA qualitatively evidenced the presence of polymer strands on the SWCNTs surface. The complementary quantitative study employing EA and XPS enabled the determination of the elemental composition of the pre-functionalized SWCNTs and the final polymer modified SWCNTs. After estimation of the conversion of the HDA reaction, a comparison of the currently shown synthetic pathway (involving a pre-treatment via oxidation of the SWCNTs) and a previously introduced direct and non-destructive ambient temperature DA approach evidences that the HDA route leads to approximatively two times higher grafting densities. Which approach is ultimately taken will depend on the desired application: higher grafting densities (pre-functionalization for HDA reaction) versus a more intact SWCNT structure (direct DA reaction).

Chapter 8 – Concluding remarks

8.1. Concluding remarks

In the present thesis, the successful functionalization of SWCNTs via a DA reaction by the use of a variety of highly defined polymer chains with a Cp end-group was pioneered for the first time. After a detailed characterization of the polymer end-group, the SWCNTs were functionalized in a one-pot reaction at ambient temperature (and at elevated temperature 80 °C) in a solvent (*N*-methylpyrrolidone). By means of several analytic methods (TGA, EA and XPS) and a systematic control study with non-functional polymer chains, the presence of covalently bound polymer chains on the SWCNT surface was evidenced and quantified.

In Chapter 4, after the polymerization of the monomer by ATRP and the Cp end-group transformation, Cp end-capped PMMA was reacted with SWCNTs leading to a grafting density of 0.0293 chain·nm^{-2} at ambient temperature and 0.0396 chain·nm^{-2} at 80 °C of the polymer chains at the surface of the SWCNTs. The use of Cp end-capped PNIPAM in Chapter 5, after RAFT polymerization of the monomer and the sequential chain-end transformation to Cp, led not only to a successful functionalization of the SWCNTs with a 0.0288 chain·nm^{-2} grafting density, yet also to SWCNTs displaying thermo-responsive behavior over 20 °C, in which individual SWCNTs with a 52–90 nm hydrodynamic diameter aggregated to 152–169 nm hydrodynamic diameter particles. The conjugated polymer P3HT, obtained by GRIM polymerization and a subsequent chain-end transformation to Cp reacted in Chapter 6 with SWCNTs to form polymer/SWCNT hybrid materials with a higher grafting density than with non-functional polymer chains. Whereas the non-functional polymer chains

are known to wrap around SWCNTs and consequently led to a loading capacity of $0.0617 \, mmol \cdot g^{-1}$, the Cp functional polymer chains functionalized the SWCNTs with an approximatively doubled grafting density of $0.0510 \, chain \cdot nm^{-2}$ at 80 °C (loading capacity close to $0.111 \, mmol \cdot g^{-1}$). The observed increase of grafting density may result from a combined *'wrapping and DA reaction'* effect. Finally, in Chapter 7, an even higher grafting density was obtained by means of a pre-treatment of the SWCNTs with a new dithioester susceptible to react via a HDA reaction with Cp end-capped PMMA chains. Although the complexity of this synthetic procedure and its somewhat destructive nature towards SWCNTs are drawbacks, the grafting density of the polymer/SWCNTs materials was higher with $0.0774 \, chain \cdot nm^{-2}$ than the grafting density obtained via the direct DA reaction with Cp end-capped PMMA $0.0293 \, chain \cdot nm^{-2}$, with the pre-treated SWCNTs being reacted under the same conditions (ambient temperature) as for the DA reaction.

8.2. Outlook

In the present thesis, the DA reaction and its hetero form (HDA reaction) were applied to SWCNTs by exploiting the dienophilic character of the SWCNTs to react with three Cp end-capped polymers. The nature of these employed polymers covers a wide spectrum of applications – PMMA is used as thermoplast, PNIPAM is useful for its thermal properties and water solubility, P3HT is employed in photovoltaics – and required to adapt the end-group transformation as a function of the employed polymerization techniques (ATRP, RAFT polymerization and GRIM polymerization) to obtain the Cp terminus.

The simplicity of the DA reaction – once the specific end-group is attached to the polymer chains – offers the unique opportunity to functionalize not only SWCNTs, but also fullerenes, MWCNTs, graphene and other carbon allotropes showing a dienophilic character, with a wide spectrum of Cp end-capped polymer chains. Particularly in the case of graphene, depending on its ability to react as diene or dienophile, the end-group modification of polymer chains (or even small molecules) to a diene or dienophile may be of great interest for diverse applications.

Appendix

Synthesis A1.

The following provides the synthesis and the characterization of the materials employed in Chapter 5.

Additional materials

1-Dodecanethiol (≥99%, Acros), Aliquot 336 (Sigma Aldrich), carbon disulfide (≥99%, VWR), 3-bromo-1-propanol (≥97%, Acros), sodium azide (≥99.5%, Sigma Aldrich), oxalyl chloride (≥98%, Acros), triethylamine (≥99%, Acros), 2-bromo-2-methylpropionyl bromide (≥98%, Acros), propargyl alcohol (≥99%, Alfa Aesar) were used as received.

Synthesis of DMP, DMP-N_3 and 2-propynyl 2-bromo-2-methylpropanoate

2-Dodecylsulfanylthiocarbonylsulfanyl-2-methylpropionic acid (DMP) was synthesized according to literature.[297] ^{1}H NMR: 0.81 (t, 3H), 1.11-1.37 (m, 18H), 1.56-1.68 (m, 8H), 3.21 (t, 2H), 13.05 (s, 1H). ^{13}C NMR (δ, ppm): 220.8 (S-C=S); 178.8 (C=O); 55.6 (-S-C(CH$_3$)$_2$-CO); 37.1 (-CH$_2$-CH$_2$-S-C=S); 31.9 (-C(10)H$_2$-CH$_2$-S); 29.6 (-C(3)H$_2$-CH$_2$-S); 29.6 (-C(4)H$_2$-CH$_2$-S); 29.5 (-C(5)H$_2$-CH$_2$-S); 29.4 (-C(6)H$_2$-CH$_2$-S); 29.1 (-C(7)H$_2$-CH$_2$-S); 29.0 (-C(8)H$_2$-CH$_2$-S); 28.0(-C(9)H$_2$-CH$_2$-S); 27.9 (-C(2)H$_2$-CH$_2$-S); 25.1 (-S-C(CH$_3$)$_2$-CO); 22.7 (-C(11)H$_2$-CH$_2$-S); 14.1 (CH$_3$-C$_{11}$H$_{22}$-S-C=S). IR (KBr) (wavenumber, cm^{-1}) for DMP: 2917 and 2856 (C-Cs), 1718 (C=O), 1070 (C=S), 1172 and 816 (C-Cb).Elemental analysis, calculated: C = 56.00, H = 8.85, O = 8.78, S = 26.38; experimental: C = 55.18, H = 8.80, O = 8.80, S = 26.52.

The synthetic route described by Gondi *et al.*[298] was used for the synthesis of 2-dodecylsulfanylthiocarbonylsulfanyl-2-methylpropionic acid 3-azidopropyl ester (DMP-N_3) and of the intermediate 3-azidopropanol. ^{1}H NMR (δ, ppm) for DMP-N_3: 4.15-4.21 (t, J=6.10 Hz, 2 H), 3.31-3.41 (t, J=6.69 Hz, 2 H), 3.23-3.30 (t, J=7.60 Hz, 2 H), 1.85-1.94 (quin, J=6.10 Hz, 2 H), 1.57-1.68 (m, 2 H), 1.19-1.42 (m, 18 H), 0.84-0.93 (td, J=6.80, 1.30 Hz, 3 H). ^{13}C NMR (δ, ppm) for DMP-N_3: 220.8 (S-C=S); 172.9 (C=O).; 62.8 (-CH$_2$-CH$_2$-O-C=O); 55.9 (-S-C(CH$_3$)$_2$-CO); 48.2 (-CH$_2$-CH$_2$-N$_3$); 37.0 (-CH$_2$-CH$_2$-S-C=S); 31.9 (-C(10)H$_2$-CH$_2$-S); 31.6 (-CH$_2$-CH$_2$-N$_3$); 29.6 (-C(3)H$_2$-CH$_2$-S); 29.5 (-C(4)H$_2$-CH$_2$-S); 29.4 (-C(5)H$_2$-CH$_2$-S); 29.3 (-C(6)H$_2$-CH$_2$-S); 29.1 (-C(7)H$_2$-CH$_2$-S); 28.9 (-C(8)H$_2$-CH$_2$-S); 28.0 (-C(9)H$_2$-CH$_2$-S); 27.9 (-C(2)H$_2$-CH$_2$-S); 25.3 (-S-C(CH$_3$)$_2$-CO); 22.7 (-C(11)H$_2$-CH$_2$-S); 14.1 (CH$_3$-C$_{11}$H$_{22}$-S-C=S). IR (KBr) (wavenumber, cm^{-1}) for DMP-N_3: 2923 and 2854 (C-Cs), 2096 (C-N=N=N), 1735 (C=O), 1064 (C=S), 1155 and 814 (C-Cb).

Elemental analysis for DMP-N$_3$, calculated: C = 53.65, H = 8.33, N = 9.39, O = 7.15, S = 21.41; experimental: C = 51.00, H = 7.10, N = 8.93, O = 7.71, S = 23.61. ^{1}H NMR (δ, ppm) for 3-azidopranol: 3.71-3.61 (t, J = 6.00 Hz, 2H, -CH$_2$-CH_2-OH), 3.42-3.23 (t, J = 6.56 Hz, 2H, -CH$_2$- CH_2-N$_3$), 2.38 (br-s, 1H, OH), 1.82-1.69 (quin, 2H, HO-CH$_2$-CH_2-CH$_2$-N$_3$).

The same procedure as Luetdke *et al.* was followed for the synthesis of 2-propynyl 2-bromo-2-methylpropanoate.[299] ^{1}H NMR (δ, ppm): 4.76-4.8 (d, *J*=2.53 Hz, 2 H), 2.51-2.56 (t, J = 3.00 Hz, 1 H), 1.93-1.99 (s, 6 H). ^{13}C NMR (δ, ppm): 170.9 (C=O), 76.9 (-C≡C-H), 75.5 (H-C≡C-), 54.9 (C-O), 53.5 (Br-C-(CH$_3$)$_2$), 30.7 (*C*H$_3$-C). IR (ATR) (wavenumber, cm^{-1}): 3296 (alkyn C-H*s*), 2975 (C-C*s*), 1732 (C=O), 1153 (C-C*b*).
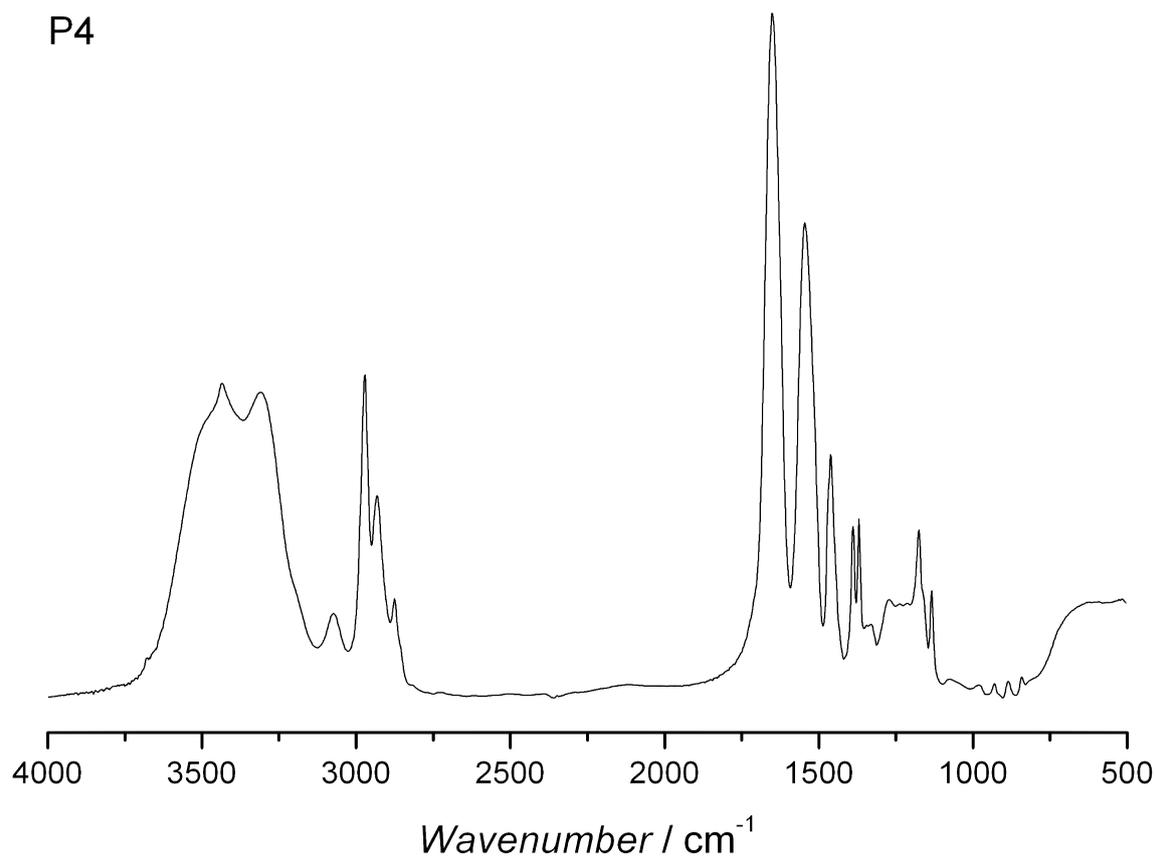
Figure A1. FTIR spectrum of PNIPAM with acidic end-group (**P4**) in a KBr pellet.
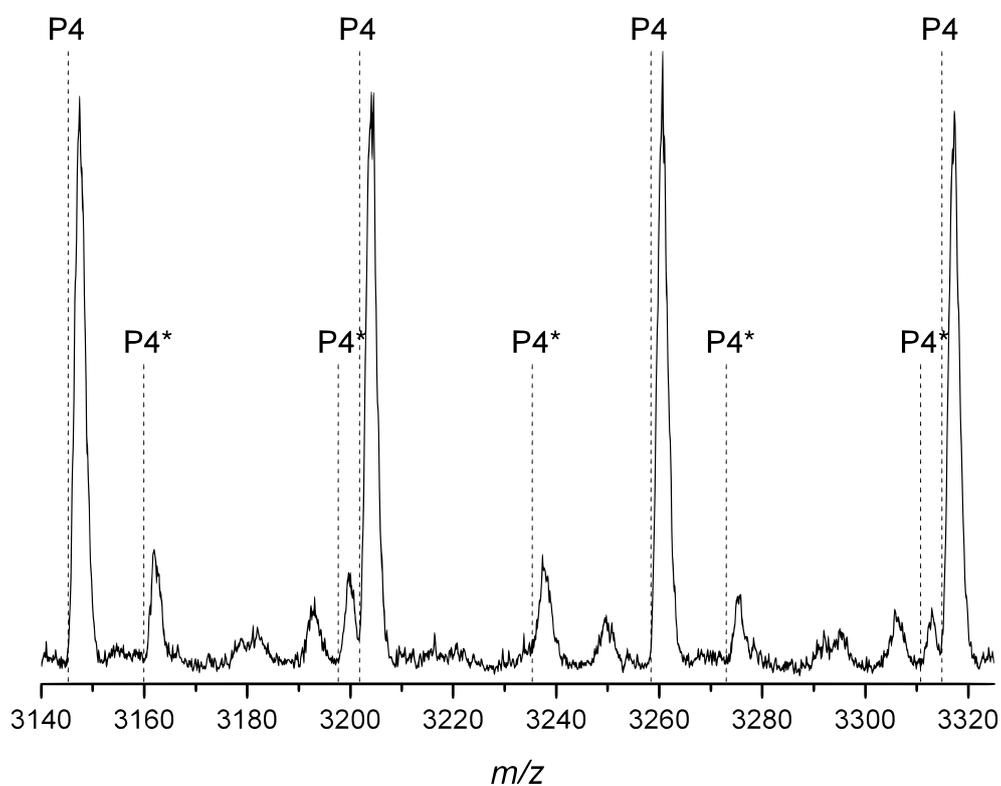
Figure A2. ESI-MS spectrum of doubly (denoted **P4**) and triply (denoted **P4***) charged PNIPAM with acidic end-group (**P4**). The spectrum is recorded via direct infusion.

Table A1. Summary of ESI-MS data for PNIPAM with acidic end-group (**P4**). The spectrum was recorded via direct infusion.

| Species	n [a]	Fomula	m/z theoretical	experimental	Δ
P4	52	$[C_{329}H_{604}N_{52}O_{54}S_3Na_2]^{2+}$	3145.25	3144.82	0.43
	53	$[C_{335}H_{615}N_{53}O_{55}S_3Na_2]^{2+}$	3201.80	3201.73	0.07
	54	$[C_{341}H_{626}N_{54}O_{56}S_3Na_2]^{2+}$	3258.34	3258.18	0.16
	55	$[C_{347}H_{637}N_{55}O_{57}S_3Na_2]^{2+}$	3314.88	3314.45	0.43
P4*	80	$[C_{497}H_{912}N_{80}O_{82}S_3Na_3]^{3+}$	3159.95	3160.45	0.50
	81	$[C_{503}H_{923}N_{81}O_{83}S_3Na_3]^{3+}$	3197.64	3197.81	0.17
	82	$[C_{509}H_{934}N_{82}O_{84}S_3Na_3]^{3+}$	3235.34	3235.73	0.39
	83	$[C_{515}H_{945}N_{83}O_{85}S_3Na_3]^{3+}$	3273.03	3273.45	0.42
	84	$[C_{521}H_{956}N_{84}O_{86}S_3Na_3]^{3+}$	3310.73	3310.36	0.37

[a] number of monomer units.
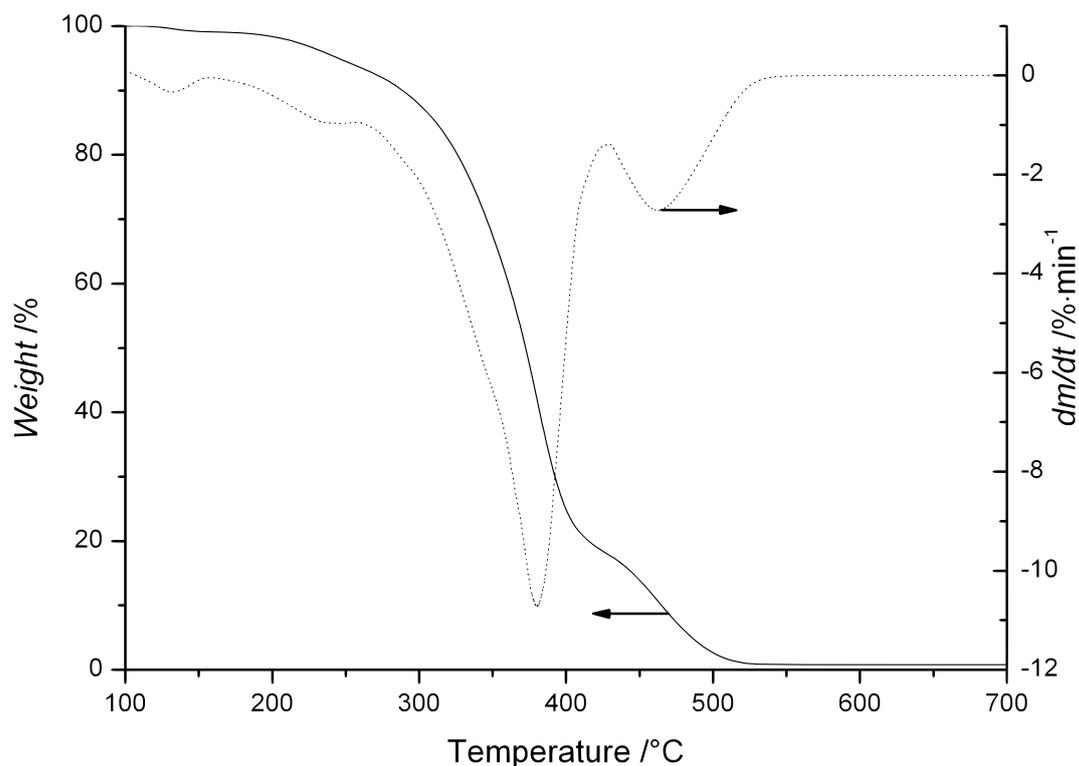
Figure A3. Thermogravimetric profile and its derivative of PNIPAM with bromine end-group (**P2**) with recognizable subsidiary degradation at 130 °C due to bromine elimination. Sample measured under ambient atmosphere with a heat flow of 10 °C·min^{-1}, with a preliminary isothermal step at 100 °C for 30 minutes.
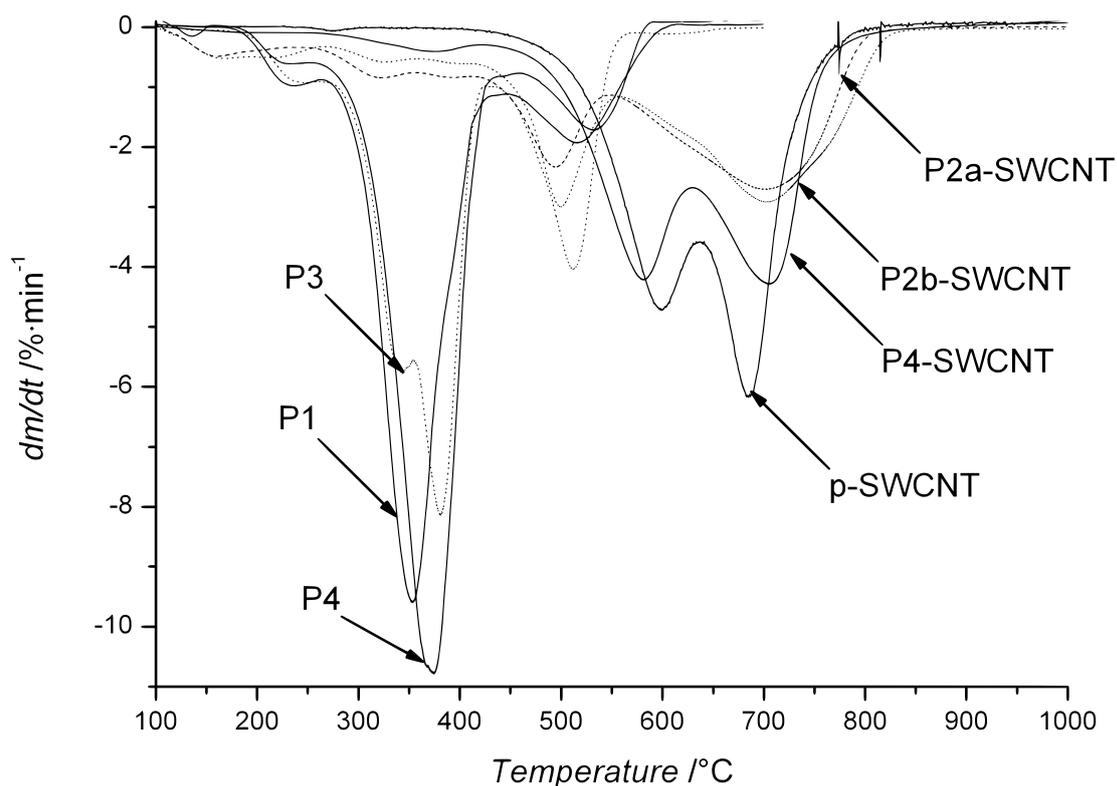
Figure A4. Derivatives of thermogravimetric profiles of PNIPAM with different end-group (azide, **P1**), (Cp, **P3**) and (acid, **P4**), and pristine SWCNTs (**p-SWCNT**), functionalized with **P3** at ambient temperature (**P3a-SWCNT**), at 80 °C (**P3b-SWCNT**), and mixed with PNIPAM with acidic end-group (**P4-SWCNT**). All samples measured under ambient atmosphere with a heat flow of 10 °C·min^{-1}, with a preliminary isothermal step at 100 °C for 30 minutes.

Table A2. Summary of thermogravimetric analysis of PNIPAM with different end-group (azide, **P1**), (bromine, **P2**), (Cp, **P3**) and with acidic end-group (**P4**).

Sample	$T_i{}^a$ /°C	$T_f{}^b$ /°C	$T_m{}^c$ /°C	wt.-% at T_f	Sample	$T_i{}^a$ /°C	$T_f{}^b$ /°C	$T_m{}^c$ /°C	wt.-% at T_f
P1	150	265	235	94.7	P3	170	270	245	94.3
	265	440	350	22.2		270	355	345	67.2
	440	620	520	2.7		355	425	380	31.6
P2	100	160	130	99.1		425	580	510	4.1
	160	260	240	93.5	P4	170	270	235	95.9
	260	430	380	17.8		270	435	375	17.3
	430	550	460	0.8		435	590	540	1.3

^aT_i: initial temperature for degradation; ^bT_f: final temperature for degradation; ^cT_m: temperature of maximal weight loss (from first derivative). All samples measured under air atmosphere with a heat flow of 10 °C·min^{-1}, with a preliminary isothermal step at 100 °C for 30 minutes.

Table A3. Summary of thermogravimetric analysis for pristine SWCNTs (**p-SWCNT**), SWCNTs functionalized with **P3** at ambient temperature (**P3a-SWCNT**), at 80 °C (**P3b-SWCNT**), and SWCNTs mixed with PNIPAM with acidic end-group (**P4-SWCNT**).

Sample	$T_i{}^a$ /°C	$T_f{}^b$ /°C	$T_m{}^c$ /°C	wt.-% at T_f	Sample	$T_i{}^a$ /°C	$T_f{}^b$ /°C	$T_m{}^c$ /°C	wt.-% at T_f
p-SWCNT	430	640	600	57.2		100	190	170	97.0
	640	810	685	13.8		190	270	220	93.5
	100	240	160	95.4	P3b-SWCNT	270	360	325	89.1
	240	355	320	88.3		360	410	395	86.2
P3a-SWCNT	355	410	390	83.9		410	560	500	62.6
	410	545	495	63.6		560	850	700	12.6
	545	815	700	13.8		100	240	200	99.2
						240	420	375	94.6
					P4-SWCNT	420	635	580	51.6
						635	810	705	10.7

^aT_i: initial temperature for degradation; ^bT_f: final temperature for degradation; ^cT_m: temperature of maximal weight loss (from first derivative). All samples measured under air atmosphere with a heat flow of 10 °C·min^{-1}, with a preliminary isothermal step at 100 °C for 30 minutes.
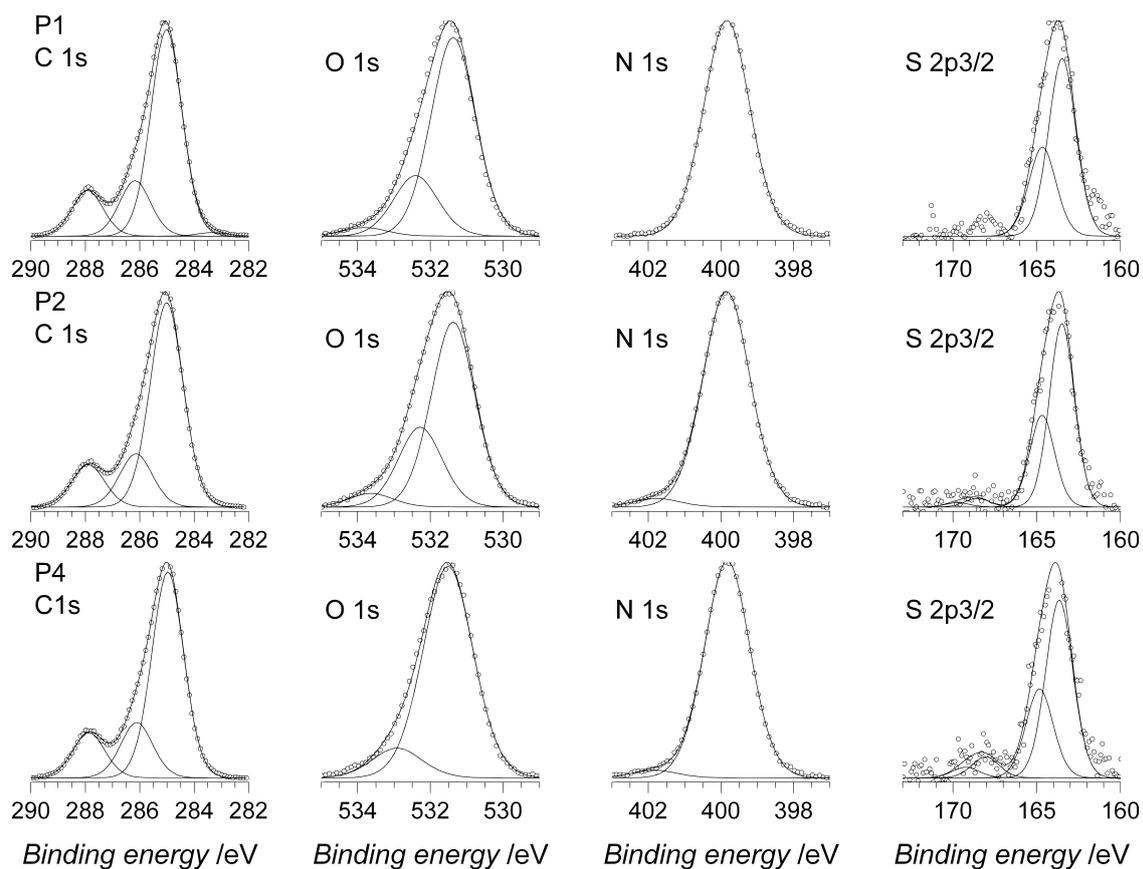
Figure A5. XPS spectra of PNIPAM with different end-groups (azide, **P1**, top), (bromine, **P2**, middle) and with acidic end-group (**P4**, bottom) for each characteristic atom (carbon, oxygen, nitrogen and sulfur). All spectra referenced at 285.0 eV for C-C sp^2.

Table A4. Assignment of binding energy and comparison of the bond contribution after the deconvolution of the XPS spectra of PNIPAM with different end-groups (azide, **P1**), (bromine, **P2**) and with acidic end-group (**P4**) for each characteristic atom (carbon, oxygen, nitrogen and sulfur). All spectra are referenced at 285.0 eV.

Atom	Binding energy /eV	at.-%			Entity
		P1	P2	P4	
S 2p3	163.5	0.51	0.45	0.38	$\underline{S}$-C
	168.5	-	0.02	0.1	$\underline{S}$=C
C 1s	285.0	49.3	51.9	49.7	$\underline{C}H_2$, $\underline{C}H_3$ sp^3
	286.1	13.3	13.5	14.0	$\underline{C}$-N, $\underline{C}$-O
	287.9	10.9	10.8	11.7	$\underline{C}$=O
N 1s	399.8	10.2	10.1	10.9	$\underline{N}$-C
	401.9	-	0.4	0.3	$\underline{N}^+$-H
O 1s	531.4	12.9	12.1	11.3	$\underline{O}$-C
	533.3	0.4	0.6	0.9	$\underline{O}$=C
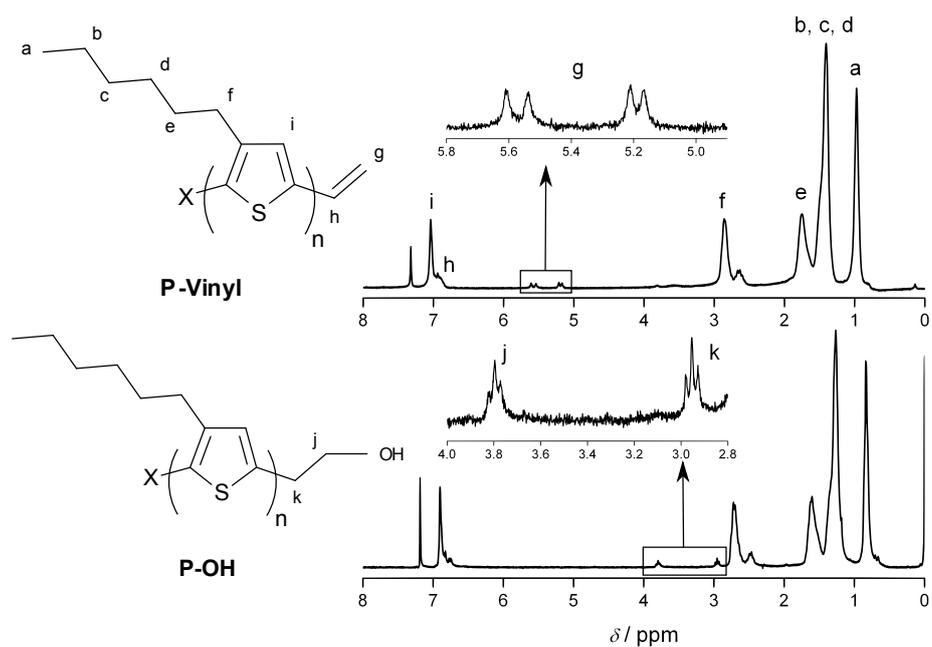
Figure A6. ^{1}H NMR spectra of **P-Vinyl** and **P-OH**.
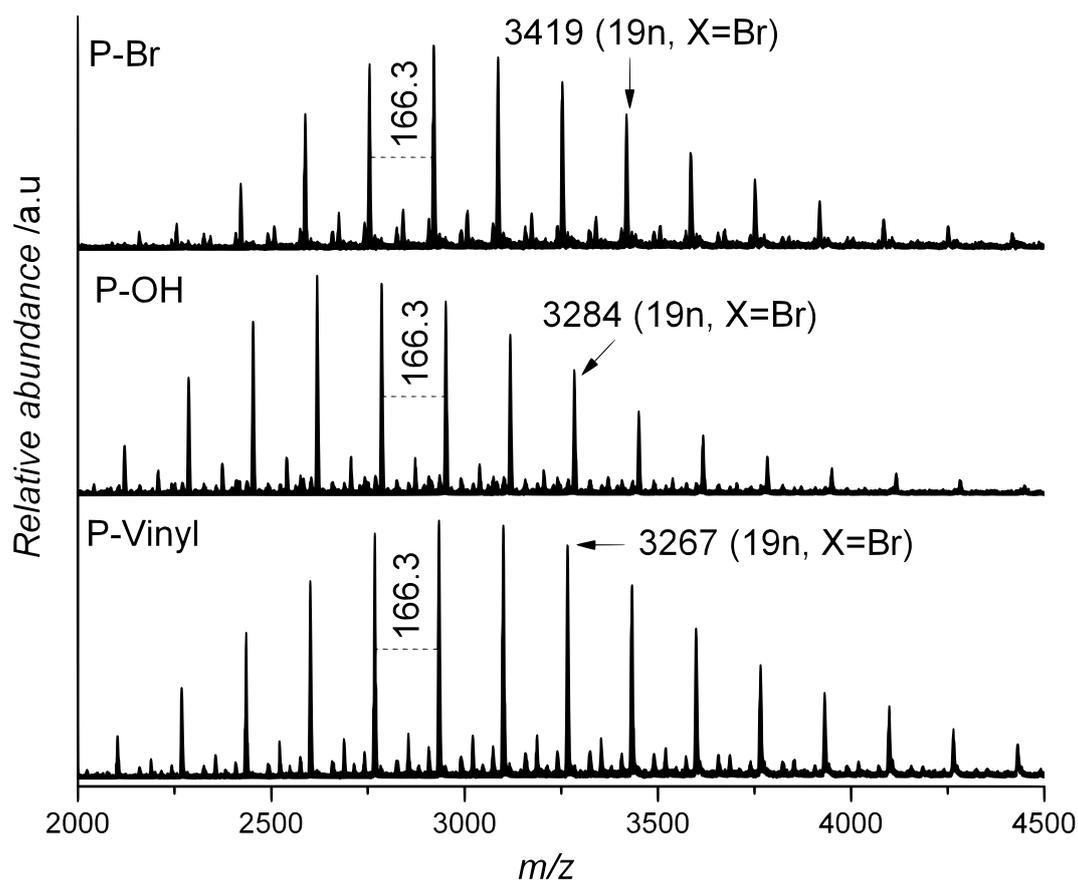
Figure A7. MALDI-ToF mass spectra of **P-Vinyl**, **P-OH** and **P-Br**.
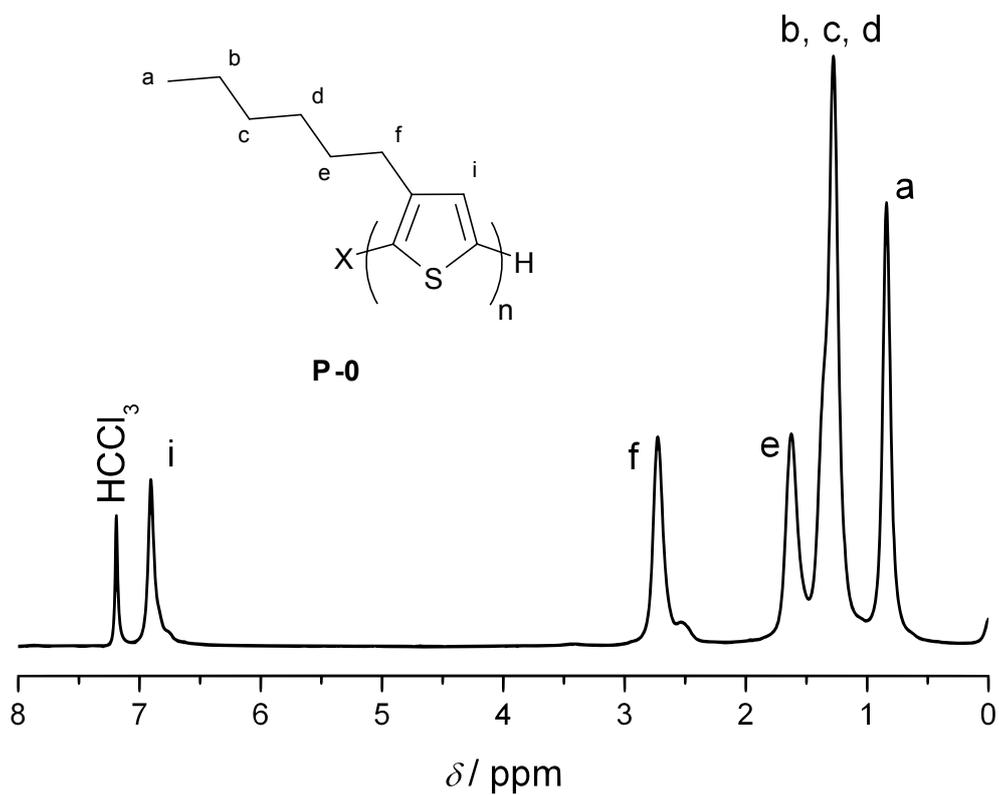
Figure A8. ^{1}H NMR spectrum of **P-0**.
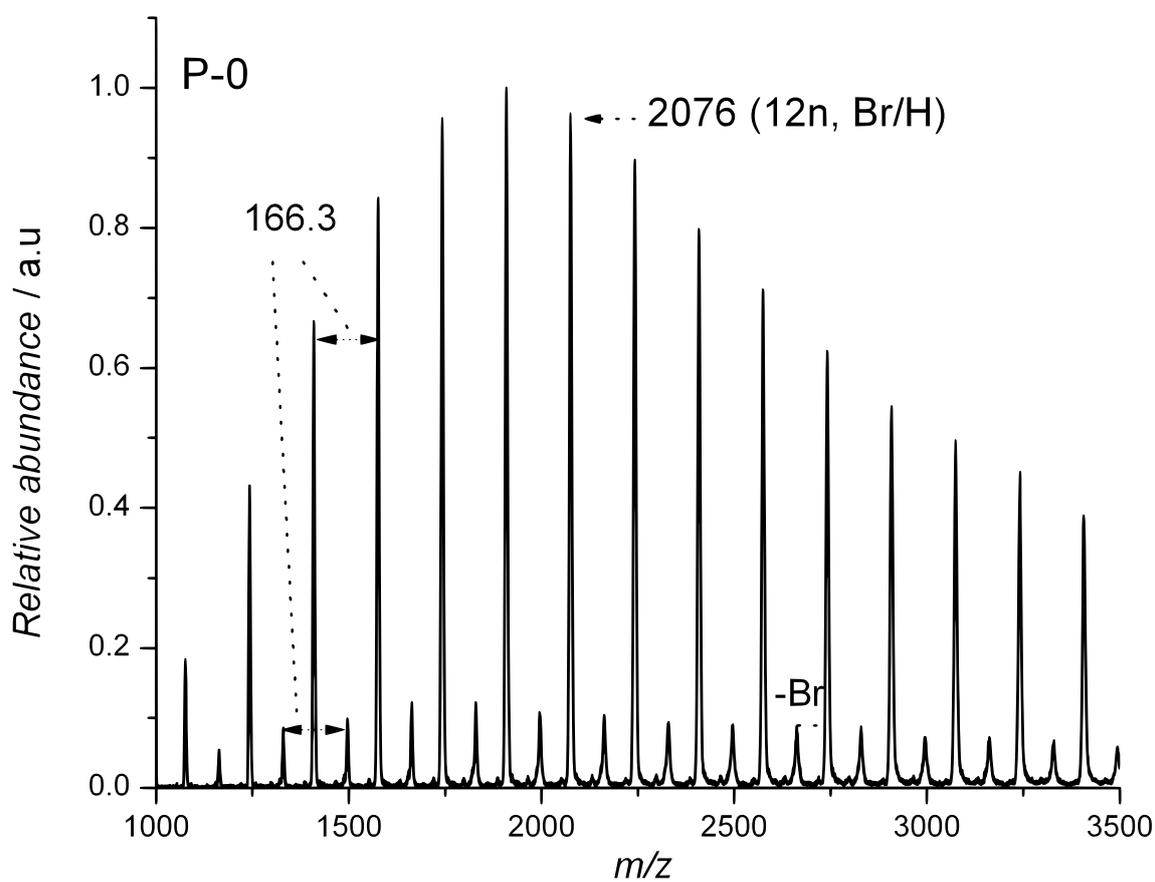
Figure A9. MALDI-ToF mass spectrum of **P-0**.
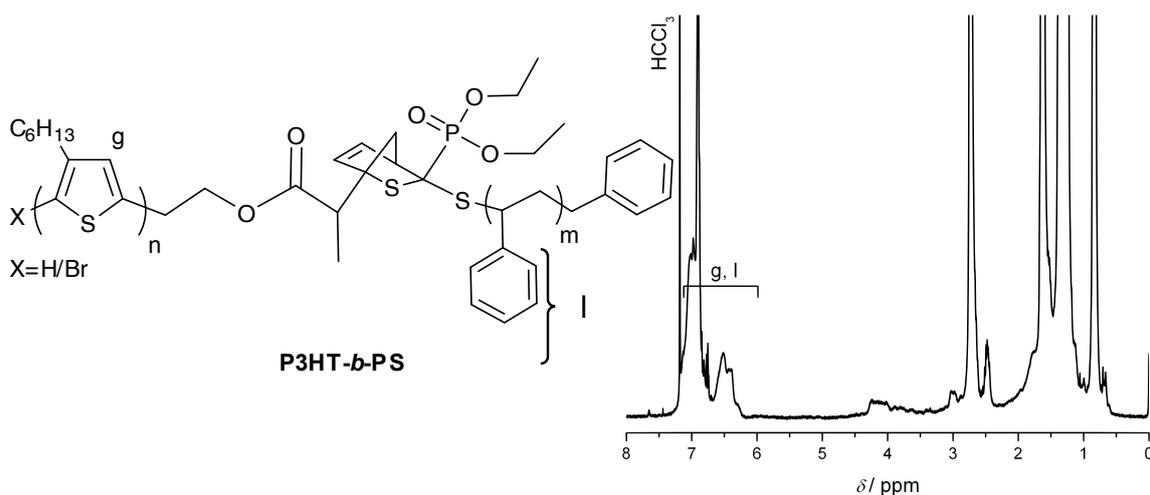
**Figure A10.** ^{1}H NMR spectrum of **P3HT-*b*-PS**.
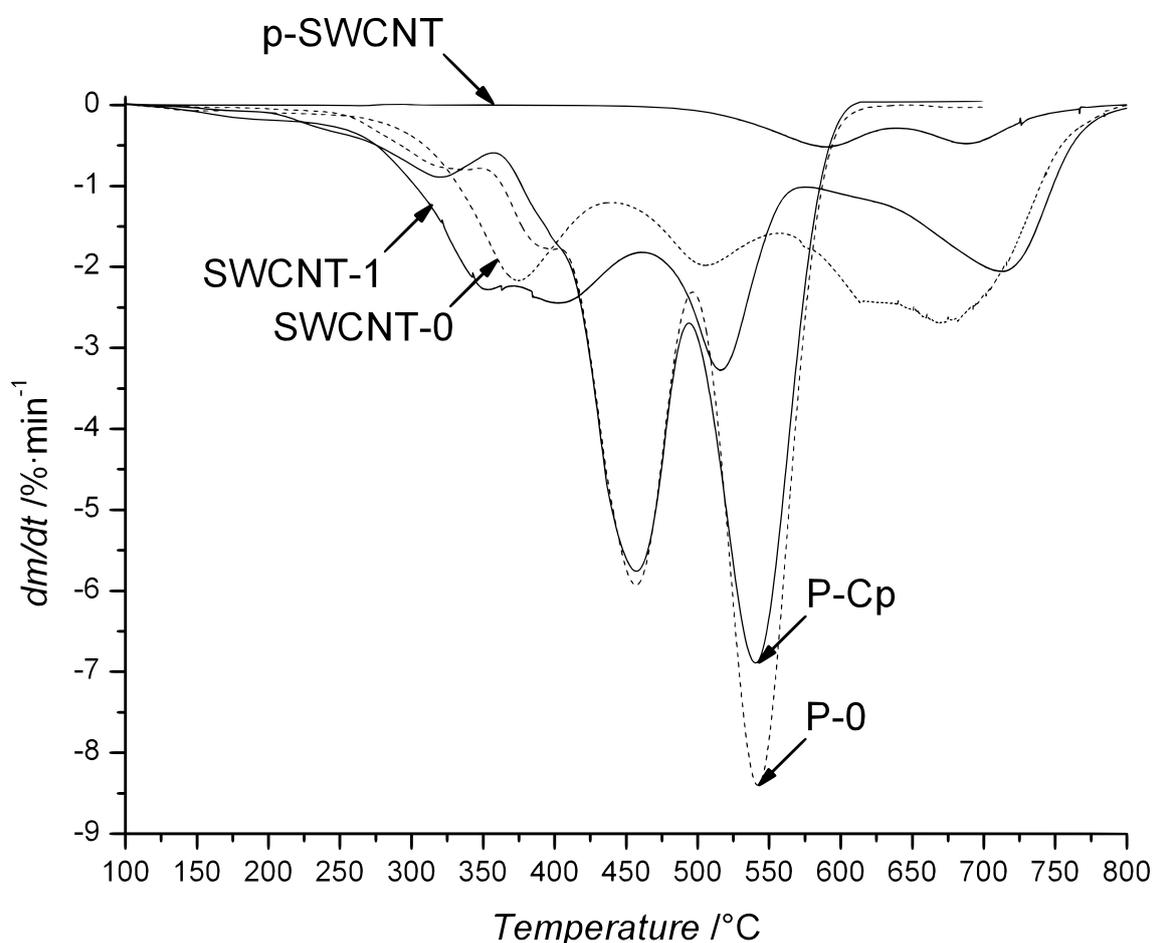
Figure A11. First derivatives of the thermogravimetric profiles of non-modified SWCNTs (**p-SWCNT**), cyclopentadienyl end-capped P3HT (**P-Cp**) and functionalized SWCNTs with **P-Cp** (**SWCNT-1**). The reference samples, non-functional P3HT (**P-0**) and the SWCNTs mixed with **P-0** (**SWCNT-0**) are represented. A heating rate of 10 °C·min^{-1} was applied initially, following a 30 minutes isothermal step at 100 °C.

Table A5. Observed thermogravimetric transformations for non-modified SWCNTs (**p-SWCNT**), cyclopentadienyl end-capped P3HT (**P-Cp**), functionalized SWCNTs with P3HT-Cp (**SWCNT-1**), as well as the reference samples: non-functional P3HT (**P-0**), and SWCNTs mixed with **P-0** (**SWCNT-0**).

Sample	$T_i{}^a$ /°C	$T_f{}^b$ /°C	$T_m{}^c$ /°C	wt.-% at T_f	Sample	$T_i{}^a$ /°C	$T_f{}^b$ /°C	$T_m{}^c$ /°C	wt.-% at T_f
p-SWCNT	440	640	590	71.6	SWCNT-1	100	240	-	99.2
	640	820	690	14.6		240	370	355	82.8
P-Cp	100	355	330	91.6		370	460	400	62.8
	355	410	-	85.0		460	570	520	38.7
	410	495	455	49.7		570	800	715	10.8
	495	630	540	8.2	SWCNT-0	100	195	-	99.5
P-0	100	360	320	93.2		195	440	375	78.2
	360	410	-	85.4		440	560	505	58.5
	410	495	455	50.4		560	800	670	17.0
	495	630	540	3.6					

[a] initial temperature for degradation; [b] final temperature for degradation; [c] temperature of maximal rate of weight loss (from first derivative).
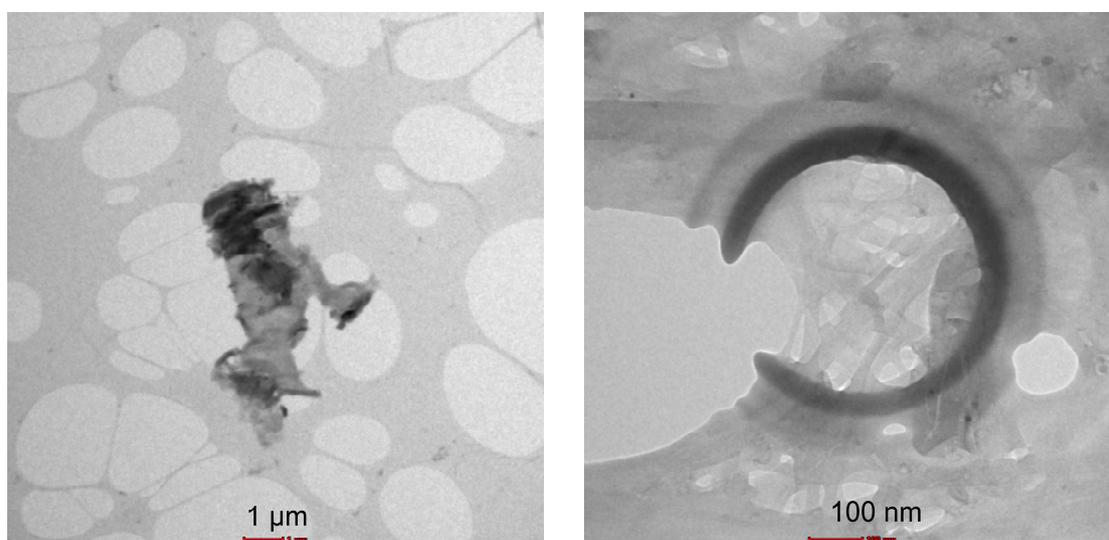

Figure A12. HRTEM pictures of coated agglomerate (left) and contamination induced by electron beam (right) of the reference sample (**SWCNT-0**).
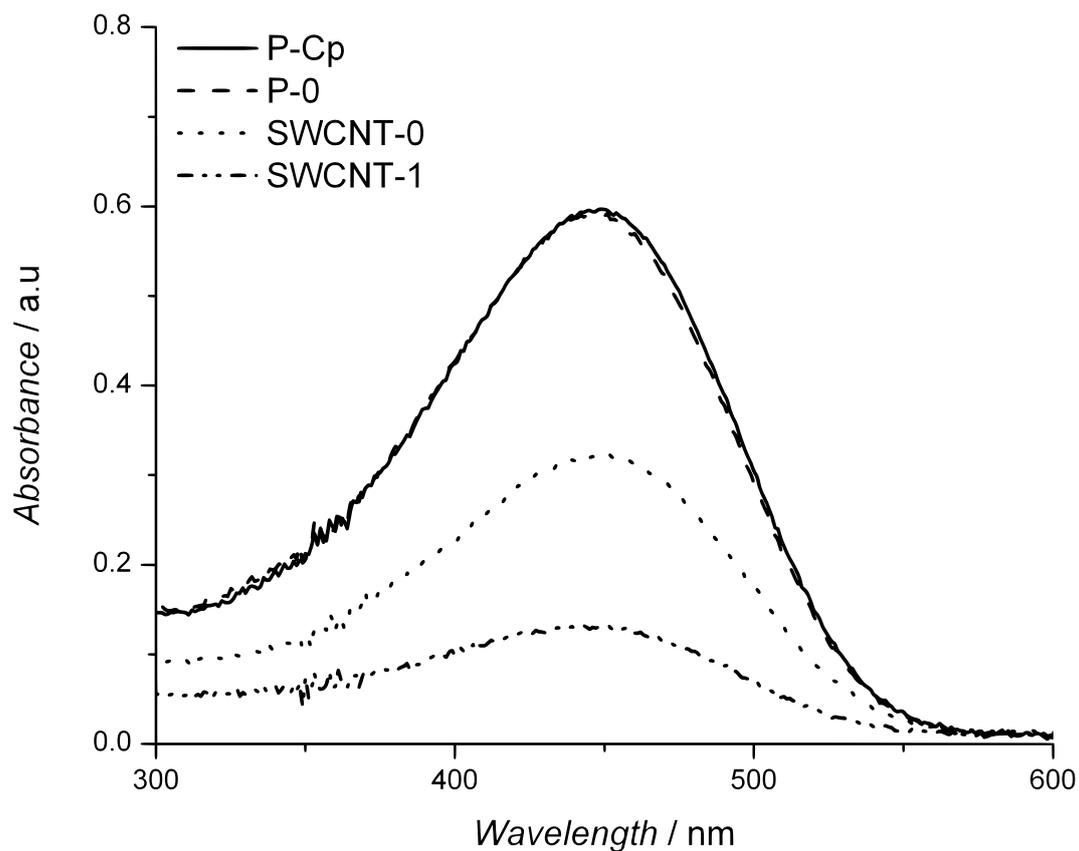
Figure A13. UV-VIS spectra of a 0.005 mM CHCl$_3$ solution of **P-Cp**, **P-0** and extracts from the dispersions prepared by 1 minute ultrasonication of 1 mg of **SWCNT-0** and **SWCNT-1** in 320 µL of CHCl$_3$.

Figure A14. Digital photograph of the dispersions prepared after 1 minute ultrasonication of 1 mg of **SWCNT-1** (left) and **SWCNT-0** (right) in 10 mL of CHCl$_3$ after 5 days.
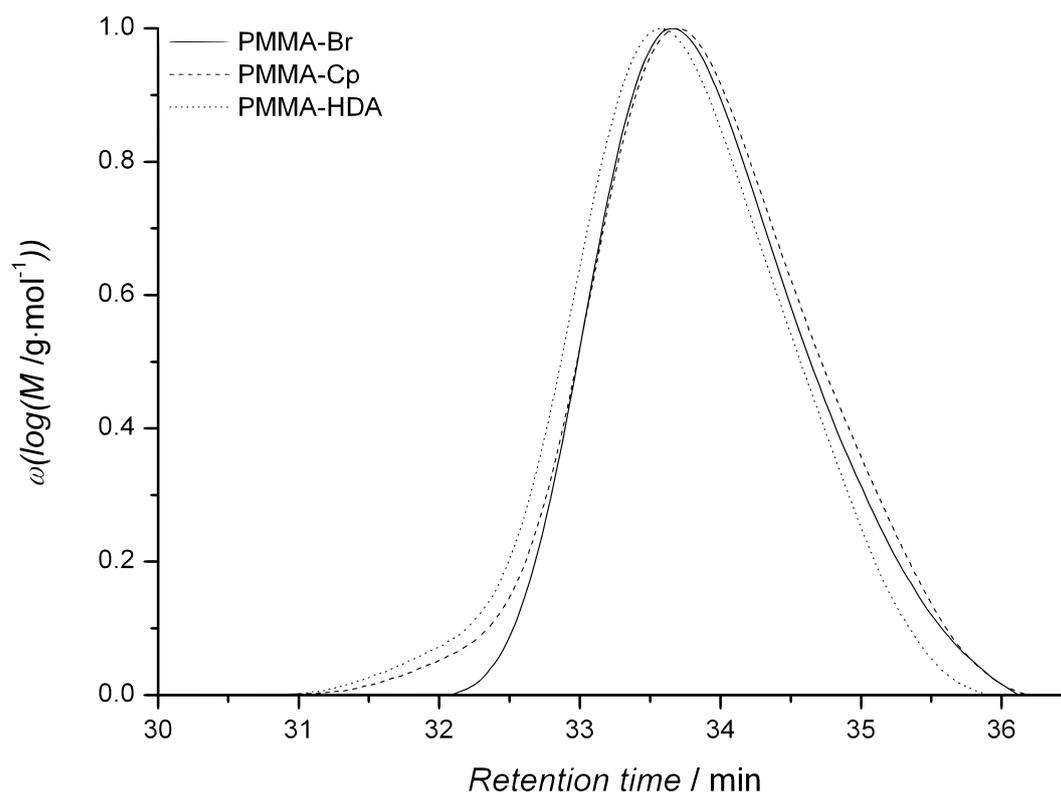
Figure A15. SEC traces of the starting material **PMMA-Br** (M_n = 2700 g·mol⁻¹, $Đ$ = 1.14), the Cp-end capped **PMMA-Cp** (M_n = 2700 g·mol⁻¹, $Đ$ = 1.17), and after the HDA reaction with **Dithio-OH** (**PMMA-HDA**, M_n = 2900 g·mol⁻¹, $Đ$ = 1.16).

**Table A6.** Summary of the identified species from the ESI-MS spectrum of **PMMA-Cp** (I-V).

n	Species	Formula	m/z exp.	m/z th.	Δm/z
	IV	$[C_{75}H_{120}O_{31}Na]^+$	1539.48	1539.77	0.29
	I	$[C_{80}H_{126}O_{30}Na]^+$	1589.56	1589.82	0.26
14	II	$[C_{75}H_{121}O_{30}BrNa]^+$	1605.36	1603.7	0.66
	III	$[C_{79}H_{126}O_{32}Na]^+$	1609.51	1609.81	0.30
	V	$[C_{80}H_{130}O_{32}Na]^+$	1625.48	1625.84	0.36
	IV	$[C_{80}H_{128}O_{33}Na]^+$	1639.48	1639.82	0.34
	I	$[C_{85}H_{134}O_{32}Na]^+$	1689.59	1689.88	0.29
15	II	$[C_{80}H_{129}O_{32}BrNa]^+$	1705.44	1703.75	0.69
	III	$[C_{84}H_{134}O_{34}Na]^+$	1709.56	1709.86	0.3
	V	$[C_{85}H_{138}O_{34}Na]^+$	1725.75	1725.9	0.15
	IV	$[C_{85}H_{136}O_{35}Na]^+$	1739.64	1739.88	0.24
	I	$[C_{90}H_{142}O_{34}Na]^+$	1789.56	1789.93	0.37
16	II	$[C_{85}H_{137}O_{34}BrNa]^+$	1805.56	1803.81	0.75
	III	$[C_{89}H_{142}O_{36}Na]^+$	1809.64	1809.92	0.28
	V	$[C_{90}H_{146}O_{36}Na]^+$	1825.84	1825.95	0.11
17	IV	$[C_{90}H_{144}O_{37}Na]^+$	1839.92	1839.93	0.01
	I	$[C_{95}H_{150}O_{36}Na]^+$	1889.75	1890.00	0.23

Table A7. Summary of the identified doubly charged species in the ESI-MS spectrum of **PMMA-Cp** (I*).

n	Species	Formula	m/z exp.	m/z th.	Δm/z
31	I*	$[C_{165}H_{261}O_{64}Na_2]^{2+}$	1656.33	1656.35	0.02
32	I*	$[C_{170}H_{269}O_{66}Na_2]^{2+}$	1706.25	1706.37	0.12
33	I*	$[C_{175}H_{277}O_{68}Na_2]^{2+}$	1756.51	1756.4	0.11
34	I*	$[C_{180}H_{285}O_{70}Na_2]^{2+}$	1806.33	1806.43	0.10
35	I*	$[C_{185}H_{293}O_{72}Na_2]^{2+}$	1856.41	1856.45	0.04
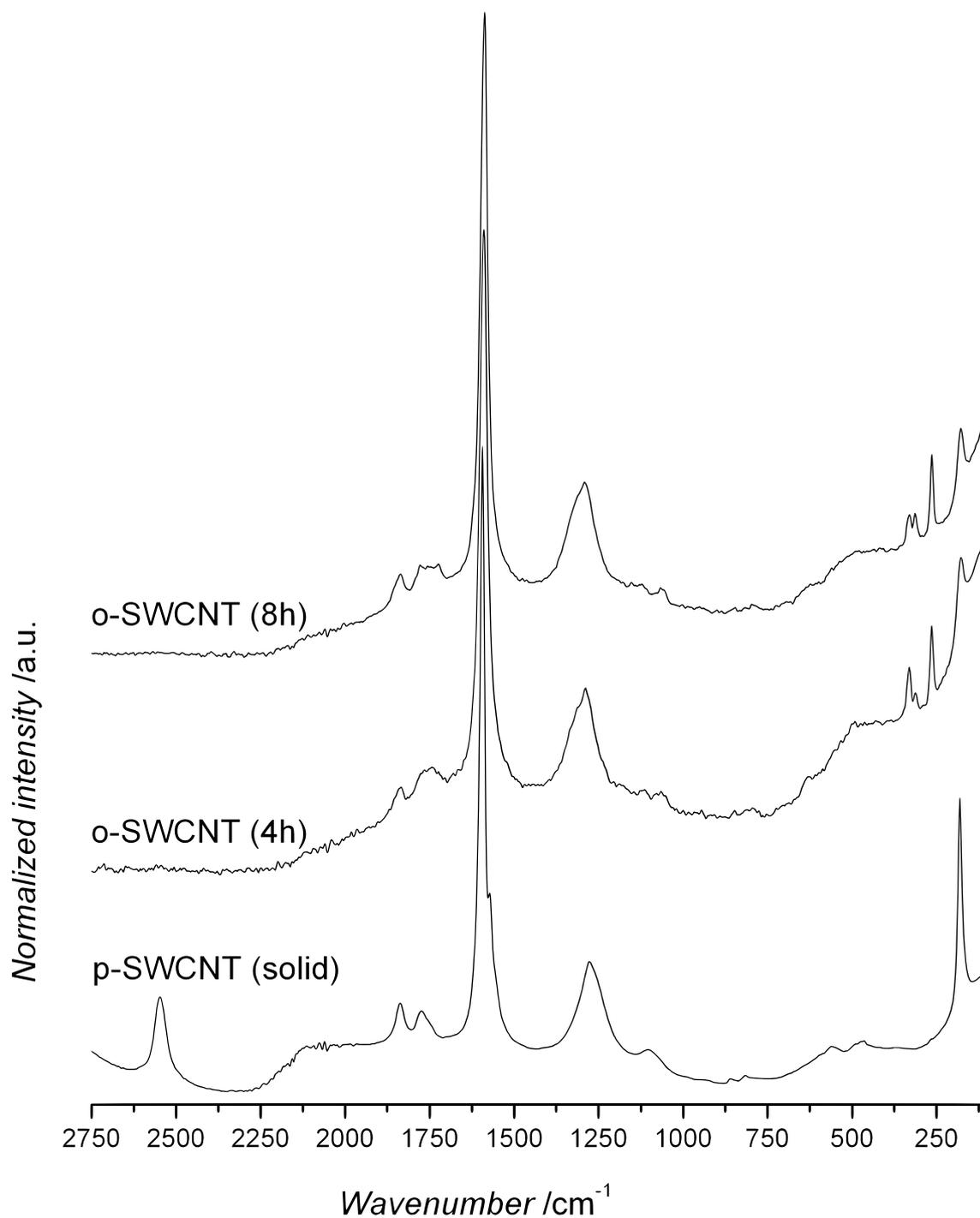
Figure A16. Raman spectra of pristine SWCNTs (**p-SWCNT**) in solid state, and of oxidized **o-SWCNT** after 4 h and 8 h acidic treatment. The spectra are recorded in water dispersion with a 1064 nm laser excitation after purification, and normalized on the G-band peak intensity.
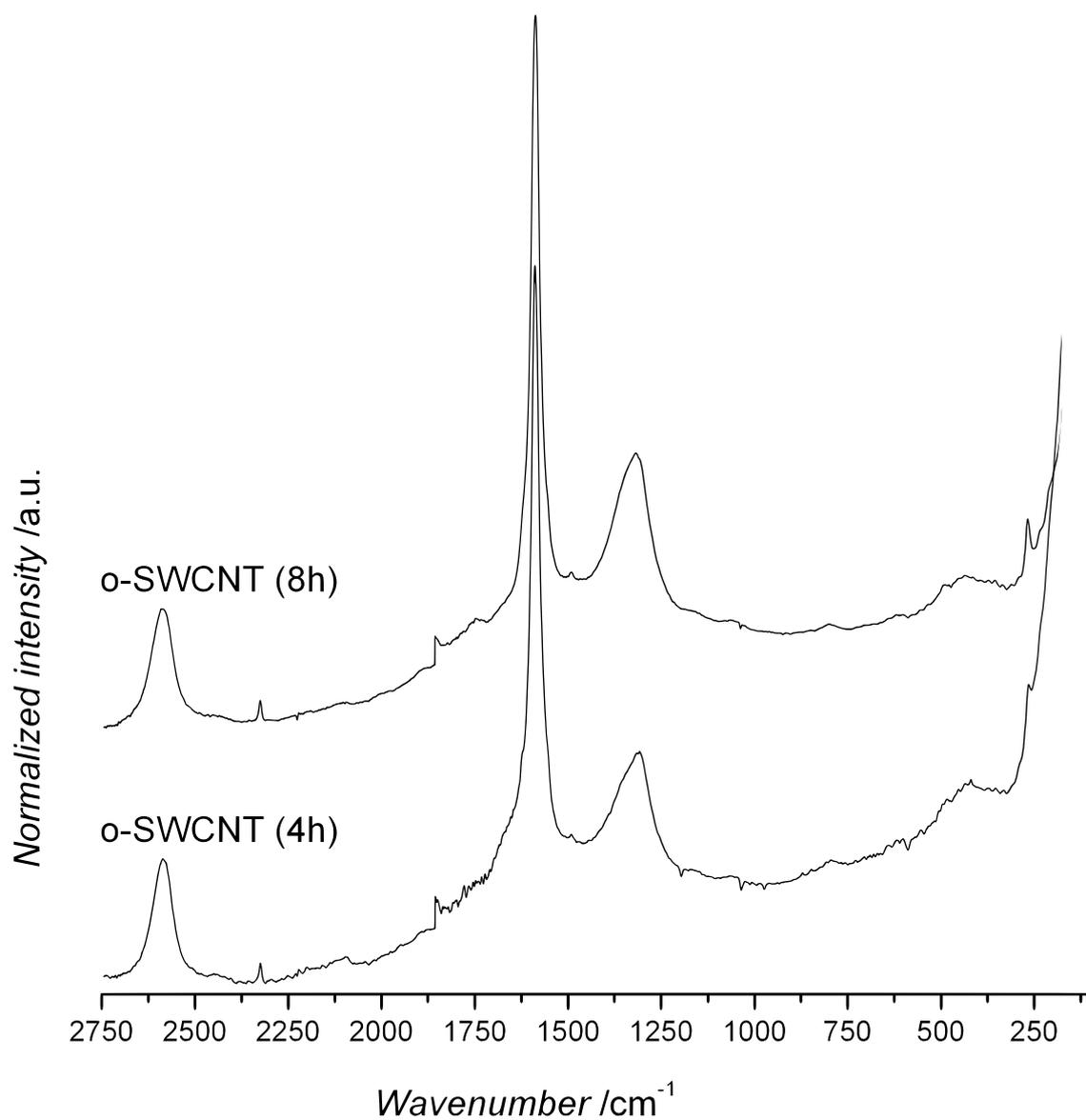
Figure A17. Raman spectra of oxidized **o-SWCNT** after 4 h and 8 h acidic treatment. The spectra were recorded in water dispersion with a 785 nm laser excitation after purification, and normalized to the G-band peak intensity.
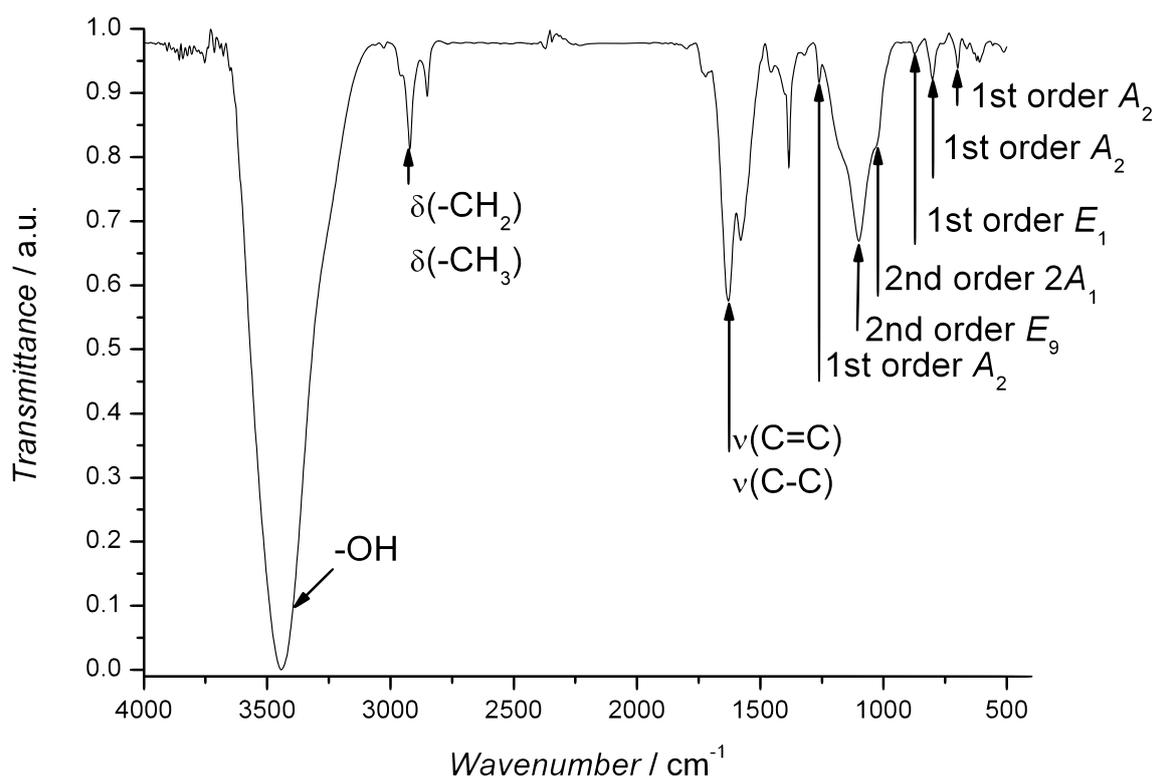
Figure A18. FTIR spectrum of the pristine SWCNTs (**p-SWCNT**) in a KBr pellet. The identified peaks agree well with those reported in the literature.[353]
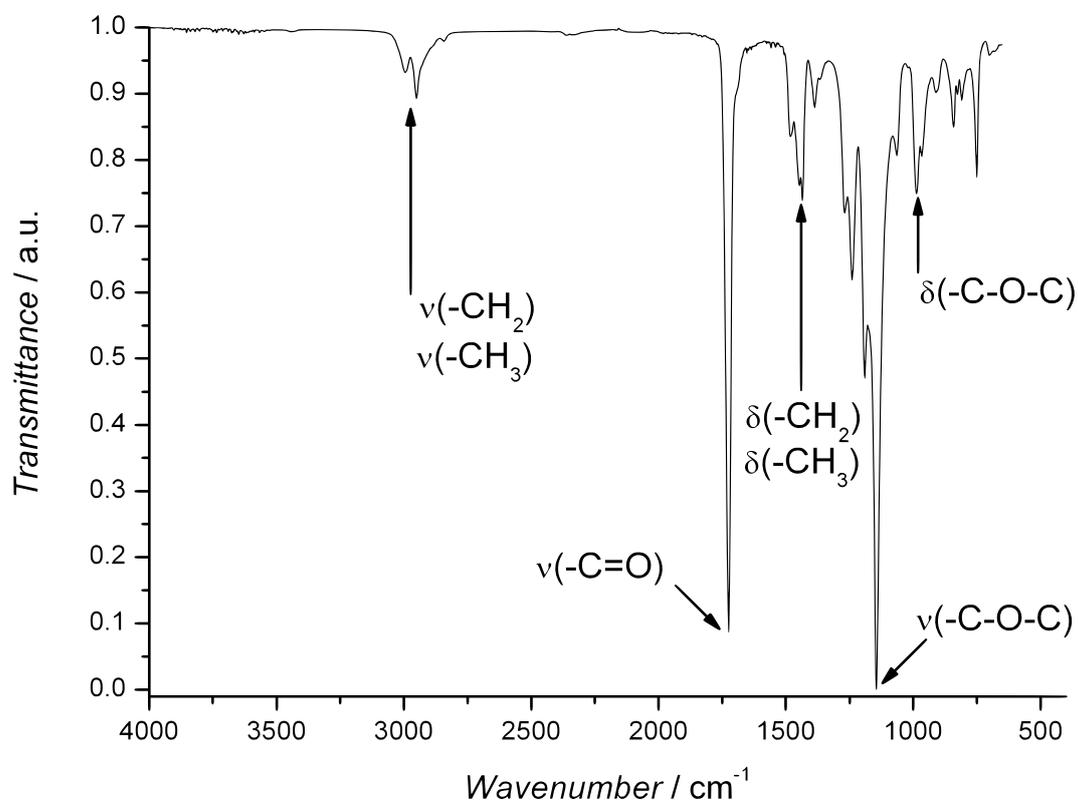
Figure A19. FTIR spectrum of **PMMA-Cp** in a KBr pellet.
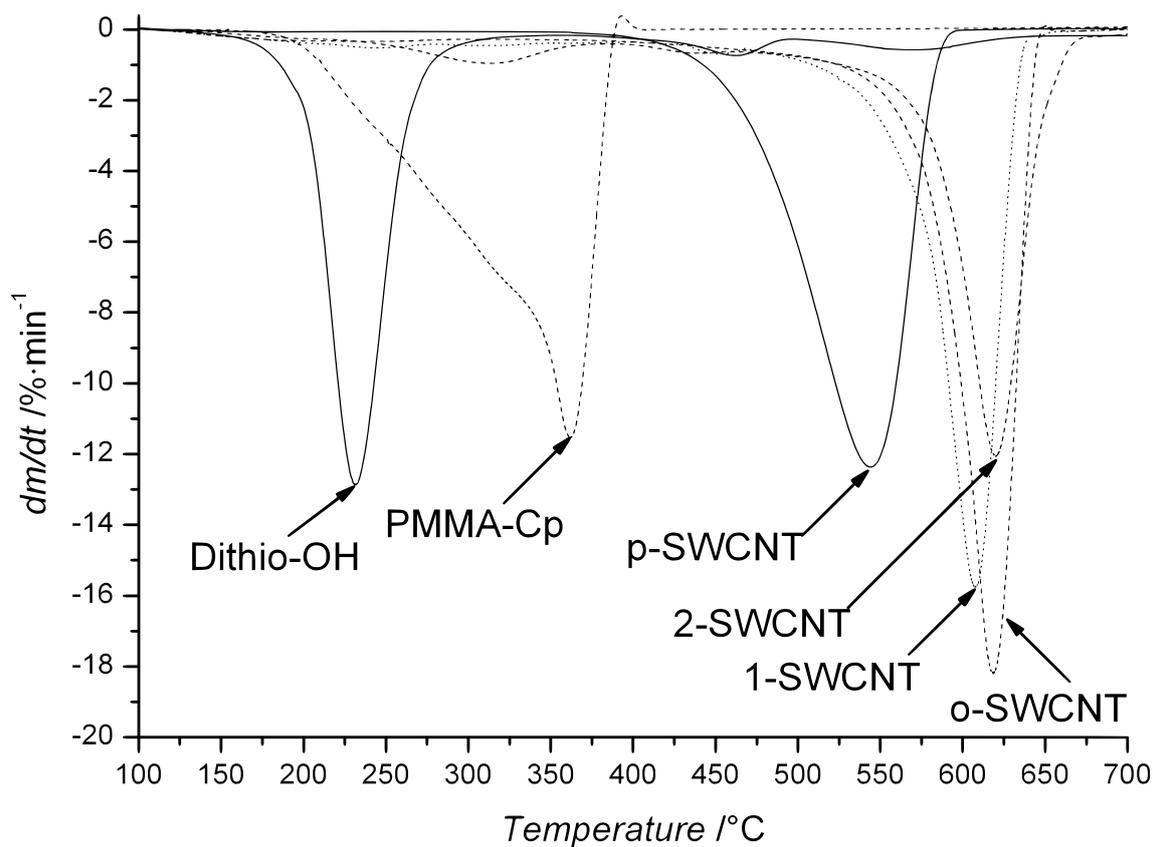
**Figure A20.** First derivatives of the thermogravimetric profiles of the pristine SWCNTs (**p-SWCNT**), after oxidation (**o-SWCNT**) and esterification (**1-SWCNT**) with the pyridine based **Dithio-OH**, and the HDA reaction (**2-SWCNT**) with **PMMA-Cp**. All samples are measured under an air atmosphere, with a heat flow of 10 °C·min^{-1}, after an isothermal step at 100 °C for 30 minutes.

Table A8. Summary of the degradation observed via thermogravimetric analysis of pristine SWCNTs (**p-SWCNT**), after oxidation (**o-SWCNT**) and esterification (**1-SWCNT**) with the pyridine based **Dithio-OH** and after the HDA reaction (**2-SWCNT**) with **PMMA-Cp**.

Sample	$T_i{}^a$ /°C	$T_f{}^b$ /°C	$T_m{}^c$ /°C	wt.-% at T_f
p-SWCNT	350	600	545	4.5
o-SWCNT	100	305	225	94.9
	305	650	610	3.9
1-SWCNT	100	280	245	94.5
	280	350	315	91.4
	350	390	370	89.9
	390	650	610	8.4
2-SWCNT	100	390	315	87.9
	390	460	440	83.9
	460	680	620	16.3

[a]initial temperature of degradation; [b]final temperature of degradation; [c]maximum temperature of degradation.

Table A9. Summary of the degradation observed via thermogravimetric analysis of the pyridine based **Dithio-OH**, and cyclopentadienyl end-capped **PMMA-Cp**.

Sample	$T_i{}^a$ /°C	$T_f{}^b$ /°C	$T_m{}^c$ /°C	wt.-% at T_f
Dithio-OH	100	360	230	32.2
	360	495	460	17.4
	495	670	570	0.44
PMMA-Cp	140	400	290	1.9

[a]initial temperature of degradation; [b]final temperature of degradation; [c]maximum temperature of degradation.

Table A10. Elemental composition of **Dithio-OH** and cyclopentadienyl end-capped **PMMA-Cp**.

Sample	C /wt.-%	H /wt.-%	N /wt.-%	O /wt.-%	S /wt.-%
Dithio-OH exp.	61.3	4.9	4.9	5.5	22.7
Dithio-OH th.	61.1	4.8	5.1	5.8	23.3
PMMA-Cp	58.3	7.7	1.0	30.2	0

Table A11. Assignment of the binding energies and the comparison of the band contribution after deconvolution of the XPS spectra of **PMMA-Cp**. The spectra referenced at 285.0 eV for C-C sp^3.

Peak	B.E.^{a} /eV	PMMA-Cp /at.-%	Entity
C1s	285.0	26.3	-$\underline{C}$H$_2$/-$\underline{C}$H$_3$ sp^3
	285.8	21.1	-CH$_2$-$\underline{C}$(CH$_3$)-COOCH$_3$
	286.8	13.7	-O$\underline{C}$H$_3$
	289.3	12.5	O=$\underline{C}$-OCH$_3$
O 1s	532.1	13.4	$\underline{O}$=C-OCH$_3$
	533.4	13.0	-$\underline{O}$-CH$_3$

^{a}binding energy.

References

[1] M.-C. Daniel, D. Astruc, *Chem. Rev.*, **2004**, *104*, 293.

[2] H. W. Kroto, *J. Chem. Soc. Faraday Trans.*, **1991**, *87*, 2871.

[3] W. Zhou, X. Bai, E. Wang, S. Xie, *Adv. Mater.*, **2009**, *21*, 4565.

[4] W. Lu, M. Zu, J.-H. Byun, B.-S. Kim, T.-W. Chou, *Adv. Mater.*, **2012**, *24*, 1805.

[5] H. Qian, E. S. Greenhalgh, M. S. P. Shaffer, A. Bismarck, *J. Mater. Chem.*, **2010**, *20*, 4751.

[6] A. Izadi-Najafabadi, S. Yasuda, K. Kobashi, T. Yamada, D. N. Futaba, H. Hatori, M. Yumura, S. Iijima, K. Hata, *Adv. Mater.*, **2010**, *22*, E235.

[7] K. Ellmer, *Nature Photonics*, **2012**, *6*, 808.

[8] A. C. Dillon, *Chem. Rev.*, **2010**, *110*, 6856.

[9] B. Esser, J. M. Schnorr, T. M. Swager, *Angew. Chem. Int. Ed.*, **2012**, *51*, 1.

[10] C. Gao, Z. Guo, J.-H. Liu, X.-J. Huang, *Nanoscale*, **2012**, *4*, 1948.

[11] L. Meng, X. Zhang, Q. Lu, Z. Fei, P. J. Dyson, *Biomaterials*, **2012**, *33*, 1689.

[12] H. Huang, Q. Yuan, J. S. Shah, R. D. K. Misra, *Adv. Drug Del. Rev.*, **2011**, *63*, 1332.

[13] E. Miyako, C. Hosowaka, M. Kojima, M. Yudasaka, R. Funahashi, I. Oishi, Y. Hagihara, M. Shichiri, M. Takashima, K. Nishio, Y. Yoshida, *Angew. Chem. Int. Ed.*, **2011**, *50*, 12266.

[14] Z. Spitalsky, D. Tasis, K. Papagelis, C. Galiotis, *Prog. Polym. Sci.*, **2010**, *35*, 357.

[15] W. Bauhofer, J. Z. Kovacs, *Compos. Sci. Technol.*, **2008**, *69*, 1486.

[16] B.-X. Yang, J.-H. Shi, K. P. Pramoda, S. H. Goh, *Nanotechnol.*, **2007**, *18*, 125606.

[17] R. Blake, J. N. Coleman, M. T. Byrne, J. E. McCarthy, T. S. Perova, W. J. Blau, J. B. Nagy, Y. K. Gun'ko, *J. Mater.Chem.*, **2006**, *16*, 4206.

[18] R. Vukićević, I. Vukovic, H. Stoyanov, A. Korwitz, D. Pospiech, G. Kofod, K. Loos, G. Binke, S. Beuermann, *Polym. Chem.*, **2012**, *3*, 2261.

[19] S. Bose, A. R. Bhattacharyya, A. R. Kulkarni, P. Pötschke, *Compos. Sci. Technol.*, **2009**, *69*, 365; Y. Y. Huang, E. M. Terentjev, *Adv. Funct. Mater.*, **2010**, *23*, 4062; Y. L. Huang, H. W. Tien, C. C. Ma, Y. H. Yu, S. Y. Yang, M. H. Wei, S. Y. Wu., *Nanotechnology*, **2010**, *21*, 185702; J. S. Hong, I. G. Hong, H. T. Lim, K. H. Ahn, S. J. Lee, *Macromol. Mater. Eng.*, **2011**, *296*, 341.

[20] L. A. Girifalco, M. Hodak, R. S. Lee, *Phys. Rev. B: Condens. Matter.*, **2000**, *62*, 13104.

[21] T. Kashiwagi, J. Fagan, J. F. Douglas, K. Yamamoto, A. N. Heckert, S. D. Leigh, J.

Obrzut, F. Du, S. Lin-Gibson, M. Mu, K. I. Winey, R. Haggenmueller, *Polymer*, **2007**, *48*, 4855.

[22] T. Fujigaya, T. Fukumaru, N. Nakashima, *Synth. Met.*, **2009**, *159*, 827.

[23] X. Li, H. Gao, W. A. Scrivens, D. Fei, X. Xu, M. A. Sutton, A. P. Reynolds, M. L. Myrick, *J. Nanosci. Nanotechnol.*, **2007**, *7*, 2309.

[24] T. Uchida, S. Kumar, *J. Appl. Polym. Sci.*, **2005**, *98*, 985.

[25] C. Backes, F. Hauke, A. Hirsch, *Adv Mater.*, **2011**, *23*, 2588.

[26] N. G. Sahoo, S. Rana, J. W. Cho, L. Li, S. H. Chan, *Prog. Poly. Sci.*, **2010**, *35*, 7, 837.

[27] M. Moniruzzaman, K. I. Winey, *Macromolecules*, **2006**, *39*, 5194.

[28] H. Liu, X. Wang, P. Fang, S. Wang, X. Qi, C. Pan, G. Xie, K. M. Liew, *Carbon*, **2010**, *48*, 721.

[29] Y. Lin, M. J. Meziani, Y.-P. Sun, *J. Mater. Chem.*, **2007**, *17*, 1143.

[30] E. Moore, P.-Y. Wang, A. P. Vogt, C. T. Gibson, V. Haridas, N. H.Voelcker, *RSC Advances*, **2012**, *2*, 1289.

[31] A. Hirsch, O. Votroswsky, *Top. Curr. Chem.*, **2005**, *245*, 193; S. Banerjee, T. Hemraj-Benny, S. S. Wong, *Adv. Mater.*, **2005**, *1*, 17; X. Peng, S. S. Wong, *Adv. Mater.*, **2009**, *21*, 625; F. Hauke, A. Hirsch, *Covalent Functionalization of Carbon Nanotubes, in Carbon Nanotubes and Related Structures: Synthesis, Characterization, Functionalization, and Applications*, D. M. Guldi and N. Martín Eds., Wiley-VCH Verlag GmbH & Co. KGaA, Weinheim, Germany, **2010**; D. Tasis, N. Tagmatarchis, A. Bianco, M. Prato, *Chem. Rev.*, **2006**, *106*, 1105; A. Hirsch, *Angew. Chem. Int. Ed.*, **2002**, *41*, 1853; P. Singh, S. Campidelli, S. Giordani, D. Bonifazi, A. Bianco, M. Prato, *Chem. Soc. Rev.*, **2009**, *38*, 2214.

[32] M. N. Tchoul, W. T. Ford, G. Lolli, D. E. Resasco, S. Arepalli, *Chem. Mater.*, **2007**, *19*, 5765.

[33] V. Datsyuk, M. Kalyva, K. Papagelis, J. Parthenios, D. Tasis, A. Siokou, I. Kallitsis, C. Galiotis, *Carbon*, **2008**, *46*, 833.

[34] H. Touhara, J. Inahara, T. Mizuno, Y. Yokoyama, S. Okanoa, K. Yaganiuch, I. Mukopadhyay, S. Kawasaki, F. Okino, H. Shirai, W. H. Xu, T. Kyotani, A. Tomita, *J. Fluor. Chem.*, **2002**, *114*, 181.

[35] Y. Ying, R. K. Saini, F. Liang, A. K. Sadana, W. E. Billups, *Org. Lett.*, **2003**, *5*, 1471.

[36] M. Holzinger, O. Votrowski, A. Hirsch, F. Hennrich, M. Kappes, R. Weiss, F. Jellen, *Angew. Chem.*, **2001**, *40*, 4002.

[37] F. Brunetti, M. Ferrrero, J. Munoz, M. Meneghetti, M. Prato, E. Vasquez, *J. Am. Chem. Soc.*, **2008**, *130*, 8094.

[38] K. S. Coleman, S. R. Bailey, S. Fogden, M. L. H. Green, *J. Am. Chem. Soc.*, **2003**, *125*, 8722.

[39] B. Gebhardt, R. Graupner, F. Hauke, A. Hirsch, *Eur. J. Org. Chem.*, **2010**, *8*, 1494.

[40] Y. Martinez-Rubi, J. Guan, S. Lin, C. Scriver, R. E. Sturgeon, B. Simard, *Chem. Comm.*, **2007**, *48*, 5146.

[41] S. Bose, R. A. Khare, P. Moldenaers, *Polymer*, **2010**, *51*, 975.

[42] P. Eaton, *J. Am. Chem. Soc.*, **1964**, *86*, 962.

[43] L. A. Paquette, *Chem. Rev.*, **1989**, *89*, 1051

[44] K. Raghavachari, J. S. Binkley, *J. Chem. Phys.*, **1987**, *87*, 2191

[45] H. W. Kroto, J. R. Heath, S. C. O'Brien, R. F. Curl, R. E. Smalley, *Nature*, **1985**, *318*, 162.

[46] W. Krätschmer, L. D. Lamb, K. Fostiropoulos, D. R. Huffman, *Nature*, **1990**, *347*, 354.

[47] L. T. Scott, M. M. Boorum, B. J. McMahon, S. Hagen, J. Mack, J. Blank, H. Wegner, A. de Meijere, *Science*, **2002**, *295*, 1500.

[48] L.T. Scott, *Angew. Chem. Int. Ed.*, **2004**, *43*, 4994.

[49] H. W. Kroto, *Nature*, **1987**, *329*, 529.

[50] F. J. Owens, C. P. Poole Jr., *The Physics and Chemistry of Nanosolids*, John Wiley and Sons, Inc., **2008**

[51] P. Avouris, C. Dimitrakopoulos, *Materials Today*, **2012**, *3*, 86.

[52] M. Terrones, *Annu. Rev. Mater. Res.*, **2003**, *33*, 419.

[53] B. Yu, C. Liu, P.-X. Hou, Y. Tian, S. Li, B. Liu, F. Li, E. I. Kauppinen, H.-M. Cheng, *J. Am. Chem. Soc.*, **2011**, *133*, 5232.

[54] M. S. Dresselhaus, G. Dresselhaus, Ph. Avouris, *Carbon Nanotubes Synthesis, Structure, Properties, and Applications*, Topics in Applied Science, 80, Springer, **2001**.

[55] S. Ijima, *Nature*, **1991**, *56*, 354.

[56] M. S. Dresselhaus, G. Dresselhaus, R. Saito, *Carbon*, **1995**, *7*, 883.

[57] O. Diels, W. E. Thiele, *Ber. dtsch. Chem. Ges. A/B*, **1938**, *71*, 1173.

[58] M. Ikeda, R. Ochi, Y.-S. Kurita, D. J. Pochan, I. Hamachi, *Chem. Eur. J.*, **2012**, *18*, 13091.

[59] R. B. Woodward, R. Hoffmann, *J. Am. Chem. Soc.*, **1965**, *87*, 395.

[60] V. K. Johns, Z. Shi, W. Dang, M. D. McInnis, Y. Weng, Y. Liao, *J. Phys. Chem. A*, **2011**, *28*, 8093.

[61] J. Sauer, R. Sustmann, *Angew. Chem. Int. Ed. Engl.*, **1980**, *19*, 779.

[62] S. Zhang, J. T. Koberstein, *Langmuir*, **2012**, *28*, 486.

[63] R. T. Chen, S. Marchesan, R. A. Evans, K. E. Styan, G. K. Such, A. Postma, K. M. McLean, B. W. Muir, F. Caruso, *Biomacromolecules*, **2012**, *13*, 889.

[64] J.-T. Wu, C.-H. Huang, W.-C. Liang, Y.-L. Wu, J. Yu, H.-Y. Chen, *Macromol. Rapid Commun.*, **2012**, *33*, 922.

[65] T. N. Gevrek, R. N. Ozdeslik, G. S. Sahin, G. Yesilbag, S. Mutlu, A. Sanyal, *Macromol. Chem. Phys.*, **2012**, *213*, 166.

[66] B. Fabre, D. M. Bassani, C. K. Liang, D. Ray, F. Hui, P. Hapiot, *J. Phys. Chem. C*, **2011**, *115*, 14786.

[67] A. S. Goldmann, T. Tischer, L. Barner, M. Bruns, C. Barner-Kowollik, *Biomacromolecules*, **2011**, *12*, 1137.

[68] H. C. Kolb, M. G. Finn, K. B. Sharpless, *Angew. Chem. Int. Edit.*, **2001**, *40*, 2004.

[69] W. H. Binder, R. Sachsenhofer, *Macromol. Rapid Commun.*, **2007**, *28*, 15; W. H. Binder, R. Sachsenhofer, *Macromol. Rapid Commun.*, **2008**, *29*, 952; R. A. Evans, *Austr. J. Chem.*, **2007**, *60*, 384; J. E. Moses, A. D. Moorhouse, *Chem. Soc. Rev.*, **2007**, *36*, 1249.

[70] K. C. Nicolaou, S. A. Snyder, T. Montagnon, G.Vassilikogiannakis, *Angew. Chem. Int. Ed.*, **2002**, *41*, 1668.

[71] B. S. Bodnar, M. J. Miller, *Angew. Chem. Int. Ed.*, **2011**, *50*, 5630.

[72] C. Barner-Kowollik, F. E. Du Prez, P. Espeel, C. J. Hawker, T. Junkers, H. Schlaad, W. Van Camp, *Angew. Chem. Int. Ed.*, **2011**, *50*, 60.

[73] M. A. Tasdelen, *Polym. Chem.*, **2011**, *2*, 2133.

[74] K. Kempe, A. Krieg, C. R. Becer, U. S. Schubert, *Chem. Soc. Rev.*, **2012**, *41*, 176.

[75] M. Glassner, K. Oehlenschlaeger, T. Gruendling, C. Barner-Kowollik, *Macromolecules*, **2011**, *44*, 4681.

[76] J. Amici, M. U. Kahveci, P. Allia, P. Tiberto, Y. Yagci, M. Sangermano, *J. Mater. Sci.*, **2012**, *47*, 412.

[77] T. Pauloehrl, G. Delaittre, V. Winkler, A. Welle, M. Bruns, H. G. Börner, A. M. Greiner, M. Bastmeyer, C. Barner-Kowollik, *Angew. Chem. Int. Ed.*, **2012**, *51*, 1071.

[78] M. D. Rowe, C.-C. Chang, D. H. Thamm, S. L. Kraft, J. F. Jr. Harmon, A. P. Vogt, B. S.

Sumerlin, S. G. Boyes, *Langmuir*, **2009**, *25*, 9487.

[79] A. P. Bapat, J. G. Ray, D. A. Savin, E. A. Hoff, D. L. Patton, B. S. Sumerlin, *Polym. Chem.*, **2012**, *3*, 3112.

[80] J. A. Syrett, G. Mantovani, W. R. S. Barton, D. Pricec, D. M. Haddleton, *Polym. Chem.*, **2010**, *1*, 102.

[81] O. Diels, K. Alder, *Ann.*, **1928**, *460*, 98.

[82] R. B. Woodward, T. J. Katz, *Tetrahedron*, **1959**, *5*, 70.

[83] J.-L. Li, T.-Y, Liu, Y.-C. Chen, *Acc. Chem. Res.*, **2012**, *45*, 1491.

[84] P. D. Bartlett , K. E. Schueller, *J. Am. Chem. Soc.*, **1968**, *22*, 6077.

[85] L. Nebhani, S. Sinnwell, C. Y. Lin, M. L. Coote, M. H. Stenzel, C. Barner-Kowollik *J. Polym. Sci. A Polym. Chem.*, **2009**, *47*, 6053.

[86] S. Sinnwell, A. J. Inglis, T. P. Davis, M. H. Stenzel, C. Barner-Kowollik, *Chem. Commun.*, **2008**, 2052.

[87] A. Bousquet, C. Boyer, T. P. Davis, M. H. Stenzel, *Polym. Chem.*, **2010**, *1*, 1186.

[88] T. Tischer, A. S. Goldmann, K. Linkert, V. Trouillet, H. G. Boerner, C. Barner-Kowollik, *Adv. Funct. Mater.*, **2012**, *22*, 3853.

[89] M. Kaupp, A. P. Vogt, J. C. Natterodt, V. Trouillet, T. Gruendling, T. Hofe, L. Barner, C. Barner-Kowollik, *Polym. Chem.*, **2012**, *3*, 2605.

[90] J. A. Isaacs, A. Tanwani, M. L. Healy, L. J. Dahlben, *J. Nanopart. Res.*, **2010**, *12*, 551.

[91] J. Q. Huang, Q. Zhang, M. Q. Zhao, F. Wei, *Chin. Sci. Bull.*, **2012**, *57*, 157.

[92] C. Ge, F. Lao, W. Li, Y. Li, C. Chen, Y. Qiu, X. Mao, B. Li, Z. Chai, Y. Zhao, *Anal. Chem.*, **2008**, *80*, 9426.

[93] J. Ma, J. N. Wang, *Chem. Mater.*, **2008**, *20*, 2895.

[94] W. Huang, Y. Wang, G. Luo, F. Wie, *Carbon*, **2003**, *41*, 2585.

[95] K. Moshammer, F. Hennrich, M. M. Kappes, *Nano Res.*, **2009**, *2*, 599.

[96] C. Blum, N. Stürzl, F. Hennrich, S. Lebedkin, S. Heeg, H. Dumlich, S. Reich, M. M. Kappes, *ACS Nano*, **2011**, *5*, 2847.

[97] D. M. Guldi, N. Martín, *Carbon Nanotubes and Related Structures*, Wiley-VCH Verlag GmbH & Co. KGAa, Weinheim, **2010**.

[98] J. Prasek, J. Drbohlavova, J. Chomoucka, J. Hubalek, O. Jasek, V. Adamand, R. Kizek, *J. Mater. Chem.*, **2011**, *21*, 15872.

[99] S. Lebedkin, P.Schweiss, B. Renker, S. Malik, F. Hennrich, M. Neumaier , C. Stoermer,

M. M. Kappes, *Carbon*, **2002**, *40*, 417.

[100] M. Kalbac, Y.-P. Hsieh, H. Farhat, L. Kavan, M. Hofmann, J. Kong, M. S. Dresselhaus, *Nano Lett.*, **2010**, *10*, 4619.

[101] R. Marquis, C. Greco, I. Sadokierska, S. Lebedkin, M. M. Kappes, T. Michel, L. Alvarez, J.-L. Sauvajol, S. Meunier, C. Mioskowski, *Nano Lett.*, **2008**, *8*, 1830.

[102] J. A. Fagan, B. J. Bauer, E. K. Hobbie, M. L. Becker, A. R. Hight Walker, J. R. Simpson, J. Chun, J. Obrzut, V. Bajpai, F. R. Phelan, D. Simien, J. Y. Huh, K. B. Migler, *Adv. Mater.*, **2011**, *23*, 338.

[103] J.-C. Charlier, *Acc. Chem. Res.*, **2002**, *35*, 1063.

[104] S. Schrettl, H. Frauenrath, *Angew. Chem. Int. Ed.*, **2012**, *51*, 6569.

[105] M. A. Tasdelen, *Polym. Chem.*, **2011**, *2*, 2133.

[106] E. H. Fort, P. M. Donovan, L. T. Scott, *J. Am. Chem. Soc.*, **2009**, *131*, 16006.

[107] E. H. Fort, M. S. Jeffreys, L. T. Scott, *Chem. Commun.*, **2012**, *48*, 8102.

[108] E. H. Fort, L. T. Scott, *J. Mater. Chem.*, **2011**, *21*, 1373.

[109] H.-B. Li, A. J. Page, S. Irle, K. Morokuma, *Chem. Phys. Chem.*, **2012**, *13*, 1479.

[110] H.-B. Li, A. J. Page, S. Irle, K. Morokuma, *J. Am. Chem. Soc.*, **2012**, *134*, 15887.

[111] R. S. Edwards, K. S. Coleman, *Nanoscale*, **2013**, *5*, 38.

[112] M. J. Allen, V. C. Tung, R. B. Kaner, *Chem. Rev.*, **2010**, *110*, 132.

[113] A. Sinitskii, A. Dimiev, D. V. Kosynkin, J. M. Tour, *ACS Nano*, **2010**, *4*, 5405.

[114] L. Zhi, K. Müllen, *J. Mater. Chem.*, **2008**, *18*, 1472.

[115] A. J. Pearson, Y. Zhou, *J. Org. Chem.* **2009**, *74*, 4242.

[116] D. Rodrìguez-Lojo, D. Peña, D. Pérez, E. Guitián, *Org. Biomol. Chem.*, **2010**, *8*, 3386.

[117] A. Criado, D. Peña, A. Cobas, E. Guitián, *Chem. Eur. J.*, **2010**, *16*, 9736.

[118] E. Logakis, C. Pandis, P. Pissis, J. Pionteck, P. Pötschke, *Compos. Sci. Technol.*, **2011**, *71*, 854.

[119] N. Roy, R. Sengupta, A. K. Bhowmick, *Prog. Polym. Sci.*, **2012**, *37*, 781.

[120] R. Simoes, J. Silva, R. Vaia, *J. Nanosci. Nanotechnol.*, **2010**, *10*, 2451.

[121] X. Zeng, X. Xu, P. M. Shenai, E. Kovalev, C. Baudot, N. Mathews, Y. Zhao, *J. Phys. Chem. C*, **2011**, *115*, 21685.

[122 C. Meng, C. Liu, S. Fan, *Adv. Mater.*, **2010**, *22*, 535.

[123] S.-L. Gao, R.-C. Zhuang, J. Zhang, J.-W. Liu, E. Mäder, *Adv. Funct. Mater.*, **2010**, *20*, 1885.

[124] Z. Lin, Y. Liu, Y. Yao, O. J. Hildreth, Z. Li, K. Moon, C.-P. Wong, *J. Phys. Chem. C*, **2011**, *115*, 7120.

[125] K. Bui, H. M. Duong, A. Striolo, D. V. Papavassiliou, *J. Phys. Chem. C*, **2011**, *115*, 3872.

[126] H. Kim, A. A. Abdala, C. W. Macosko, *Macromolecules*, **2010**, *43*, 6515; Q. Song, K.-Z. Li, H.-L. Li, H.-J. Li, C. Ren, *Carbon*, **2012**, *50*, 3943; H.-B. Zhang, W.-G. Zheng, Q. Yan, Z.-G. Jiang, Z.-Z. Yu, *Carbon*, **2012**, *50*, 5117; D. Galpaya, M. Wang, M. Liu, N. Motta, E. Waclawik, C. Yan, *Graphene*, **2012**, *1*, 30.

[127] S. Bose, R. A. Khare, P. Moldenaers, *Polymer*, **2010**, *51*, 975.

[128] M. Rahmat, P. Hubert, *Compos. Sci. Technol.*, **2011**, *72*, 72.

[129] T. P. Selvin, A. G. Salihu, A. A.-J. Abdulhadi, M. Khaled, S. K. De, A. A. Muataz, *Polym. Eng. Sci.*, **2012**, *52*, 525; M. Mu, K. I. Winey, *J. Phys. Chem. C*, **2007**, *111*, 17923; A. E. Daugaard, K. Jankova, J. M. Roman Marín, J. Bøgelund, S. Hvilsted, *Eur. Polym. J.*, **2012**, *48*, 743.

[130] G. V. Dubacheva, C.-K. Liang, D. M. Bassani, *Coord. Chem. Rev.*, **2012**, *256*, 2628.

[131] C. Bounioux, E. A. Katz, R. Yerushalmi-Rozen, *Polym. Adv. Technol.*, **2012**, *23*, 1129.

[132] G. Yu, J. Gao, J. C. Hummelen, F. Wudi, A. J. Heeger, *Science*, **1995**, *270*, 1789; G. Dennler, M. C. Scharber, C. J. Brabec, *Adv. Mater.*, **2009**, *21*, 1323; G. Li, R. Zhu, Y. Yang, *Nature Photon.*, **2012**, *6*, 153.

[133] H. Zhu, J. Wei, K. Wang, D. Wu, *Sol. Energy Mater. Sol. Cells*, **2009**, *93*, 1461.

[134] S. H. Lee, D. H. Lee, W. J. Lee, S. O. Kim, *Adv. Funct. Mater.*, **2011**, *21*, 1338.

[135] E. Kymakis, G. A. J. Amaratunga, *Rev. Adv. Mater. Sci.*, **2005**, *10*, 300.

[136] S. D. Stranks, C. Weisspfennig, P. Parkinson, M. B. Johnston, L. M. Herz, R. J. Nicholas, *Nano Lett.*, **2011**, *11*, 66.

[137] M.-H. Ham, G. L. C. Paulus, C. Y. Lee, C. Song, K. Kalantar-Zadeh, W. Choi, J.-H. Han, M. S. Strano, *ACS Nano*, **2010**, *4*, 6251.

[138] E. Kymakis, P. Servati, P. Tzanetakis, E. Koudoumas, N. Kornilios, I. Rompogiannakis, Y. Franghiadakis, G. A. J. Amaratunga, *Nanotechnology*, **2007**, *18*, 435702.

[139] R. M. Jain, R. Howden, K. Tvrdy, S. Shimizu, A. J. Hilmer, T. P. McNicholas, K. K. Gleason, M. S. Strano, *Adv. Mater.*, **2012**, *24*, 4436.

[140] T. Winzer, A. Knorr, E. Malic, *Nano Lett.*, **2010**, *10*, 4839.

[141] D. Jariwala, V. K. Sangwan, L. J. Lauhon, T. J. Marks, M. C. Hersam, *Chem. Soc. Rev.*,

2012, *42*, 2824.

[142] A. Iwan, A. Chuchmała, *Prog. Polym. Sci.*, **2012**, *37*, 1805.

[143] G. H. Jun, S. H. Jin, S. H. Park, S. Jeon, S. H. Hong, *Carbon*, **2012**, *50*, 40.

[144] S. Cataldo, P. Salice, E. Menna, B. Pignataro, *Energy Environ. Sci.*, **2012**, *5*, 5919.

[145] L. Wei, Y. Lei, H. Fu, J. Yao, *ACS Appl. Mater. Interfaces*, **2012**, *4*, 1594; E. Morales-Narváez, A. Merkoçi, *Adv. Mater.*, **2012**, *24*, 3298; J. Qian, D. Wang, F.-H. Cai, W. Xi, L. Peng, Z.-F. Zhu, H. He, M.-L. Hu, S. He, *Angew. Chem. Int. Ed.*, **2012**, *51*, 10570; L. Feng, Z. Liu, *Nanomedicine*, **2011**, *6*, 317; A. De La Zerda, C. Zavaleta, S. Keren, S. Vaithilingam, S. Bodapati, Z. Liu, J. Levi, B. R. Smith, T.-J. Ma, O. Oralkan, Z. Cheng, X. Chen, H. Dai, B. T. Khuri-Yaku, S. S. Gambhir, *Nat. Nanotech.*, **2008**, *3*, 557; D. A. Heller, H. Jin, B. M. Martinez, D. Patel, B. M. Miller, T.-K. Yeung, P. V. Jena, C. Hörbartner, T. Ha, S. K. Silverman, M. S. Strano, *Nat. Nanotech.*, **2009**, *4*, 114.

[146] G. P. Kotchey, S. A. Hasan, A. Kapralov, S. H. Ha, K. Kim, A. A. Shvedova, V. E. Kagan, A. Star, *Acc. Chem. Res.*, **2012**, *10*, 1770.

[147] A. Bianco, K. Kostarelos, M. Prato, *Chem. Commun.*, **2011**, *47*, 10182.

[148] S. Bhattacharya, D. Roxbury, X. Gong, D. Mukhopadhyay, A. Jagota, *Nano Lett.*, **2012**, *12*, 1826; Q. Mu, G. Su, L. Li, B. O. Gilbertson, L. H. Yu, Q. Zhang, Y.-P. Sun, B. Yan, *ACS Appl. Mater. Interfaces*, **2012**, *4*, 2259.

[149] C. Fabbro, H. Ali-Boucetta, T. Da Ros, K. Kostarelos, A. Bianco, M. Prato, *Chem. Commun.*, **2012**, *48*, 3911; K. Yang, Y. Li, X. Tan, R. Peng, Z. Liu, *Small*, DOI: 10.1002/smll.201201417; X. Yang, G. Niu, X. Cao, Y. Wen, R. Xiang, H. Duana, Y. Chen, *J. Mater. Chem.*, **2012**, *22*, 6649.

[150] a) X. Lu, F. Tian, N. Wang, Q. Zhang, *Org. Letters*, **2002**, *24*, 4313; b) C.-M. Chang, Y.-L. Liu, *Carbon*, **2009**, *47*, 3041; c) F. Mercuri, A. Sgamellotti, *Phys. Chem. Chem. Phys.*, **2009**, *11*, 563; d) M. R. McPhail, J. A. Sells, Z. He, C. C. Chusuei, *J. Phys. Chem. C*, **2009**, *113*, 14102; e) M. C. Paiva, W. Xu, M. F. Proença, R. M. Novais, E. Lægsgaard, F. Besenbacher, *Nano Lett.*, **2010**, *10*, 1764.

[151] M. Sola, J. Mestres, J. Marti, M. Duran, *Chem. Phys. Lett.*, **1994**, *231*, 325.

[152] A. Chikama, H. Fueno, H. Fujimoto, *J. Phys. Chem.*, **1995**, *99*, 8541.

[153] J. B. Briggs, G. P. Miller, *C. R. Chimie*, **2006**, *9*, 916.

[154] a) J. A. Schleuter, J. M. Seaman, S. Taha, H. Cohen, K. R. Lykke, H. H. Wang, J. M. Williams, *J. Chem. Soc.*, *Chem. Commun.*, **1993**, 972; b) K. Komatsu, Y. Murata, N. Sugita,

K. Takeuchi, T. S. M. Wan, *Tetrahedron Lett.*, **1993**, *34*, 8473; c) P. de la Cruz, A. de la Hoz, F. Langa, B. Illescas, N. Martín, *Tetrahedron*, **1997**, *53*, 2599.

[155] M. Tsuda, T. Ishida, T. Nogami, S. Kurono, M. Ohashi, *J. Chem. Soc., Chem. Commun.*, **1993**, 1296

[156] a) Y. Murata, N. Kato, K. Fujiwara, K. Komatsu, *J. Org. Chem.*, **1999**, *64*, 3483; b) G.-W. Wang, Z.-X. Chen, Y. Murata and K. Komatsu, *Tetrahedron*, **2005**, *61*, 4851.

[157] K. Mikami, S. Matsumoto, T. Tonoi, Y. Okubo, *Tetrahedron Lett.*, **1998**, *39*, 3733.

[158] B. Kräutler, T. Müller, J. Maynollo, K. Gruber, C. Kratky, P. Ochsenbein, D. Schwarzenbach, H. Bürgi, *Angew. Chem. Int. Ed. Engl.*, **1996**, *35*,1204.

[159] T. Tago, T. Minowa, Y. Okada, J. Nishimura, *Tetrahedron Lett.*, **1993**, *34*, 8461.

[160] A. Herrera, R. B. Alvarez, N. Martin, M. Chioua, R. Chioua, D. Molero, A. Sanchez-Vasquez, J. Almy, *Tetrahedron*, **2009**, *65*, 5817.

[161] Y. Rubin, S. Khan, D. I. Freedberg, C. Yeretzian, *J. Am. Chem. Soc.*, **1993**, *115*, 344.

[162] R. N. Warrener, R. A. Russel, I. G. Pitt, *J. Chem. Soc., Chem. Commun.*, **1984**, 1675.

[163] W. Bidell, R. E. Douthwaite, M. L. H. Green, A. H. H. Stephens, J. F. C. Turner, *J. Chem. Soc., Chem. Commun.*, **1994**, 1641.

[164] R. F. Enes, A. C. Tome, J. A. S. Cavaleiro, *Tetrahedron*, **2005**, *61*, 1423.

[165] B. Illescas, N. Martin, C. Seoane, P. de la Cruz, F. Langa, F. Wudl, *Tetrahedron Lett.*, **1995**, *36*, 8307.

[166] M. Ohno, S. Kojima, Y. Shirakawa, S. Eguchi, *Tetrahedron Lett.*, **1995**, *36*, 6899.

[167] H. T. Yang, G. W. Wang, Y. Xu, J. C. Huang, *Tetrahedron Lett.*, **2006**, *47*, 4129.

[168] H. Ishida, H. Asaji, T. Hida, K. Itoh, M. Ohno, *Tetrahedron Lett.*, **2000**, 2153.

[169] M. Ohno, T. Azuma, S. Kojima, Y. Shirakawa, S. Eguchi, *Tetrahedron*, **1996**, *52*, 4983.

[170] B. Kräutler, M. Puchberger, *Helv. Chim. Acta.*, **1993**, *76*, 1626.

[171] B. Kräutler, J. Maynollo, *Tetrahedron*, **1996**, *52*, 5033.

[172] M. Ohno, S. Kojima, S. Eguchi, *J. Chem. Soc., Chem. Commun.*, **1995**, 565.

[173] J. Sauer, R. Sustmann, *Angew. Chem. Int. Ed. Engl.*, **1980**, *19*, 779.

[174] B. S. Jursic, *Can. J. Chem.*, **1996**, *74*, 114.

[175] A. Puplovskis, J. Kacens, O. Neilands, *Tetrahedron Lett.*, **1997**, *38*, 285.

[176] T. C. Dinadayalane, R. Vijaya, A. Smitha, G. N. Sastry, *J. Phys. Chem. A*, **2002**, *106*, 1627.

[177] B. Nie, V. Rotello, *J. Phys. Chem. Sol.*, **1997**, *58*, 1897.

[178] A. Tovar, U. Pena, G. Hernandez, R. Portillo, R. Gutierrez, *Synthesis*, **2007**, *1*, 22.

[179] a) D. Ray, C. Belin, F. Hui, B. Fabre, P. Hapiot, D. M. Bassani, *Chem. Commun.*, **2011**, *47*, 2547; b) B. Fabre, D. M. Bassani, C.-K. Liang, D. Ray, F. Hui, P. Hapiot, *J. Phys. Chem. C*, **2011**, *115*, 14786.

[180] Y. He, C. Chen, E. Richard, L. Dou, Y. Wu, G. Li, Y. Yang, *J. Mater. Chem.*, **2012**, *22*, 13391.

[181] J.-I. Aihara, *J. Phys. Chem.*, **1994**, *98*, 9773.

[182] J. Li, G. Jia, Y. Zhang, *Chem. Eur. J.*, **2007**, *13*, 6430.

[183] Z. Chen, W. Thiel, A. Hirsch, *Chem. Phys. Chem.*, **2003**, *1*, 93; Z. Chen, S. Nagase, A. Hirsch, R. C. Haddon, W. Thiel, P. von Ragu Schleyer, *Angew. Chem.*, **2004**, *116*, 1578; S. Osuna, K. N. Houk, *Chem. Eur. J.*, **2009**, *15*, 13219.

[184] F. Mercuri, A. Sgamellotti, *Phys. Chem. Chem. Phys.*, **2009**, *11*, 563.

[185] X. Lu, F. Tian, N. Wang, Q. Zhang, *Org. Lett.*, **2002**, *24*, 4313.

[186] L. Zhang, J. Yang, C. L. Edwards, L. B. Alemany, V. N. Khabashesku, A. R. Barron, *Chem. Commun.*, **2005**, 3265.

[187] J. L. Delgado, P. de la Cruz, F. Langa, A. Urbina, J. Casado, J. T. López Navarrete, *Chem. Commun.*, **2004**, 1734.

[188] G. Sakellariou, H. Ji, J. W. Mays, D. Baskaran, *Chem. Mater.*, **2008**, *20*, 6217.

[189] G. Sakellariou, H. Ji, J. W. Mays, D. Baskaran, *Chem. Mater.*, **2008**, *20*, 6217.

[190] C. Ménard-Moyon, F. Dumas, E. Doris, C. Mioskowski, *J. Am. Chem. Soc.*, **2006**, *128*, 14764.

[191] A. Gergely, J. Telegdi, E. Mészáros, Z. Pászti, G. Tárkányi, F. H. Kármán, E. Kálmán, *J. Nanosci. Nanotechnol.*, **2007**, *7*, 2795.

[192] C.-M. Chang, Y.-L. Liu, *Carbon*, **2009**, *47*, 3041.

[193] S. Munirasu, J. Albuerne, A. Boschetti-de-Fierro, V. Abetz, *Macromol. Rapid Commun.*, **2010**, *31*, 574.

[194] Y. Nakamura, N.Takano, T. Nishimura, E. Yashima, M. Sato, T. Kudo, J. Nishimura, *Org. Lett.*, **2001**, *3*, 1193.

[195] H. Pellissier, M. Santelli, *Tetrahedron*, **2003**, *59*, 701.

[196] A. Criado, M. J. Gómez-Escalonilla, J. L. G. Fierro, A. Urbina, D. Peña, E. Guitián, F. Langa, *Chem. Commun.*, **2010**, *46*, 7028.

[197] S. Sarkar, E. Bekyarova, S. Niyogi, R. Haddon, *J. Am. Chem. Soc.*, **2011**, *133*, 3324.

[198] X. Zhong, J. Jin, S. Li, Z. Niu, W. Hu, R. Li, J. Ma, *Chem. Commun.*, **2010**, *46*, 7340.

[199] G. Sakellariou, D. Priftisa, D. Baskaran, *Chem. Soc. Rev.*, **2013**, *42*, 677.

[200] J.-T. Sun, L.-Y. Zhao, C.-Y. Hong, C.-Y. Pan, *Chem.Commun.*, **2011**, *47*, 10704.

[201] G. Sakellariou, H. Ji, J. W. Mays, D. Baskaran, *Chem. Mater.*, **2008**, *20*, 6217.

[202] D. Priftis, G. Sakellariou, D. Baskaran, J. W. Mays, N. Hadjichristidis, *Soft Matter*, **2009**, *5*, 4272.

[203] D. Priftis, N. Petzetakis, G. Sakellariou, M. Pitsikalis, D. Baskaran, J. W. Mays, N. Hadjichristidis, *Macromolecules*, **2009**, *42*, 3340.

[204] M. M. Bernal, M. Liras, R. Verdejo, M. A. López-Manchado, I. Quijada-Garrido, R. París, *Polymer*, **2011**, *52*, 5739.

[205] A. J. Inglis, S. Sinnwell, M. H. Stenzel, C. Barner-Kowollik, *Angew. Chem. Int. Ed.*, **2009**, *48*, 2411.

[206] L. Nebhani, C. Barner-Kowollik, *Macromol. Rapid Commun.*, **2010**, *31*, 1298.

[207] J. Yuan, G. Chen, W. Weng, Y. Xu, *J. Mater. Chem.*, **2012**, *22*, 7929.

[208] M. C. Iovu, M. Jeffries-El, E. E. Sheina, J. R. Cooper, R. D. McCollough, *Polymer*, **2005**, *46*, 8582.

[209] A. H. Müller, K. Matyjaszewski, *Controlled and living polymerizations: methods and materials, from mechanisms to applications*, Wiley-VCH Verlag, **2009**.

[210] M. Buback, R. G. Gilbert, R. A. Hutchinsin, B. Klumperman, F.-D. Kuchtam B. G. Manders, K. F. O'Driscoll, G. T. Russel, J. Schweer, *Macromol. Chem. Phys.*, **1995**, *196*, 3267.

[211] K. Matyjaszewski, T. P. Davis, *Handbook of Radical Polymerization*, K. Matyjaszewski, T. P. Davis Eds., Wiley and Sons, Inc., **2002**.

[212] K. Matyjaszewski, J. Xia, *Chem. Rev.*, **2001**, *101*, 2921.

[213] M. Matyjaszewski, A. K. Nanda, W. Tang, *Macromolecules*, **2005**, *38*, 2015.

[214] V. Percec, T. Guliashvili, J. S. Ladislaw, A. Wistrand, A. Stjerndahl, M. J. Sienkowska, M. J. Monteiro, S. Sahoo, *J. Am. Chem. Soc.*, **2006**, *128*, 14156.

[215] W. A. Braunecker, K. Matyjaszewski, *Prog. Polym. Sci.*, **2007**, *32*, 93.

[216] W. Jakubowski, K. Matyjaszewski, *Macromolecules*, **2005**, *38*, 4139.

[217] Y. Kwak, A. J. D. Magenau, K. Matyjaszewski, *Macromolecules*, **2010**, *44*, 811.

[218] R. Nicolaÿ, Y. Kwak, *Isr. J. Chem.*, **2012**, *52*, 288.

[219] C. Barner-Kowollik, *Handbook of RAFT Polymerization*, C. Barner-Kowollik Ed.,

Wiley-VCH, Weinheim, **2008**, 423.

[220] C. Barner-Kowollik, M. Buback, B. Charleux, M. L. Coote, M. Drache, T. Fukuda, A. Goto, B. Klumperman, A. B. Lowe, J. B. McLeary, G. Moad, M. J. Monteiro, R. D. Sanderson, M. P. Tonge, P. Vana, *J. Polym. Sci. A*, **2006**, *44*, 5809.

[221] A. Feldermann, M. L. Coote, M. H. Stenzel, T. P. Davis, C. Barner-Kowollik, *J. Am. Chem. Soc.*, **2004**, *126*, 15915.

[222] A. Theis, T. P. Davis, M. H. Stenzel, C. Barner-Kowollik, *Polymer*, **2006**, *47*, 999.

[223] M. A. Harvison, P. J. Roth, T. P. Davis, A. B. Lowe, *Austr. J. Chem.*, **2011**, *64*, 992.

[224] H. Willcock, R. K. O'Reilly, *Polym.Chem.*, **2010**, *1*, 149.

[225] D. L. Patton, M. Mullings, T. Fulghum, R. C. Advincula, *Macromolecules*, **2005**, *38*, 8597.

[226] D. B. Thomas, A. J. Convertine, R. D. Hester, A. B. Lowe, C. L. McCormick, *Macromolecules*, **2004**, *37*, 1735.

[227] A. Postma, T. P. Davis, G. Li, G. Moad, M. S. O'Shea, *Macromolecules*, **2006**, *39*, 5307.

[228] A. Postma, T. P. Davis, R. A. Evans, G. Li, G. Moad, M. S. O'Shea, *Macromolecules*, **2006**, *39*, 5293.

[229] G. Moad, E. Rizzardo, S. H. Thang, *Polym. Int.*, **2011**, *60*, 9.

[230] C. Schmid, J. Falkenhagen, C. Barner-Kowollik, *J. Polym. Sci. A Polym. Chem.*, **2011**, *49*, 1.

[231] M. Dietrich, M. Glassner, T. Gruendling, C. Schmid, J. Falkenhagen, C. Barner-Kowollik, *Polym. Chem.*, **2010**, *1*, 634.

[232] C. L. McCornick, A. B. Lowe, *Acc. Chem. Res.*, **2004**, *37*, 312.

[233] C. Li, B. C. Benicewicz, *Macromolecules*, **2005**, *38*, 5929.

[234] Y. Zaho, S. Perrier, *Macromolecules*, **2006**, *39*, 8603.

[235] A. Kiriy, V. Senkovskyy, M. Sommer, *Macrol. Rapid Commun.*, **2011**, *32*, 1503.

[236] K. Tamao, K. Sumitani, M. Kumada, *J. Am. Chem. Soc.*, **1972**, *94*, 4374.

[237] R. S. Loewe, P. C. Ewbank, J. Liu, L. Zhai, R. D. McCullough, *Macromolecules*, **2001**, *34*, 4324.

[238] I. Osaka, R. D. McCollough, *Accounts of chemical research.*, **2008**, *9*, 1202.

[239] M. Jeffries-El, G. Sauvé, R. D. McCullough, *Adv. Mater.*, **2004**, *16*, 1017.

[240] M. C. Stefan, A. E. Javier, I. Osaka, R. D. McCollough, *Macromolecules*, **2009**, *42*, 30.

[241] S. Wu, Y. Sun, L. Huang, J: Wang, Y. Zhou, Y. Geng, F. Wang, *Macromolecules*, **2010**, *43*, 4438.

[242] M. Yuan, K. Okamoto, H. A. Bronstein, C. K. Luscombe, *ACS macro Lett.*, **2012**, *1*, 392.

[243] Z.-Q. Wu, R. J. Ono, Z. Chen, C. W. Bielawski, *J. Am. Chem. Soc.*, **2010**, *132*, 14000.

[244] R. J. Ono, S. Kang, C. W. Bielawski, *Macromolecules*, **2012**, *45*, 2321.

[245] M. C. Stefan, M. P. Bhatt, P. Sista, H. D. Magurudeniya, *Polym. Chem.*, **2012**, *3*, 1693; M. C. Iovu, C. R. Craley, M. Jeffries-El, A. B. Krankowski, R. Zhang, T. Kowalewski, R. D. McCullough, *Macromolecules*, **2007**, *14*, 4733; A. Britze, V. Möllmann, G. Grundmeier, H. Luftmann, D. Kückling, *Macromol. Chem. Phys.*, **2011**, *212*, 679; M. G. Alemseghed, S. Gowrisanker, J. Servello, M. C. Stefan, *Macromol. Chem. Phys.*, **2009**, *210*, 2007.

[246] C. Enders, S. Tanner, W. H. Binder, *Macromolecules*, **2010**, *43*, 8436.

[247] B. Trathnigg, *Size-exclusion Chromatography*, Encyclopedia of Analytical Chemistry, R. A. Meyers Ed., John Wiley Sons Ltd, Chichester, **2000**.

[248] Y. Guillaneuf, P. Castignolles, *J. Polym. Sci. A Polym Chem.*, **2007**, *46*, 897.

[249] Z. Grubisic, P. Rempp, H. J. Benoit, *J. Polym. Sci. B Polym. Lett.*, **1967**, *5*, 753.

[250] M. Stickler, D. Panke, W. Wunderlich, *Die Makromolekulare Chemie - Macromolecular Chemistry and Physics*, **1987**, *188*, 2651.

[251] C. Strazielle, H. Benoit, O. Vogl, *Eur. Polym. J.*, **1978**, *14*, 331.

[252] J. B. Fenn, M. Mann, C. K. Meng, S. F. Wong, C. M. Whitehouse, *Mass Spectrom. Rev.*, **1990**, *9*, 37.

[253] R. E. March, *Int. J. Mass Spectrom.*, **2000**, *200*, 285.

[254] K. Tanaka, H. Waki, Y. Ido, S. Akita, Y. Yoshida, T. Yoshida, T. Matsuo, *Rapid Commun. Mass Sp.*, **1988**, *2*, 151.

[255] N. C. Fenner, N. R. Daly, *Rev. Sci. Instrum.*, **1966**, *37*, 1068.

[256] G. R. Heal, *Principles of thermal analysis and calorimetry*, Chapter 2, Thermogravimetry and derivative thermogravimetry, Ed. Peter Haines, **2002**; D. M. Price, D. J. Hourston, F. Dumont, *Thermogravimetry of polymers*, Encyclopedia of Analytical Chemistry, R. A. Meyers Eds., John Wiley & Sons Ltd, Chichester, **2000**.

[257] R. A. Nadkarni, *A review of modern Instrumental Methods of Elemental Analysis of Petroleum Related Material: Part II – Analytical Techniques, Modern Instrumentaltion methods of elemental analysis of petroleum products and lubricants*, ASTM STP 1109, R. A.

Nadkarni, Ed., Amercian Society for Texting and Materials, Philadelphia, **1991**.

[258] J. F. Watts, *An introduction to Surface Analysis by Electron Spectroscopy*, Oxford University Press, Oxford, **1990**; D. Briggs, M. P. Seah, *Practical Surface Analysis*, Volume 1 – Auger and X-ray Photoelectron Spectroscopy, Second Edition, John Wiley and Sons, Chichester, **1990**.

[259] K. L. Parry, A. G. Shard, R. D. Short, R. G. White, J. D. Whittle, A. Wright, *Surf. Interface Anal.*, **2006**, *38*, 1497.

[260] J. H. Scofield, *J. Electron Spectr. Relat. Phen.*, **1976**, *8*, 129.

[261] S. Tanuma, C. J. Powell, D. R. Penn, *Surf. Interface Anal.*, **1994**, *21*, 165.

[262] R. F. Egerton, *Physical Principles of Electron Microscopy*, An Introduction to TEM, SEM and AEM, Springer, **2005**.

[263] F. Ernst, W. Sigle, *High-Resolution Imaging and Spectrometry of Materials*, F. Ernst, W. Sigle Eds., Springer-Verlag Berlin Heidelberg New York, **2003**.

[264] J. C. H. Spence, *Experimental High Resolution microscopy*, Oxford University Press, New York, **1988**.

[265] T. J. Michael, D. J. David, *Ultraviolet and visible spectroscopy*, 2nd Ed., John Wiley and Sons, Chichester, **1996**.

[266] W. Schärtl, *Light scattering from polymer solutions and nanoparticles dispersions*, Springer, Berlin, **2007**.

[267] R. Xu, *Particle Characterization: Light Scattering Method*s, Particle Technology Series, Kluwer Academic Publishers, **2002**; B. J. Berne, R. Pecora, *Dynamic Light Scattering: With Applications to Chemistry, Biology, and Physics*, Dover Publicationns, Inc., **2000.**

[268] G. de Haseth, *Fourier Transform Infrared Spectroscopy*, John Wiley and Sons, New York, **1986**.

[269] R. L. McCreery, *Raman Spectroscopy for Chemical Analysis*, Wiley Interscience, John Wiley and Sons, Inc., New York, Chichester, Weinheim, Brisbane, Singapore, Toronto, **2000**.

[270] Z. Yu, L. Brus, *J. Phys. Chem. B*, **2001**, *105*, 1123.

[271] K. Kneipp, H. Kneipp, J. Kneipp, *Acc. Chem. Res.*, **2006**, *39*, 443; K. Kneipp, H. Kneipp, M. S. Dresselhaus, S. Lefrant, *Phil. Trans. R. Soc. Lond. A*, **2004**, *362*, 2361.

[272] E. Bailoa, V. Deckert, *Chem. Soc. Rev.*, **2008**, *37*, 921; N. Hayazawa, T. Yano, H. Watanabe, Y. Inouye, S. Kawata, *Chem. Phys. Lett.*, **2003**, *376*, 174; N. Anderson, A. Hartschuh, S. Cronin, L. Novotny, *J. Am. Chem. Soc.*, **2005**, *127*, 2533.

[273] T. Gruendling, S. Weidner, J. Falkenhagen, C. Barner-Kowollik, *Polym. Chem.*, **2010**, *1*, 599; S. M. Advoshenko, I. N. Ioffe, A. A. Kozlov, V. Y. Markov, E. N. Nikolaev, L. N. Sidorov, *Rapid Commun. Mass Spectrom,.* **2008**, *22*, 1372.

[274] A. J. Inglis, T. Paulöhrl, C. Barner-Kowollik, *Macromolecules*, **2010**, *43*, 33.

[275] A. Peigney, C. Laurent, E. Flahaut, R. R. Bacsa, A. Rousset, *Carbon*, **2001**, *39*, 507.

[276] M. S. Dresselhaus, G. Ph. Avouris, *Carbon Nanotubes: Synthesis, Structure, Properties, and Applications*; M. S. Dresselhaus, G. Ph. Avouris, Eds.; Springer Verlag Berlin Heidelberg New York, Topics in Applied Physics, Vol. 80, **2001**.

[277] M. Rubinstein, R. Colby, *Polymer physics*, M. Rubinstein, R. Colby, Eds.; Oxford University Press Inc. **2001**.

[278] I. Retzko, W. E. S. Unger, *Adv. Eng. Mater.*, **2003**, *5*, 519.

[279] M. Pumera, B. Smid, K. Veltruska, *J. Nanosci. Nanotechnol.*, **2009**, *9*, 2671.

[280] C. De Marco, S. M. Eaton, R. Suriano, S. Turri, M. Levo, R. Rampino, G. Cerullo, R. Osellame, *Appl. Mater. Interfaces*, **2010**, *2*, 2377.

[281] L. Hsu, C. Weder, S. J. Rowan, *J. Mater. Chem.*, **2011**, *21*, 2812.

[282] X. Zhang, C. L. Pint, M. H. Lee, B. E. Schubert, A. Jamshidi, K. Takei, H. Ko, A. Gillies, R. Bardhan, J. J. Urban, M. Wu, R. Fearing, A. Javey, *Nano Lett.*, **2011**, *11*, 3239.

[283] H. Kong, W. Li, C. Gao, D. Yan, Y. Jin, D. R. M. Walton, H. W. Kroto, *Macromolecules*, **2004**, *37*, 6683.

[284] F. J. Xu, J. Li, F. Su, X. S. Zhao, E. T. Kang, K. G. Neoh, *J. Nanosci. Nanotechnol.*, **2008**, *8*, 5858.

[285] C.-Y. Hong, Y.-Z. You, C.-Y. Pan, *Chem. Mater.*, **2005**, *17*, 2247.

[286] Y.-Z. You, C.-Y. Hong, C.-Y. Pan, *Adv. Funct. Mater.*, **2007**, *17*, 2470.

[287] G. Xu, W.-T. Wu, Y. Wang, W. Pang, P. Wang, Q. Zhu, F. Lu, *Nanotechnology*, **2006**, *17*, 2458.

[288] G. Xu, W.-T. Wu, Y. Wang, W. Pang, Q. Zhu, P. Wang *Nanotechnology*, **2007**, *18*, 145606.

[289] J. Liu, Z. Nie, Y. Gao, A. Adronov, H. Li, *J. Polym. Sci. A. Polym. Chem.*, **2008**, *46*, 7187.

[290] Y. Li, D. Yan, A. Adronov, Y. Gao, X. Luo, H. Li, *Macromolecules*, **2012**, *45*, 4698.

[291] M. Teodorescu, K. Matyjaszewski, *Macromolecules*, **1999**, *32*, 4826.

[292] K. Matyjaszewski, D. A. Shipp, J.-L. Wang, T. Grimaud, T. E. Patten, *Macromolecules*,

1998, *31*, 6836.

[293] J. T. Rademacher, M. Baum, M. E. Pallack, W. J. Brittain, W. J. Simonsick Jr., *Macromolecules*, **2000**, *33*, 284.

[294] G. Masci, L. Giacomelli, V. Creczenci, *Macrmol. Rapid Comm.*, **2004**, *25*, 559.

[295] Y. Xia, X. Yin, N. A. D. Burke, H. D. H. Stöver, *Macromolecules*, **2005**, *38*, 5937.

[296] A. P. Vogt, B. S. Sumerlin, *Macromolecules*, **2006**, *39*, 5286.

[297] J. T. Lai, D. Filla, R. Shea, *Macromolecules*, **2002**, *35*, 6754.

[298] S. R. Gondi, A. P. Vogt, B. S. Sumerlin, *Macromolecules*, **2007**, *40*, 474.

[299] A. E. Luetdke, J. W. Timberlake, *J. Org. Chem.*, **1985**, *50*, 270.

[300] E. C. Cho, Y. D. Kim, K. Cho, *Polymer*, **2004**, *45*, 3195.

[301] J. Zhang, R. Pelton, *Langmuir*, **1996**, *12*, 2611.

[302] P. Kujawa, F. Segui, S. Shaban, C. Diab, Y. Okada, F. Tanaka, F. M. Winnik, *Macromolecules*, **2006**, *39*, 341.

[303] A. P. Vogt, B. Summerlin, *Macromolecules*, **2008**, *41*, 7368.

[304] A. S. Goldmann, A. Walther, L. Nebhani, R. Joso, D. Ernst, K. Loos, C. Barner-Kowollik, L. Barner, A. H. E. Müller, *Macromolecules*, **2009**, *42*, 3707.

[305] L. Barner, A. S. Quick, A. P. Vogt, V. Winkler, T. Junkers, C. Barner-Kowollik, *Polym. Chem.*, **2012**, *3*, 2266.

[306] C.-Y. Hong, Y.-Z. You, C.-Y. Pan, *Chem. Mater.*, **2005**, *17*, 2247.

[307] Q. Zaib, I. A. Khan, Y. Yoon, J. R. V. Flora, Y.-G. Park, N. B. Saleh, *J. Nanosci. Nanotechnol.*, **2012**, *12*, 3909.

[308] K. C. Etika, F. D. Jochun, M. A. Cox, P. Schattling, P. Theato, J. C. Bruhan, *Macromol. Rapid Commun.*, **2010**, *31*, 1368.

[309] D. Bouchard, W. Zhang, T. Powell, U. Rattanaudompol, *Environ. Sci. Technol.*, **2012**, *46*, 4458.

[310] C. Desai, S. Addo, S. Mitra, *J. Colloid Interface Sci.*, **2012**, *368*, 115.

[311] C. Branca, V. Magazu, A. Mangione, *Diamond Relat. Mater.*, **2005**, *14*, 846.

[312] J. Gigault, I. Le Hécho, S. Dubascoux, M. Potin-Gautier, G. Lespes, *J. Chromatogr. A*, **2010**, *1217*, 7891.

[313] J. Gigault, B. Grassl, G. Lespes, *Analyst*, **2012**, *137*, 917.

[314] J. Nelson, *Current Opinion in Solid State and Materials Science*, **2002**, *6*, 87; A. Pivrikas, N. S. Sariciftci, G. Juska, R. Osterbacka, *Prog. Photovoltaics*, **2007**, *15*, 677; J. A.

Turner, *Science*, **1999**, *285*, 687; G. M. Whitesides, G. W. Crabtree, *Science*, **2007**, *315*, 796; P. Szuromi, B. Jasny, D. Clery, J. Austin, B. Hanson, *Science*, **2007**, *315*, 781; N. Lewis, *Science*, **2007**, *315*, 798; A. Shah, *Science*, **1999**, *285*, 692.

[315] V. Sgobba, D. M. Guldi, *Chem. Soc. Rev.*, **2009**, *38*, 165.

[316] D. E. Carlson, C. R. Wronski, *Appl. Phys. Lett.*, **1976**, *28*, 671; N. Naghavi, S. Spiering, M. Powalla, B. Cavana, D. Lincot, *Prog. Photovoltaics*, **2003**, *11*, 437; B. O'Regan, M. Grätzel, *Nature*, **1991**, *353*, 737; W. Huynh, J. Dittmer, A. P. Alivisatos, *Science*, **2002**, *295*, 2425.

[317] J. Holt, S. Singh, T. Drori, Y. Zhang, Z. V. Vardeny, *Phy. Rev. B*, **2009**, *79*, 195.

[318] D. Yu, Y. Yang, M. Durstock, J.-B. Baek, L. Dai, *ACS Nano*, **2010**, *4*, 5633; G. Araújo, C. Arantes, L. S. Roman, A. J. G. Zarbin, M. L. M. Rocco, *Surf. Sci.*, **2009**, *603*, 647.

[319] Y. Liang, Z. Xu, J. Xia, S.-T. Tsai, Y. Wu, G. Li, C. Ray, L. Yu, *Adv. Energy Mater.*, **2010**, *22*, E135.

[320] R. Radbeh, E. Parbaile, M. Chakaroun, B. Ratier, M. Aldissi, A. Moliton, *Polym. Int.*, **2010**, *59*, 1514.

[321] Y. Kanai, J. C. Grossman, *Nano Lett.*, **2008**, *8*, 908; S. D. Stranks, C. Weisspfennig, P. Parkinson, M. B. Johnston, L. M. Herz, R. J. Nicholas, *Nano Lett.*, **2011**, *11*, 66; S. Ren, M. Bernardi, R. R. Lunt, V. Bulovic, J. C. Grossman, S. Gradečak, *Nano Lett.*, **2011**, *11*, 5316.

[322] R. J. Chen, Y. Zhang, D. Wang, H. Dai, *J. Am. Chem. Soc.*, **2001**, *123*, 3838.

[323] B. K. Kuila, K. Park, L. Dai, *Macromolecules*, **2010**, *16*, 6699.

[324] N. A. Kumar, S. H. Kim, B. G. Cho, K. T. Lim, Y. T. Jeong, *Colloid Polym. Sci.*, **2009**, *287*, 97.

[325] F. Boon, S. Desbief, L. Cutaia, O. Douhéret, A. Minoia, B. Ruelle, S. Clément, O. Coulembier, J. Cornil, P. Dubois, R. Lazzaroni, *Macromol. Rapid Commun.*, **2010**, *31*, 1427.

[326] L. Niu, P. Li, Y. Chen, J. Wang, J. Zhang, B. Zhang, W. J. Blau, *J. Poly. Sci. Part A: Poly. Chem.*, **2011**, *49*, 101

[327] V. Sadhu, N. A. Nismy, A. A. D. T. Adikaari, S. J. Henley, M. Shkunov, S. R. P. Silva, *Nanotechnology*, **2011**, *22*, 265607.

[328] A. Phuong, T.-M. Huang, P.-T. Chen, A. C.-M. Yang, *J. Poly. Sci. Part B: Poly. Phys.*, **2011**, *49*, 581.

[329] M. Jeffries-El, G. Sauvé, R. D. McCullough, *Macromolecules*, **2005**, *38*, 10346.

[330] M. Giulianini, E. R. Waclawik, J. M. Bell, M. De Crescenzi, P. Castrucci, M. Scarselli,

N. Motta1, *Appl. Phys. Lett.*, **2009**, *95*, 013304.

[331] M. Bernardi, M. Giulianini, J. C. Grossman, *ACS Nano*, **2010**, *4*, 6599.

[332] C. Caddeo, C. Melis, L. Colombo, A. Mattoni, *J. Phys. Chem. C*, **2010**, *114*, 21109.

[333] T. Matrab, M. M. Chehimi, J. Pinson, S. Slomkowski, T. Basinska, *Surf. Interface Anal.*, **2006**, *38*, 565.

[334] S. Yuan, D. Wan, B. Liang, S. O. Pehkonen, Y. P. Ting, K. G. Neoh, E. T. Kang, *Langmuir*, **2011**, *27*, 2761.

[335] Y. Joseph, I. Besnard, M. Rosenberger, B. Guse, H.-G. Nothofer, J. M. Wessels, U. Wild, A. Knop-Gericke, D. Su, R. Schloegl, A. Yasuda, T. Vossmeyer, *J. Phys. Chem. B*, **2003**, *107*, 7406.

[336] E. H. Lock, D. Y. Petrovykh, P. Mack, T. Carney, R. G. White, S. G. Walton R. F. Fernsler, *Langmuir*, **2010**, *26*, 8857.

[337] M. Bruns, U. Geckle, V. Trouillet, M. Rudolphi, H. Baumann, *J. Vac. Sci. Technol. A*, **2005**, *23*, 1114.

[338] a) S. A. Al-Bataineh, L. G. Britcher, H. J. Griesser, *Surf. Sci.*, **2006**, *600*, 952; b) S. A. Al-Bataineh, L. G. Britcher, H. Griesser, *Surf. Interface Anal.*, **2006**, *38*, 1512.

[339] K. M. Wiggins, J. A. Syrett, D. M. Haddleton, C. W. Bielawski, *J. Am. Chem. Soc.*, **2011**, *133*, 7180.

[340] C. M. Homenick, U. Sivasubramaniam, A. Adronov, *Polym. Int.*, **2008**, *57*, 1007.

[341] R. C. Chadwick, U. Khan, J. N. Coleman, A. Adronov, *Small*, **2013**, *5*, 552.

[342] H. Hu, B. Zhao, M. E. Itkis, R. C. Haddon, *J. Phys. Chem.*, **2003**, *107*, 13838.

[343] C.-H. Andersson, H. Grennberg, *Eur. J. Org. Chem.*, **2009**, 4421.

[344] G.-W. Lee, S. Kumar, *J. Phys. Chem. B*, **2005**, *109*, 17128.

[345] G.-W. Lee, S. Jagannathan, H. G. Chae, M. L. Minus, S. Kumar, *Polymer*, **2008**, *49*, 1831.

[346] M. W. Marshall, S. Popa-Nita, J. G. Shapter, *Carbon*, **2006**, *44*, 1137.

[347] Z. Špitalsky, C. A. Krontiras, S. N. Georga, C. Galiotis, *Compos. Part A-Appl. S.*, **2009**, *40*, 778.

[348] I. Abrunhosa, M. Gulea, S. Masson, *Synthesis*, **2004**, *6*, 0928.

[349] Leena Nebhani, *Doctor of Science*, Karlsruhe Institute for Technology (Karlsruhe, Germany), July, **2010**.

[350] S. Vassiliou, M. Xeilari, A. Yiotakis, J. Grembecka, M. Pawełczak, P. Kafarski, A.

Mucha, *Bioorg. Med. Chem.*, **2007**, *15*, 3187.

[351] M. S. Dresselhaus, G. Dresselhaus, R. Saito, A. Jorio, *Phys. Rep.*, **2005**, *409*, 47.

[352] J. Kastner, T. Pichler, H. Kuzmany, S. Curran, W. Blau, D.N. Weldon, M. Delamesiere, S. Draper, H. Zandbergen, *Chem. Phys. Lett.*, **1994**, *221*, 53.

[353] U. Kim, X. Liu, C. Furtado, G. Chen, R. Saito, J. Jiang, M. Dresselhaus, P. C. Eklund. *Phys. Rev. Lett.*, **2005**, *95*, 157402.

[354] S. Lefrant, M. Baibarac, I. Baltog, *J. Mater. Chem.*, **2009**, *19*, 5690.

[355] a) H. Estrade-Schwarckopf, *Carbon*, **2004**, *42*, 1713; b) S. Maldonado, S. Morin, K. J. Stevenson, *Carbon*, **2006**, *44*, 1429; c) T. I. T. Okpalugo, P. Papakonstantinou, H. Murphy, J. McLaughlin, N. M. D. Brown, *Carbon*, **2005**, *43*, 153.

[356] W. H. Lee, S. J. Kim, W. J. Lee, J. G. Lee, R. C. Haddon, P. J. Reucroft, *Appl. Surf. Sci.*, **2001**, *181*, 121.

[357] M. T. Martínez, M. A. Callejas, A. M. Benito, M. Cochet, T. Seeger, A. Anson, J. Schreiber, C. Gordon, C. Marhic, O. Chauvet, J. L. G. Fierro, W. K. Maser, *Carbon*, **2003**, *41*, 2247.

[358] a) L.-P. Wang, Y.-P. Wang, K. Yuan, Z.-Q. Lei, *Polymer. Adv. Techn.* **2008**, *19*, 285; b) N. Gurbuz, S. Demirci, S. Yavuz, T. Caykara, *J. Polym. Sci. Pol. Chem.*, **2011**, *49*, 423.

[359] a) R. I. Kvon, G. N. Il'inich, A. L. Chuvilin, V. A. Likholobov, *J. Mol. Catal. A- Chem.*, **2000**, *158*, 413; b) X. M. Zeng, C. M. Chan, L. T. Weng, L. Li, *Polymer*, **2000**, *41*, 8321.

List of abbreviations

3HT	3-hexylthiophene
a_{C-C}	Distance between 2 sp^2 hybridized carbon atoms in a graphene sheet
ATRP	Atom Transfer Radical Polymerization
CNTs	Carbon Nanotubes
CLRP	Controlled/living radical polymerization
Cp	Cyclopentadienyl
DA	Diels-Alder
e.g.	*exempli gratia*
GRIM	Grignard Metathesis
HDA	hetero Diels-Alder
i.e.	*id est*
KCTP	Kumada Catalyst Transfer Polymerization
MMA	(methyl)methacrylate
MWCNTs	Multi-Walled Carbon Nanotubes
NIPAM	*N*-isopropylacrylamide
P3HT	poly(3-hexylthiophene)
PMMA	poly(methyl)methacrylate
PNIPAM	poly(*N*-isopropylacrylamide)
RAFT	Reversible Addition Fragmentation chain Transfer
rDA	retro-Diels-Alder
SWCNTs	Single-Walled Carbon Nanotubes

Curriculum Vitæ

Date of birth	06.08.1982
Place of birth	Thiais
Nationality	French

Education

Since 01.2010	**Doctoral studies in Chemistry** at the Karlsruhe Institute of Technology (KIT), Karlsruhe, Germany, under the supervision of Prof. C. Barner-Kowollik in cooperation with the Fraunhofer Institute for Chemical Technology (ICT), Pfinztal, Germany
09.2002-09.2005	**Engineering Diploma** at the National Graduate School of Chemistry and Physics of Bordeaux (ENSCPB), Bordeaux, France, with emphasis on polymers science
09.2002-06.2002	**Undergraduate Cycle** in Lycée Gay-Lussac, Limoges, France, for physics, chemistry and mathematics for French Engineer School competitive examination
06.2000	**Scientific general certificate of education** with honours, Limoges, France

Employment history

since 01.2010	**Scientific co-worker** in the group of Prof. C. Barner-Kowollik at the Karlsruhe Institute of Technology (KIT), Karlsruhe, Germany
since 10.2005	**Scientific co-worker** at the Fraunhofer Institute for Chemical Technology (ICT), Pfinztal, Germany
05.2005-10.2005	**Research training** in Fraunhofer Institute for Chemical Technology (ICT), Pfinztal, Germany, for the development of photocatalytic coatings
07.2004-12.2004	**Engineer training** in ZENTARIS GmbH, Frankfurt-am-Main, Germany, for the development of a HPLC method
07-08.2003	**Worker training** in FERRO COULEUR FRANCE S.A., Limoges, France, for the production of enamel for ceramics

List of publications and

Conference contributions

Refereed Journal Publications (presenter underlined)

[7] *Conducting Polymer/SWCNTs Modular Hybrid Materials via Diels-Alder Ligation*

B. Yameen, N. Zydziak, S. M. Weidner, M. Bruns, C. Barner-Kowollik, *Macromolecules*, **2013**, *46*, 2606.

[6] *Diels-Alder Reactions for Carbon Materials Synthesis and Surface Functionalization*

N. Zydziak, B. Yameen, C. Barner-Kowollik, *Polym. Chem.*, **2013**, doi: 10.1039/c3py00232b.

[5] *Hetero Diels-Alder Chemistry for the Functionalization of Single-Walled Carbon Nanotubes with Cyclopentadienyl End-Capped Polymer Strands*

N. Zydziak, C. M. Preuss, V. Winkler, C. Hübner, C. Barner-Kowollik, *Macromol. Rapid Commun.*, **2013**, *34*, 672.

[4] *Modular Ambient Temperature Functionalization of Carbon Nanotubes with Stimuli-Responsive Polymer Strands*

N. Zydziak, C. Hübner, M. Bruns, A. P. Vogt, C. Barner-Kowollik, **2013**, *4*, 1525.

[3] *One-step Functionalization of Single-Walled Carbon Nanotubes (SWCNTs) with Cyclopentadienyl Capped Macromolecules via Diels-Alder Chemistry*

N. Zydziak, C. Hübner, M. Bruns, C. Barner-Kowollik, **2011**, *44*, 3374.

[2] *Pyrolysis of Wood-Based Polymer Compounds*

T. Haensel, A. Comouth, N. Zydziak, E. Bosch, A. Kaufmann, J. Pfitzer, S. Krischok, J. A. Schaefer, S. I.-U. Ahmed, *J. Anal. Appl. Pyrolysis*, **2010**, *87*, 124.

[1] *Pyrolysis of Cellulose and Lignin*

T. Haensel, A. Comouth, P. Lorenz, S. I.-U. Ahmed, S. Krischok, N. Zydziak, A. Kauffmann, J. A. Schaefer, *Appl. Surf. Sci.*, **2009**, *255*, 8183.

Conference contributions

[4] *Cyclopentadienyl End-Capped Polymers for a One-Step Functionalization of Carbon Nanotubes* (Poster Presentation)

<u>N. Zydziak</u>, C. Hübner, M. Bruns, C. Barner-Kowollik, **Polymer Conference**, Warwick, UK, July **2012**.

[3] *Pericyclic Reactions for High Resolution (Bio)Surface Design* (invited talk)

<u>C. Barner-Kowollik</u>, T. Paulöhrl, G. Delaittre, M. Kaupp, T. Tischer, A. S. Goldmann, N. Zydziak, **Polymer Conference**, Warwick, UK, July **2012**.

[2] *Designing Polymer Hybrid Materials via Modular Synthetic Strategies* (invited talk)

<u>C. Barner-Kowollik</u>, G. Delaittre, J. P. Blinco, T. Paulhörl, K. Oehlenschlaeger, M. Glassner, A. S. Goldmann, T. Tischer, M. Dietrich, H. Gliemann, C. Hübner, M. Bruns, M. Bastmeyer, N. Zydziak, **Macromolecular Colloquium**, Freiburg, Germany, February **2012**.

[1] *XPS-Characterization of Surface Functionalized Materials via (Hetero) Diels-Alder Chemistry* (Poster Presentation)

<u>V. Trouillet</u>, C. Barner-Kowollik, A. S. Goldmann, J. P. Blinco, T. Tischer, N. Zydziak, M. Bruns, **ECASIA 11**, Cardif, UK, September **2011**.

Acknowledgments